Fire Resistance Simulation for High Strength Reinforced Concrete

A thesis submitted in partial fulfilment

of the requirements for the

Degree of Doctor of Philosophy

By

Samson Ezekiel

Department of Urban Engineering

School of Built Environment and Architecture

London South Bank University

September, 2015

Declaration

The author declares that to the best of his knowledge the work presented in this thesis is original and has not been produced or submitted to any university or learning institute for the award of a higher degree.

Dedication

I dedicate this Thesis to God almighty for granting me wisdom, knowledge, strength and inspiration in my PhD programme.

Acknowledgements

I would like to offer my appreciation and gratitude to the following people who advised and assisted me during my research programme:

- My first supervisor, Director of studies Professor Robert Xiao and my supervisor Dr Ivana Kraincanic for their unfailing and invaluable guidance, motivation and assistance during my research. I will forever remain grateful.
- The Management team of Petroleum Technology Development Fund (PTDF) for granting me a research scholarship.
- Professor Michael Gunn for his support and assistance.
- Dr Andy Lim and my colleagues Dominic Wu, Saba Al-Zoehairi, Haider Alsabty and Zoheir Kichou for their support, assistance, team working and creating a good working environment.
- Mrs Louise Thompson and Mr Andre Etheridge for granting me regular and timely feedback on my progress reports.
- The staff of Urban Engineering who has provided their support and advice.
- My Parents, family and friends for their encouragement and understanding during this period.

Abstract

High strength reinforced concrete (HSRC) has been used more frequently in the construction of high rise buildings and other concrete structures in recent decades due to its advantages and excellent performance over normal strength and conventional reinforced concrete. Some of these advantages include: higher strength, better durability and allowance for provision of using less concrete and smaller section sizes. Although HSRC performs better than normal strength reinforced concrete (NSRC) at ambient temperatures, NSRC has been found to perform better than HSRC at elevated temperatures and fire conditions.

Provision of adequate fire resistance for reinforced concrete (RC) structures is essential as fire represents an extreme loading and hazardous condition to which a structure might be exposed during its life span. The fire resistance of RC members is evaluated using a prescriptive approach which is irrational and conservative. Current codes of practice and construction in industry are moving towards performance based fire design method with computing software, which is a rationally based method with each structure designed to meets its own need. This method requires comprehensive knowledge and modelling of concrete and reinforcement material behaviour and their response at elevated temperatures.

The fire resistance of HSRC members (columns and beams) in this study was evaluated using a three-dimensional Finite Element (FE) model created in ANSYS. The stress – strain behaviour of concrete proposed in this research was used in modelling the behaviour of concrete in ANSYS, while other concrete and steel material properties were accounted for by using models proposed by other researchers. The fire resistance of the HSRC members is evaluated using coupled field analysis (thermal – structural analysis) with performance based failure criteria provided in the code of practice.

The accuracy of the FE model was verified by comparing the thermal response, structural response and predicted fire resistance with fire test results obtained. Using the validated FE model, parametric studies were conducted to investigate the influence of various parameters affecting the fire performance of HSRC members exposed to fire. From the parametric studies conducted, simplified calculation models were developed for evaluating the resistance of HSRC members (columns and beams) exposed to fire. These models were validated with results from ANSYS and a fire resistance test. The simple model accounts for major factors such as member

size, load ratio and fire scenario, and therefore can be easily incorporated into structural design. The FE model and simple calculation model provide a rational approach for evaluating the fire resistance of HSRC (members) and predict a more accurate fire resistance than the prescriptive approach.

Contents

List of Tables

List of Figures

Notations

A_f Floor area of enclosure (m^2)

A_t Total compartment or enclosure area (m^2)

A_v Total vertical opening area (m^2)

b Thermal absorptivity of the enclosure ($Ws^{0.5}/m^2 K$)

B_b Beam sectional width (mm)

B_c Column sectional width (mm)

C Specific heat capacity (J/kg K)

C_c Specific heat capacity of concrete (J/kg K)

C_l Limiting axial contraction (mm)

C_s Specific heat capacity of steel (J/kg K)

d Depth of the tensile zone (mm)

d_a Aggregate size (mm)

D Thermal diffusivity (m^2/s)

D_b Beam sectional depth (mm)

D_c Column sectional depth (mm)

D_l Limiting deflection (mm)

E Elastic modulus (MPa)

E_{c0} Elastic modulus of concrete at ambient temperature (MPa)

E_{cT} Elastic modulus of concrete at elevated temperature (MPa)

E_{sT} Elastic modulus of steel (MPa)

f_c Applied compressive stress (MPa)

f_f Fire factor

f_{c0} Compressive strength of concrete at ambient temperature (MPa)

f_{cT} Compressive strength of concrete at elevated temperature (MPa)

f_{t0} Tensile strength of concrete at ambient temperature (MPa)

f_{tT} Tensile strength of concrete at elevated temperature (MPa)

f_{sT} Applied steel stress (MPa)

f_{spT} Strength of steel at proportional limit (MPa)

f_{syT} Yield strength of steel (MPa)

F Yield criterion

F_{rb} Beam fire resistance (min)

F_{rc} Column fire resistance (min)

$\{F^a\}$ Applied structural load vector or applied heat load vector

G_{cT} Compressive fracture energy at elevated temperatures (N/mm)

G_{fT} Fracture energy at elevated temperatures (N/mm)

$\{F_i^{nr}\}$ Restoring force or restoring heat load

h Height of axial and vertical load bearing members (mm)

h_e Average window height (m)

h_s Element size (mm)

k Thermal conductivity (W/m K)

k_c Thermal conductivity of concrete (W/m K)

k_s Thermal conductivity of steel (W/m K)

k_x Thermal conductivity in x direction (W/m K)

k_y Thermal conductivity in y direction (W/m K)

k_z Thermal conductivity in z direction (W/m K)

k_{cT} Reduction factor of concrete strength at elevated temperature

k_{eT} Incremental factor of concrete strain at elevated temperature

$[K]$ Stiffness or conductivity matrix

$\left[K_i^T\right]$ Tangential stiffness or tangential conductivity matrix

L Length (mm)

L_b Beam length factor

L_r Load ratio

L_{rb} Beam load ratio factor

L_{rc} Column load ratio factor

$[M]$ Mass matrix (kg)

O Ventilation opening factor

P_t Applied load at time t (N)

P_{ta} Total applied load (N)

q_{fd} Design fire load density (MJ/m^2)

Q Internally generated heat (J)

Q_c Convection heat flux (J)

Q_f Flow potential

Q_r Radiation heat flux (J)

R Gas constant (J/kmol K)

$\{S\}$ Deviatoric stress vector (MPa)

t Time (min)

$t_{\max}$ Time at which maximum temperature is reached (min)

t^* Ventilation compensated time (min)

T Temperature (°C)

T_g Fire or furnace temperature (°C)

T_s Surface temperature (°C)

$T_{\max}$ Maximum fire or furnace temperature (°C)

$\{u\}$ Displacement or temperature vector

X Clear concrete cover (mm)

X_b Concrete cover factor for beam

X_c Concrete cover factor for column

α Pressure sensitivity parameter

α_0 Aggregate type factor

α_c Convective heat coefficient

α_f Flow potential pressure sensitivity parameter

α_s Concrete tensile strength factor

ε Strain of concrete due to applied compressive stress

ε_r Resultant emissivity

ε_{c0} Peak strain of concrete at ambient temperature

ε_{cT} Peak strain of concrete at elevated temperature

ε_{cr} Creep strain

ε_{th} Free thermal strain or thermal expansion

ε_{σ} Strain due to applied stress and load

$\varepsilon_{tot.cr}$ Total creep strain

ε_{tr} Transient strain

ε_{thc} Thermal strain of concrete

ε_{ths} Thermal strain of steel

ε_{spT} Strain at proportional limit for steel

ε_{syT} Yield strain of steel

ε_{stT} Limiting strain of steel

ε_{suT} Ultimate strain of steel

σ Applied stress (MPa)

σ_e Equivalent stress (MPa)

σ_k Yield stress (MPa)

σ_m Mean or hydrostatic stress (MPa)

σ_r Stephan Boltzmann constant

Γ Time factor

ρ Density of concrete (kg/m^3)

ρ_s Effective reinforcement ratio

μ Load ratio

w/c Water cement ratio

FE Finite element

HSC High strength concrete

HSRC High strength reinforced concrete

LITS Load induced thermal strain

NSC Normal strength concrete

NSRC Normal strength reinforced concrete

RC Reinforced concrete

Chapter 1 : Introduction

Concrete is widely used as a construction material for different structures, including bridges, houses, tunnels, offshore structures, reservoirs, dams, liquefied petroleum and gas (LPG/LNG) terminals and other applications. Concrete is extensively used because it can be easily moulded into any desirable shape, size and form. It competes particularly well with other building materials due to its versatility in use. It also possesses good water resistance without fast deterioration, and the materials required in its production, namely water, aggregate and cement are readily available almost in everywhere worldwide (Mehta and Monteiro, 1993).

In recent years a significant amount of research has been performed to improve the properties of concrete, such as strength, durability and other properties. This has given rise to the production of new types of concrete, such as high strength concrete (HSC) and fibre reinforced concrete (FRC). High strength concrete is characterised by higher strength and durability, whilst fibre reinforced concrete is characterised by higher ductility.

1.1 High Strength Concrete (HSC)

Concrete strength determines the amount of load which a concrete structure can carry and support. Therefore, higher strength concrete performs better when subject to structural loadings. With advances in technology, the production of concrete with high strength is easily achieved. In the past, high strength concrete (HSC) has been viewed as concrete with a compressive strength of 40MPa and above (Mehta and Monteiro, 1993; Nawy, 2001; Neville, 1995). In more recent times, HSC is viewed as concrete with a compressive strength of 55MPa and above (BS EN 1992-1-2:2004).

After the introduction of high strength concrete (HSC) in the construction industry, most reinforced concrete high rise buildings, tunnels, bridges, oil platforms, dams, LPG/LNG terminals, offshore structures and other massive structures have been built with HSC (Kodur and Phan, 2007; Gawin *et al.*, 2004). High strength concrete is produced by using a lower water/cement ratio and by adding admixtures to the concrete mix. Compared with normal strength concrete (NSC), high strength concrete has a higher strength, low porosity, low permeability, higher density, less ductility and more durability. Smaller sizes of the member can

be designed by using high strength concrete, which provides more usable space (Kodur and Phan, 2007; Phan and Carino, 1998; Slate *et al.*, 1986).

1.1.1 Characteristics of High Strength Concrete (HSC)

High strength concrete has high compressive strength, high tensile strength, low permeability, low porosity, good resistance to freeze-thaw attack, good resistance to salt penetration, good resistance to chemical attack, high density, and resistance to reinforcement corrosion. When compared with NSC, HSC has low ductility and less fire resistance at elevated temperatures (Nawy, 2001; Neville, 1995). This is mainly due to the fact that HSC loses a higher percentage of its strength and stiffness in fire conditions when compared with NSC and is more susceptible to spalling (this is when pieces of concrete fall away or break away when exposed to fire conditions). When compared with NSC, HSC relies more on the degree of compaction and the water cement ratio for its higher strength; therefore the effect of loss of stiffness and compactness is felt more in HSC. Admixtures are usually added to the concrete mix in the production HSC. These admixtures help to reduce the water cement ratio, increasing the compactness and decreasing the porosity and voids within the concrete, which eventually leads to an increase in strength and stiffness of the concrete. Types of admixture include silica fumes, superplasticisers, water reducing agents and others.

1.1.2 Fire Performance of High Strength Concrete (HSC)

Structural design requires the structure to resist fire for a period of time before the fire can be terminated and lives and properties saved. Using high strength concrete the fire resistance is less in comparison with normal strength concrete (NSC). High strength concrete is more susceptible to spalling due to its brittle behaviour and high tendency of build-up of pore pressure due to resistance of migration of vapour at elevated temperatures or fire situations (Park *et al.*, 2011; Li *et al.*, 2004; Han *et al.*, 2005).

As HSC concrete is subjected to elevated temperatures or fire, the concrete absorbs heat. As heat energy is transferred within the concrete, the water in the concrete is heated up and as the temperature increases the water is converted to vapour. The vapour tries to escape the concrete, but due to the dense and microspore nature of HSC, it cannot escape easily. Therefore, pressure builds up and causes the concrete to expand, increasing the size of micro-cracks and it gradually begins to loss its cohesion (Kodur and Phan, 2007; Arioz, 2007). With continuous pressure build

up, cracks that are induced in the concrete reduce the fire resistance of high strength concrete, which leads to brittle failure.

It was reported that the use of silica fumes in concrete causes spalling when the concrete is subjected to elevated temperature and fire (Hertz, 1984). This spalling effect is more detrimental to the concrete as a small percentage loss in weight, area and mass of concrete could be accompanied by a greater loss of strength (Li *et al.*, 2004; Li *et al.*, 2011).

1.2 Fire Safety Design

In the design of concrete structures, one major criterion is the provision of adequate fire resistance for the structural members and the structure as a whole. It is very important that, when a structure is exposed to high temperatures and fire conditions, it does not fail abruptly but still can resist the fire loading for some time in order to save lives. Fire safety design for concrete structures is achieved by active and passive methods.

The active method includes fitting the structure with an alarm system, smoke detector and control system, automatic sprinklers, fire extinguishers, access route for fire service men and fire safety management units. Alternatively, the passive method includes the provision of escape access routes, provision of barriers to repel the spread of the fire and sufficient fire resistance of the structural members. Fire resistance is the duration for which a structure can maintain its load bearing capacity, integrity, stability and insulation capabilities when exposed to fire. This study is focused on the fire resistance of structures as it is the last line of action when all other fire safety precautionary measures fail to combat the fire (Purkiss, 1996).

Achieving the fire resistance of structures has been based on meeting some requirements, which include the arrangement of the structural members to satisfy fire ratings specified in codes of practice; this method is known as the prescriptive approach. Using this approach significant factors influencing the fire performance of structures, such as load ratio, fire type and restraint condition are not fully considered. Therefore, the prescriptive approach does not provide an accurate and rational approach for evaluating the fire resistance of structures.

Contemporary design codes are moving towards the direction of performance based design (Purkiss, 1996). The performance based approach can be made by creating a replica representative specimen to be tested in a furnace or by using numerical programs to simulate the

member behaviour and performance under fire conditions. In order to achieve performance based fire design and analysis of concrete structures with numerical programs, a material model and the mechanical properties of concrete have to be obtained (Youssef and Moftah, 2007; Hertz, 2005). These properties are applied in using numerical methods to determine the fire resistance and performance of the structure under fire conditions and elevated temperatures. With performance based design, all major factors governing the fire performance of structures can be accounted for; therefore a performance based approach with numerical programs provides a cost effective and rational method for evaluating the fire resistance of structures. As discussed earlier, high strength concrete has a lower fire resistance and is more susceptible to spalling than normal strength concrete; therefore, the main focus of this research will be on high strength concrete and its performance under fire.

1.2.1 Fire Resistance Simulation

Fire resistance simulation involves modelling a structure system or an individual member by subjecting it to similar fire conditions in a furnace or by using FE software in order to obtain its response and performance under fire. This includes simulating the individual member, the thermal and structural restraint condition of the system, thermal and structural load which the system undertakes. The material properties need to be included when using software. It also involves the variation of well-known parameters to ascertain the influences on the performance of the system under fire.

1.3 High Strength Reinforced Concrete (HSRC) under Fire

When high strength reinforced concrete (HSRC) is exposed to fire, the temperature increases in both the concrete and steel material. This rise in temperature is accompanied with degradation, loss of strength and stiffness of concrete and steel. With sustained fire exposure, the high strength reinforced concrete is continually weakened, with crack propagation within the concrete, loss of cohesion and load bearing capacity, until failure. Some of the major factors governing the fire performance of high strength reinforced concrete are discussed in the section below.

1.3.1 Factors Affecting the Fire Performance of High Strength Reinforced Concrete

The strength of concrete and steel affects the fire performance of high strength reinforced concrete. HSC, which has high strength and low permeability, resists the dissipation of vapour at

elevated temperatures and therefore this leads to the build-up of pressure on the concrete, which eventually leads to spalling. It loses its strength faster than normal strength concrete (NSC) due to its brittle nature (Kodur, 1999).

The permeability of a concrete at elevated temperatures influences the performance of the high strength reinforced concrete. It was reported from obtained results that concrete with high permeability performed better than concrete with lower permeability, as spalling was observed in concrete with lower permeability at elevated temperatures (Noumowe *et al.*, 2009).

The fire intensity to which the structure is subject to also affects the fire performance of high strength reinforced concrete. The risk of spalling of concrete in hydrocarbon fires is greater than for standard fire in buildings. The temperature rise and heating rate due to hydrocarbon fires are higher than those in standard fires (ISO 834-1:1999). Experimental investigation was conducted on the fire performance of high strength concrete subjected to high and low heating rates. The results indicated that low heating rates reduced the risk of spalling in high strength concrete (Ali *et al.*, 2010).

Load intensity also affects the performance of concrete subjected to elevated temperatures. With higher loads the tendency for spalling increases. Stress in concrete is higher with higher loads; therefore the intensity of load would affect the fire performance of HSC. An increase in load level increases the risk of occurrence of spalling and early failure of the structure (Ali *et al.*, 2010).

The moisture content of concrete expressed in terms of relative humidity affects the fire endurance and spalling in high strength reinforced concrete. Concrete with high relative humidity spalls more than concrete with lower relative humidity and concrete with relative humidity of 80% and above shows significant spalling under fire (Kodur and Phan, 2007).

The size of a member affects the fire performance and spalling in HSC. Heat transfer and temperature evolution occur at a faster rate in reinforced concrete with a smaller cross-sectional area. Concrete with a larger sectional area could experience thermal shock, which could lead to cracking and spalling (Park *et al.*, 2011). Experimental studies on concrete subjected to elevated temperatures indicated that larger specimens retained more strength than smaller specimens with the same unfired strength (Li *et al.*, 2004). The concrete reinforcement cover also affects the fire

performance of reinforced concrete, as with a smaller concrete cover, heat is transferred quicker from the heated surface to the reinforcement.

The type of aggregate used in the concrete influences the fire performance of the concrete, as concrete with calcareous aggregate (limestone) has a better resistance to fire and spalling than concrete made with siliceous aggregate (Kodur and Phan, 2007). This is due to the fact that calcareous aggregate possesses a lower coefficient of thermal expansion (Kodur and Phan, 2007).

1.4 Aims of Research

The aims of this research are to evaluate the fire resistance and performance of high strength reinforced concrete (HSRC) structures under fire conditions and elevated temperatures by using a performance based approach with numerical program, ANSYS. Most international codes of practice are moving away from the traditional prescriptive approach to a performance based method by using numerical techniques and software, which is a rational approach. This is important as it allows every structure and system to be analysed and designed uniquely to meet its own specific design needs and requirements. There is a significant knowledge gap to be overcome in order to achieve this as there is a lack of research information. Through this research programme, HSRC structures can be better analysed and designed in the future. A simple rational design model will be developed for evaluating the fire resistance of HSRC members based on the results obtained and parametric studies conducted.

1.4.1 Objectives of Research

The following research tasks are set in order to achieve the aims of this research:

- Conduct a comprehensive literature review on fire performance of reinforced concrete members subjected to fire conditions. This review will cover previous testing and numerical studies on fire response of reinforced concrete, methods for evaluating fire resistance and general behaviour of concrete and reinforcement under fire.
- Carry out a review on the existing proposed models for HSC under fire and propose a new material model for HSC to address the inadequacies of the existing models. Apply the proposed model into ANSYS to perform an analysis of HSRC members under fire conditions.

- Model HSRC members (column and beam) subjected to fire with ANSYS and validate with experimental test data and evaluate the fire performance and failure pattern of these members.
- Perform parametric studies to determine the influence of various main parameters on the fire resistance of high strength reinforced concrete.
- Propose simple equations for evaluating fire resistance of HSRC columns and beams which would account for major factors influencing the fire performance of HSRC columns and beams exposed to fire.

1.4.2 Research Scope

The researches performed to achieve the above stated objectives are presented in eight chapters. Chapter 1 provides a general introduction to fire resistance simulation of high strength reinforced concrete and presents the aims and objective of this study.

Chapter 2 presents a critical review on fire performance of reinforced concrete, approaches for evaluating fire resistance, previous numerical studies on reinforced concrete exposed to fire conditions and material behaviour of concrete and steel.

Chapter 3 presents a review on some of the existing HSC material temperature dependent relationships and the proposed new material model for HSC exposed to fire.

Chapter 4 deals with three-dimensional (3D) Finite Element (FE) modelling of reinforced concrete members (columns and beams) using ANSYS APDL software.

Chapter 5 presents an FE model validation of a high strength reinforced concrete column, RC column performance under fire, model sensitivity analysis and parametric studies to determine the influence of major factors on fire performance of the column.

Chapter 6 covers FE model validation of a high strength reinforced concrete beam under fire, fire response and resistance of the beam, sensitivity analysis and parametric studies to determine the significance of major factors affecting the fire performance of reinforced concrete beams.

Chapter 7 presents the proposed model for computing the fire resistance of HSRC columns and beams exposed to fire.

Chapter 8 presents the major findings, recommendations and conclusions of the research.

1.5 Contribution to Knowledge

The research will evaluate the performance of HSRC members at elevated temperatures and fire conditions using a performance based approach and numerical methods with ANSYS. Based on the verified numerical model, parametric studies will be conducted and a simple rational design model will be developed for evaluating the fire resistance of HSRC members with major influencing factors accounted for. Through this research, high strength concrete structures would be better designed and safely used under fire. The research conducted is original and will have strong impact for the practical design and the codification of concrete structures.

Chapter 2 : Literature Review

This is a review on high strength reinforced concrete, its response during fire and elevated temperatures and work carried out by other researchers on the fire performance of reinforced concrete, the fire design method of reinforced concrete, spalling of concrete and properties of concrete and reinforcements exposed to fire conditions.

2.1 Fire

Fire involves the reaction between combustible fuel and air. The combustible fuel refers to materials which would burn during ignition or spark. Fire is domestically used for cooking, in industry for material processing, power and also heat energy (Drysdale, 2011). When it is not properly controlled in the case of an accident, fire could cause the loss of lives and damage to properties. It is, therefore, necessary to provide a guide against the improper use of fire, which can lead to fire disasters. This requires that fire resistance and safety are taken into account when designing a structure.

2.1.1 Fire Requirements of Structures

Structures need to maintain their stability, strength and integrity for a given period of time under fire in order to aid saving of lives and properties. In this period of time, the structure is expected to withstand the extra loads and stresses induced on it as a result of fire and elevated temperature while the fire service men try to terminate the fire (BS EN 1992-1-2:2004; Choi and Shin, 2011).

The structure should be designed and built in such a way that in the event of a fire, the edifice can still maintain its load-bearing capacity for a period of time. The structure should maintain its integrity, the fire should not spread to the surrounding environment, and the occupants of the building can be evacuated without posing a high risk to the rescue team (BS EN 1992-1-2:2004).

2.2 Fire Models

The development of fire, in a fire scenario, involves three main stages, namely fire growth stage, burning or fully developed fire stage and decay stage (Buchanan, 2001; Dwaikat, 2009). In the growth stage, heat energy is supplied to combustible material or fuel and the temperature within the compartment increases at a gradual and slow rate (Lie, 1992). In the burning stage, the combustible material or fuel ignites and the fire spreads throughout the compartment. This is

accompanied by rapid rise in temperatures, which can be in excess of 1000°C. The decay stage begins with decomposition and burning out of the combustible material or fuel, which leads to continual decease of fire temperatures. For simplified analysis and design purpose, fires are represented using a temperature – time curve which is approximately similar to the temperature increment in fire scenarios. The fire growth stage is neglected as at this point the fire is at the initiation phase. The fire can be represented using a standard fires model, a hydrocarbon fires model and a parametric design fires model.

2.2.1 Standard Fires

The standard fire nominal temperature – time curve represents fires with low heating rates, which occur mostly in residential buildings, offices and other structures. Figure 2.1 and Equation 2.1 represent the nominal temperature – time curve of a standard fire proposed in BS EN 1991-1-2:2002. The temperature – time curve for the standard fire only represents the fully developed fire stage and does not represent the fire decay. Therefore, a structural member can be subjected to standard fire conditions by exposing it to elevated temperature in a furnace with the temperature gradient controlled in order to achieve the standard fire curve given below:

$$T_g = 20 + 345 \log_{10}(8t + 1) \qquad 2.1$$

where T_g is the temperature of the fire or furnace in degree Celsius and t is the time in minutes.

2.2.2 Hydrocarbon Fires

The hydrocarbon fire temperature – time curve represents temperatures of fire with high heating rates and for this type of fire the temperature reaches about 1000°C within 10 minutes. This occurs mainly in hydrocarbon processing plants, industries, oil rigs, LNG/LPG terminals and other massive structures associated with hydrocarbons and petro-chemical products. Figure 2.1 and Equation 2.2 given by BS EN 1991-1-2:2002 represent the nominal temperature – time curve of hydrocarbon fire. As in the standard fire, the temperature – time curve for hydrocarbon fire does not include the decay stage of the fire:

$$T_g = 1080\left(1 - 0.325e^{-0.167t} - 0.675e^{-2.5t}\right) + 20 \qquad 2.2$$

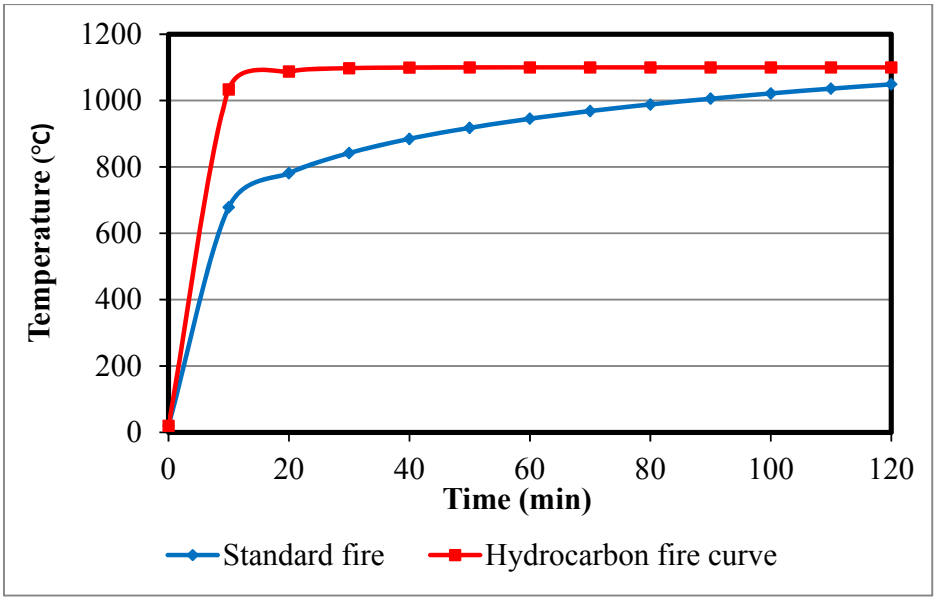

Figure 2:1: Nominal temperature – time curve for standard and hydrocarbon fires (BS EN 1991-1-2:2002)

2.2.3 Design Parametric Fires

The parametric fire model presents a more accurate temperature – time relation of the fire than standard and hydrocarbon fire models (Buchanan, 2001; BS EN 1991-1-2:2002). In the parametric fire model the temperature – time curve of the fully developed fire and decay of the fire are accounted for and can be taken into consideration in the fire design. The temperature – time curve is derived based on solving the heat balance and equilibrium equation within the compartment or enclosure due to the fire (Lie, 1974; Harmathy, 1972a; Harmathy, 1972b; Tsuchiya and Sumi, 1971). The major heat balance components which are considered are heat generated from combustion, heat losses due to radiation and outflowing gases through openings, heat content of inflowing air and heat losses to walls and enclosure (Purkiss, 1996; Lie, 1974). These heat components are a function of the fuel load of the combustible material, the dimension of the compartment or enclosure, size of ventilation opening, boundary conditions of the compartment and thermal properties of the compartment.

The Eurocodes (BS EN 1991-1-2:2002) present a parametric fire temperature – time curve that accounts for the influence of fire load, compartment size, vertical ventilation opening size and thermal properties. This temperature – time curve is given by Equation 2.3.

$$T_g = 1325\left(1 - 0.324e^{-0.0033t^*} - 0.204e^{-0.0283t^*} - 0.472e^{-0.3167t^*}\right) \quad 2.3$$

$$t^* = \Gamma \times t$$

$$\Gamma = \frac{(O/b)^2}{(0.04/1160)^2}$$

where Γ is time factor due to the ventilation opening factor (O) and thermal absorptivity (b) of the enclosure and t^* is the ventilation compensated time.

$$b = \sqrt{(\rho C k)}$$

$$O = \frac{A_v \sqrt{h_e}}{A_t}$$

where C, k and ρ are specific heat capacity, thermal conductivity and density of enclosure respectively. A_v is the total vertical opening area, A_t is the total compartment or enclosure area including openings and h_e is the average window height.

The maximum temperature $T_{\max}$ during heating occurs when $t^* = t^*_{\max}$

$$t^*_{\max} = t_{\max}\Gamma$$

$$t_{\max} = \left(120 \times 10^{-4} \frac{q_{fd} A_f}{A_t}\right) \geq 15 \text{ minutes for fast fire growth}$$

$$t_{\max} = \left(120 \times 10^{-4} \frac{q_{fd} A_f}{A_t}\right) \geq 20 \text{ minutes for medium fire growth}$$

$$t_{\max} = \left(120 \times 10^{-4} \frac{q_{fd} A_f}{A_t}\right) \geq 25 \text{ minutes for slow fire growth}$$

where q_{fd} is the fire load density and A_f is the floor area of the enclosure.

Fire load density and fire growth rate are based on occupancy classifications and the function of the building, which are provided by BS EN 1991-1-2:2002 for various classes of occupancies. BS EN 1991-1-2:2002 also presents a temperature – time curve which can be used to evaluate the temperature decrement of the fire in the decay stage. This relationship is expressed by Equation 2.4.

$$T_g = \begin{bmatrix} T_{\max} - 625\left(t^* - t^*_{\max}\right) & t^*_{\max} \le 30\,\min \\ T_{\max} - 250\left(3 - t^*_{\max}\right)\left(t^* - t^*_{\max}\right) & 30\,\min < t^*_{\max} < 120\,\min \\ T_{\max} - 250\left(t^* - t^*_{\max}\right) & t^*_{\max} \ge 120\,\min \end{bmatrix} \qquad 2.4$$

2.3 Reinforced Concrete under Fire

Reinforced concrete under fire undergoes many changes, which include transformation of the material used for the production of concrete, the microstructure and macrostructure of the concrete, its mechanical properties, thermal properties and others. These changes govern the behaviour of the concrete structure during the fire and in the cooling stage. A reinforced concrete member can be heated to standard or hydrocarbon fire conditions by subjecting it to elevated temperature in a furnace with the temperature gradient controlled in order to attain the standard or hydrocarbon fire curve (Purkiss, 1996).

2.3.1 Transformation in Reinforced Concrete at Elevated Temperatures

Temperature variation in reinforced concrete due to elevated temperatures leads to changes in the structure of the concrete. When concrete is subjected to elevated temperatures, dehydration of cement paste occurs at about 114℃ to 270℃, releasing water trapped in the concrete. Gaseous discharge occurs at about 300℃; decomposition of calcium hydroxide occurs at about 400℃ to 600℃ and above 600℃ decomposition of CSH takes place (Arioz, 2007; Hertz, 2005). When the temperature is continuously increased, the decomposition of the cement paste and concrete as a whole is increased with crack propagation. The effect of the temperature change is greater on the interfacial transition zones and cement paste than on the aggregate, as the aggregate is more structurally stable and denser. It has been reported that a crack propagation network was

observed at about 600℃ on the surface of the concrete as the temperature was increased, and the crack propagation network increased until the specimen spalled (Arioz, 2007). Figure 2.2 shows the physiochemical changes in concrete due to elevated temperatures. At elevated temperatures the bond between reinforcement and concrete weakens; reinforcement loses 10 – 15% of its yield strength as the temperature increases from 20°C to 400°C (BS EN 1992-1-2:2004). As the reinforcement attains temperatures of 500 - 700°C, it weakens extensively with large strains. (Harmathy, 1993).

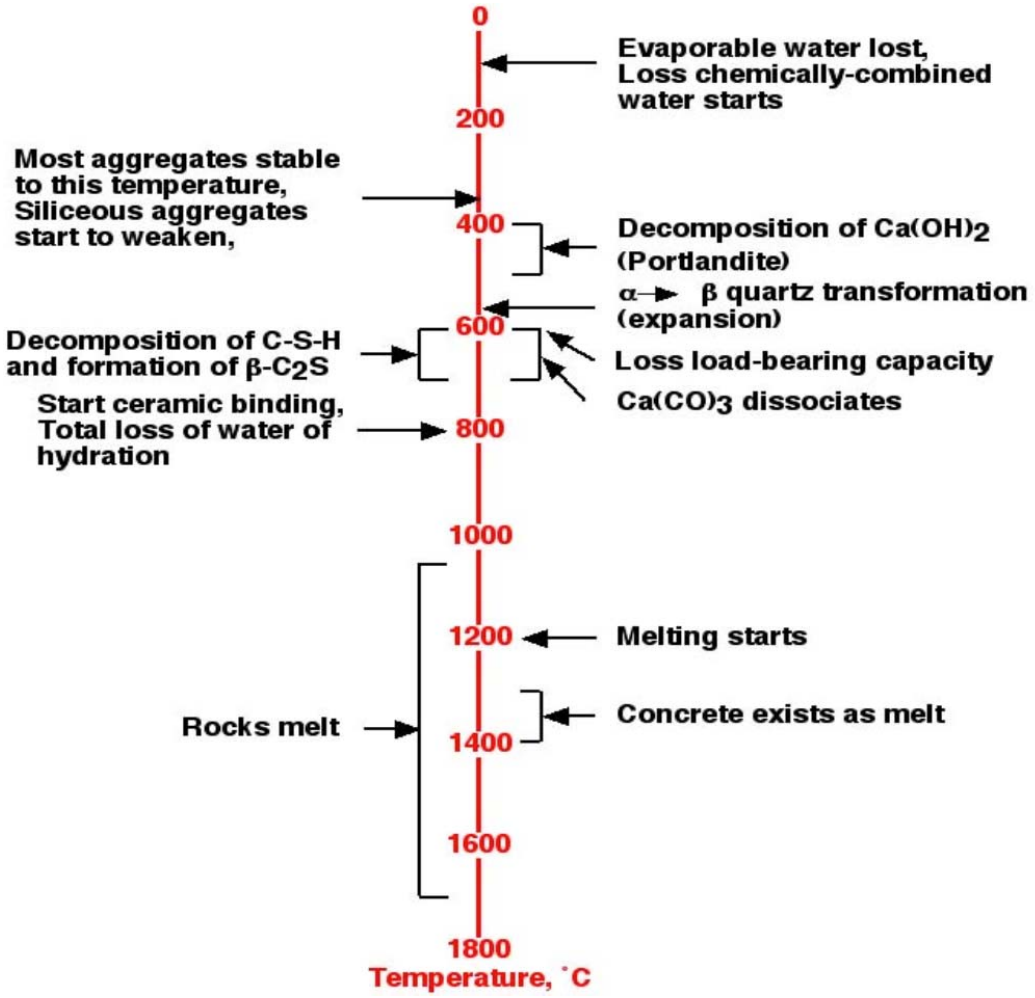

Figure 2:2: Physiochemical changes in concrete at elevated temperatures (Naus, 2010)

2.3.2 Thermal Stresses in Concrete

Stresses in concrete at ambient temperatures are a function of the structural load. These stresses are mainly in compression, tension and bending. They produce a deformation that has an approximate linear relationship when the concrete is loaded to about 30% of the failure load. As the load is increased, the degree of linearity decreases until it reaches its peak stress (Yip, 1998).

Thermal stresses in concrete are caused by the change in temperature due to either the heat of hydration or fire scenarios. Depending on the temperature change, thermal gradient and co-efficient of thermal expansion, the values of thermal stresses could be high enough to initiate cracks in the concrete (Mehta and Monteiro, 1993; Neville and Brooks, 1987). Thermal stresses in concrete induce thermal strain in the concrete.

2.4 Reinforced Concrete Fire Design

The design of concrete structures to satisfy fire structural requirements and adequate performance under fire can be performed by fire testing, the prescriptive method, calculation or the performance based method with numerical programs. The prescriptive method is well established and is the most commonly used and widely accepted method for fire design of structures. In the reinforced concrete fire designs, the structural members are required to meet specified design criteria depending on their functionality (BS EN 1992-1-2:2004). These criteria include: criterion R (load bearing capacity of the member); criterion I (insulation capability of the structural element); and criterion E (integrity of the elements) (BS EN 1992-1-2:2004). The load bearing criterion is satisfied when the structural element maintains its load bearing capacity without exceeding a specified deformation value and rate of deformation (ISO 834-1:1999; BS EN 1363-1:1999). The insulation criterion is satisfied when a separating structural element, which is exposed to fire on one side, limits the temperature increment of the unexposed surface by a specified amount. The integrity criterion is satisfied when a separating element resists the passage of flames and hot gases to the unexposed surface and resists the occurrence of opening gaps and holes through the separation elements.

2.4.1 Fire Design using Fire Test

Evaluating fire performance of reinforced concrete members can be carried out through fire testing of a replica concrete member in a specially built furnace. The principal objective of the fire test is to determine the fire resistance of the member while maintaining its load bearing

capacity and preventing the spread of the fire. In the fire test the reinforced concrete specimens to be tested are required to be similar and replicas of the actual element in practice, in accordance to design codes and standards.

Accordingly, ISO 834-1:1999 and BS EN 1363-1:1999 specify that at the time of the fire test, the test specimen should have material properties and conditions, such as strength and moisture content, similar to the actual element in service. These codes require the test specimen to be installed in a furnace with similar restraints and boundary conditions to the element in service. It is also required that the test specimen be subjected to structural loading for load bearing elements and with the furnace temperature closely controlled to attain the desired fire temperature curve, as presented in Section 2.2. The furnace and test specimen are required to be fitted with thermocouples to measure the temperature of the furnace and temperatures at the exposed surface, the unexposed surface and across the heated section of the specimen. The furnace and specimen are also required to be constructed with adequate load and deformation measuring devices.

In the fire test, structural load is initially applied and maintained on the test specimen for a period of time to replicate a member under structural loading and to obtain the deformation due to structural loading alone. Elevated temperatures are subsequently applied to the element once the structural deformation is constant. The test continues until a specified design criterion is exceeded. The specified fire design criteria recommended in (ISO 834-1:1999) are reviewed in the section 2.4.5. Major shortcomings of this method include the high cost of test equipment, the time taken and restraint on element size due to availability of space and large furnace.

2.4.2 Fire Design using Prescriptive Method

This method is based upon actual results of standard fire tests conducted on structural members in a furnace. From the results obtained in the fire tests, fire ratings of structural members are selected based mainly on their dimensions and reinforcement cover. These fire ratings are given by the regulatory codes of practice. Using the fire test in this method produced a lot of data, which have been incorporated into the code of practices for the structural fire design of concrete (Purkiss, 1996).

One of the shortcomings of this method is that it does not provide an actual representation of the performance of the member under fire. The prescriptive approach for the design of a reinforced concrete structural element in accordance to BS EN 1992-1-2:2004 is reviewed in the section below. This prescriptive design, recommended by BS EN 1992-1-2:2004, is only valid for standard fire exposure and normal weight concrete, with concrete density between 2000 to 2600kg/m^3.

Reinforced Concrete (RC) Columns

The prescriptive design approach for RC columns in accordance to BS EN 1992-1-2:2004 is based on the minimum column width, concrete cover thickness, load level and number of sides exposed to fire. BS EN 1992-1-2:2004 specifies the minimum concrete cover thickness, minimum column width, maximum load ratio and number of column sides exposed to fire required to achieve a specified fire resistance rating of an RC column. These fire resistance ratings are presented in Table 2.1.

Table 2:1: Minimum width and concrete cover specification for RC column fire resistance rating (BS EN 1992-1-2:2004)

Fire resistance rating (min)	Minimum column width/Minimum concrete cover (mm/mm)			
	Column exposed to fire on more than one side			Column exposed to fire on one side
	$\mu = 0.2$	$\mu = 0.5$	$\mu = 0.7$	$\mu = 0.7$
30	200/25	200/25	200/32 300/27	155/25
60	200/25	200/36 300/31	250/46 350/40	155/25
90	200/31 300/25	300/45 400/38	350/53 450/40	155/25
120	250/40 350/35	350/45 450/40	350/57 450/51	175/35
180	350/45	350/63	450/70	230/55
240	350/61	450/75	-	295/70

where μ represents the load ratio.

Reinforced Concrete Beams

The prescriptive design approach for reinforced concrete beams in accordance to BS EN 1992-1-2:2004 is based on the minimum beam width, concrete cover thickness and shape of the beam (rectangular and flange beams). Accordingly, BS EN 1992-1-2:2004 specifies the minimum concrete cover thickness, minimum beam width and minimum beam web thickness required to achieve a specified fire resistance rating of reinforced concrete beams. These fire resistance ratings are presented in Table 2.2.

Table 2:2: Minimum width and concrete cover specification for simply supported RC beam fire resistance rating (BS EN 1992-1-2:2004)

Fire resistance rating (min)	Rectangular beams				Flange beams		
	Minimum beam width/Minimum concrete cover thickness (mm/mm)				Minimum web thickness b_w (mm)		
					Class WA	Class WB	Class WC
30	80/25	120/20	160/15	200/15	80	80	80
60	120/40	160/35	200/30	300/25	100	80	100
90	150/55	200/45	300/40	400/35	110	100	100
120	200/65	240/60	300/55	500/50	130	120	120
180	240/80	300/70	400/65	600/60	150	150	140
240	280/90	350/80	500/75	700/70	170	170	160
The choice of Class WA, Class WB and Class WC for flange beams varies within the European Countries depending on the specified choice in their National Annex.							

Reinforced Concrete Slab

The prescriptive design approach for evaluating the fire performance of reinforced concrete slabs in accordance to BS EN 1992-1-2:2004 considers the major parameters affecting the slab performance to be the minimum slab thickness, concrete cover thickness and type of slab. Accordingly, BS EN 1992-1-2:2004 takes these major parameters into account for evaluating the fire performance of the slab and therefore specifies the minimum concrete cover thickness,

minimum slab thickness and slab type required to achieve a specified fire resistance rating of reinforced concrete slabs. These fire resistance ratings are presented in Table 2.3.

Table 2:3: Slab thickness specification for RC slab fire resistance rating (BS EN 1992-1-2:2004)

Fire resistance rating (min)	Minimum slab thickness (mm)	Minimum concrete cover thickness (mm)		
		One way spanning	Two way spanning	
			$l_y / l_x \leq 1.5$	$1.5 < l_y / l_x \leq 2.0$
30	60	10	10	10
60	80	20	10	15
90	100	30	15	20
120	120	40	20	25
180	150	55	30	40
240	175	65	40	50
l_x and l_y are the shorter and longer spans of the slab respectively				

Reinforced Concrete Load Bearing Walls

The prescriptive design approach for reinforced concrete load bearing walls in accordance to BS EN 1992-1-2:2004 is presented in Table 2.4.

Table 2:4: Specification for RC walls fire resistance rating (BS EN 1992-1-2:2004)

Fire resistance rating (min)	Minimum wall thickness/Minimum concrete cover thickness (mm/mm)			
	$\mu = 0.35$		$\mu = 0.70$	
	One side exposed to fire	Two sides exposed to fire	One side exposed to fire	Two sides exposed to fire
30	100/10	120/10	120/10	120/10
60	110/10	120/10	130/10	140/10
90	120/20	140/10	140/25	170/25
120	150/25	160/25	160/35	220/35
180	180/40	200/45	210/50	270/55
240	230/55	250/55	270/60	350/60

where μ represents the load ratio.

Accordingly, BS EN 1992-1-2:2004 specifies the minimum concrete cover thickness, minimum wall thickness and minimum load ratio required to achieve a specified fire resistance rating of reinforced concrete walls.

2.4.3 Fire Design using Calculation Method

Fire design using calculation methods is performed based on mathematical models and equations developed from heat transfer and fire tests. These calculations are computed in four stages. In the first stage the temperatures of the fire are evaluated based on fire type and scenario. These are achieved by selecting a suitable temperature – time profile or by using a parametric design fire model. The second stage involves calculating the temperature profile and distribution within the member. The structural members are sub-divided into small regions and the temperature distribution and evolution are evaluated as a function of the distance of each region from the heated surface. These temperatures are subsequently determined using heat transfer equations, finite difference or finite element methods. The temperatures can also be determined by using standard time-temperature profiles of a reinforced concrete column, beam and slab provided in codes of practice.

In the third stage, the strength reduction of each region of the member is evaluated based on a temperature dependent strength model and the load bearing of the whole member is re-evaluated based on retained strength of each region. In the fourth stage, the fire resistance times are evaluated by comparing the design applied load with the load bearing capacity of the member for load bearing elements. For separating elements such as partition walls, the fire resistance is determined by comparing the temperature of the unexposed surface with maximum allowable temperatures specified in the codes of practice.

Accordingly, BS EN 1992-1-2:2004 provides a simplified cross-section calculation method for evaluating the fire performance of reinforced concrete members. In the approach recommended in BS EN 1992-1-2:2004 the fire temperatures are determined by using the required temperature – time model, while the temperature profiles are evaluated using temperature profile curves specified by BS EN 1992-1-2:2004. In this approach, BS EN 1992-1-2:2004 specifies that regions and sections having a temperature above 500°C should be considered and analysed as

having 0% retained strength and load bearing capacity, while regions with temperatures below 500°C should be considered to have 100% retained load bearing capacity and strength. The fire resistance of the member is subsequently determined by comparing the re-evaluated maximum load resistance of the section with the applied load and temperature of the unexposed surface with the maximum temperature specified by BS EN 1992-1-2:2004. These methods are based on many approximations in evaluating the load bearing capacity and therefore would not provide an actual fire performance of the reinforced concrete member.

2.4.4 Fire Design using Performance Based Method with Computing Programs

The performance based method is carried out based on the performance of the structural member at elevated temperatures and fire conditions. This method requires temperature dependent material properties, which are used to evaluate the response of the concrete structure under fire and elevated temperatures. New codes of practice are moving towards performance based and numerical design approaches as these are less expensive, with no specimen size constraint and every design is unique to the actual structure. Four major factors must be considered when using the performance based approach with numerical computing program, namely fire type, material properties, loading conditions and failure criteria.

In the performance based approach the type of fire is required. This is to ensure that the heat transfer due to the fire scenario is properly modelled and replicated with the numerical programs. This can be achieved by using the standard, hydrocarbon or parametric temperature – time curve in Section 2.2, depending on the nature of the fire. The material properties and behaviour are also of great importance, as fire performance of materials varies depending on their stiffness, strength, moisture content and resistance to heat transfer. Loading conditions are accounted for extensively in the performance approach in order to obtain a more realistic and effective fire design, as it has been reported by numerous researches that the load level has a major influence on the fire performance of structures.

Failure criteria of the member should be considered based on the design criteria in Section 2.4.5, depending on the functionality of the member. For reinforced concrete columns and beams, the load bearing failure criterion should be considered, while for slabs, load bearing should be taken into account, and for partition walls, insulation and integrity failure criteria should be taken into account.

2.4.5 Design Criteria

When using the fire test method or performance based design approach with numerical programs, failure of a member should be considered if the designated design criteria, based on the functionality of the structural element, are exceeded. These design criteria are: load bearing design criterion, insulation design criterion and integrity design criterion.

Load Bearing Fire Design Criterion

ISO 834-1:1999; ISO 834-4:2000; ISO 834-7:2000 specify that a vertical load bearing element fails when the measured contraction or rate of contraction exceeds the limits given by Equations 2.5 and 2.6, while a load bearing horizontal and flexural element fails when the measured deflection or rate of deflection exceeds the limits given by Equations 2.7 and 2.8 (ISO 834-1:1999; ISO 834-5:2000; ISO 834-6:2000).

Limiting axial contraction $C_l = \frac{h}{100} mm$ 2.5

Limiting rate of axial contraction $\frac{dC_l}{dt} = \frac{3h}{1000} mm/\min$ 2.6

where h is the initial height of axial and vertical load bearing elements.

Limiting deflection $D_l = \frac{L^2}{400d} mm$ 2.7

Limiting rate of deflection $\frac{dD_l}{dt} = \frac{L^2}{9000d} mm/\min$ 2.8

where L and d are the span and depth of the tensile zone of flexural and horizontal load bearing elements.

Insulation Design Criterion

ISO 834-1:1999; ISO 834-4:2000; ISO 834-5:2000 specify two conditions for which a separating horizontal or vertical element exposed to fire on one side is considered to have failed. The first condition is when the temperature rise above ambient temperature at any point of the unexposed surface exceeds 180°C, while the second condition is when the average temperature of the unexposed surface rises above ambient temperature by more than 140°C.

Integrity Design Criterion

Two methods are specified in (ISO 834-1:1999) for evaluating the integrity fire performance of horizontal and vertical separating elements. This first method involves placing a cotton wool pad in a wire frame against an opening on the unexposed surface of the separating element. The separating element would be considered to have failed when the cotton wool pad ignites into flames or charring. The second method involves using gap gauges; the separating element would be considered to have failed if either of the following two conditions occurs. The first is if a 6mm gap gauge can be inserted through the element to the exposed surface and can be stretched along the length by up to 150mm without undue force or with a very little force. The second is if a 25mm gap gauge can be passed through the element to the exposed surface with little or no resistance.

Overall, for an element having a load bearing and separation function, such as loading bearing walls and slabs, the minimum fire resistance obtained from the load bearing criterion, insulation criterion and integrity criterion should be selected as the fire resistance time of the element.

2.5 Concrete Spalling in Fire

Spalling is the sudden or progressive breaking off of surface layers or pieces of concrete from a structural element exposed to fire and high temperatures, and which happens in a violent or non-violent manner (Bailey, 2002; Comsa, 2013; Fu and Li, 2011). Spalling is mainly attributed to evaporation and migration of free and chemically bonded moisture, thereby resulting in complete dryness at the heated surface, which leads to cracks and progressive breaking off of the surface layer (Comsa, 2013; Phan, 2008). Spalling is also attributed to the inability of concrete, due to its low porosity, high compactness and low permeability, to allow adequate migration and evaporation of moisture within the inner section of the concrete. This resistance to moisture migration results in build-up of internal pore pressures and can eventually result in sudden and violent breaking off of the concrete, (Phan, 2008; Mugume and Horiguchi, 2014; Suhaendi and Horiguchi, 2006). Spalling of concrete can occur in three major ways, namely aggregate, local spalling or sloughing off and explosive spalling (Institution of Structural Engineers, 1975).

2.5.1 Aggregate Spalling

Aggregate spalling is the splitting and breaking of aggregate which is very close and around the heated surface. Aggregate spalling involves the splitting and flying of aggregate pieces at the

heated surface. It also involves forceful displacement and removal of concrete surface at the heated surface. This type of spalling occurs at the early stages of heating between 20 to 30 minutes from fire exposure (Fu and Li, 2011). Aggregate spalling is mainly attributed to mineral content of the aggregate and thermal shock (Connolly, 1995).

2.5.2 Sloughing Off

Sloughing off, is the gradual, progressive and non-violent breaking off of concrete surface and corners at elevated temperatures. This spalling occurs in the later stages of fire and is mainly attributed to cracks in completely dry regions due to evaporation of moisture and loss of cohesion and strength of concrete (Purkiss, 1996; Comsa, 2013).

2.5.3 Explosive Spalling

Explosive spalling is the violent and sudden breaking away of concrete which occurs at the early stages of fire. This type of spalling, which results in the loss of concrete cover, may lead to extensive damage and early failure of the structure (Phan and Carino, 1998; Purkiss, 1996; Comsa, 2013). Figure 2.3 shows spalling in an HSRC column.

Figure 2:3: Spalling of high strength concrete column which was exposed to fire (Kodur, N.D).

This type of spalling is mainly attributed to build up of vapour pressure and thermal stresses as illustrated in Figure 2.4. When concrete is heated, free and chemically bound water in the concrete are converted to vapour at around 100°C. Some of these vapours migrate out of concrete through the surface and some migrate inwards away from the heated surface, as shown in Figure

2.4a. If the vapour which migrates inwards gets to regions of temperatures lower than 100°C, it condenses back to water and combines with the available water at that region as shown in Figure 2.4b. The concrete is therefore divided into two regions, one completely dry and the other with a high level of moisture content. With continual migration and condensation of vapour at cooler sections, a fully water saturated wall region and moisture clog are formed as shown in Figure 2.4c, with the moisture clog preventing further migration of vapour. Continual building up of vapour pressure and thermal stresses may result in expansion of the concrete volume and explosive spalling, as shown in Figure 2.4d, paving an escape route for the water vapour.

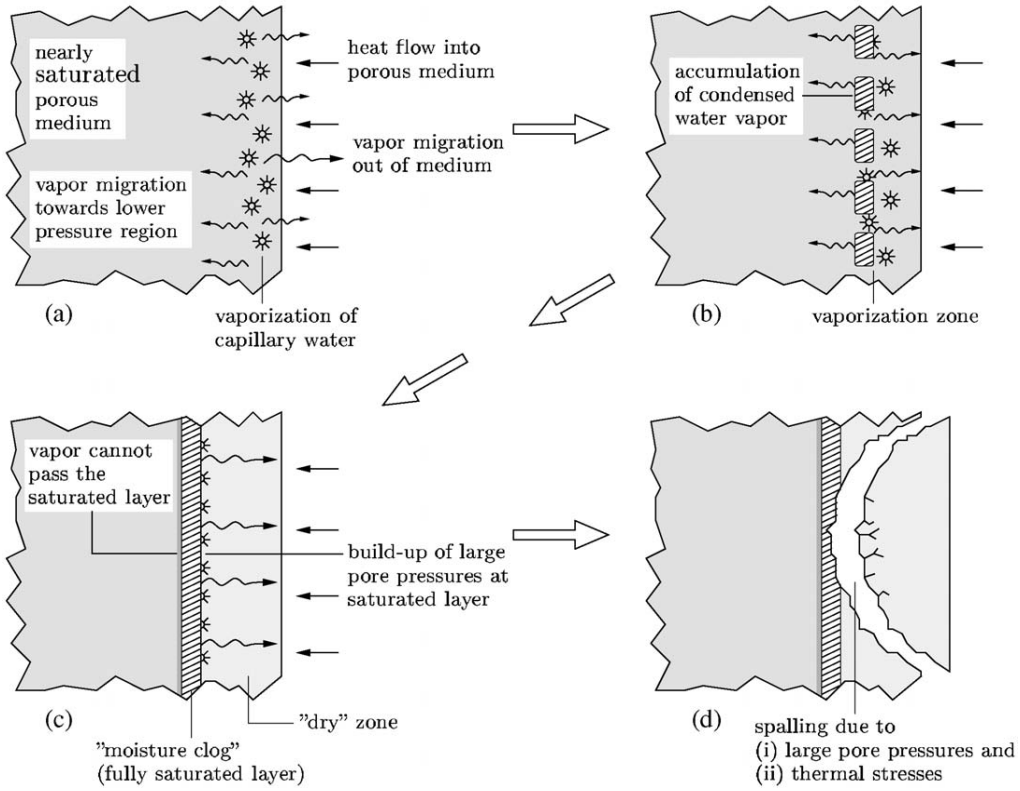

Figure 2:4: Explosive spalling mechanism in concrete (Zeiml *et al.*, 2006)

2.6 Mechanical Properties of Concrete

The mechanical properties of concrete include the compressive strength, flexural bending strength, elastic modulus, Poisson's ratio and other properties. At ambient temperature these mechanical properties are dependent on the age of the concrete, the water/cement ratio of the concrete, the degree of compactness, concrete mix, concrete material used and others. These

properties vary with elevated temperature due to the change in the micro-structures and chemical composition of the concrete. The main mechanical properties of concrete that change at elevated temperatures are the strength, peak strain and modulus of elasticity.

2.6.1 Stress – Strain Relationship of Concrete

The stress – strain relationship of a concrete is the relationship between applied load and deformation of the concrete. The relationship is approximately linear when loaded to about 30% of its maximum strength and above 30% its non-linear (Mehta and Monteiro, 1993). Micro-cracks, which exist in the transition zone in concrete even before being loaded, are mainly responsible for the non-linear behaviour of concrete (Mehta and Monteiro, 1993; Ollivier *et al.*, 1995). Micro-cracks in the concrete lead to a slight reduction in the effective surface area of the concrete, and on application of stress to the concrete, the localised stress due to stress concentration is more than the applied stress, therefore resulting in a higher value of strain (Neville and Brooks, 1987).

The separate stress – strain curves of hydrated cement paste and aggregate are linear, but the stress –strain curve of their corresponding concrete is non-linear as shown in Figure 2.5. The size of the micro-cracks increases with increase in applied load and stress, therefore resulting in crack prorogation through the section. Figure 2.6 shows a relationship between micro-cracks, applied stress and the elasticity of the concrete. From the figure it can be seen that as the load increases, the size of the micro-cracks begins to increase and the stress is no longer linear with strain, which eventually leads to failure.

The loss of water present in the microstructure of hydrated cement paste due to drying leads to drying shrinkage which contributes to microcracks and crack propagation in the concrete. A sustained load also leads to the increase in microcracks and propagation of these cracks, and therefore contributes to the non-linear behaviour of the concrete (Mehta and Monteiro, 1993). At the initial stage, when the concrete load is very small and is applied for a short period with fewer microcracks, the concrete exhibits a linear stress − strain relation, but as the load is increased and sustained over a longer period of time, the stress-strain relationship is no longer linear (Mehta and Monteiro, 1993).

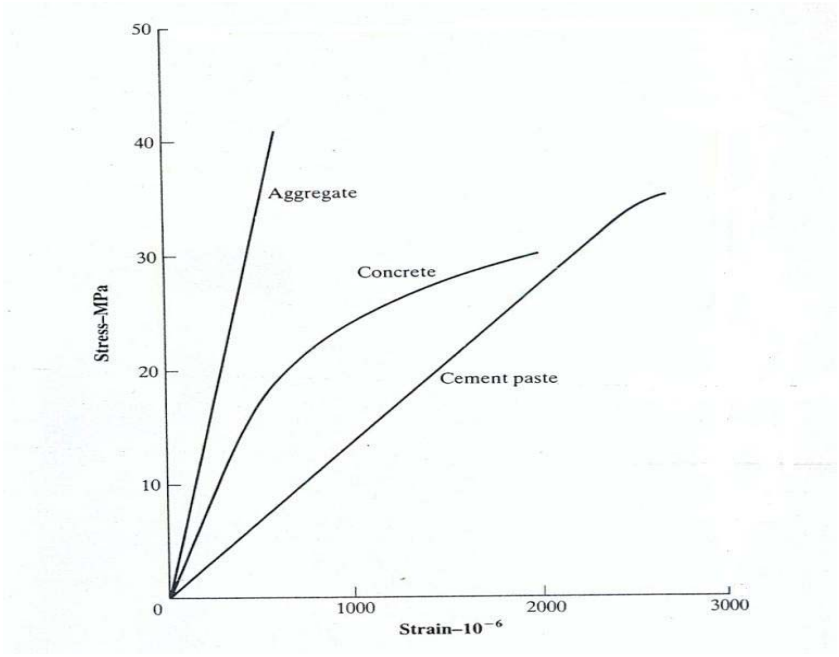

Figure 2:5: Stress – strain curve for cement paste, aggregate and concrete (Neville and Brooks, 1987)

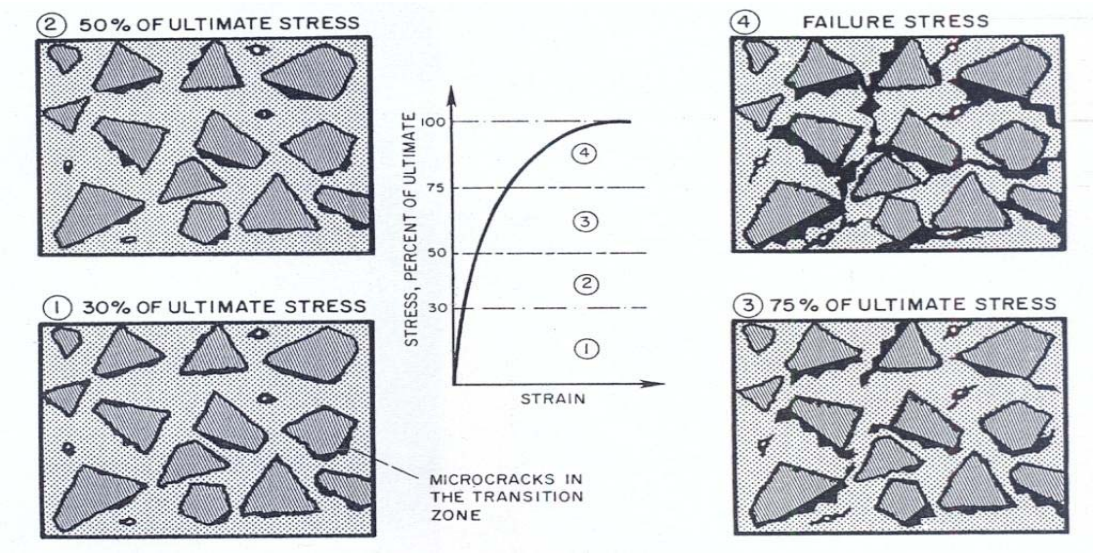

Figure 2:6: Effect of stress on microcracks and elasticity of concrete (Mehta and Monteiro, 1993)

At elevated temperatures or temperatures due to fire, the change in temperature causes the concrete to expand, dehydrate and experience thermal stresses. These thermal stresses cause propagation of microcracks in the concrete as the elevated temperature is sustained or increased

(Arioz, 2007). The determination of the stress – strain relationship of concrete at elevated temperatures can be achieved using two test methods (Anderberg and Thelandersson, 1976; Fu *et al.*, 2005):

i. Constant load and increase in temperature until failure (transient method). In this test method the specimen is prepared and placed in the furnace, the load is kept constant and the temperature is gradually increased until the concrete fails.
ii. Constant temperature and loading to failure (steady state method). In this method the specimen is prepared and placed in the furnace and temperature is increased until the target temperature is reached. The target temperature is kept constant for some time to ensure that the target temperature is attained throughout the concrete. The concrete is then loaded gradually until failure.

Anderberg and Thelandersson (1976) from their experimental research reported that the stress – strain relationship obtained using the transient method produced similar results and in good agreement with those obtained from the steady state test method. The stress – strain relationship of concrete under uniaxial compressive load at elevated temperatures using the steady state test method has been carried out in three states: the stressed test, unstressed test and unstressed residual test (Abrams, 1971; Bastami and Aslani, 2010). In the stressed test the concrete sample is preloaded and placed in the furnace, and after attaining the required test temperature the load is gradually increased until failure. This is carried out while the concrete is still in the hot state (Abrams, 1971; Bastami and Aslani, 2010). In the unstressed test the concrete is not preloaded before thermal testing; the concrete is heated to the required temperature and then loaded gradually until failure while still in the hot state (Abrams, 1971; Bastami and Aslani, 2010). In the unstressed residual test the concrete is not preloaded before testing; after heating the specimen in the furnace, its temperature is allowed to drop back to ambient temperature and it is gradually loaded to failure. This test is useful for post fire analysis of concrete structures and repairs (Abrams, 1971; Bastami and Aslani, 2010). The schematic diagram of these tests is shown in Figure 2.7.

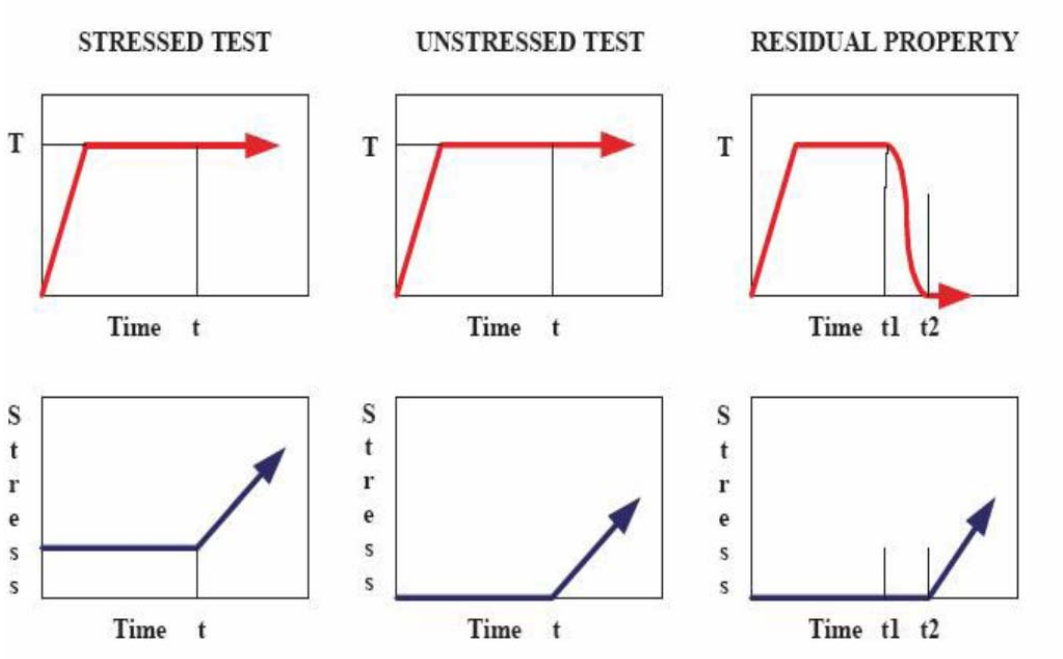

Figure 2:7: Schematic diagram of stressed, unstressed and residual test for concrete at elevated temperatures (Naus, 2010)

2.6.2 Compressive Strength

The compressive strength of concrete is a measure of the load bearing capacity of the concrete in compression. At ambient temperature the compressive strength of concrete is influenced by the age of the concrete, water/cement ratio, admixture used in the concrete, type of aggregate used in the concrete, the compactness of the concrete and the type of cement used in the concrete.

At elevated temperatures, the compressive strength of concrete decreases with the increase in temperature (Phan and Carino, 1998; Hertz, 2005). The rate of decrease in the compressive strength at elevated temperatures varies with the type of test carried out (stressed, unstressed and unstressed residual test) (Cheng *et al.*, 2004; Phan and Carino, 2003). Abrams (1971) reported that results from his test indicated the lowest decrease in the strength of concrete to be in the stressed test, followed by the unstressed test, and the residual test had the highest decrease in strength.

This reduction in strength results from weakening of the bond and crack propagation in the concrete due to elevated temperatures. The original compressive strength and water/cement ratio

has little or no effect on the normalised compressive strength of concrete at elevated temperatures (Schneider, 1988; Xiao and König, 2004).

2.6.3 Elastic Modulus of Concrete

The elastic modulus of concrete is a measure of the stiffness of the concrete. It can be determined as secant modulus, tangent modulus and initial tangent modulus. At ambient temperature the elastic modulus of concrete is influenced by the strength of the concrete, the stiffness of the aggregate, the water/cement ratio of the concrete and the age of the concrete. Concrete with higher strength, stiffer aggregate and with lower water/cement ratio possesses a higher elastic modulus (Naus, 2006).

At elevated temperatures the elastic modulus of concrete decreases with the increase in temperature; this is due to the weakening of the bond between the cement paste and aggregate and also the loss of stiffness of the concrete. The initial strength and water/cement ratio of the concrete has little or no influence on the normalised elastic modulus temperature relationship (Schneider, 1988; Sabeur *et al.*, 2007). The decrease in the normalised elastic modulus of concrete is higher in the unstressed test than in the stressed test and also when tested in the hot state, the type of cement used in the concrete has little or no influence on the elastic modulus temperature relationship (Naus, 2010; Schneider, 1988).

2.6.4 Strain of Concrete at Elevated Temperatures

At ambient temperature the strain in concrete is a combination of strain due to the instantaneous stress and creep. The strain of concrete at elevated temperatures includes the elastic instantaneous strain, the free thermal strain, transient strain and creep strain (Sadaoui and Khennane, 2009; Hassen and Colina, 2006). Li and Purkiss (2005) stated that the transient strain is due to the change of chemical composition of concrete and externally applied stress. The creep strain is dependent on external applied stress, temperature and the duration of the applied stress. The instantaneous and transient strains are dependent on the external applied stress and temperature, while the free thermal strain is a function of temperature (Li and Purkiss, 2005). The instantaneous peak strain is the value of strain which corresponds to the maximum stress of concrete; it increases with elevated temperature (Chang *et al.*, 2006). The increase in peak strain at elevated temperatures is due to degradation of material and thermal incompatibility of the aggregate and cement paste (Xiao and König, 2004; Chang *et al.*, 2006). Youssef and Moftah

(2007) and Li and Purkiss (2005) gave the expression, Equation 2.9, for the total strain in concrete at elevated temperature:

$$\varepsilon_{tot} = \varepsilon_{th}(T) + \varepsilon_{\sigma}(\sigma,T) + \varepsilon_{cr}(\sigma,T,t) + \varepsilon_{tr}(\sigma,T) \quad 2.9$$

Where ε_{th} is the free thermal strain or thermal expansion;

ε_{σ} is the strain due to applied stress and load;

ε_{cr} is creep strain; and

ε_{tr} is transient strain.

Sadaoui and Khennane (2009) and Hassen and Colina (2006) suggested that the transient thermal strain occurs due to change in chemical and thermo-mechanical interactions in the concrete. The non-inclusion of transient thermal strain in the evaluation of the total strain of concrete at elevated temperatures would lead to an erroneous result (Sadaoui and Khennane, 2009). Anderberg and Thelandersson (1976), Jensen *et al.* (2010) and Li and Purkiss (2005) suggested that creep strain is very small and can be neglected.

Khoury *et al.* (1985), Khoury *et al.* (1986) and Terro (1998) considered the total strain of concrete at elevated to be a combination of three strains as expressed in Equation 2.10.

$$\varepsilon_{tot} = \varepsilon_{th} + \varepsilon_{\sigma} + \varepsilon_{tot.cr} \quad 2.10$$

Where $\varepsilon_{tot.cr}$ is total creep strain and it's a combination of basic creep, thermal creep and drying creep.

Khoury *et al.* (1985), Khoury *et al.* (1986) and Terro (1998) combined total creep strain and instantaneous stress related strain as load induced thermal strain (LITS) and is given by

$$LITS = \varepsilon_{tot.cr} + \varepsilon_{\sigma} \quad 2.11$$

The load induced thermal strain LITS is a function of applied load (stress level) and temperature. Load induced thermal strain at 30% stress level at elevated temperatures is given by

$$LITS(T,0.3f_{c0}) = \left(2.73T + \frac{6.35T^2}{10^2} - \frac{2.19T^3}{10^4} + \frac{2.77T^4}{10^7} - 43.87\right) \times 10^{-6} \quad 2.12$$

For other stress level the LITS is given by

$$LITS(f_c / f_{c0}) = LITS(T,0.3f_{c0}) \times (0.032 + 3.226\, f_c / f_{c0}) \quad 2.13$$

Where T is temperature, f_c is applied stress and f_{c0} is compressive strength at ambient temperature.

The free thermal strain or thermal expansion of concrete is a measure of volume change in the concrete due to change in temperature. Thermal expansion is significant as it accounts for the structural movement and thermal stresses due to temperature change and could eventually result in cracking and spalling of the concrete (Naus, 2006).

Concrete with lower thermal expansion is desirable in order to reduce the risk of high thermal expansion and stresses of the concrete at elevated temperatures, as concrete are weak in tension. At ambient temperature the coefficient of thermal expansion is influenced by the type of aggregate. Figure 2.8 shows the coefficient of thermal expansion of concrete with different aggregates. At elevated temperatures the free thermal strain of concrete, a heterogeneous material, is influenced by the thermal expansion of the cement paste and the aggregate, the two having different values. A large difference between the thermal expansion of the cement paste and that of the aggregate leads to thermal incompatibility and differential action at the interface, and would eventually result in cracking at the interface (Naus, 2010).

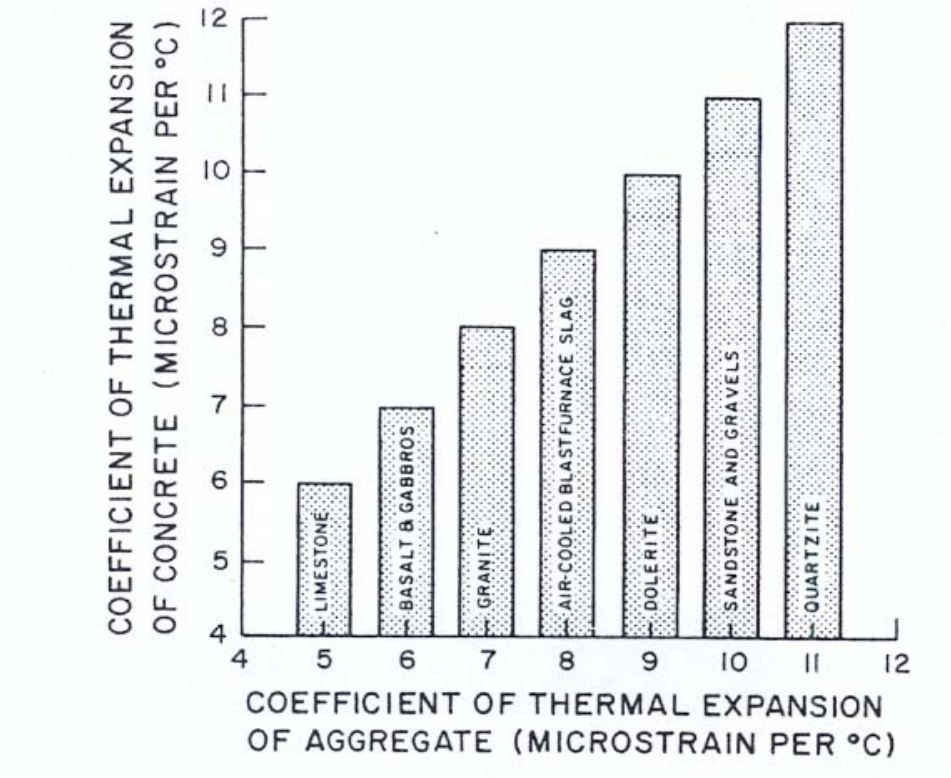

Figure 2:8: Bar graph showing the relationship between the coefficient of thermal expansion of aggregate and concrete (Mehta and Monteiro, 1993)

Cement paste subjected to elevated temperature undergoes thermal expansion up to about 150℃ and begins to contract above this temperature, while aggregate subjected to elevated temperature undergoes thermal expansion throughout the period of elevated temperature (Naus, 2010; Cruz and Gillen, 1980). In concrete the expansion of the aggregate exceeds the contraction of the cement paste and therefore concrete experiences thermal expansion at elevated temperatures (Cruz and Gillen, 1980). Figure 2.9 shows the thermal expansion of cement paste and its corresponding mortar and concrete. Cruz and Gillen (1980) and Kodur and Sultan (2003) reported that the type of aggregate used in concrete is the major factor influencing the thermal expansion of concrete at elevated temperatures.

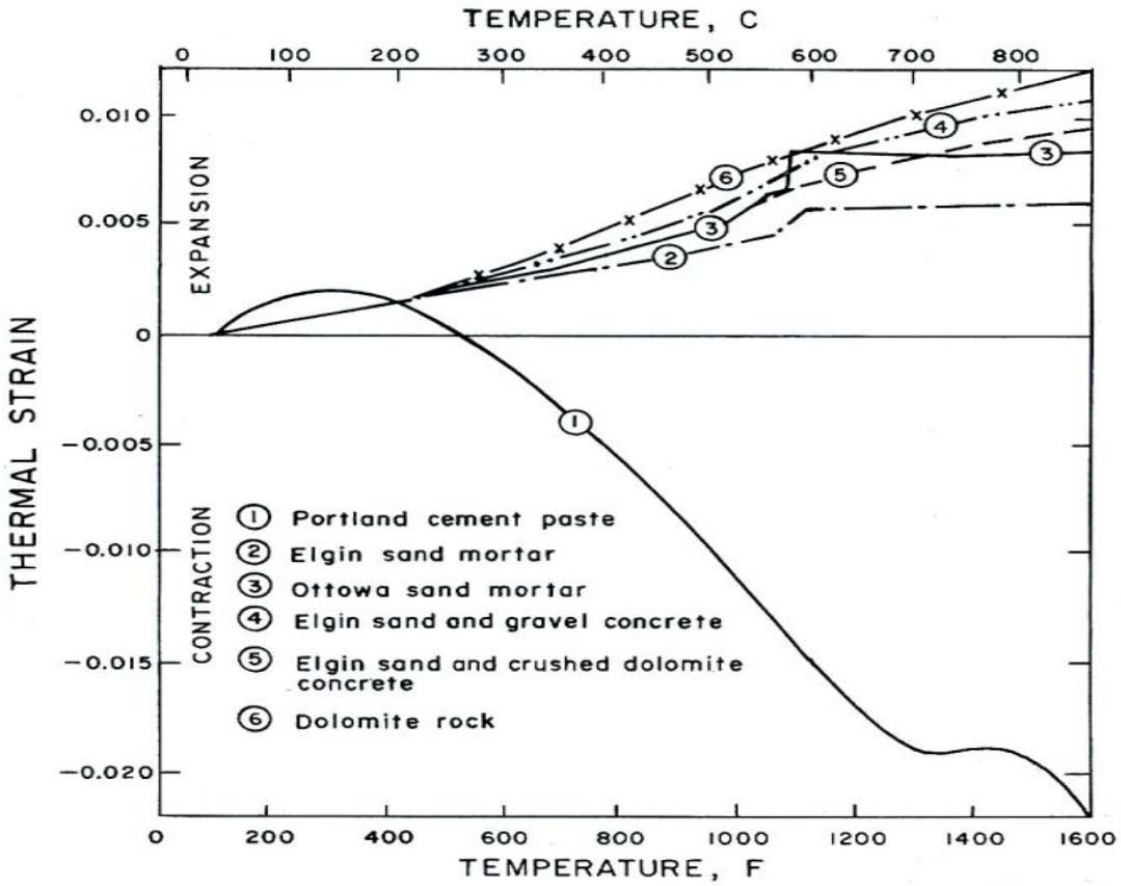

Figure 2:9: Thermal expansion of cement paste and its corresponding mortar and concrete at elevated temperatures (Naus, 2010)

Aggregate with a high coefficient of thermal expansion would produce concrete with a high thermal expansion, The thermal expansion of the aggregate is influenced by the percentage of silica content in the aggregate, as aggregate with a higher percentage of silica content would have a high value of thermal expansion and would correspondingly produce concrete with a higher free thermal strain and vice versa (Naus, 2010). Moisture content also influences thermal expansion as saturated concrete has a higher thermal expansion than dry concrete. At elevated temperatures, siliceous aggregate concrete undergoes a higher thermal expansion than carbonate aggregate. Figure 2.10 gives the thermal expansion of concrete with siliceous and carbonate aggregate.

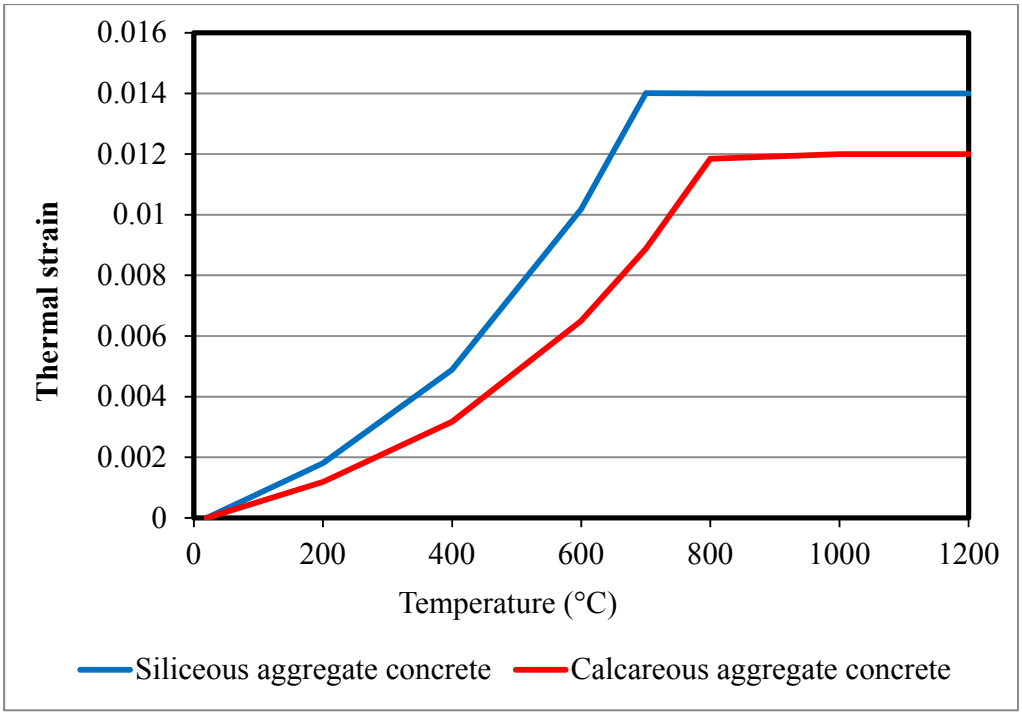

Figure 2:10: Thermal expansion of siliceous and carbonate aggregate concrete at elevated temperatures (BS EN 1992-1-2:2004)

2.6.5 Density of Concrete

At ambient temperature the density of concrete depends mainly on the density of the aggregate and the moisture content of the concrete, as lightweight aggregate concrete has a lower density than normal weight aggregate concrete and saturated concrete has higher density than dry concrete. The density of concrete decreases slightly with elevated temperature due to the dehydration of free and chemical bound water in the concrete, decomposition of calcium hydroxide and decarbonation in carbonate aggregate concrete (Naus, 2010).

2.7 Thermal Properties of Concrete

Concrete's thermal properties dictate its thermal behaviour and response at elevated temperatures. The properties include thermal conductivity, thermal diffusivity and specific heat capacity. These thermal properties are not constant but are dependent mainly on the water/cement ratio, compactness, porosity and type of aggregate used in the concrete, and at elevated temperatures these thermal properties undergo some changes and variation (Kodur and Sultan, 2003; Yang *et al*., 2003).

2.7.1 Thermal Conductivity of Concrete

Thermal conductivity is a measure of heat conduction in concrete; it is evaluated as the ratio of heat flux to temperature change and it is responsible for the rate of temperature change in the concrete at elevated temperatures. At ambient temperature the thermal conductivity of concrete is higher with lower water/cement ratio and low porosity. It is required that concrete should have a high thermal conductivity in other to achieve a low temperature gradient across the concrete. Concrete with a high temperature gradient would lead to thermal shock and eventually could lead to spalling and failure of concrete (Naus, 2010; Shin *et al.*, 2002; Zha, 2003).

The thermal conductivity of concrete is influenced by the hardened cement paste, the moisture content of the concrete and pore sizes and distribution (Naus, 2006; Shin *et al.*, 2002). Normal weight aggregate concrete has a much higher thermal conductivity than light weight aggregate concrete at ambient and elevated temperatures (Harmathy, 1970). Kodur and Sultan (2003) from their test results reported that the thermal conductivity of concrete with carbonate and siliceous aggregate decreases with increase in temperature. Figure 2.11 presents thermal conductivity of concrete as given in (BS EN 1992-1-2:2004).

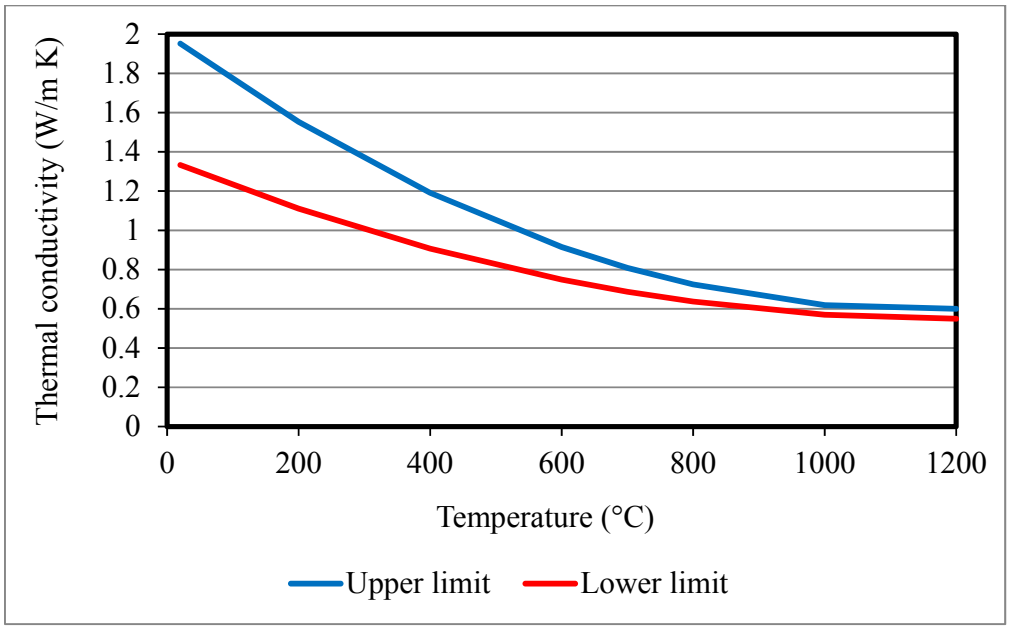

Figure 2:11: Thermal conductivity of normal weight aggregate concrete (BS EN 1992-1-2:2004)

2.7.2 Thermal Diffusivity

Thermal diffusivity of concrete is the rate at which heat is dissipated through the concrete in all directions due to change in temperature. It is the rate of heat flow through the concrete at elevated temperatures. Concrete with high thermal diffusivity is desirable in order to increase heat flow rate through the concrete, as low rate of heat flow would lead to build-up of thermal stresses and pressure (Naus, 2010). At elevated temperatures, the thermal diffusivity of concrete decreases with increasing temperature.

The thermal diffusivity is given by;

$$D = \frac{k}{pC_c} \qquad 2.14$$

where $D =$ thermal diffusivity (m^2/s);

$k =$ thermal conductivity (W/mK);

$p =$ density (kg/m^3); and

$C_c =$ specific heat capacity (J/kg K).

2.7.3 Specific Heat Capacity

The specific heat capacity of concrete is the amount of heat required to raise the temperature of a unit mass of the concrete through a unit rise in temperature. At ambient temperature, the type of aggregate and mix proportion have little or insignificant effect on the specific heat capacity, whereas at lower temperatures the moisture content of concrete affects the specific heat capacity, as concrete with high moisture content has high specific heat capacity (Naus, 2006). This is due to the fact that not all the heat transferred to the concrete is used up by the concrete, as some of the heat is consumed in the heating and evaporation process of the moisture in the concrete. At elevated temperatures the specific heat capacity of concrete varies depending on the composition change which takes place in the concrete. The specific heat capacity of concrete increases at temperatures between 100℃ – 400℃, where both free water and water in the cement paste evaporates.

2.8 Mechanical Properties of Reinforcement

The mechanical properties of reinforcement include the yield strength, ultimate strength, elastic modulus, Poisson's ratio, strain and other properties. At ambient temperature these mechanical properties of reinforcement are dependent mainly on chemical composition and steel type (Harmathy, 1993). These properties are more consistent in value in comparison with concrete due to the homogeneity of reinforcements. These properties vary at elevated temperatures due to degradation, loss of strength and stiffness of the reinforcement. The reinforcement steel mainly used in construction are reinforcing steel and prestressing steel.

The reinforcing steel is used as rebar inside concrete to provide tensile resistance. While prestressing steel are pre-stressed to produces compressive stresses which balances the tensile stresses in the concrete. The prestressed steel exert a prestressed longitudinal force on the concrete thereby producing compressive stresses and eliminating or considerably reducing tensile stresses at critical sections of the member (Nawy, 2006; O'Brien *et al.*, 2012).

2.8.1 Stress – Strain Relationship of Reinforcing steel

The stress – strain relationship of reinforcement is the relationship between applied load and deformation of the reinforcement. This relationship is linear and elastic until the reinforcing steel starts to yield. At normal temperature reinforcing steel yields abruptly with increment in applied load, while at elevated temperatures the yielding softens, which is mainly attributed to loss of stiffness of the bar (Buchanan, 2001). Yield strength and modulus of elasticity of reinforcing steel decrease with increasing temperature.

At ambient temperature the strain in reinforcing steel is a combination of strain due to the instantaneous stress and creep. At high temperatures, total strain of reinforcement is a combination of thermal, elastic and creep strain (Li and Purkiss, 2005). The thermal strain of reinforcing steel is a function of temperature, while the elastic strain is a function of temperature and applied stress, and creep strain is a function of temperature, applied stress and time. Unlike concrete, steel reinforcements do not encounter transient strain effects as the structure of the reinforcement is more homogenous and stable. Total strain component in reinforcing steel at elevated temperatures is expressed by Equation 2.15.

$$\varepsilon_{tot} = \varepsilon_{th}(T) + \varepsilon_{\sigma}(\sigma, T) + \varepsilon_{cr}(\sigma, T, t) \qquad 2.15$$

2.8.2 Stress – Strain Relationship of Prestressing steel

At ambient temperature the stress strain curve of prestressing steel is linear and elastic, it becomes nonlinear and in elastic at about 70% of the tensile strength (Nawy, 2006). Just as with reinforcing steel, the stiffness and yield strength of prestressing steel decreases with elevated temperatures. This degradation of stiffness and strength of prestressed steel is caused by changes in the microstructure, recovery of dislocation and recrystallization of the reinforcement at elevated temperatures. At ambient temperatures prestressed steel possesses a stable microstructure (martensite), when subjected to elevated temperatures the martensite structures is converted to pearlite structure (Hou *et al.*, 2014). This pearlite microstructure is less stable and has a high ductility which leads to the degradation of stiffness and strength of the material. In comparison with reinforcing steel, the rate of loss of strength and stiffness is higher in prestressing steel reinforcement (Hou *et al.*, 2014).

The strain in prestressed reinforcement also increases with elevated temperatures. Just as with reinforcing steel the total strain for prestressed is a combination of strain due to the instantaneous stress, temperature and creep as expressed in Equation 2.15.

2.9 Thermal Properties of Steel Reinforcement

The thermal properties of steel reinforcement that influence its thermal behaviour and response at elevated temperatures include thermal conductivity and specific heat capacity (Buchanan, 2001). These thermal properties vary with increasing temperature.

2.9.1 Thermal Properties of Reinforcing Steel

The thermal conductivity of steel reinforcement decreases with increasing temperature between 20 − 800°C and above this temperature range it is approximately constant (BS EN 1992-1-2:2004; Purkiss, 1996). The specific heat capacity of steel reinforcement increases with increasing temperature between 20 − 600°C with a peak value at 700 − 800°C, and above 900°C the specific heat capacity is approximately constant. This variation in thermal conductivity and specific heat capacity with elevated temperatures are presented in Figure 2.12 and 2.13 respectively.

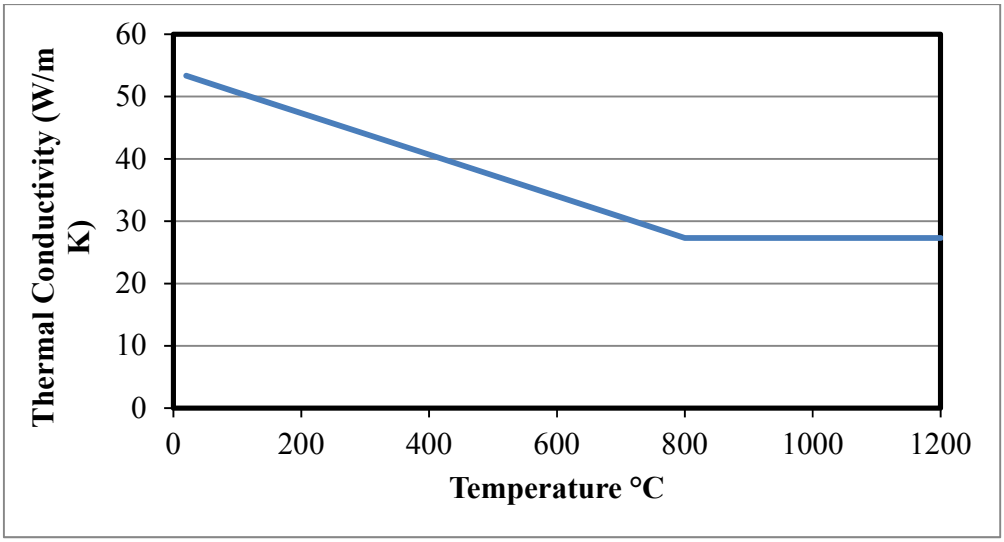

Figure 2:12: Thermal conductivity of reinforcing steel at elevated temperatures (BS EN 1993-1-2:2005)

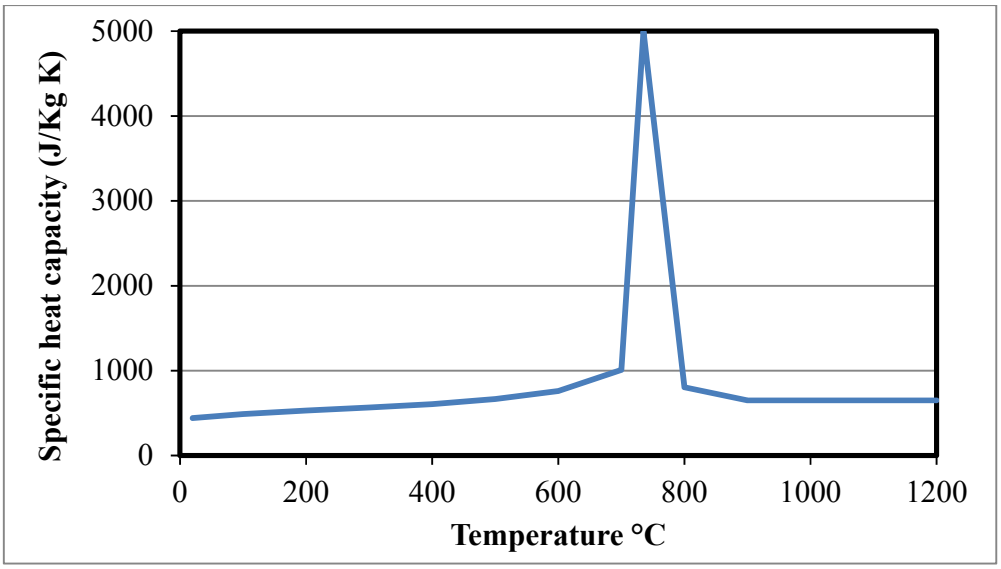

Figure 2:13: Specific heat capacity of reinforcing steel at elevated temperatures (BS EN 1993-1-2:2005)

2.9.2 Thermal Properties of Prestressing Steel

Thermal conductivity of prestressed reinforcement is the ability of the material to transfer heat within its structure. While specific heat capacity is the amount of heat required to raise the

temperature of a unit mass of steel through a unit rise in temperature. There have been very few and limited research conducted on the thermal properties of prestressing steel, BS EN 1992-1-2:2004 and BS EN 1993-1-2:2005 recommends that thermal conductivity and specific capacity of reinforcing steel can be used for prestressing steel.

2.10 Previous Studies on Reinforced Concrete under Fire

In this section, previous research studies on fire performance of reinforced concrete members are reviewed. These include numerical research work on normal and high strength reinforced concrete members, as most numerical research work carried out has been for normal strength reinforced concrete.

Gao *et al.* (2013) performed a numerical study on fire performance of reinforced concrete beams exposed to fire. They developed a three-dimensional (3D) finite element model using FE software ABAQUS. The standard temperature – time curve was used to model the fire temperatures and structural load was applied to the beam that was simply supported. Newton-Raphson iteration was used to perform a non-linear analysis of the beams and load bearing performance based failure criteria were used to evaluate fire resistance of the RC beams. The effect of perfect and non-perfect bonds between concrete and reinforcement was also investigated. Gao *et al.* (2013) concluded that the numerical model was suitable, cost effective and valid for evaluating fire performance of normal strength reinforced beams. They also established that although a slightly more accurate fire performance was predicted with non-perfect concrete reinforcement bonds, the effect of the bond type is negligible and therefore a perfect bond can be used for contact between concrete and reinforcement. The numerical model is only valid for normal strength reinforced concrete (NSRC) and therefore it should be extended to cover HSRC.

Zha (2003) performed a numerical study on the behaviour and fire performance of reinforced concrete columns and beams exposed to fire. Three-dimensional (3D) non-linear finite element models were developed with FE software DYNA3D. A standard temperature – time curve was used to model the fire temperatures and the temperature distribution and profile were evaluated using Hertz's simplified heat transfer formula (Hertz, 1981). The time dependent temperatures were input to DYNA3D to perform thermal structural non-linear analysis of the RC columns and beams. Fire resistance of the RC columns and beams was evaluated using performance based

failure criteria. Parametric studies were performed to determine the influence of load ratio, concrete cover, member size and reinforcement ratio on fire performance of RC beams and columns.

Zha (2003) concluded that failure of a column was attributed to compressive load and material degradation, while the failure of the beam was due to excessive deflection of the beam caused by high temperatures. Zha (2003) established that decreasing load level, increasing concrete cover, increasing member sizes and increasing reinforcement ratio resulted in increased fire resistance. The influence of these parameters on fire performance of RC columns and beams was not considered in relationship to member resistance, which usually increases or decreases due variation in reinforcement ratio and member sizes. The numerical model is suitable and valid for evaluating fire performance of NSRC members and therefore cannot be used to evaluate the fire performance of HSRC members.

Lie and Irwin (1993) established a mathematical model for evaluating the fire resistance of RC columns with rectangular sections. Using this numerical model the cross-section of the columns is subdivided into elements. The combined fire response of all elements is used in predicting the fire performance of RC columns. The standard temperature – time curve was used to model the fire temperatures and heat transfer within the elements was evaluated using a Finite Difference method. The model accounted for moisture content by considering that all heat energy supplied to the element at 100°C would be used up for moisture evaporation and temperature dependent material model. Column failure and fire resistance were evaluated as the time when the applied load was greater than the computed column strength. Lie and Irwin (1993) concluded that the model is valid for normal strength RC columns and can be used for predicting the fire resistance of columns in practice. The model is not valid for HSRC columns and therefore is limited to only NSRC columns.

Kodur and Dwaikat (2008) developed a numerical program for modelling and predicting fire response of RC beams exposed to fire. Using this program, a macroscopic finite element model was developed by subdividing the beams into sections along their longitudinal span. The collated fire responses of all sections are used in predicting the fire performance of RC beams. The model accounted for temperature dependent material properties and fire induced spalling of concrete. Thermal structural analysis was conducted and performance based failure criteria were utilized in

predicting fire resistance of the RC beams. Kodur and Dwaikat (2008) established that the type of fire model and load level significantly influence fire performance of RC beams. The model is cost effective and valid for normal and high strength RC beams. The proposed numerical program is not commercially available to the design industry, unlike commercially available program such as ANSYS, ABAQUS and other software which can be easily accessed and used in the design industry.

Kodur *et al.* (2004) carried out a numerical study on fire performance and response of RC columns exposed to fire. They developed a numerical model for predicting fire response of RC columns, similar to that proposed by Lie and Irwin (1993), which they incorporated into their computer program written with FORTRAN. The model accounted for temperature dependent material properties and fire induced spalling of concrete by assuming that all concrete spalls above 350°C. Structural analysis was performed and failure was based on strength reduction criteria for predicting fire resistance of the RC columns. Kodur *et al.* (2004) validated the model for HSC and recommended the model to be suitable for predicting the fire performance of RC columns. Again, the developed numerical program is not commercially available to the design industry. A proper mesh sensitivity analysis and adequacy check was not conducted as the model is based on macroscopic finite discretisation.

Dotreppe and Franssen (1985) developed a numerical model for analysis of reinforced concrete beams exposed to fire. The model simulated fire conditions by using the ISO 834 standard temperature curve and temperature distribution within the RC beam was evaluated using a finite difference method and heat balance. The temperature dependent material relationship of steel and concrete was used in order to evaluate the fire response of the element and RC beam as a whole and Newton-Raphsons iterative method was applied for the solution. Dotreppe and Franssen (1985) established that the model is valid for fire analysis of NSRC beams under fire. In the study, parametric analysis was not conducted and the model was not verified for HSRC beams and therefore it is only valid for NSRC beams exposed to fire.

2.11 Knowledge Gap

Many temperature dependent material models have been proposed for normal strength concrete (NSC), but only very few such models have been available for high strength concrete (HSC) under fire and elevated temperatures. Therefore in this research the existing material models for

HSC at elevated temperatures will be reviewed and a new model will be proposed in order to address some of the inadequacies of these models. The material model will be implemented into FE software to conduct numerical analysis of concrete members under fire and at elevated temperatures.

At present the design of reinforced concrete structures to meet the fire requirements is achieved through the prescriptive approach, which is dependent on empirical methods or laboratory testing. The structure is designed in such a way to meet the required fire ratings. These methods do not require knowledge of the temperature dependent material properties of concrete. New international codes of practice are all moving towards numerical and performance based fire design for structures, which require temperature dependent material properties and the application of these properties to perform numerical analysis and design of concrete under fire and elevated temperatures. Hence this research has become important to bridge this gap of knowledge.

Fire design of a structure based on an experimental test takes an excessive time of up to six months before construction starts. Therefore, it is important that fire designs of structures are performed using numerical and FE analysis as this would save time and resources. This research has been defined to conduct numerical and FE analysis of concrete structural members under fire and elevated temperatures. Therefore, each structure can be designed uniquely to attain its specific needs, rather than a generalised fire design, which is based on fire rating, sizes and shapes of the member. Using the performance based approach with FE software, the strength, loading conditions, restraint, moisture content, aggregate type, reinforcement arrangement, material properties, sizes and shapes are all taken into consideration, as these factors influence the performance of structures under fire. By means of the verified FE model, simple design equations are developed for evaluating the fire resistance RC members exposed to fire conditions.

From the review on previous numerical studies, it can be seen that most of these have been limited to NSC and therefore this research will be focused on HSC under fire conditions and elevated temperatures. As reported by several researchers, HSC is more vulnerable than NSC under such conditions and loading (Kodur, 1999). Most of this numerical research has been executed with non-commercial software and programs that are not available to the construction

industry. Therefore in this research ANSYS software is used as it is commercially available and can perform coupled field analysis between several engineering fields and multi-physics fields.

Chapter 3 : Material Model for High Strength Concrete (HSC) at Elevated Temperatures

3.1 Scope

In this chapter, some of the existing models for HSC subjected to elevated temperatures are reviewed and also evaluated are the advantages and limitations of these models. In order to address some limitations of these models, a new model for HSC will be proposed through this research programme. The new model will be further compared with the already reviewed existing models and will be used in ANSYS to evaluate the performance of HSC structural members under fire in further chapters.

3.2 Material Model Overview

Understanding concrete material properties at elevated temperatures is essential in order to perform numerical analysis of concrete members subjected to fire conditions. These material properties are classified mainly as the thermal and mechanical or structural material properties. The thermal properties include specific heat capacity and thermal conductivity. The mechanical properties that mainly influence the performances of concrete under fire are; compressive strength, stress-strain, thermal strain, elastic modulus and transient strain. The mechanical properties determine the loss of stiffness, strength and deformation of the concrete while the thermal properties control the heat transfer and distribution across the concrete.

There are still many on-going improvements and experimental studies for the material properties of HSC, as it has been reported by numerous researchers that HSC concrete performs differently from normal strength and conventional concrete (Kodur *et al.*, 2008). The experimental test to determine the mechanical properties has been carried out mainly either as steady state test or transient state test. The steady state test involves heating the concrete specimen in a furnace to a target temperature and keeping the temperature constant for a while in order to achieve an approximate constant temperature across the section before gradually loading to failure. In transient test a constant stress is applied to the specimen, which is then heated to failure in the furnace. The steady state tests are mostly used to determine the mechanical properties of concrete. The steady state test is mainly used as it is easier and it is quite rigorous to monitor the

temperature distribution across the specimen and also the deformation with increasing temperatures.

The steady state test is further categorised as a stressed, unstressed or residual test method. In the stressed test the concrete is preloaded to a certain stress level (usually 20 – 40% of the maximum strength) and heated to constant temperature. When the required temperature is attained the stress level is gradually increased until it fails in the hot state. An unstressed test is performed by heating the specimen to constant temperature and loading to failure in the hot state without any preload. The residual test involves heating the specimen to the desired target temperature and allowing the temperature to drop back to ambient temperature before loading to failure.

3.3 Kodur's Model

Kodur *et al.*'s (2008) model for HSC was based on the ASCE (Lie, 1992) suggested model. They modified the ASCE (Lie, 1992) model as it was based on conventional concrete. The modification considers the higher deterioration, loss of strength and stiffness of the concrete. Kodur's model for compressive strength of HSC is expressed as Equation 3.1 and presented in Figure 3.1. This model can be used for all types of HSC, The model accounts for three temperature regimes that indicate the variation in the response of HSC at the given temperature range. The peak strain model is represented as Equation 3.2 and Figure 3.2. The single equation is used to represent the peak strain for HSC for all types of HSC and temperature ranges. The stress – strain curve model in Equation 3.3 and as shown in Figure 3.3, accounts for both the ascending and descending branch of the stress strain curve. Kodur's model for thermal strain, which is expressed as Equation 3.4 and as presented in Figure 3.4, can be used for all types of HSC and temperature regimes.

Hence, the compressive strength of HSC is represented as:

$$f_{cT} = f_{c0}\begin{bmatrix} 1-0.003125(T-20) & T<100°C \\ 0.75 & 100°C \le T \le 400°C \\ 1.33-0.00145T & T>400°C \end{bmatrix} \qquad 3.1$$

where f_{c0} and f_{cT} are compressive strength of concrete at ambient and elevated temperatures, respectively.

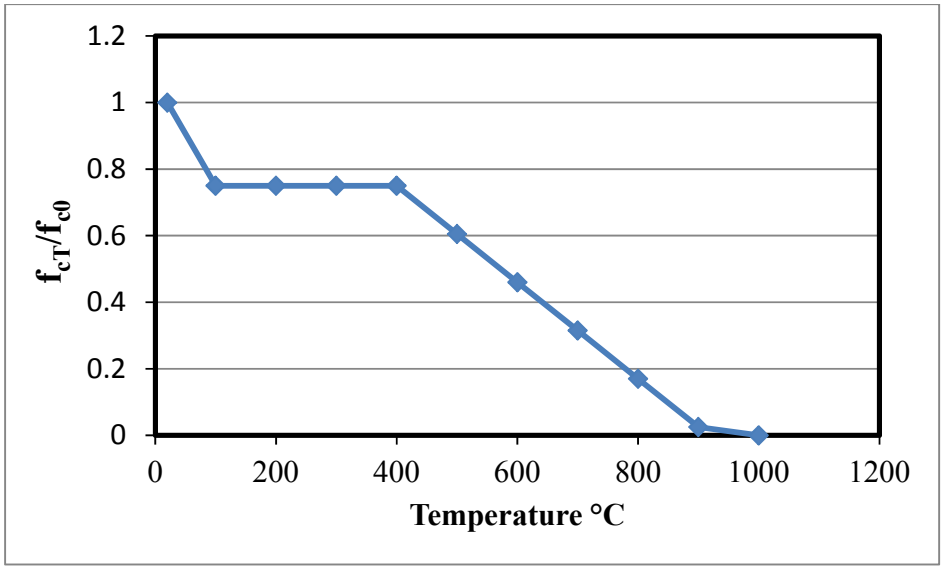

Figure 3:1: Kodur's model for concrete compressive strength

For the peak strain:

$$\varepsilon_{cT} = 0.0018 + \left(6.7 f_{c0} + 6.0T + 0.03T^2\right) \times 10^{-6} \qquad 3.2$$

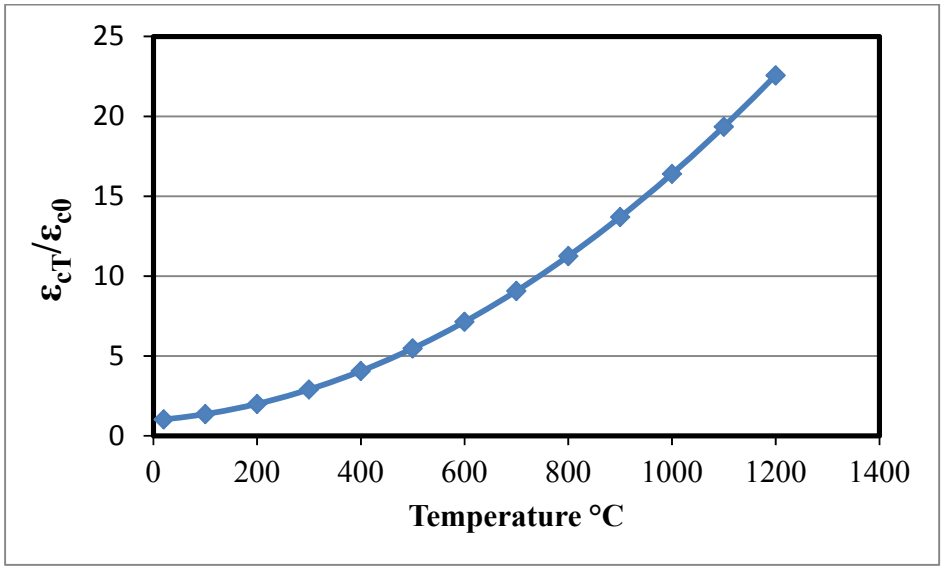

Figure 3:2: Kodur's model for concrete peak strain

where ε_{c0} and ε_{cT} represent the peak strain of concrete at ambient and elevated temperatures.

For the stress – strain curve:

$$f_c = f_{cT}\begin{bmatrix} 1-\left(\dfrac{\varepsilon_{cT}-\varepsilon}{\varepsilon_{cT}}\right)^H & \varepsilon \le \varepsilon_{cT} \\ 1-\left(\dfrac{30(\varepsilon-\varepsilon_{cT})}{(130-f_{c0}).\varepsilon_{cT}}\right) & \varepsilon > \varepsilon_{cT} \end{bmatrix} \qquad 3.3$$

$$H = 2.28 - 0.012\, f_{c0}$$

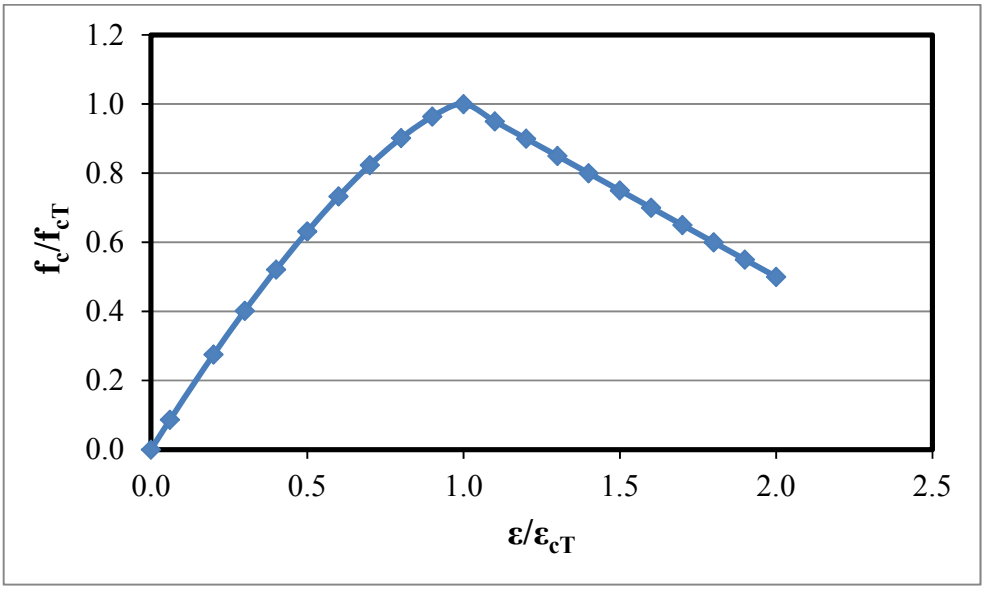

Figure 3:3: Kodur's model for concrete stress – strain curve

For thermal strain:

$$\varepsilon_{thc} = \left(0.004\left(T^2 - 400\right) + 6(T-20)\right)\times 10^{-6} \qquad 3.4$$

where ε_{thc} is the thermal strain of concrete.

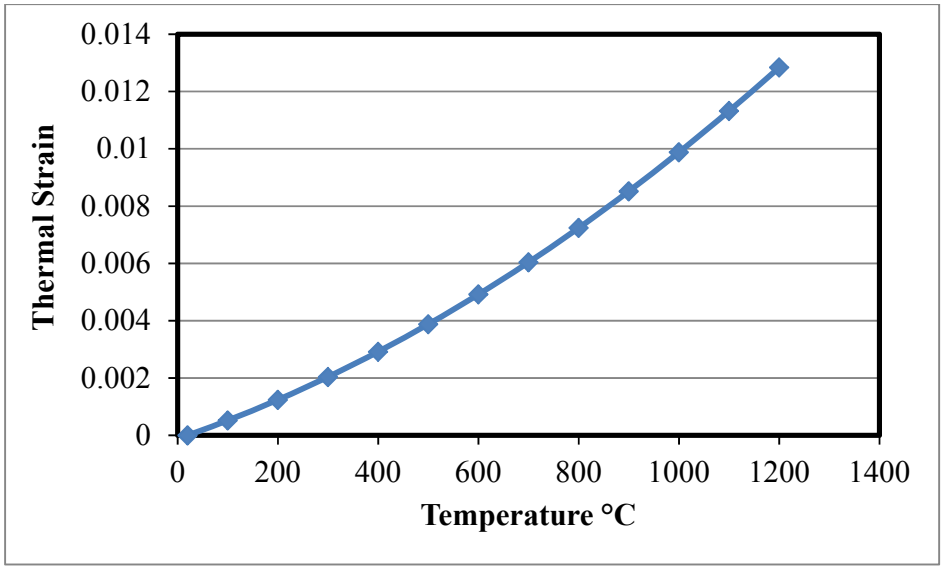

Figure 3:4: Kodur's model for concrete thermal strain

Kodur's model for specific heat capacity of HSC is given by Equations 3.5 - 3.6 and as shown in Figure 3.5. Two models have been presented for specific heat capacity of HSC based on the type of aggregate (siliceous or carbonate) used in the concrete. Equations 3.5 and 3.6 represent the models for siliceous and carbonate aggregate concrete, respectively. The model considers 5-6 regime of temperature, which represents the complex nature of the variation of the specific heat capacity of concrete at elevated temperatures. The model for thermal conductivity is categorised based on the type of aggregate used in concrete. These models are expressed as Equations 3.7 and 3.8 for siliceous and carbonate aggregate concrete respectively and as shown in Figure 3.6.

Hence, the specific heat of siliceous aggregate HSC is described as:

$$C_c = \frac{1}{\rho}\begin{bmatrix} 0.005T + 1.7 & 20°C \le T \le 200°C \\ 2.7 & 200°C < T \le 400°C \\ 0.013T - 2.5 & 400°C < T \le 500°C \\ 10.5 - 0.013T & 500°C < T \le 600°C \\ 2.7 & 600°C < T \le 635°C \end{bmatrix} \qquad 3.5$$

and for carbonate aggregate HSC:

$$C_c = \frac{1}{\rho}\begin{bmatrix} 2.45 & 20°C \le T \le 400°C \\ 0.026T - 12.85 & 400°C < T \le 475°C \\ 0.0143T - 6.295 & 475°C < T \le 650°C \\ 0.1894T - 120.11 & 650°C < T \le 735°C \\ -0.263T - 212.4 & 735°C < T \le 800°C \\ 2 & 800°C < T \le 1000°C \end{bmatrix} \quad 3.6$$

where C_c and ρ are the specific heat capacity and density of concrete, respectively.

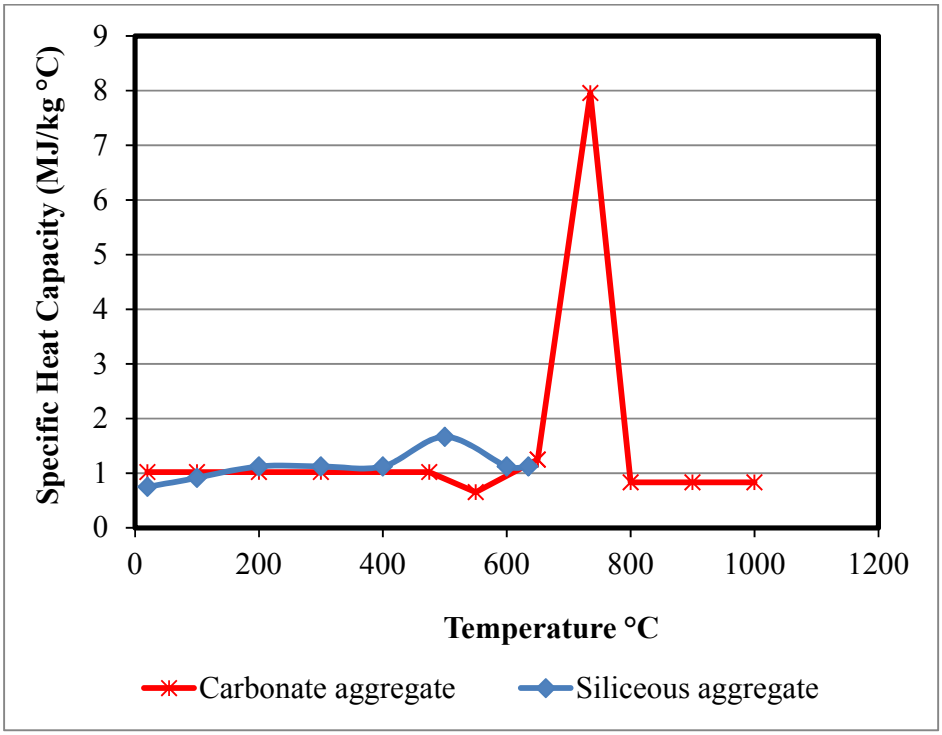

Figure 3:5: Kodur's model for concrete specific heat capacity

For the thermal conductivity of siliceous aggregate HSC:

$$k_c = 0.85(2 - 0.0011T) \qquad 20°C < T \le 1000°C \quad 3.7$$

and for carbonate aggregate HSC:

$$k_c = \begin{bmatrix} 0.85(2 - 0.0013T) & 20°C \le T \le 300°C \\ 0.85(2.21 - 0.002T) & 300°C < T \end{bmatrix} \quad 3.8$$

where k_c is the thermal conductivity of concrete.

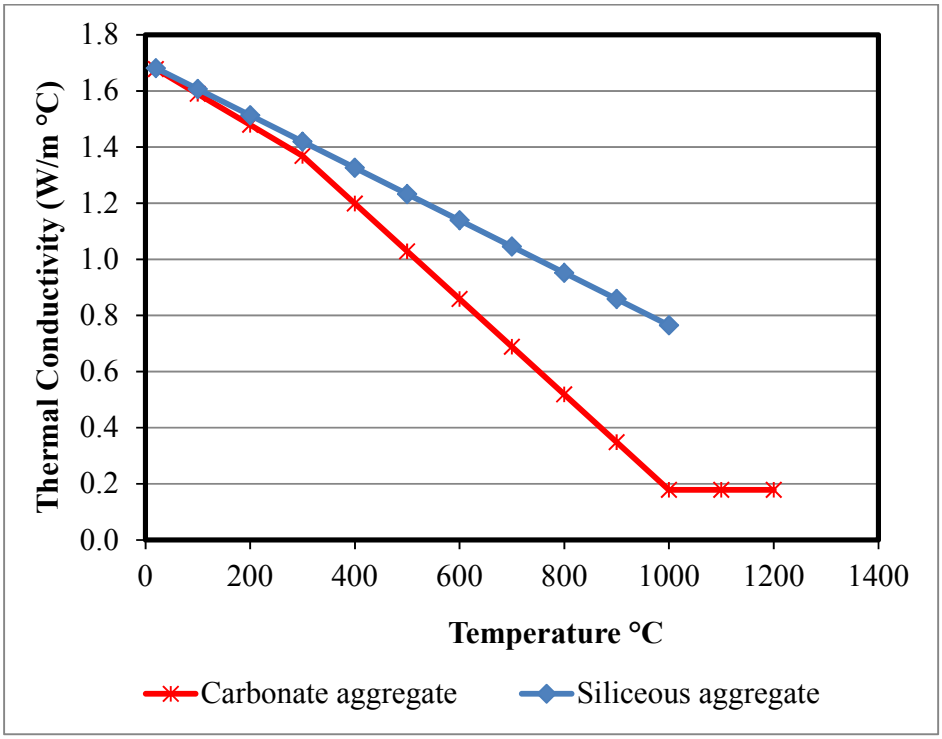

Figure 3:6: Kodur's model for concrete thermal conductivity

3.3.1 Advantages of Kodur's Model

Kodur's model for the compressive strength, peak strain, stress-strain curve and thermal strain for HSC are advantageous as a single model is proposed for all types of HSC and therefore it is easy to be used for numerical analysis. The model also accounts for the descending branch of the stress – strain curve, which can be used to model the response of HSC members after failure.

3.3.2 Disadvantages of Kodur's Model

Kodur considers HSC as a concrete having a compressive strength of 70MPa and above and therefore does not cover HSC within the strength range 55 – 69MPa. The models proposed by Kodur for specific heat capacity and thermal conductivity are less favourable as two different relationships are presented based on the type of aggregate used. The model accounts for variation in response of concrete due to aggregate type through the specific heat capacity and thermal conductivity rather than the thermal strain. It has been reported by numerous researchers (Mehta and Monteiro, 1993; Neville, 1995; Arioz, 2007) that siliceous aggregate concrete expands more

than carbonate aggregate concrete at elevated temperatures. As specific heat capacity and thermal conductivity do not influence the deformation of the concrete directly, these properties mainly offset and affect the time when a given temperature is attained and not the deformation. The model fails to account for the effect of moisture content on concrete subjected to elevated temperatures.

3.4 Eurocodes Model

The proposed Eurocode model for HSC was based on steady state and transient state experiments (BS EN 1992-1-2:2004). The model includes specific heat capacity for both siliceous and carbonate aggregate concrete, thermal conductivity, thermal strain for siliceous and carbonate aggregate concrete, strength of concrete and stress – strain curves. The model also takes into account the moisture content through the specific heat capacity model. The Eurocodes model accounts for the moisture in the concrete by setting peak values of the specific heat capacity at temperatures ranging from 100°C to 115°C and dropping linearly between 115°C to 200°C. This is due to the fact that at temperatures between 100°C and 115°C evaporation of water takes place. Therefore, at this temperature range heat transferred to the concrete is used up for the evaporation of water and is not transferred into the inner layer of the concrete until the water evaporates completely.

The compressive strength model of HSC presented by Eurocodes is given by Equation 3.9 and as shown in Figure 3.7. The model is categorised into three classes of concrete based on the value of the concrete compressive strength. The model for compressive strength does not consider any variation in the response of HSC due to the aggregate type. Equation 3.10 and Figure 3.8 represents the peak strain temperature dependent relationship from Eurocodes and can be used for all types of HSC. It does not include any variation due to the compressive strength of the concrete or aggregate type. The stress – strain model proposed in the Eurocodes model only considers the ascending branch and does not consider the descending branch after failure. This relationship is presented as Equation 3.11 and Figure 3.9. The Eurocodes thermal strain model accounts for the difference in response of HSC made with siliceous and carbonate aggregates. It presents two different sets of relationship based on the aggregate type. These relationships are expressed as Equations 3.12 and 3.13 for siliceous and carbonate aggregate respectively and as shown in Figure 3.10.

Hence, we have for the compressive strength model of HSC presented by Eurocodes:

$$f_{cT} = f_{c0} k_{cT} \qquad 3.9$$

where k_{cT} is the reduction factor of concrete strength at elevated temperature and its values are given in Table 3.1.

Table 3:1: Reduction factor of compressive strength of HSC

Temperature °C	k_{cT}		
	Class 1	Class 2	Class 3
20	1	1	1
100	0.9	0.75	0.75
200	0.9	0.75	0.70
300	0.85	0.75	0.65
400	0.75	0.75	0.45
500	0.60	0.60	0.30
600	0.45	0.45	0.25
700	0.30	0.30	0.20
800	0.15	0.15	0.15
900	0.08	0.113	0.08
1000	0.04	0.075	0.04
1100	0.01	0.038	0.01
1200	0	0	0

Class 1 represents concrete with compressive strength between C55 to C60;
Class 2 is for concrete with compressive strength ranging from C70 to C80;
Class 3 represents concrete with compressive strength of C90 and above.

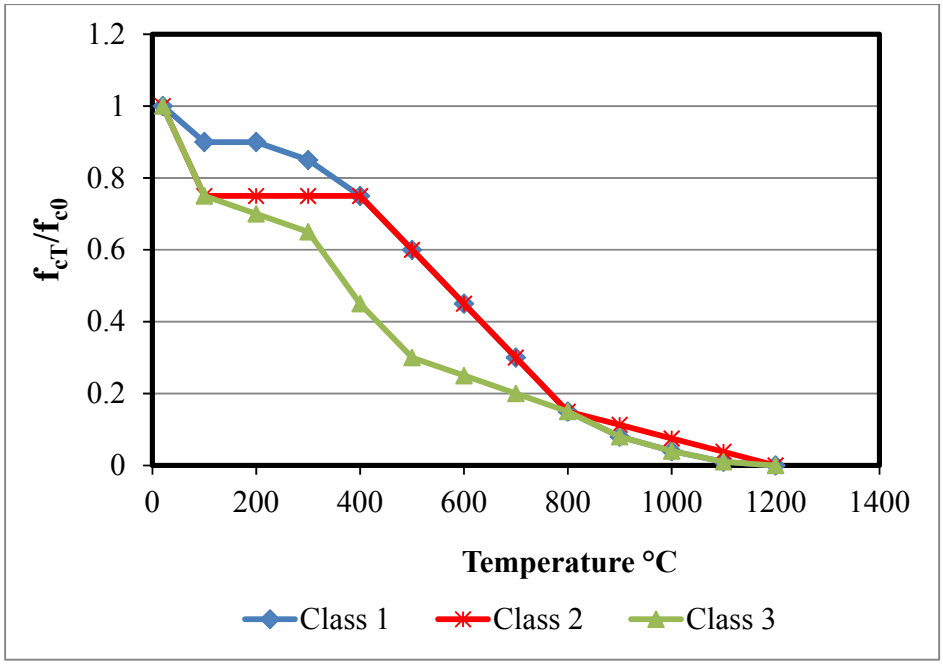

Figure 3:7: Eurocodes model for concrete compressive strength

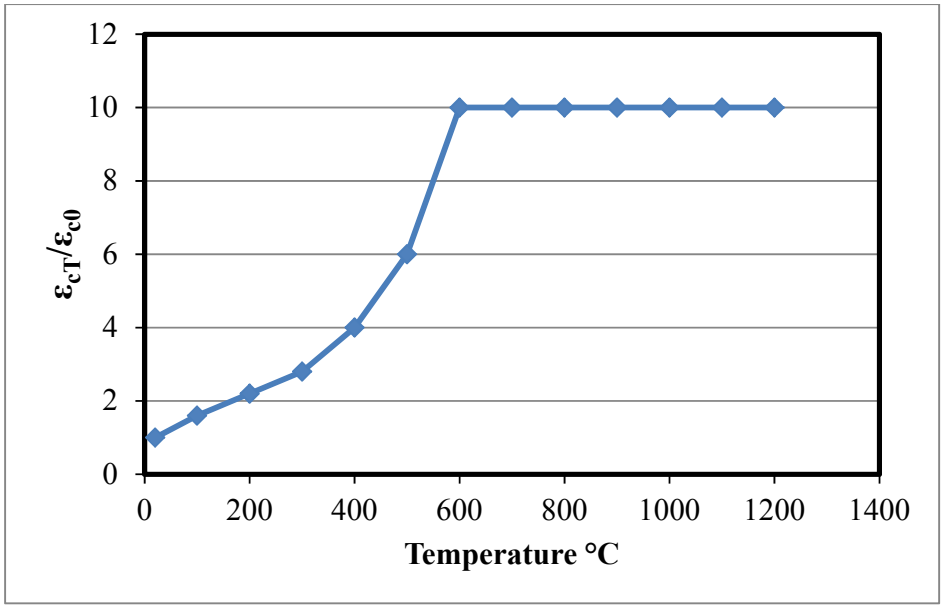

Figure 3:8: Eurocodes model for concrete peak strain

For the peak strain relationship:

$$\varepsilon_{cT} = \varepsilon_{c0} k_{eT} \qquad 3.10$$

where k_{eT} is the incremental factor of concrete strain at elevated temperature and its values are given in Table 3.2.

Table 3:2: Increment factor of peak strain of concrete

Temperature °C	k_{eT}
20	1.0
100	1.6
200	2.2
300	2.8
400	4.0
500	6.0
600	10.0
700	10.0
800	10.0
900	10.0
1000	10.0
1100	10.0
1200	10.0

For the stress – strain relationship:

$$f_c = f_{cT}\left[\left(\frac{3\varepsilon \times f_{cT}}{\varepsilon_{cT}\left(2+\left(\frac{\varepsilon}{\varepsilon_{cT}}\right)^3\right)}\right) \qquad \varepsilon \le \varepsilon_{cT}\right] \tag{3.11}$$

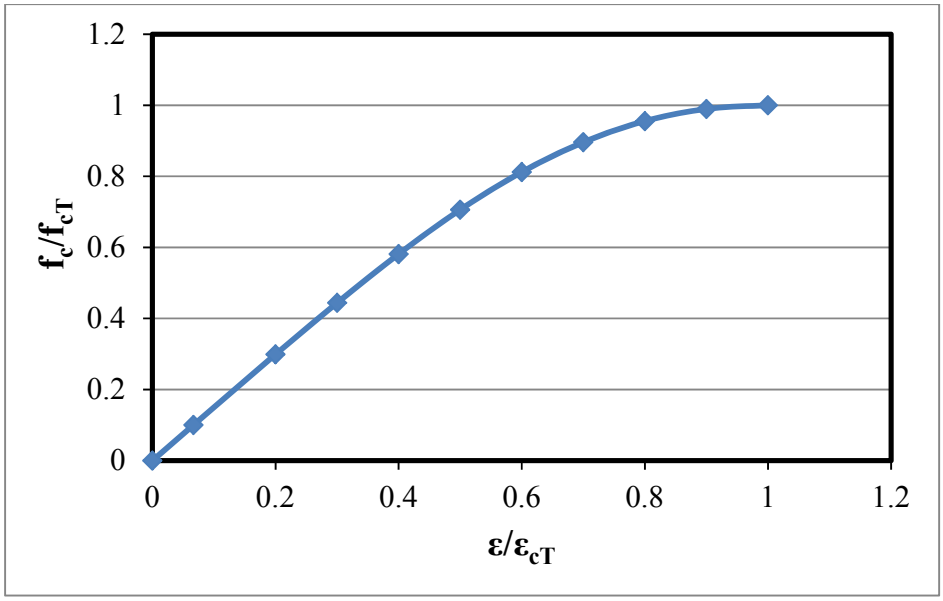

Figure 3:9: Eurocodes model for concrete stress – strain curve

For the thermal strain relationship of siliceous aggregate HSC:

$$\varepsilon_{thc} = \begin{bmatrix} -1.8\times10^{-4} + 9\times10^{-6}T + 2.3\times10^{-11}T^3 & 20°C \le T \le 700°C \\ 14\times10^{-3} & 700°C < T \le 1200°C \end{bmatrix} \quad 3.12$$

and for the thermal strain relationship of carbonate aggregate HSC:

$$\varepsilon_{thc} = \begin{bmatrix} -1.2\times10^{-4} + 6\times10^{-6}T + 1.4\times10^{-11}T^3 & 20°C \le T \le 805°C \\ 12\times10^{-3} & 805°C < T \le 1200°C \end{bmatrix} \quad 3.13$$

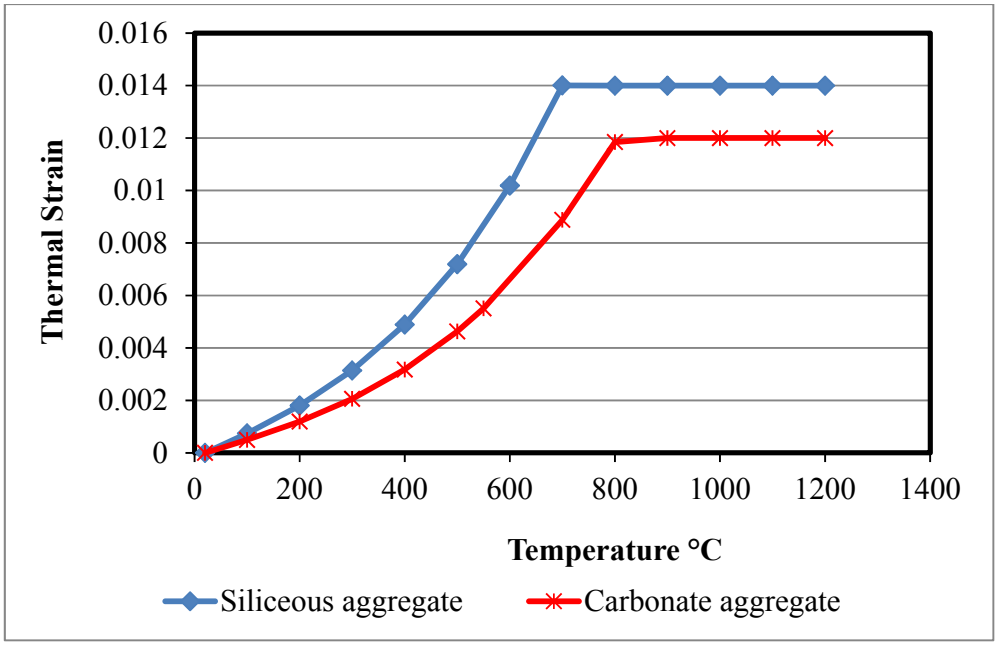

Figure 3:10: Eurocodes model for concrete thermal strain

The specific heat capacity temperature dependent relationship for HSC in Eurocodes is given by Equation 3.14 and as shown in Figure 3.11. The model does not consider any variation in the heat capacity response of HSC due to the aggregate type or strength. The model however considers variation due to the moisture content. This has been considered by setting the peak value to 900 J/kg °C at 0% moisture content, 1470 J/kg°C at 1.5% moisture content and 2020J/kg°C at 3% moisture of concrete weight within the peak temperature 100°C to 115°C. The Eurocodes model for the thermal conductivity is expressed as Equations 3.15 and 3.16 and as shown in Figure 3.12. The model presents two sets of relationship as upper limit and lower limit but does not specify the condition for using the upper limit or lower limit.

For the specific heat capacity of HSC in Eurocodes:

$$c_c = \begin{bmatrix} 900 & 20°C \le T \le 100°C \\ 900 + (T - 100) & 100°C < T \le 200°C \\ 1000 + \left(\frac{T - 200}{2}\right) & 200°C < T \le 400°C \\ 1100 & 400°C < T \le 1200°C \end{bmatrix} \quad 3.14$$

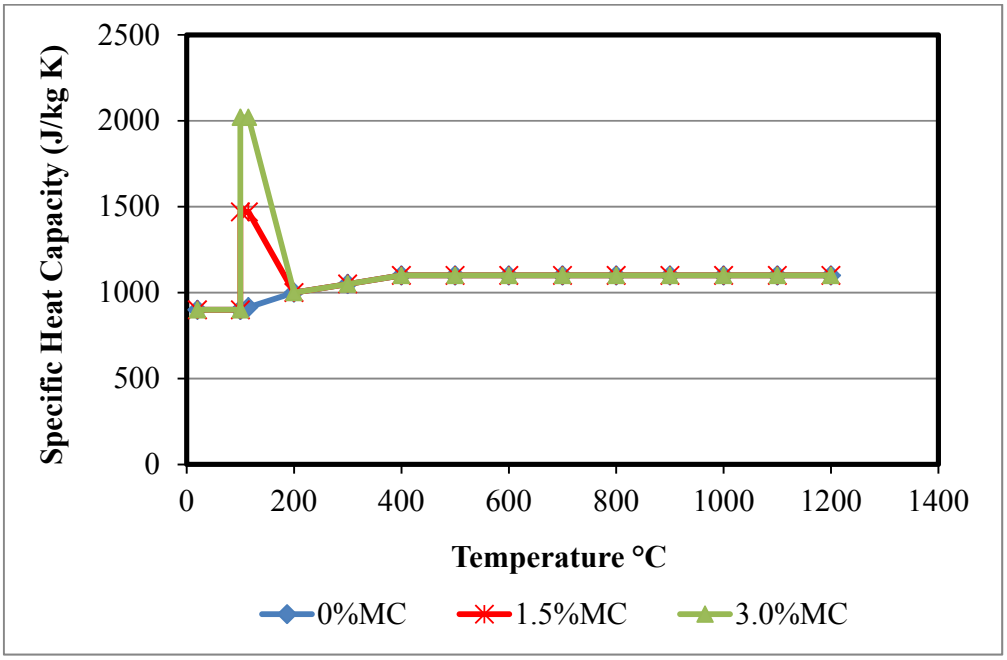

Figure 3:11: Eurocodes model for concrete specific heat capacity

For the thermal conductivity (upper limit):

$$k_c = 2 - 0.2451\left(\frac{T}{100}\right) + 0.0107\left(\frac{T}{100}\right)^2 \qquad 3.15$$

and for the lower limit:

$$k_c = 1.36 - 0.136\left(\frac{T}{100}\right) + 0.0057\left(\frac{T}{100}\right)^2 \qquad 3.16$$

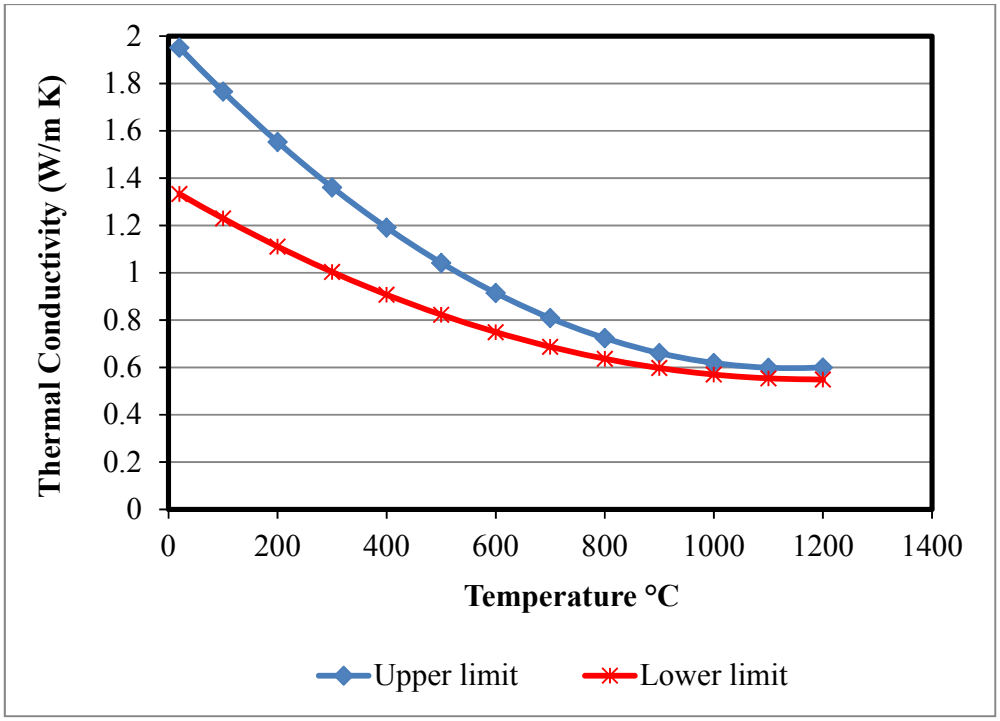

Figure 3:12: Eurocodes model for concrete thermal conductivity

3.4.1 Advantages of Eurocodes Model

The Eurocodes model accounts for the effect of the moisture content through the specific heat capacity of the concrete. Numerous researchers have reported that the moisture contents of concrete influence its response at elevated temperatures and fire conditions (Kodur and Phan, 2007). The models considered the difference in response of HSC due to the aggregate type by proposing different relationships for the thermal strain of siliceous and carbonate aggregate concrete.

3.4.2 Disadvantages of Eurocodes Model

The Eurocodes model proposes two sets of relationship for the thermal conductivity of concrete but it does not specify the condition for which a relationship should be adopted. The stress – strain model does not take into account the descending branch of the curve. The model proposed for the compressive strength is less favourable as there are different relationships based on the strength of the concrete.

3.5 Knaack's Model

Knaack *et al.* (2010) and Knaack *et al.* (2011) proposed a model for HSC concrete at elevated temperatures based on North American aggregate concrete. They used experimental test data from North American aggregate, tested in steady state (stresses, unstressed and residual test). The model is categorised based on the test type as stressed, unstressed and residual. This is further grouped based on the aggregate as siliceous and carbonate aggregate concrete.

The compressive strength and elastic modulus models proposed by Knaack are represented by Equations 3.17 and 3.18 respectively. The compressive strength and elastic modulus models proposed are also presented in Figure 3.13 and 3.14, respectively. The relationships cover only carbonate aggregate concrete and consist of three different expressions, each based on the test type. The peak strain model in Equation 3.19 and Figure 3.15 can be used for all types of HSC in the unstressed state and the stress – strain curve model expressed as Equation 3.20 and shown in Figure 3.16 is valid for all types of HSC. Knaack adopted the model proposed by Cruz and Gillen (1980) for the thermal strain of concrete; this model is expressed as Equation 3.21 and shown in Figure 3.17. The model is valid for all types of HSC.

For the compressive strength of HSC (Knaack model):

$$f_{cT} = f_{c0}\begin{bmatrix} 1.15 - 2.45\times10^{-3}T + 4.52\times10^{-6}T^2 - 2.41\times10^{-9}T^3 & \textit{Stressed} \\ 1.10 - 1.51\times10^{-3}T + 2.22\times10^{-6}T^2 - 1.08\times10^{-9}T^3 & \textit{Unstressed} \\ 1.09 - 1.37\times10^{-3}T + 1.76\times10^{-6}T^2 - 1.05\times10^{-9}T^3 & \text{Re}\textit{sidual} \end{bmatrix} \qquad 3.17$$

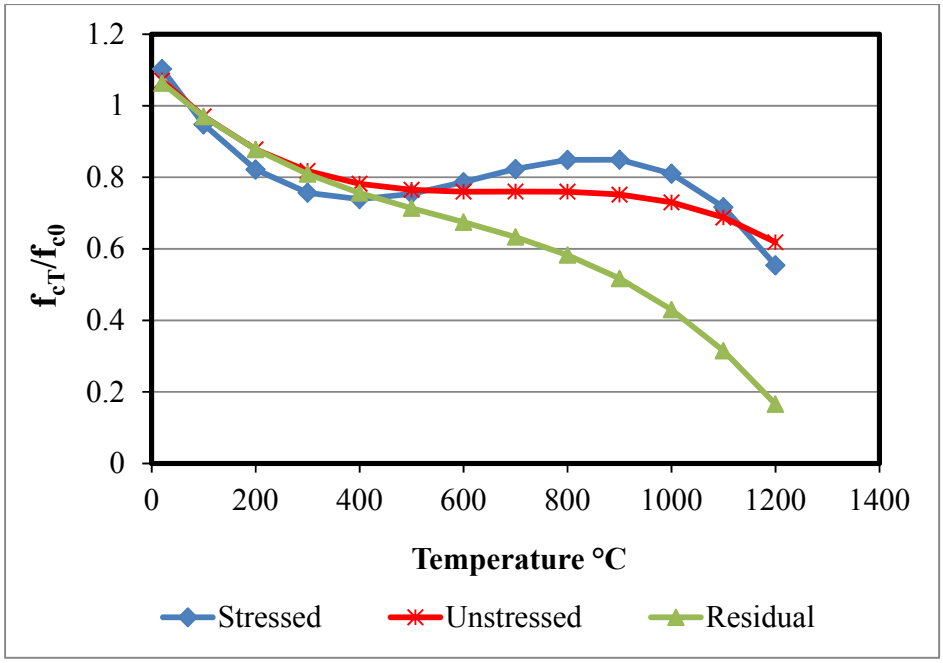

Figure 3:13: Knaack's model for concrete compressive strength

For the elastic modulus:

$$E_{cT} = E_{c0}\begin{bmatrix} 1.058 - 1.168\times10^{-3}T + 3.180\times10^{-7}T^2 & Stressed \\ 1.055 - 1.146\times10^{-3}T + 4.654\times10^{-7}T^2 & Unstressed \\ 1.351 - 2.037\times10^{-3}T + 9.671\times10^{-7}T^2 & Residual \end{bmatrix} \quad 3.18$$

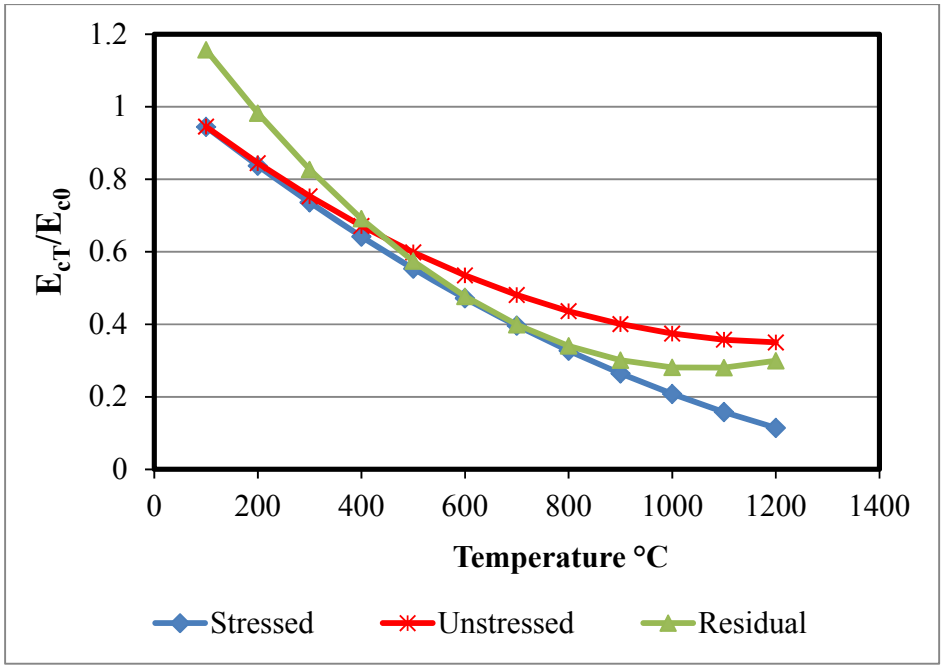

Figure 3:14: Knaack's model for concrete elastic modulus

For the peak strain:

$$\varepsilon_{cT} = \varepsilon_{c0}\left[0.896+1.431\times10^{-3}T+8.772\times10^{-8}T^{2}\right] \qquad 3.19$$

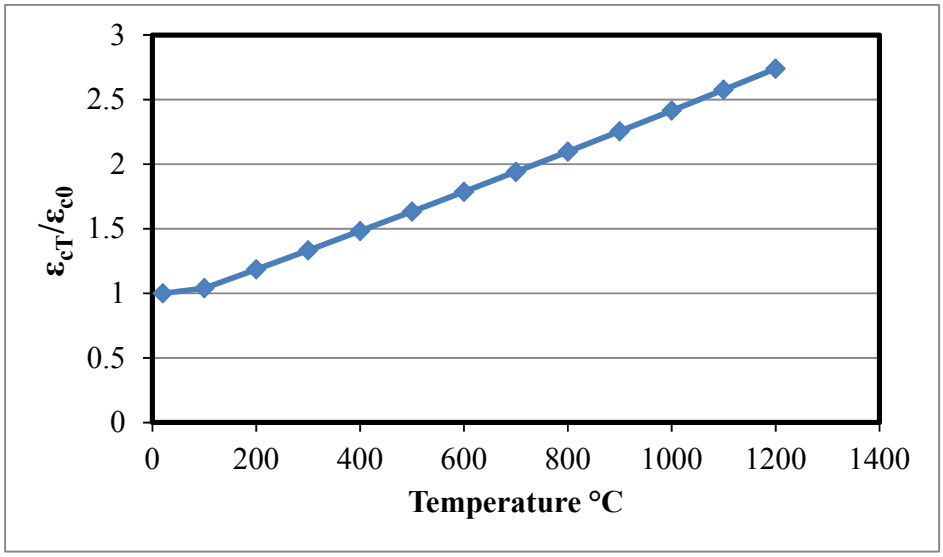

Figure 3:15: Knaack's model for concrete peak strain

For the stress – strain curve model:

$$f_c = \frac{f_{cT}\varepsilon \times r}{\varepsilon_{cT}\left(r - 1 + \left(\frac{\varepsilon}{\varepsilon_{cT}}\right)^r\right)} \qquad 3.20$$

where $r = \frac{E_{cT}}{E_{cT} - \frac{f_{cT}}{\varepsilon_{cT}}}$

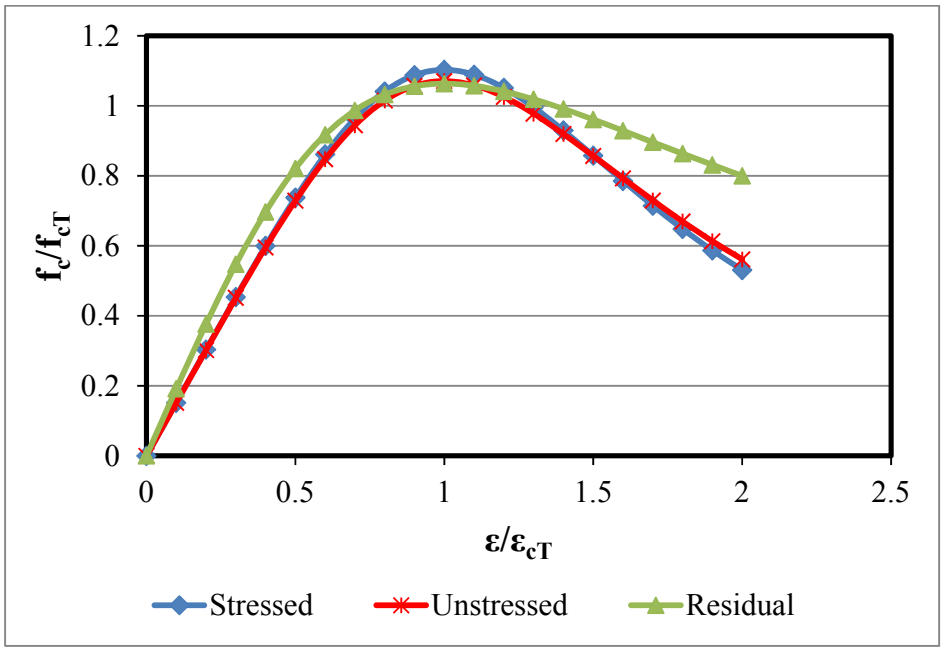

Figure 3:16: Knaack's model for concrete stress – strain curve

For the thermal strain model:

$$\varepsilon_{thc} = 12.6 \times 10^{-6}(T - 20) \qquad 3.21$$

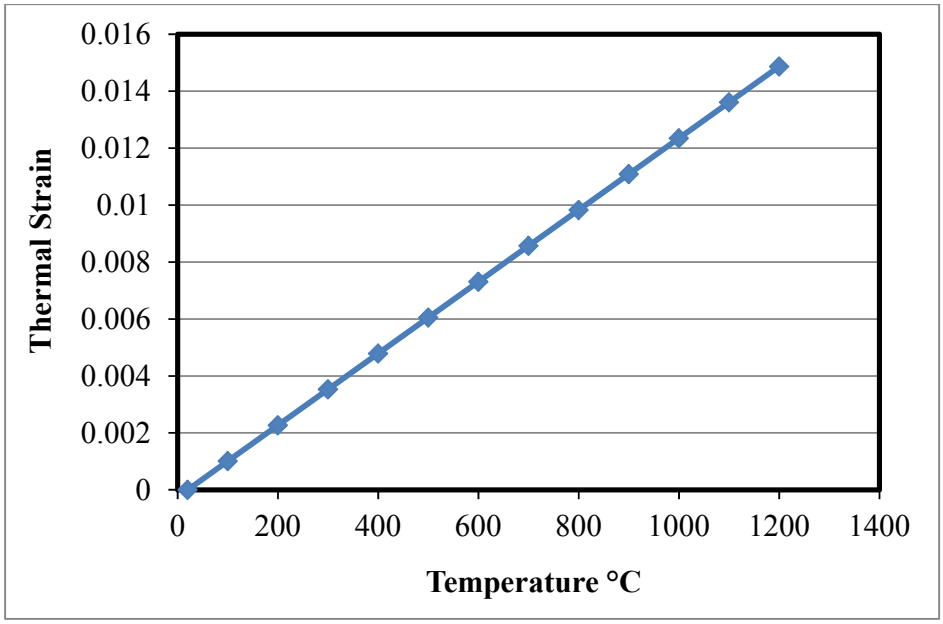

Figure 3:17: Knaack's model for concrete thermal strain

3.5.1 Advantages of Knaack Model

The model takes into consideration the variation in response of the concrete due to the test type and also presents a single equation for all temperature regimes.

3.5.2 Disadvantages of Knaack Model

Knaack's models for compressive strength and elastic modulus are only valid for carbonate aggregate concrete. The peak strain model is also only valid for concrete tested in the unstressed state and therefore the model is limited to this condition alone.

From the evaluation of the above reviewed models on HSC, it has been identified that there are limitations. The stress − strain model present in BS EN 1992-1-2:2004 does not account for a descending branch. The stress – strain, compressive strength and peak strain models recommended by Kodur only cover HSC with compressive strength of 70MPa and above. The compressive strength model proposed by Knaack is only valid for carbonate aggregate concrete. From the outlined shortcomings of the reviewed material models for HSC, a new model for the elastic stress-strain curve, compressive strength and peak strain is proposed in this study. The proposed model is derived based on data of HSC at elevated temperatures, which were collected

from numerous experimental research studies on HSC at high temperatures. Experimental data on the mechanical properties of concrete were collected from the literature. These data were either in tabular format, graphs or charts in the literature. The data in tabular formats were collected directly from the literature, while those in form of graphs and charts were collected via the aid of Enguage digitizer software. The graph and charts were imported from an electronic version of the literature to Enguage digitizer software, which was used to digitize and obtain the data from the graphs and charts.

Each paper and literature was carefully studied in detail concerning materials, methods and testing procedures used by this research program. This information and the data collected were then sorted. For the data on compressive strength and peak strain, an individual data represents the value of that mechanical property of a concrete specimen at a given temperature with the average of 2 ~ 3 concrete specimens under the same condition and temperature.

For the full stress − strain curve, a data point represents the strain of a concrete specimen at a given stress level and temperature or the stress of the concrete specimen at a given strain level and temperature depending on the method used for the experiment. For the stress − strain curve of concrete with specific data points, data were collected by digitizing each data point, and for those without data points, data were collected by using the segment fill command in the Enguage digitizer software which automatically extracted data at regular intervals on the curve.

Quantitative data analysis was conducted with full set of data by using regression analysis to obtain the optimum mathematical fit model for the compressive strength, peak strain and stress – strain curve of the concrete at elevated temperatures. The data were copied to Curve expert professional, which was used to perform regression analysis.

3.6 Proposed Model for High Strength Concrete (HSC)

The proposed models in this research have been based on experimental data collected from a number of experimental studies conducted on HSC at elevated temperatures by several research groups. These describe the full set of mechanical properties of concrete at elevated temperatures, such as compressive strength, peak strain and stress − strain properties. The test data collected on HSC have been obtained from cylindrical and cubic specimens, with calcareous and siliceous aggregate, and tested in stressed, unstressed and residual states. The proposed models for HSC

material at elevated temperatures were further implemented into Finite Element software (ANSYS) for thermal and structural analysis of concrete members subjected to elevated temperatures in chapter 5 and chapter 6.

3.6.1 Proposed Model for Compressive Strength of Concrete at Elevated Temperatures

The compressive strength of concrete is the most important property of concrete. It decreases at elevated temperatures. HSC retains about 70 – 80% of its original compressive strength at 300 − 400°C and retains about 20% at 800°C (Cheng *et al.*, 2004; Behnood and Ghandehari, 2009). Sancak *et al.* (2008) reported that HSC retains 60% to 79% of its original compressive strength at 400°C. Test data for compressive strength of concrete were collected from seven literatures (Fu *et al.*, 2005; Cheng *et al.*, 2004; Phan and Carino, 2003; Behnood and Ghandehari, 2009; Sancak *et al.*, 2008; Poon *et al.*, 2004; Xu *et al.*, 2003). These data consisted of high strength concrete, with siliceous and carbonate aggregate concrete, tested in stressed, unstressed and residual states. The collected data were normalised by dividing the strength at elevated temperature by the ambient temperature strength. Original and normalised collected data are plotted in Figures 3.18 and 3.19, respectively.

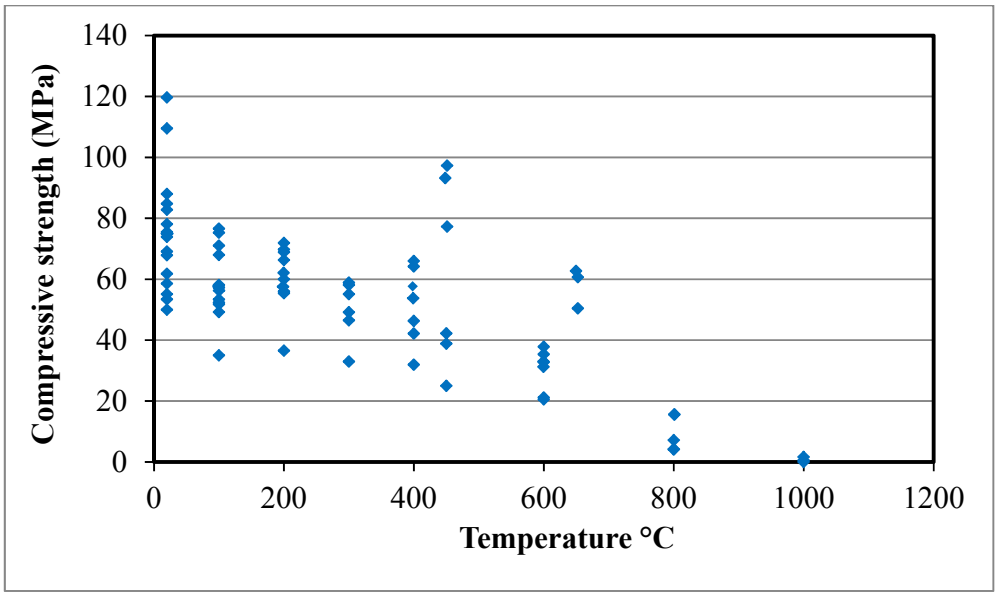

Figure 3:18: Compressive strength data

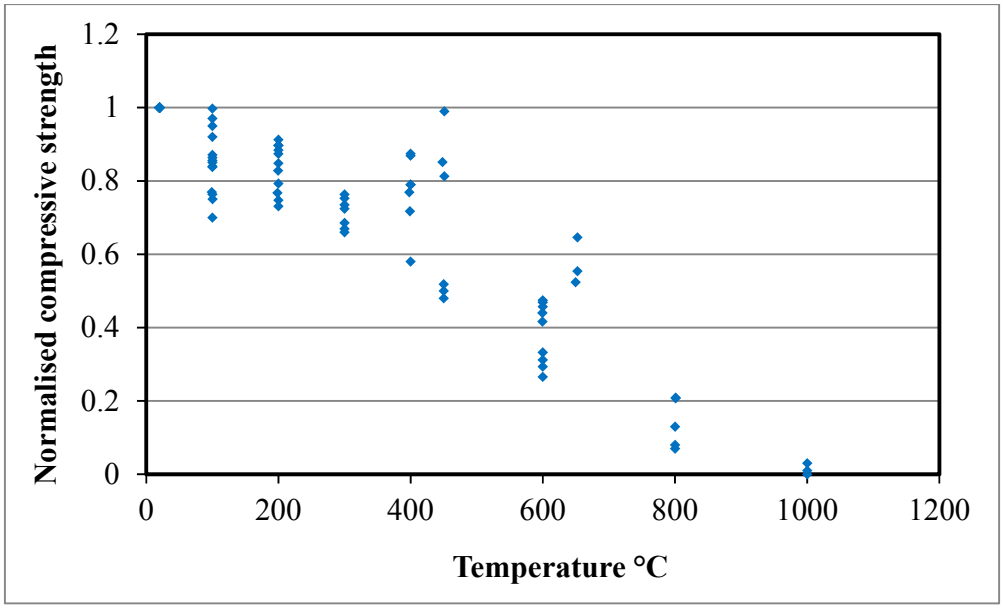

Figure 3:19: Normalised compressive strength data

The large variation of the normalised test data values can be attributed to the moisture content of the concrete, the curing method, quantity of the admixture used, heating rates, loading rate and condition of testing. In this study, a generalised model for compressive strength of HSC was developed based on regression analysis performed on normalised test data. The proposed relationship is given by Equation 3.22 and as shown in Figure 3.20.

$$f_{cT} = f_{c0}\begin{bmatrix} 1-0.00085(T-20) & 20 \le T \le 300 \\ 0.9417-1.379\times10^{-6}T^{2}-1.029\times10^{-13}T^{4}+5.497\times10^{-19}T^{6} & 300 < T \le 1000 \\ 0 & T > 1000 \end{bmatrix} \quad 3.22$$

Where f_{cT} and f_{c0} are the compressive strengths of concrete at elevated and ambient temperatures respectively.

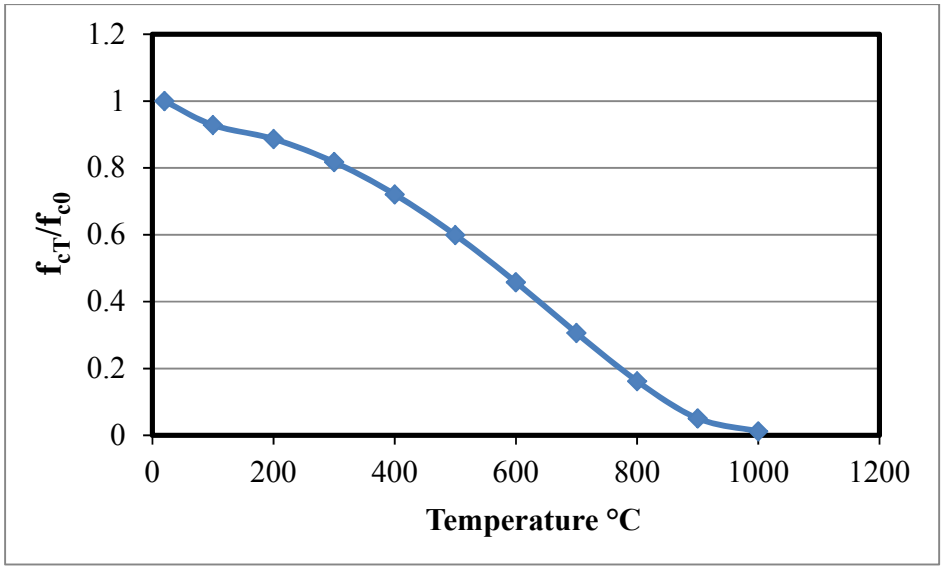

Figure 3:20: Proposed model for concrete compressive strength

The proposed model has three crucial temperature zones, which reflect the design needs and main concrete behaviour and evolution in fire. From 20 − 300°C the strength decomposition of concrete occurs at a less rapid rate than at 400 − 1000°C, where the strength loss is more rapid. This is mainly because calcium oxide (portlandite), which is a major binder component in cement, starts to decompose at around 400°C, thereby making the concrete decompose at a faster rate (Naus, 2010). This variation in rate of compressive strength decomposition is captured in the model. Above 1000°C, the compressive strength of concrete is taken to be zero as the binder component within the cement would have fully decomposed. The proposed model has an index form of temperature change which is convenient for both manual design calculations and computational analysis.

The model is valid for HSC with siliceous and carbonate aggregate. Figure 3.21 shows the comparison between the proposed model with the experimental test data and other models. Table 3.3 presents the correlation coefficient (r) and coefficient of determination (r^2) of the proposed model. Correlation coefficient (r) is a measure of how well the proposed model fits the data, while coefficient of determination (r^2) indicates how much variation of the test data is captured by the proposed model (Gibson, 1994; Larson and Farber, 2012).

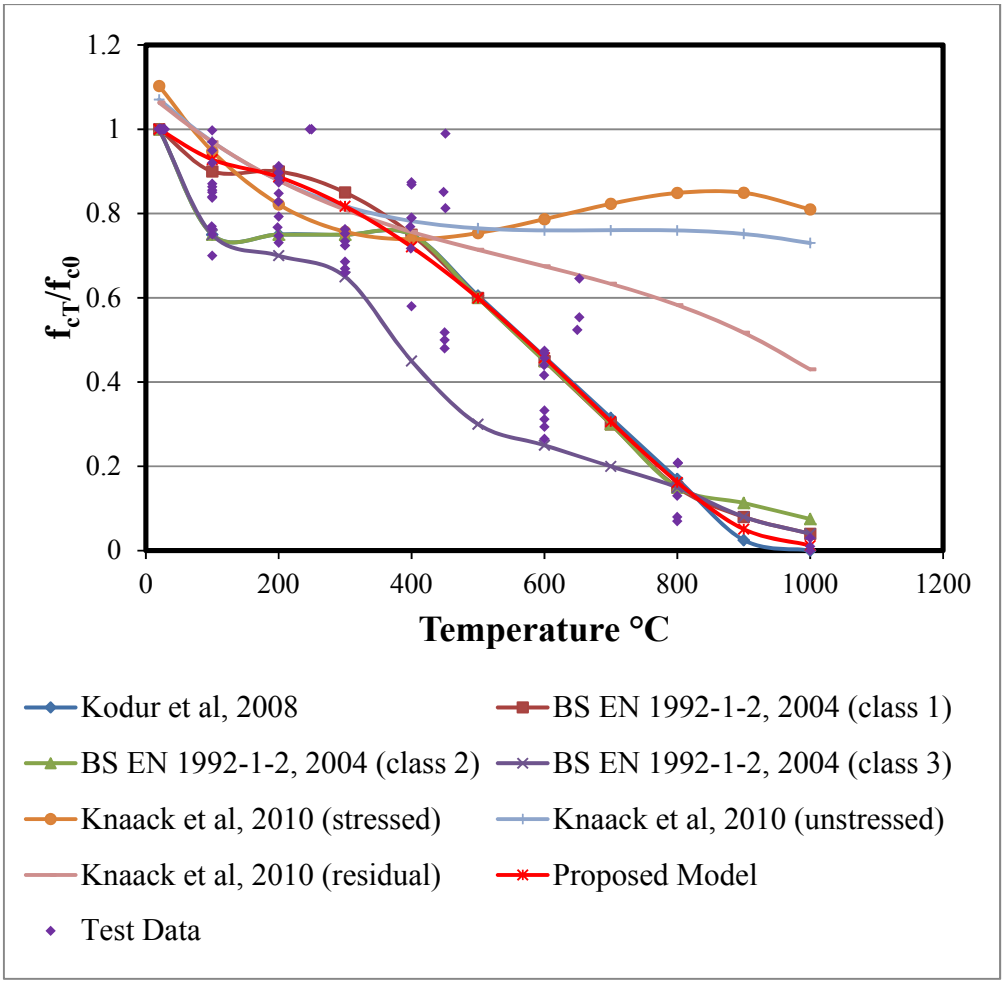

Figure 3:21: Comparison of the proposed model for compressive strength of concrete at elevated temperatures with test data and other models

From Figure 3.21 it can be seen that the proposed model for the compressive strength of concrete fits fairly well with the experimental data. The coefficients of determination (r^2) of the proposed model with the test data are 0.58 and 0.849 at 20 − 300°C and 301 − 1000°C respectively. At 20 − 300°C temperature range the model accounts for about 58% of the variation of the concrete strength test data with temperature. At 301 − 1000°C the model accounts for 84% of the variation of the concrete strength test data with temperature.

Table 3:3: Correlation coefficient and coefficient of determination

Model	Correlation coefficient (r)	Coefficient of determination (r^2)
Compressive strength ($20°C \leq T \leq 300°C$)	0.762	0.581
Compressive strength ($300°C < T \leq 1000°C$)	0.905	0.849
Peak strain $200°C < T \leq 800°C$	0.965	0.932
Stress – strain (ascending branch)	0.993	0.986
Stress – strain (descending branch)	0.901	0.812

The compressive strength model partially accounts for the effect of aggregate and sloughing off spalling implicitly by ensuring that concrete retained strengths at 800 − 1000°C are very low, with a retained compressive strength of about 16%, 5% and 1% at 800°C, 900°C and 1000°C respectively. The following assumptions are made in respect to aggregate and sloughing off spalling:

- Aggregate spalling is associated with aggregate at and very close to the heated surface as discussed in Chapter 2.
- At the moment aggregate spalling occurs, the temperature at and around the heated surface is about 800°C and, with the proposed compressive strength model, its retained strength is about 16% of unfired concrete strength. Therefore, using this model the displaced concrete is extensively weakened and its contribution to the load bearing capacity of structural members is negligible.
- Sloughing off spalling is associated with the gradual falling off of the heated surface. This spalling occurs at late stages of the fire as discussed in chapter 2.
- At the moment this spalling occurs, the temperature of the displaced concrete is between 800 − 1000°C. Using this compressive strength model, the average retained compressive

strength over these temperatures is approximately 7.5% of unheated concrete strength. Therefore, the load bearing capacity of the displaced concrete due to spalling is very small and negligible.

3.6.2 Tensile Strength of Concrete at elevated Temperatures

Tensile strength of concrete is the maximum stress concrete can resist in tension. Concrete's tensile strength is about 10% of its compressive strength and it decreases when subjected to elevated temperatures BS EN 1992-1-1:2004. There have been a lot of studies conducted to investigate tensile strength of concrete at ambient temperatures but very few and limited studies have been carried out under elevated temperature. Very limited test data are available for the model validation. This limitation can be attributed to the complex nature of the tensile test and require accurate instrumentation measurement under elevated temperatures. Therefore for this study, the rate of decrease of concrete's tensile strength is assumed to be same with rate of decrease of compressive strength at elevated temperatures. Tensile strength of concrete at elevated is therefore expressed as equation 3.23 and as shown in Figure 3.22. This can be reviewed in the future when more solid experimental results are obtained from research.

$$f_{tT} = f_{t0}\begin{bmatrix} 1-0.00085(T-20) & 20 \le T \le 300 \\ 0.9417 - 1.379\times10^{-6}T^2 - 1.029\times10^{-13}T^4 + 5.497\times10^{-19}T^6 & 300 < T \le 1000 \\ 0 & T > 1000 \end{bmatrix} \quad 3.23$$

Where f_{tT} and f_{t0} are the tensile strengths of concrete at elevated and ambient temperatures respectively.

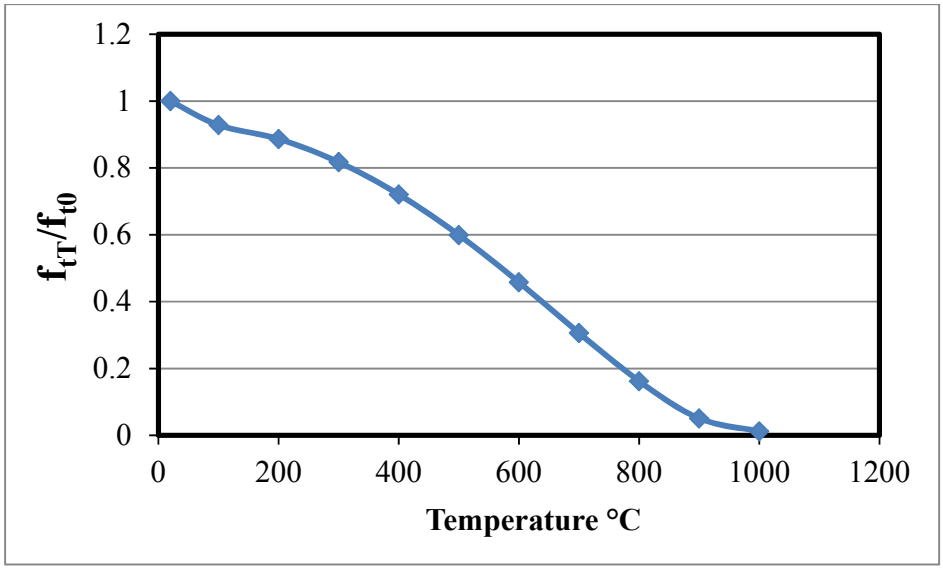

Figure 3:22: Proposed model for concrete tensile strength

3.6.3 Proposed Model for Peak Strain of Concrete at Elevated Temperatures

Concrete's peak strain increases at elevated temperatures due to the decrease in stiffness and loss of load bearing capacity. Data for peak strain of high strength concrete at elevated temperatures were collected from Cheng *et al.* (2004) and Felicetti and Gambarova (1998). The collected data were normalised by taking the ratio of peak strain at elevated temperatures to the values at ambient temperature. Figures 3.23 and 3.24 present the peak strain and normalised peak strain data. A temperature dependent relationship for peak strain was proposed based on normalised peak strain data. The model is expressed as Equation 3.24 and as presented in Figure 3.25. The correlation coefficient (r) and coefficient of determination (r^2) were presented in Table 3.3. The model is valid for both siliceous and calcareous aggregate HSC tested at elevated temperatures.

$$\varepsilon_{cT} = \varepsilon_{c0}\begin{bmatrix} 1 & 20°C \le T \le 200°C \\ \dfrac{1}{\left(1.17073 - 8.70402\times10^{-5}T^{1.40173}\right)} & 200°C < T \le 800°C \\ 8 & T > 800°C \end{bmatrix} \qquad 3.24$$

where ε_{cT} and ε_{c0} are the peak strains of concrete at elevated and ambient temperature respectively. The value of peak strain at room temperature (ε_{c0}) is taken as 0.003, as the average

value of peak strain data collected at ambient temperature was about 0.003. At 20 − 200°C the normalised peak strain data shows little variation and therefore in the model the peak strain is taken to be constant over this temperature range. At 800°C the concrete losses about 85% of its stiffness and strength so it is assumed that above this temperature the concrete has failed and there is less variation in the peak strain. Therefore, the peak strain value above 800°C is considered to be constant.

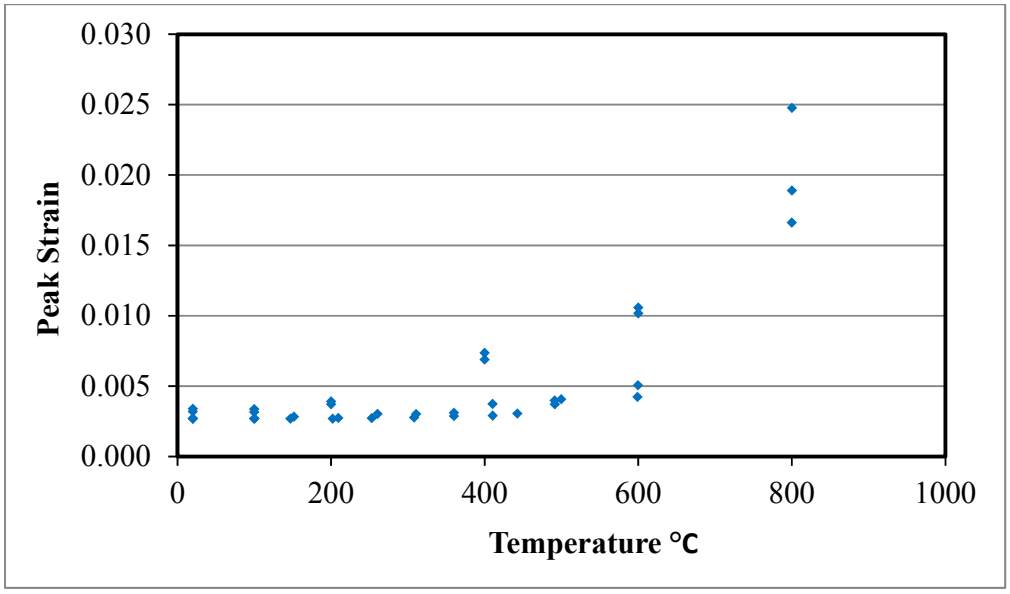

Figure 3:23: Peak strain data

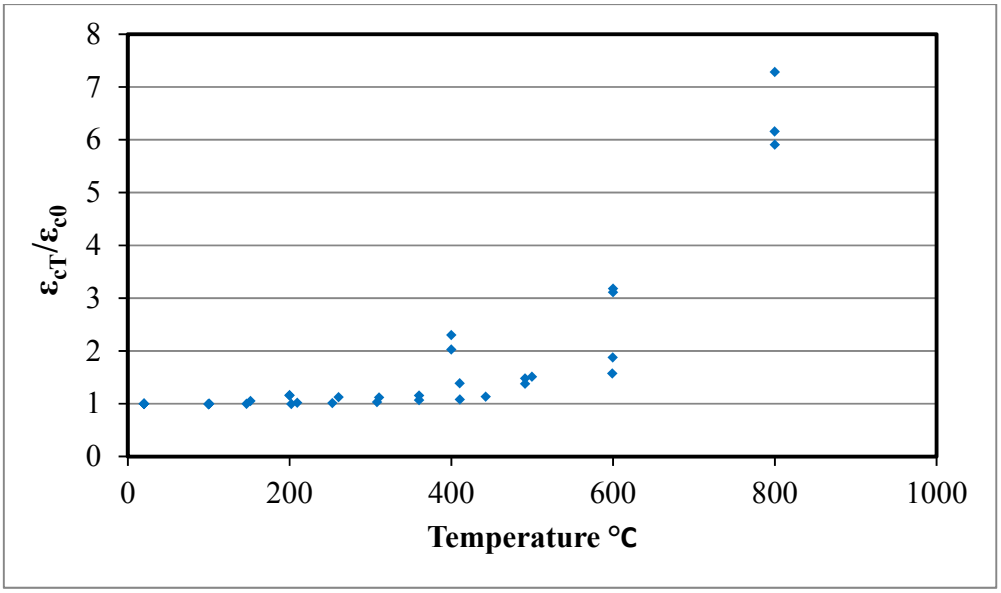

Figure 3:24: Normalised peak strain data

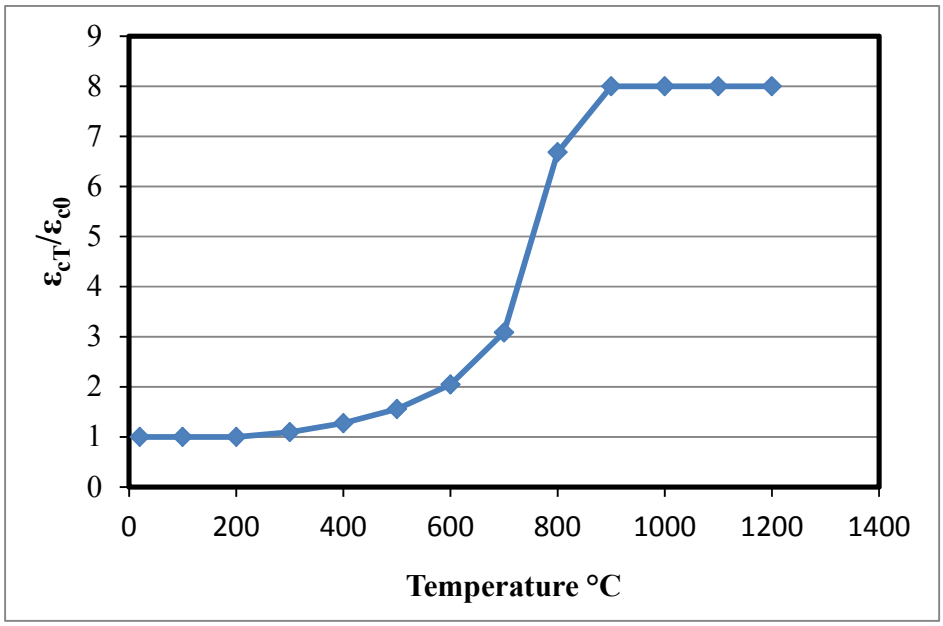

Figure 3:25: Proposed model for concrete peak strain

In Figure 3.26 the comparison between the proposed model with the experimental test data and other proposed models is made.

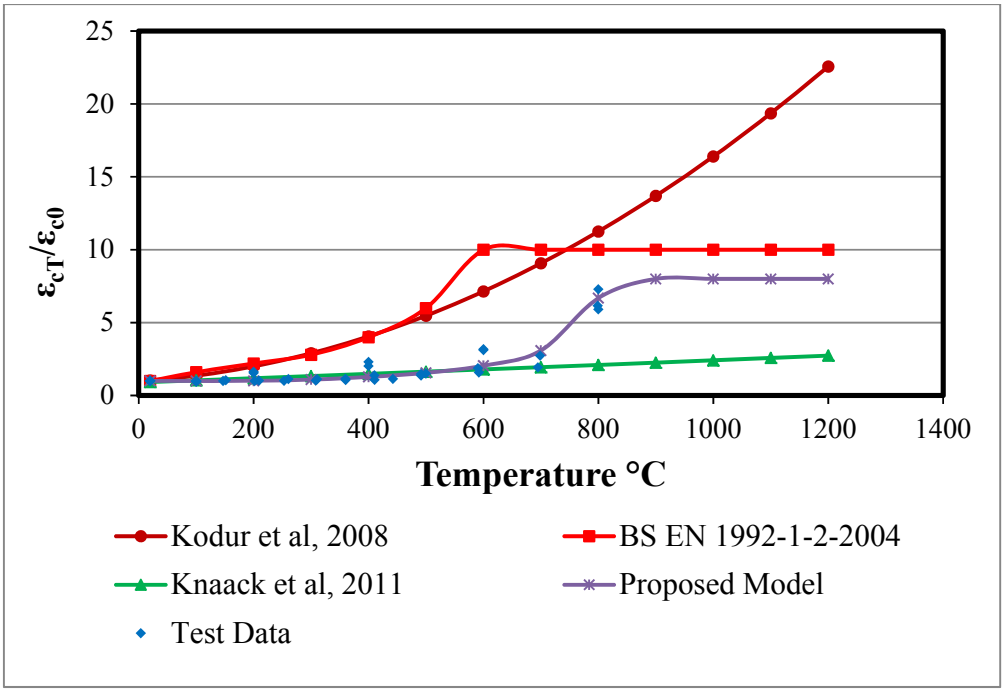

Figure 3:26: Comparison of the proposed model for peak strain with test data and other models

3.6.4 Proposed Model for Stress-Strain of Concrete at Elevated Temperatures

For the complete stress – strain curve of concrete, experimental data were collected from Cheng *et al.* (2004) and Felicetti and Gambarova (1998). These data were normalised by taking the ratio of the applied stress to the concrete strength at elevated temperatures with the corresponding ratio of strain to the peak strain at elevated temperatures. This normalised data was used to propose a stress – strain model for concrete at elevated temperatures. Regression analysis was performed on the experimental data using Curve expert professional software. The data used includes data on siliceous aggregate concrete and carbonate aggregate concrete. The model can be used for any type of HSC, irrespective of the test and aggregate type. It also considers the descending branch of the curve after failure. The proposed model for stress − strain of concrete at elevated temperatures is given by Equation 3.25. Figures 3.27 – 3.30 present the comparison of the proposed model with test data and the reviewed model and the correlation coefficient and coefficient of determination were presented in Table 3.3.

$$f_c = f_{cT}\begin{bmatrix} 1.7425\left(\frac{\varepsilon}{\varepsilon_{cT}}\right) - 0.7437\left(\frac{\varepsilon}{\varepsilon_{cT}}\right)^{2.4119} & \varepsilon \le \varepsilon_{cT} \\ 1.0275\left(\frac{\varepsilon}{\varepsilon_{cT}}\right)^{-1.7356} - 0.0114\left(\frac{\varepsilon}{\varepsilon_{cT}}\right) & \varepsilon > \varepsilon_{cT} \end{bmatrix} \quad 3.25$$

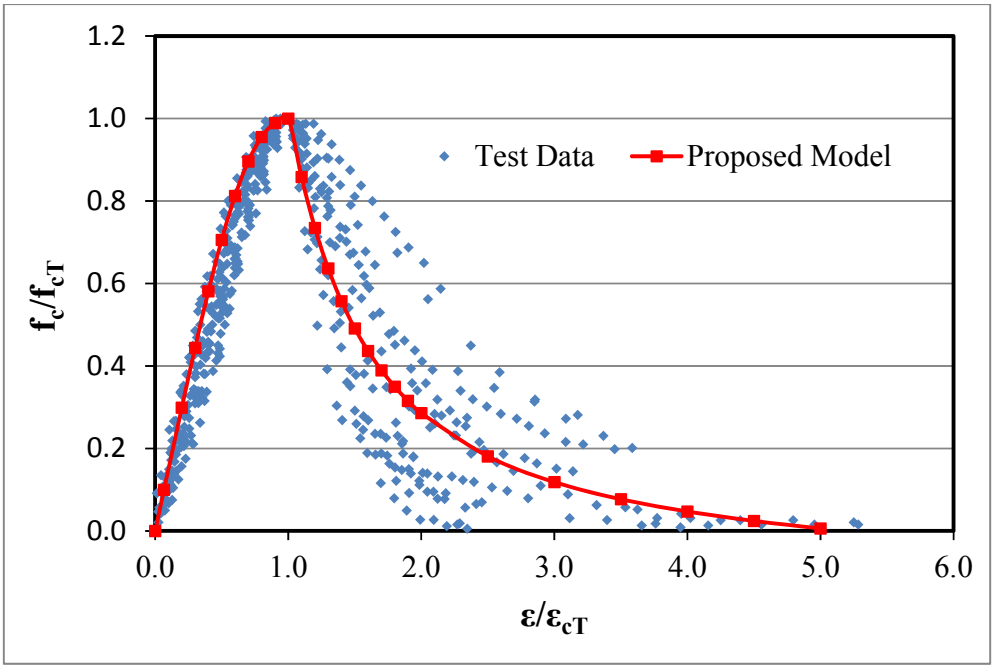

Figure 3:27: Normalised model for stress – strain curve with test data

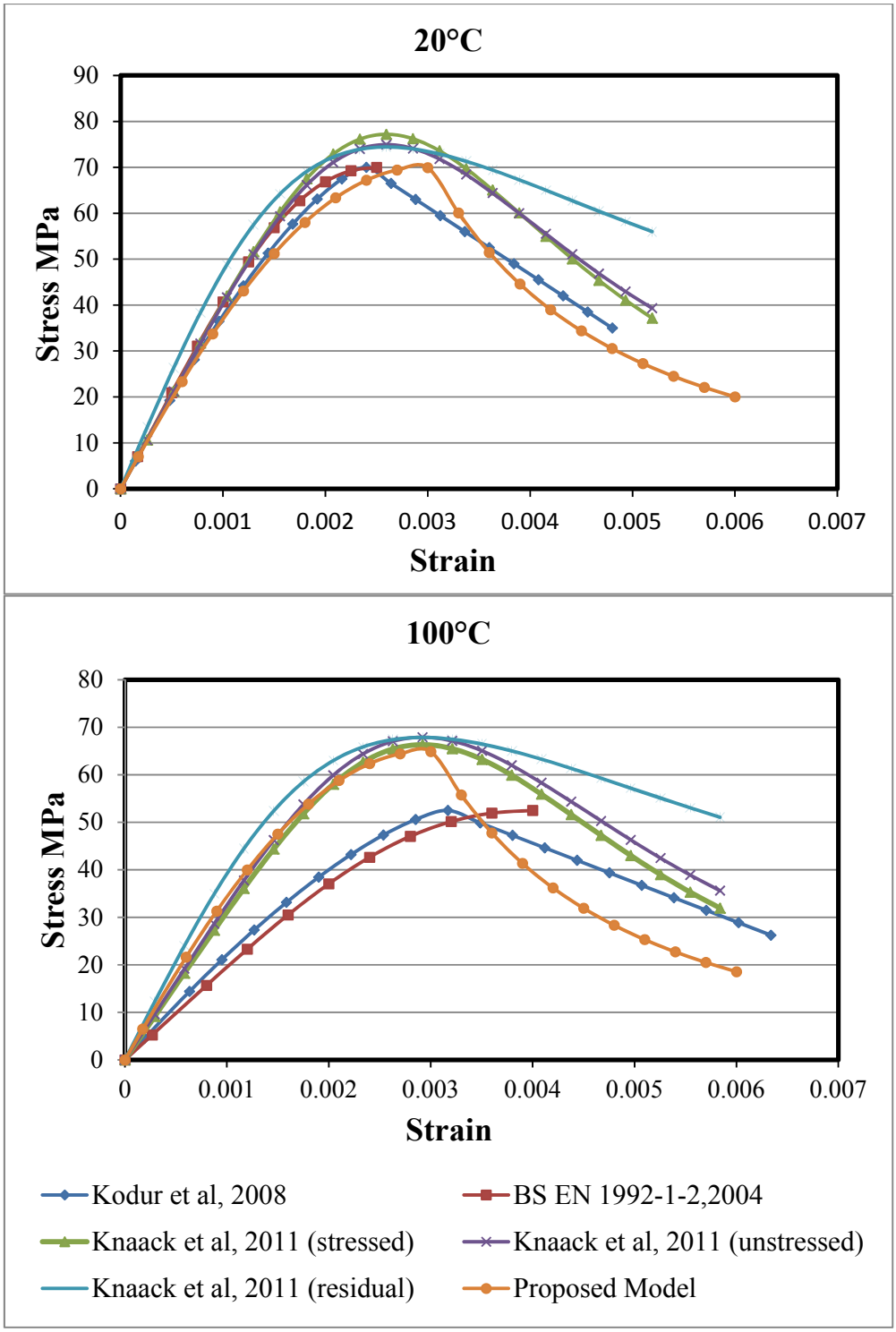

Figure 3:28: Comparison of proposed model for stress − strain curve of concrete at elevated temperatures with other models at 20°C and 100°C

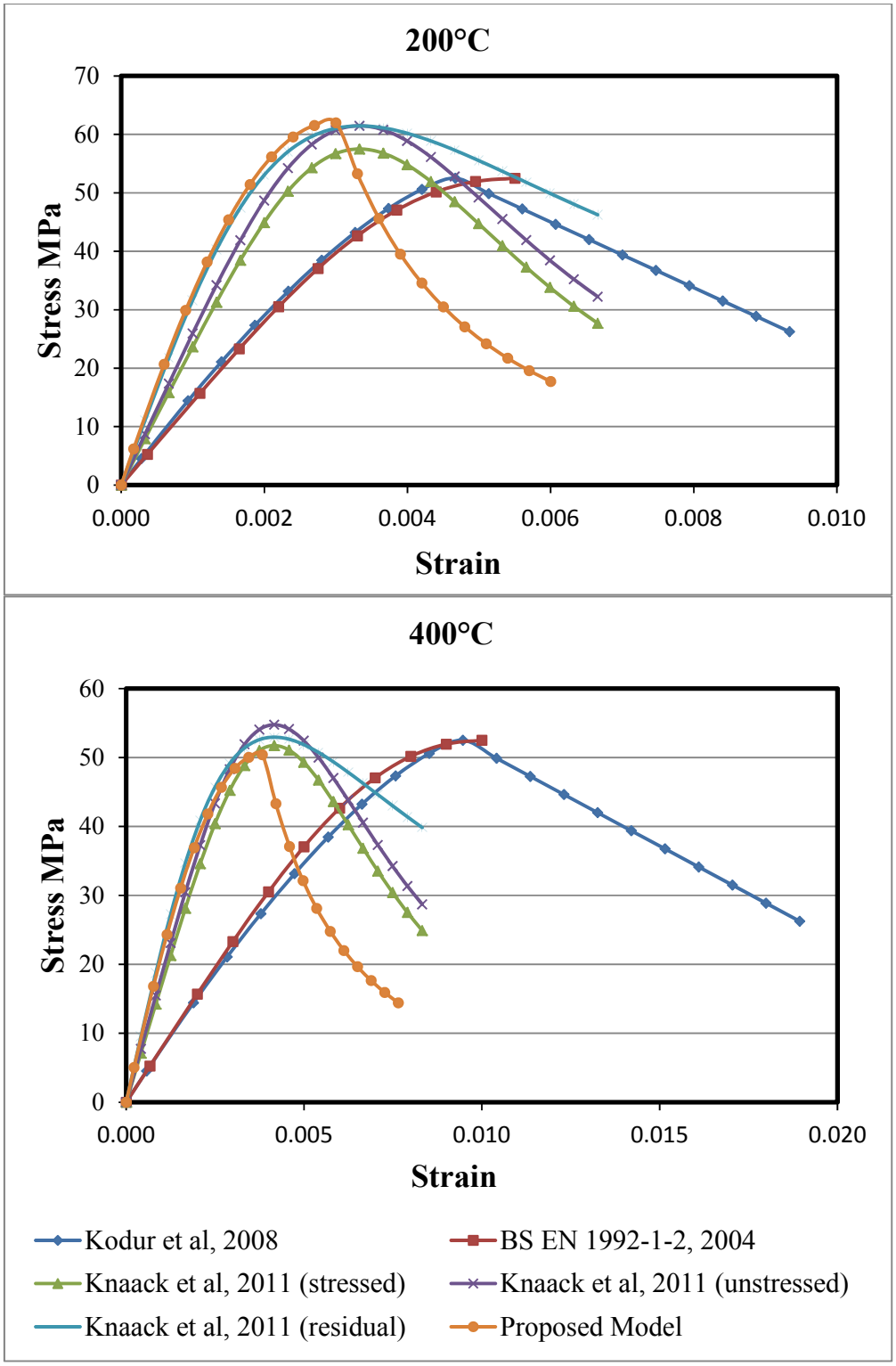

Figure 3:29: Comparison of proposed model for stress − strain curve of concrete at elevated temperatures with other models at 200°C and 400°C

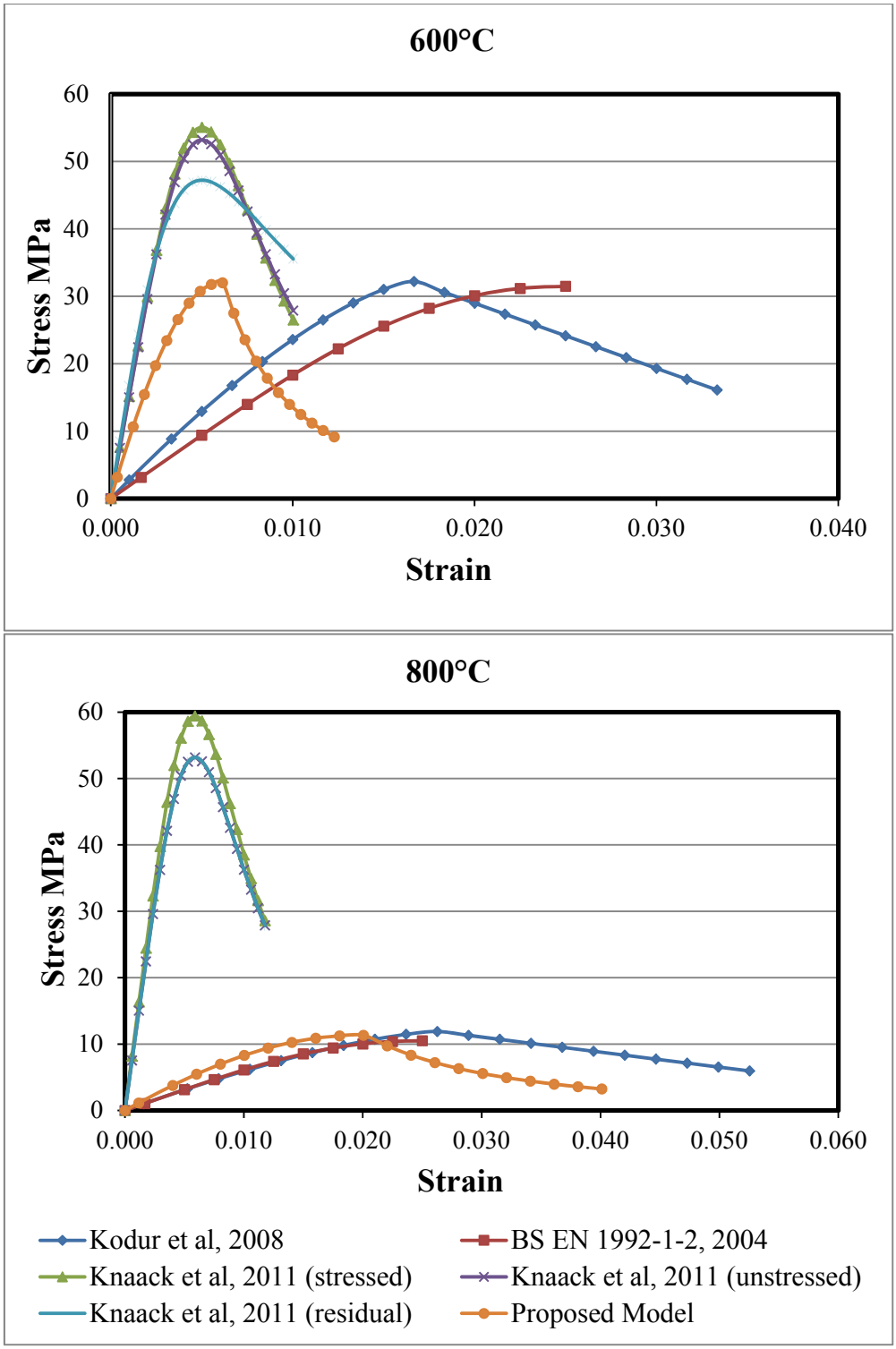

Figure 3:30: Comparison of proposed model for stress − strain curve of concrete at elevated temperatures with other models at 600°C and 800°C

From Figures 3.27 – 3.30 it can be seen that the proposed model fits well with the test data and at 20˚C, 100˚C and 800°C the proposed model is in close agreement with the models proposed by Kodur and Eurocodes. The model shows some variations with other models at 200˚C to 600˚C, which are attributed to the differences in the values of peak strain and compressive strength between the proposed model and the other models at these temperatures.

3.7 Summary

Some of the existing material models of HSC exposed to fire have been reviewed and based on their limitations a new model for elastic stress – strain, compressive strength and peak strain of HSC was proposed. The new models takes account of the descending branch of HSC at elevated temperatures and covers HSC with a compressive strength of 50MPa and above made with siliceous and carbonate aggregate. It also partially accounts for the effect of aggregate and sloughing off spalling implicitly through the compressive strength by ensuring that at a temperature range of 800 − 1000°C the concrete retains an average strength of 7.5% of its unfired strength. In the scenario where this type of spalling occurs, the affected region is assumed to be within this temperature range and therefore its load bearing capacity is small and negligible. The proposed model is simple and convenient for both manual design calculations and computational analysis.

Chapter 4 : Finite Element Techniques

This chapter presents an introduction to Finite element (FE) method for modelling and analysis of materials and structures. It also presents a brief overview of ANSYS software. Modelling of RC columns and beams using ANSYS are presented in detail. This includes the development of the geometric and FE model with ANSYS. It presents the computation of the material behaviour of the concrete and reinforcement bars in ANSYS. The simulation of the fire, structural loading, heat transfer and boundary conditions are also presented.

4.1 Overview of Finite Element Analysis

Finite element analysis (FEA) is a numerical tool for modelling and analysing structures, heat transfers, fluid flow, electromagnetics, acoustics problem and other simple and complex numerical problems. The fundamental principle of FEA is providing a solution for a complicated or large problem by representing it with a set of smaller or simpler models with aid of an FEA computer program and software (Rao, 1999; Kurowski, 2004). Major benefits of FEA include reduction in design time, provision of cost effective analysis methods and simplification and solution of complex numerical problem. Without FEA and other numerical analyses, analysis and design of structures would have to done by hand. It is virtually impossible now for complicated structural systems and loading conditions to be analysed without computational modelling. Analysis of complex structures and problems would require a prototype model and field testing of this prototype model to determine its viability to represent the response and analysis of the problem in a real scenario. Irrespective of the computer program or software used in FEA, it involves the following major tasks (Cook *et al.*, 1989):

1. The first step involved in FEA is to create a geometric model to accurately represent the problem to be solved in the virtual space of a computer based program and software.
2. Setting material properties and formulation of a mathematical model that simulates the behaviour and response of the element under loading.
3. Discretisation (meshing) and dividing the geometric model into an assembly of smaller and finite elements. This converts a complex structure or problem with infinite degrees of freedom to a combination of smaller and simplified systems with finite degrees of freedom.

4. Combination of each finite element behaviour and response under load to simulate the performance of the whole structure.
5. Application of load and boundary conditions. These include moments, forces, pressure, restraint for structural analysis and temperature, heat fluxes in thermal analysis and heat transfer problems.
6. Perform solution of the problem to determine nodal and element deformation, stresses for structural problems and temperature, heat fluxes for heat transfer problems.

Task 4 is performed automatically by the computer program and software, while tasks 1,2,3,5 and 6 are determined by the user and input as data in the software or computer program.

For this research, FE modelling and analysis of HSRC columns and beams were performed using ANSYS.

4.2 ANSYS Software

ANSYS software has the capability to perform linear and non-linear static, dynamic and transient analyses of various engineering problems. These include fluid analysis, structural analysis, multi-physics analysis, mechanical analysis, thermal analysis, geotechnical analysis, electromagnetic analysis and other complex analyses across the engineering discipline. The ANSYS program provides the opportunity to use a user defined material model and perform analyses across different engineering disciplines. It also allows models created in CAD software, such as AutoCAD, to be imported.

4.3 Finite Element (FE) Modelling and Analysis Techniques

Coupled field modelling and analysis techniques were used in ANSYS for modelling and analysing of HSRC members at elevated temperatures. Coupled field analysis in ANSYS allows the combination of analysis between two engineering fields, called load transfer method, or using an element type which possesses the necessary degree of freedom, called the direct method. For this work, the load transfer method was used. This allows the result and analysis from one field to be transferred to another field or between both fields in an iterative manner. It also supports substituting element types with the appropriate elements having the required degree of freedom in that field. The coupling could be either one-way or two-way coupling. For one-way coupling, the result and analysis from the second field is dependent on the result from the first field, but the

result from the first field is independent of the result from the second field. While in the two-way coupling the results from both fields are dependent on each other in an iterative manner.

For this research the simulation performed was from thermal to structural fields using one-way coupling analysis, as the results from the structural field are dependent on the results from the thermal field but the results from the thermal field are independent of the results from the structural field. The modelling and analysis procedures are presented in Figure 4.1.

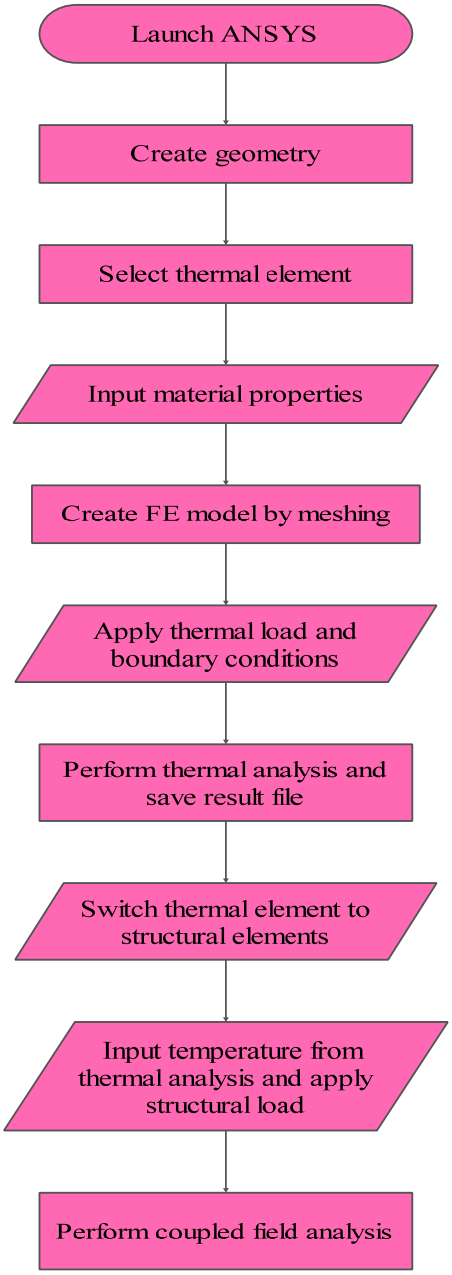

Figure 4:1: Flowchart of FE modelling and analysis procedure

4.3.1 Geometrical Model

The geometry of the concrete and reinforced steel was created as volume and lines, respectively using the solid modelling and direct generation method. The interaction between the concrete and reinforced steel was assumed to be perfectly bond in order to simplify the analysis and aid in the convergence of the solution.

4.3.2 Element Types and Attributes

SOLID70

The concrete was meshed using SOLID70, which is a 3-D element with thermal conductivity capabilities. The element is an eight node element with a temperature degree of freedom at each node. The element can be used to carry out 3-D steady state or transient analyses. The element supports convection or heat flux surface load and heat generation body load. Its material properties, which are orthotropic, include specific heat capacity, thermal expansion and thermal conductivity (ANSYS, 2010b). Its solution output includes nodal temperature, heat flux and thermal gradient and it was replaced with SOLID185 in the structural field modelling.

SOLID185

SOLID185 is a 3-D solid element with structural capabilities. This element has three degree of translational freedom at each node in the x, y and z directions. The element can be used to simulate plasticity, hyperelasticity, large deflections and strain in structures. The element supports pressure load, concentrated load and temperature load. Its material properties include elastic modulus, density, damping, thermal strain and shear modulus. Its output results are stresses, deformation and stress intensity (ANSYS, 2010b). Figure 4.2 presents the geometry of SOLID70 and SOLID185 elements.

LINK33

The steel reinforced bars were meshed with LINK33, which is a line element with a thermal conductivity function. It is an element with a single temperature degree of freedom at each node. This element has the capability to simulate steady state and transient temperature distribution, thermal gradient and thermal flux. The element supports heat generated loads and its material properties include specific heat capacity, enthalpy change, thermal conductivity, density and coefficient of thermal expansion. The output results include nodal temperature, thermal flux and heat flow rate (ANSYS, 2010b). The element was substituted with LINK180 to carry out structural analysis.

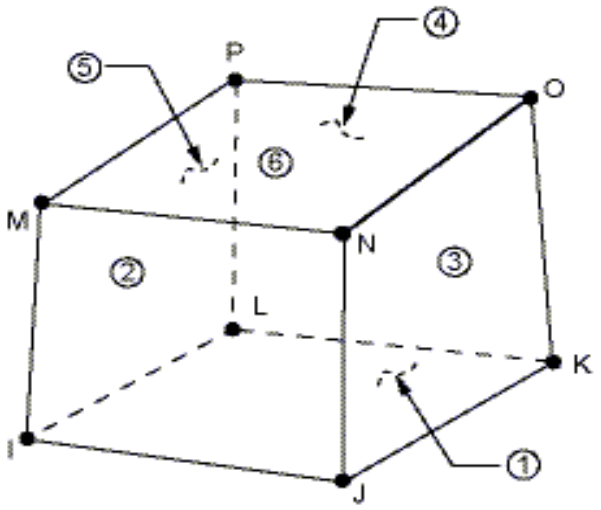

Figure 4:2: SOLID70 and SOLID185 geometry (ANSYS, 2010b)

LINK180

This is a line element which has 3 degrees of freedom at each node. The degree of freedom is translational in the x, y and z directions. This element has structural capabilities and can be used to simulate beams, trusses, bars and cables under structural loading. The element supports the simulation of plasticity, large deformation and strain. It has the function of temperature load and material properties that include elastic modulus, damping, Poisson's ratio and thermal strain. The solution outputs are nodal displacement, axial forces and others (ANSYS, 2010b). Figure 4.3 shows the geometrical shape of LINK33 and LINK180 elements.

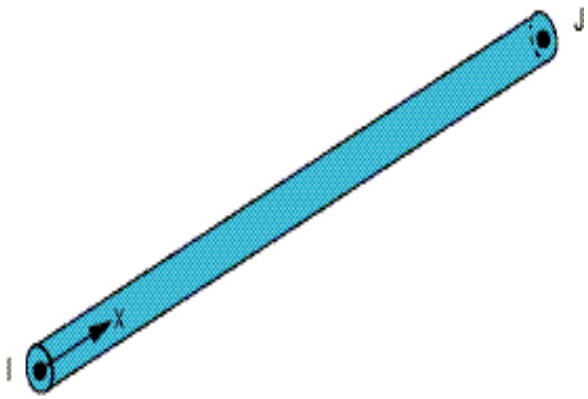

Figure 4:3: LINK33 and LINK180 geometry (ANSYS, 2010b)

SURF152

This is a 3-D surface thermal element with thermal capabilities. The element supports 3-D transient analysis and its material properties include density, emissivity, convection, heat flux and heat generation. SURF152 was used for modelling the radiating (receiving and emitting) surface on the exposed surface of the member. This was achieved by overlaying the element on fire exposed surface of the member. Figure 4.4 presents the geometrical shape of SURF152 element.

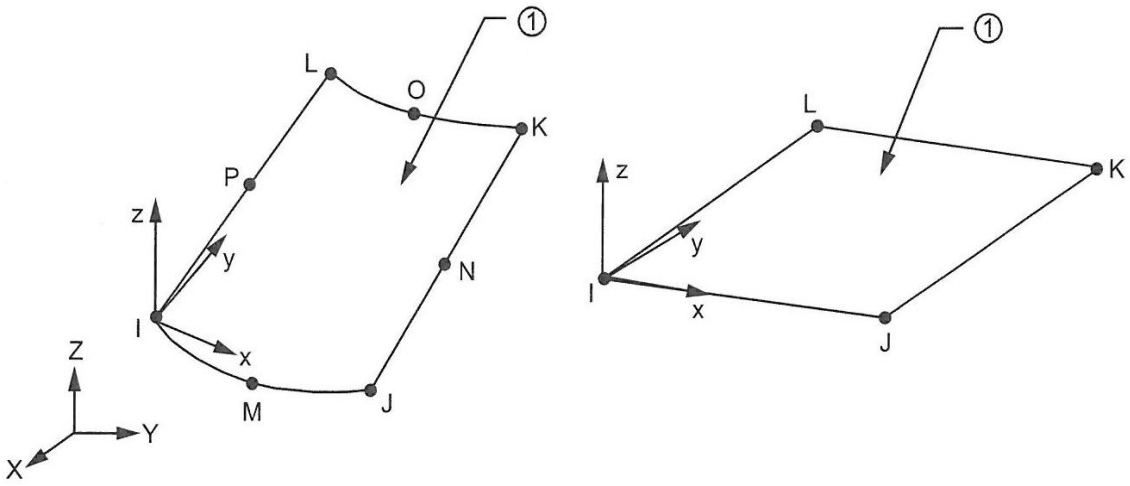

Figure 4:4: SURF152 geometry (ANSYS, 2010b)

4.3.3 Concrete Material Model at Elevated Temperatures

For the concrete properties, the proposed elastic stress − strain model in this study was used and concrete's tensile strength was taken as 10% of its compressive strength at elevated temperatures. Transient strain model was taken from Anderberg and Thelandersson (1976), which is expressed as in Equations 4.1. For the thermal properties and thermal strain of HSC, the model proposed in the Eurocodes was adopted, as it considers the moisture content of the concrete and the variation of response of concrete at elevated temperatures due to aggregate type. These models were presented in Chapter 3. Concrete density was taken as a constant value of 2400kg/m^3 without considering any variation due to elevated temperatures. Creep strain was not considered in the model due to computational and convergence difficulties as it has been

reported by Anderberg and Thelandersson (1976), Jensen *et al.* (2010) and Li and Purkiss (2005) that creep strain is very small and can be neglected.

$$\varepsilon_{tr} = -2.35\left(\frac{f}{f_{c0}}\right)\varepsilon_{thc} \qquad 4.1$$

where ε_{tr} and ε_{thc} are transient strain and thermal strain of concrete at high temperatures respectively.

Most engineering materials have a proportional limit within which the material behaviour is elastic and beyond this point the material behaviour is inelastic. Beyond the yield point the material behaviour becomes plastic. In modelling plasticity of a material, three major factors are taken into account, namely yield criterion, flow rule and hardening rule. Yield criterion or yield point is the stress level at which yielding and development of plastic strain occurs (Chen, 1982; Chen, 1988;). Uniaxial compressive test or tensile test provides test data which are used to obtain one dimension stress – strain curve. The actual structure usually exhibit multi axial stress state and the yield criterion present a scalar invariant relationship of the stress state (multi axial) of the material which is similar in form to the uniaxial cases. The yield point presented in three dimensional spaces is called the yield surface. The material is elastic when stresses lie inside the yield surface and the material yields and develops plastic strain when the stresses lie on the yield surface as shown in Figure 4.5. Flow rule accounts for the direction of plastic straining of the material. Flow rule is associative when the direction of plastic straining is normal to yielding surface and non-associative when plastic straining is not normal to the yield surface. The hardening rule describes the transformation of the yield surface under cyclic loading. The hardening rule is classified into isotropic and kinematic hardening. In isotropic hardening, the yield surface maintains its initial centre line and the progressive yield surface increases. In kinematic hardening, the yield surface drifts away from its initial centre line with the yield surface being constant.

For metals and steel the most widely used yield criteria is the Von Mises yield, which considers yielding of the material when equivalent stress is equal to yield stress. Drucker and Prager (1952), modified the Von Mises yield criteria to account for the effect of hydrostatic stresses on

plastic behaviour of brittle material such as soil, rocks and concrete, the Drucker-Prager yield surface is presented in Figure 4.6.

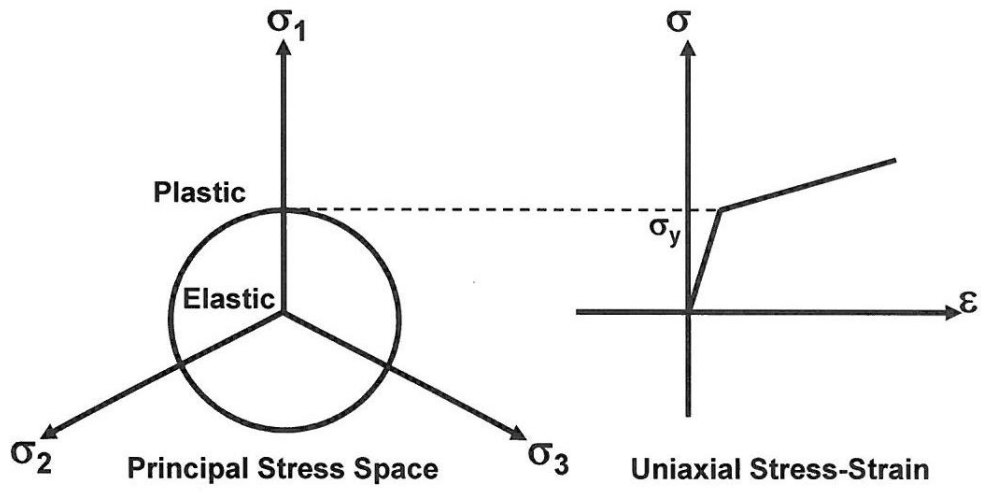

Figure 4:5: Von Mises yield surface and uniaxial stress-strain curve (ANSYS, 2010a)

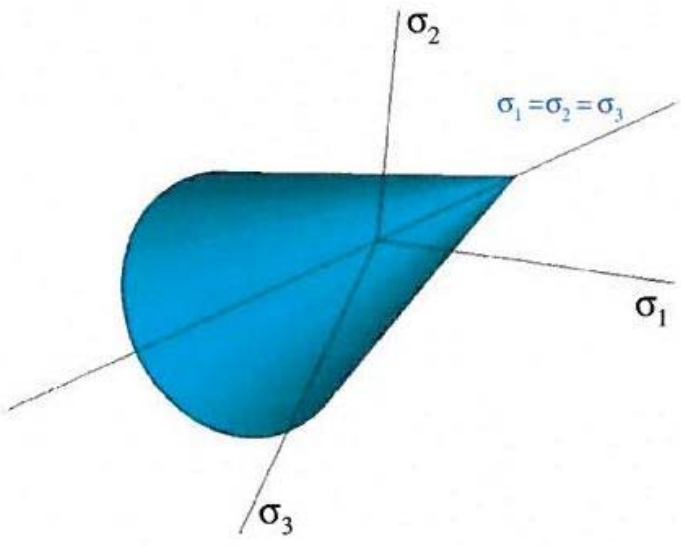

Figure 4:6: Drucker-Prager yield surface (ANSYS, 2010a)

For modelling brittle behaviour of concrete in ANSYS, Extended Drucker-Prager (ANSYS, 2010a) model was selected. This model is suitable for modelling soils, rocks, concrete and other brittle material. This model is adequate for modelling concrete because it accounts for tensile and compressive behaviour of concrete and it has temperature dependency. The yield function is given by Equation 4.2 (ANSYS, 2010a).

$$F = \sigma_e + \alpha\sigma_m - \sigma_k = 0 \qquad 4.2$$

Where F is yield function, α is pressure sensitivity parameter and σ_k is yield stress

$$\sigma_e = \sqrt{\frac{3}{2}\{S\}^T [M]\{S\}} \qquad 4.3$$

where σ_e is the equivalent stress and $\{S\}$ is deviatoric stress vector

$$\{S\} = \{\sigma\} - \sigma_m [1 \quad 1 \quad 1]^T \qquad 4.4$$

$[M] = \begin{bmatrix} 1 & 0 & 0 \\ 0 & 1 & 0 \\ 0 & 0 & 1 \end{bmatrix}$ is mass matrix

σ_m is the mean or hydrostatic stress

$$\sigma_m = \frac{1}{3}(\sigma_x + \sigma_y + \sigma_z) \qquad 4.5$$

The flow potential is given by Equation 4.6

$$Q_f = \sigma_e + \alpha_f \sigma_m \qquad 4.6$$

Where Q_f is flow potential and α_f is flow potential pressure sensitivity parameter

For associative flow $\alpha_f = \alpha$ and for non-associative flow $\alpha_f < \alpha$

4.3.4 Steel Material Model at Elevated Temperatures

The models suggested by BS EN 1992-1-2:2004 and BS EN 1993-1-2:2005 were used for the thermal and structural steel material models; these models are given by Equations 4.7 – 4.13. Reinforcement density was taken as a constant value of 7850kg/m^3 without considering any variation due to elevated temperatures.

$$\varepsilon_{ths} = \begin{bmatrix} -2.416\times10^{-4} + 1.2\times10^{-5}T + 0.4\times10^{-8}T^2 & 20°C \le T \le 750°C \\ 11\times10^{-3} & 750°C < T \le 860°C \\ -6.2\times10^{-3} + 2\times10^{-5}T & 860°C < T \le 1200°C \end{bmatrix} \quad 4.7$$

$$C_s = \begin{bmatrix} 425 + 7.73\times10^{-1}T - 1.69\times10^{-3}T^2 + 2.22\times10^{-6}T^3 & 20°C \le T < 600°C \\ 666 + \dfrac{13002}{738 - T} & 600°C \le T < 735°C \\ 545 + \dfrac{17820}{T - 731} & 735°C \le T < 900°C \\ 650 & 900°C \le T \le 1200°C \end{bmatrix} \quad 4.8$$

$$k_s = \begin{bmatrix} 54 - 3.33\times10^{-2}T & 20°C \le T < 800°C \\ 27.3 & 800°C \le T \le 1200°C \end{bmatrix} \quad 4.9$$

where $\varepsilon_{ths}, C_s,$ and k_s represent the thermal strain, specific heat capacity and thermal conductivity of steel, respectively.

$$f_{sT} = \begin{bmatrix} \varepsilon E_{sT} & 0 \le \varepsilon \le \varepsilon_{spT} \\ f_{spT} - c + \left(\dfrac{b}{a}\right)\left[a^2 - (\varepsilon_{syT} - \varepsilon)^2\right]^{0.5} & \varepsilon_{spT} \le \varepsilon \le \varepsilon_{syT} \\ f_{syT} & \varepsilon_{syT} \le \varepsilon \le \varepsilon_{stT} \\ f_{syT}\left[1 - \dfrac{(\varepsilon - \varepsilon_{stT})}{(\varepsilon_{suT} - \varepsilon_{stT})}\right] & \varepsilon_{stT} \le \varepsilon \le \varepsilon_{suT} \\ 0 & \varepsilon = \varepsilon_{suT} \end{bmatrix} \quad 4.10$$

where f_{sT}, f_{spT}, f_{syT} and E_{sT} represent stress, strength at elastic limit, yield strength and the elastic modulus of steel at elevated temperatures, while $\varepsilon, \varepsilon_{spT}, \varepsilon_{syT}, \varepsilon_{stT}$ and ε_{suT} are the strain,

strain at elastic limit, yield strain, limiting strain and ultimate strain of steel at elevated temperatures, respectively.

$$a = \sqrt{(\varepsilon_{syT} - \varepsilon_{spT})(\varepsilon_{syT} - \varepsilon_{spT} + c/E_{sT})} \quad 4.11$$

$$b = \sqrt{c(\varepsilon_{syT} - \varepsilon_{spT})E_{sT} + c^2} \quad 4.12$$

$$c = \frac{(f_{syT} - f_{spT})^2}{(\varepsilon_{syT} - \varepsilon_{spT})E_{sT} - 2(f_{syT} - f_{spT})} \quad 4.13$$

The plastic steel material behaviour was modelled using a multi-linear isotropic hardening material model in ANSYS, with the von Mises yield criterion. The von Mises yield criterion considers yielding of a material and development of plastic strain when the equivalent stress is equal to the yield stress (Chen, 1982). The von Mises yield surface in three-dimensional space is presented in Figure 4.7.

The multi-linear isotropic model was selected as it has up to 20 temperature regimes and 100 different stress − strain points for each temperature curve. The yield function is expressed as Equation 4.14 (ANSYS, 2010a).

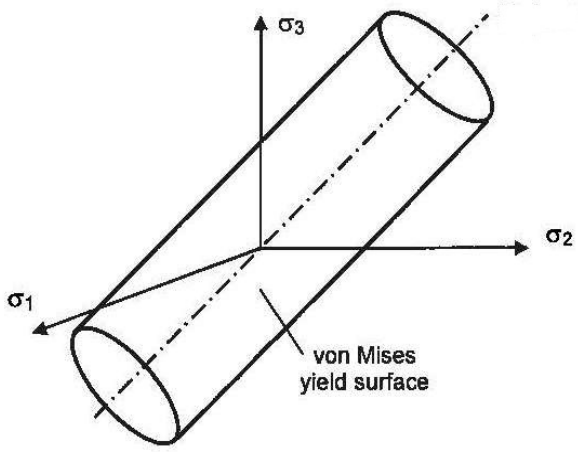

Figure 4:7**:** Von Mises yield criteria in 3-D plane (Espinós Capilla *et al.*, 2012)

$$F = \sigma_e = \sqrt{\frac{3}{2}\{S\}^T [M]\{S\}} = \sigma_k \qquad 4.14$$

Where σ_e is the equivalent stress, σ_k is the yield stress. and $\{S\}$ is deviatoric stress vector

$$[M] = \begin{bmatrix} 1 & 0 & 0 \\ 0 & 1 & 0 \\ 0 & 0 & 1 \end{bmatrix} \text{ is mass matrix}$$

4.3.5 Fracture Energy Element Size Determination Method

The concrete and steel reinforced bars were meshed with SOLID70 and LINK33 elements respectively. These elements were subsequently replaced with SOLID185 and LINK180 in structural phase with the mesh size maintained. Fracture energy element size determination method for reinforced concrete at elevated temperature proposed by Carstensen *et al.*, (2013) was used in the modelling. The model proposed by Carstensen *et al.*, (2013) is given by

$$\frac{2G_{fT}}{f_{tT}\left(\varepsilon_y - \frac{\alpha_s f_{tT}}{\rho_s E_{sT}}\right)} \le h_s \le \min\left\langle \frac{\frac{2E_{cT}G_{fT}}{f_{tT}^{\,2}}}{\frac{9E_{cT}G_{cT}}{8 f_{cT} f_{c0}}} \right\rangle \qquad 4.15$$

G_{fT} is tensile fracture energy at elevated temperature and is given by

$$G_{fT} = 0.0025\alpha_0 \left(\frac{f_{c0}}{0.051}\right)^{0.46} \left(1 + \frac{d_a}{11.27}\right)^{0.22} \left(\frac{f_{cT}}{f_{c0}}\right) (w/c)^{-0.3} \qquad 4.16$$

Where w/c is water cement ratio, d_a is aggregate size and α_0 is aggregate type factor and should be taken as 1 for rounded aggregate and 1.44 for crushed or angular aggregate.

G_{cT} is compressive fracture energy at elevated temperature and is given by

$$G_{cT} = 8.8 f_{cT} (f_{c0})^{-0.5} \qquad 4.17$$

Where h_s is element size, ρ_s is effective reinforcement ratio, f_{tT} is tensile strength of concrete at elevated temperature, f_{cT} is compressive strength of concrete at elevated, E_{cT} is elastic modulus of concrete at elevated temperature, E_{sT} is elastic modulus of steel at elevated temperatures and α_s is concrete tensile strength factor and should be taken as (0.4 – 1.0).

4.3.6 Thermal Analysis

Thermal analysis was performed in the thermal field in order to determine nodal temperature and temperature distribution and profile in the member. In the thermal field the heat transfer was modelled using radiation, convection and conduction;

Radiation was modelled in ANSYS by creating a space node which represents the fire environment or furnace and a radiating (receiving and emitting) surface on the exposed surface of the member. The fire was simulated by applying the appropriate temperature – time curve on the space node which represents the fire or furnace temperature. An example of a temperature − time function used in ANSYS is given in Equation 4.18. The ambient and reference temperature for thermal calculations was taken as 20°C.

$$T_g = \begin{bmatrix} 20 & 0 \le t \le 0.1 \\ 20 + 345\log_{10}(8t+1) & t > 0.1 \end{bmatrix} \quad 4.18$$

where T_g is fire or furnace temperature and t is fire exposure time.

The heat transfer from the space node to exposed element surface in ANSYS is determined by Equation 4.19 (ANSYS, 2010a; Lamont *et al.*, 2001).

$$Q_r = \varepsilon_r \sigma_r \left(T_g{}^4 - T_s{}^4\right) \quad 4.19$$

Where Q_r is radiation heat flux, ε_r is resultant emissivity, σ_r is the Stephan Boltzmann constant and T_s is surface temperature of the member.

Convection was modelled in ANSYS with the law governing convective heat transfer given by Equation 4.20 (ANSYS, 2010a; Lamont *et al.*, 2001).

$$Q_c = \alpha_c \left(T_g - T_s\right) \quad 4.20$$

Where Q_c is convection heat flux and α_c is the convective heat coefficient

Heat transfer by conduction within the element in ANSYS was evaluated using the Fourier law of heat transfer as stated below (ANSYS, 2010a):

$$\rho C \frac{\partial T}{\partial t} = Q + \frac{\partial}{\partial x}\left(k_x \frac{\partial T}{\partial x}\right) + \frac{\partial}{\partial y}\left(k_y \frac{\partial T}{\partial y}\right) + \frac{\partial}{\partial z}\left(k_z \frac{\partial T}{\partial z}\right)$$

where T is temperature, k_x, k_y and k_z are the thermal conductivities in x, y and z directions, Q is internally generated heat, C is specific heat capacity and t is time.

The nodal temperatures and output obtained from the thermal analysis were afterwards applied as thermal loading in the structural model and analysis.

4.3.7 Structural Analysis

In the structural analysis, the load was applied at as a function of time and kept constant once the target load value was attained. This was done in order to enhance the accuracy of the FE model, as applying the load gradually gives a better result and a better representation of a structure exposed to fire. The user defined function of the applied load is given in Equation 4.21. The restraint of column was taken as pinned-fixed, pinned at the top and fixed at the bottom, while the beam was simply supported.

$$P_t = \begin{bmatrix} 100P_{ta}t & 0 \le t \le 0.01 \\ P_{ta} & t > 0.01 \end{bmatrix} \qquad 4.21$$

where P_t is the applied load at time t and P_{ta} is the target applied load before the member is subjected to elevated temperatures.

Non-linear structural analysis was performed in ANSYS, with the thermal element substituted with equivalent structural elements, with the mesh size, nodes and element position maintained. The nodal and element temperatures were accounted for by reading the temperature results from the thermal analysis.

4.3.8 Non-Linear Solution Method

The finite element model is non-linear due to the plasticity and temperature dependent properties of the material and therefore iterative solutions were required. For a linear model in the structural field, the stiffness is constant while the displacement is linear and directly proportional to the applied load, while for a linear thermal analysis the conductivity is constant and heat flow is directly proportional to temperature gradient, as given in Equation 4.22 (ANSYS, 2010a).

$$\{F^a\} = [K]\{u\} \tag{4.22}$$

Where $\{F^a\}$ is applied structural load vector or applied heat load vector, $\{u\}$ is the displacement or temperature vector and $[K]$ is the stiffness or conductivity matrix depending on the analysis field.

In this study, the degradation of material is due to plasticity and changes in the thermal properties, and the stiffness in the structural field varies and continues to change depending on the material behaviour with variation in thermal conductivity in the thermal phase. This makes the analysis non- linear and requires an iterative solution. Therefore, the stiffness or effective applied load becomes a function of deformation (ANSYS, 2010a).

The Newton-Raphson method was selected in ANSYS for these solutions due to simplicity and convergence rate over other methods (such as modified Newton-Raphson and initial stiffness Newton-Raphson method). This solution is expressed in Equation 4.23 (ANSYS, 2010a). The Newton-Raphson method evaluates the out-of-balance load vector, which is the difference between the applied load and the restoring load. The program initially performs a linear solution with the out-of-balance load, and if the problem fails to converge, the out-of-balance load and the tangent matrix are re-evaluated and a new linear solution is performed with the new updated tangent matrix and out-of-balance load. This iterative procedure is repeated until a convergence solution is obtained. This iterative procedure is presented in Figure 4.8 (ANSYS, 2010a).

$$\{F^a\} - \{F_i^{nr}\} = [K_i^T] \times \{\Delta u_i\} \tag{4.23}$$

$$\{\Delta u_i\} = \{u_{i+1}\} - \{u_i\} \tag{4.24}$$

Where $\{F_i^{nr}\}$ is the restoring force or restoring heat load and $[K_i^T]$ is the tangential stiffness or tangential conductivity matrix depending on the engineering field, and i is the number of iterations.

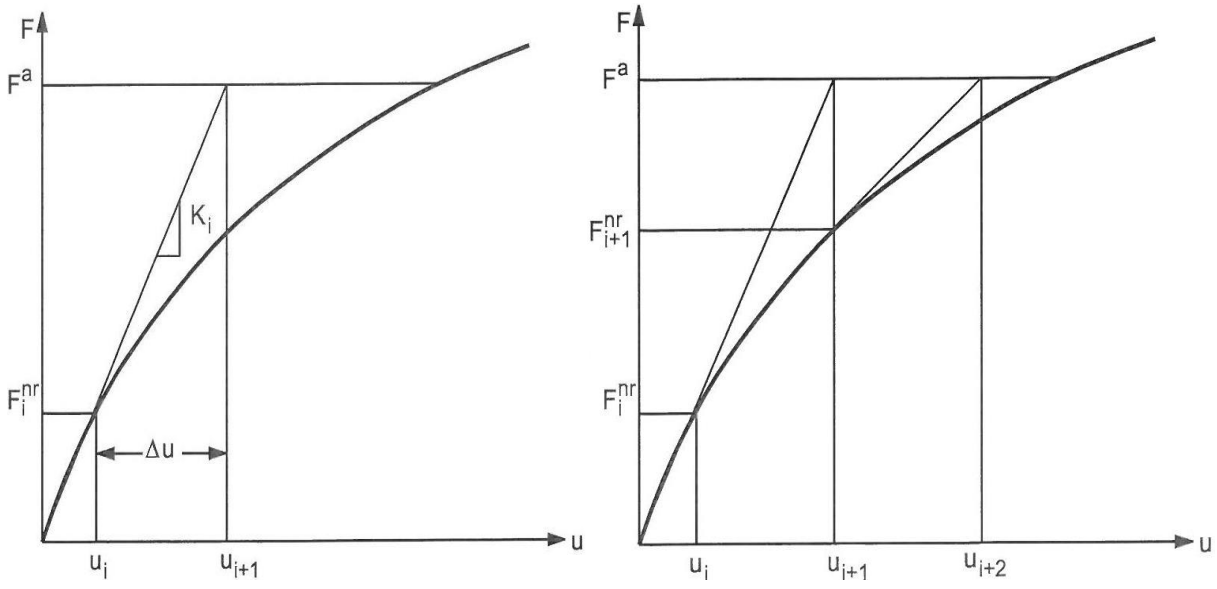

Figure 4:8: Newton-Raphson method showing first and second iterations (ANSYS, 2010a)

In the thermal field, a convergence solution is obtained when the applied heat is equal to the resisting heat load, with some allowable tolerance. While in the structural field, a convergence solution is attained when the applied load is equal to the restoring load and their corresponding displacements are equal, with some tolerance limits. In this study, the tolerance values were taken as 0.1%, 0.5% and 5% for heat, force and displacement respectively. These were the default tolerance limits set by the program.

For the non-linear transient analysis, time steps were used as both temperature and applied structural load were applied as a function of time. With time increment, the applied load, temperature, stiffness and conductivity matrix are updated. For this study the time step was selected as 0.001 minutes with a minimum and maximum value of 0.001 minutes and 20 minutes respectively. This implies that if a solution convergence smoothly, then ANSYS automatically increases the time step by 50% until a maximum time step of 20 minutes is attained and the time

step increment is maintained at 20 minutes. If the solution fails to converge, ANSYS decreases the time step down to a minimum value of 0.001 minutes.

Chapter 5 : Fire Resistance Simulation for HSRC Column

This chapter covers the development and validation of the FE high strength reinforced concrete column model. It also presents FE analysis of HSRC column subjected to fire. Sensitivity analyses of major aspects of the model are presented, and parametric studies on major factors influencing the fire performance of HSRC columns are evaluated. Fire resistance using a performance based approach with ANSYS is evaluated and compared with that obtained using a prescriptive design approach given in Eurocodes 2 (BS EN 1992-1-2:2004).

5.1 Development of HSRC Column Model

A high strength reinforced concrete column under fire conditions was simulated by developing a three-dimensional (3D) Finite Element (FE) model using commercial Finite Element software ANSYS. The model includes the thermal and mechanical properties of concrete, the thermal and mechanical properties of reinforced steel, restraint conditions, heat transfer, fire model and structural loads. The geometric parameters of the model include the column height, breadth and depth, the concrete cover and the size of the reinforcement bars. The model comprises concrete and steel reinforcement bars, owing to symmetry of the column only one quarter was modelled. Concrete was created as volume while the reinforcement bars were created as lines inside the concrete. This was achieved by creating the volume using the down-up modelling techniques and applying reinforcement bar sizes and steel properties for the required lines. The thermal and mechanical contacts between the reinforcement and concrete were assumed to be perfect bond in order to simplify convergence of the solution and be less complicated. Temperature dependent material properties are assigned to the concrete and steel.

The concrete was meshed using SOLID70 hexagonal (8-node) thermal solid element with thermal capabilities, while the reinforcement bars were meshed with LINK33, which is a 2-node line element with thermal functions. In the structural phase of the analysis, these elements are substituted with their structural equivalent of SOLID185 and LINK180. The properties and attributes of these elements are given in Chapter 4. Element size was determined by using fracture energy method proposed by Carstensen *et al.*, (2013). From this method the suitable element sizes obtained was 24 – 58mm and therefore 25mm element size was selected, which proved to be satisfactory for controlling the mesh density. Thermal and structural loads were

applied in their respective fields and the Newton-Raphson method was used to obtain the non-linear solution of the problem. The FE of the column is shown in Figure 5.1.

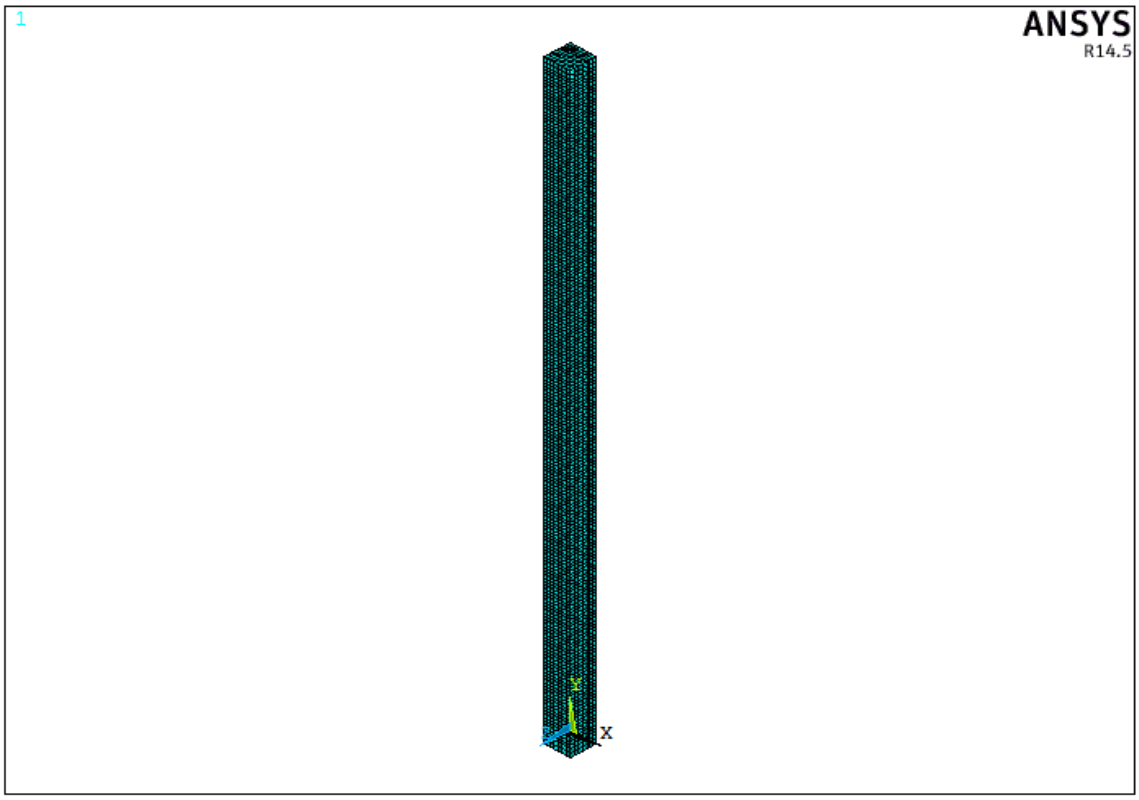

Figure 5:1: Finite element model for HSRC column

5.2 Column Model Validation

The validation of the FE model for the reinforced concrete column under fire conditions was carried out in two stages. In the first stage the predicted thermal result obtained from the simulation was validated against experimental results. In the second stage the predicted structural response was compared with experimental test.

Validation of the three-dimensional (3D) FE model was established by comparing the predicted fire performance of the column with fire test results from Kodur and Richard (2003) and Kodur *et al.* (2003) on the structural behaviour of reinforced concrete columns under fire. The thermal response was validated with temperature variation within the reinforced concrete column, while the structural performance was validated with temperature – time dependent axial deformation at the top of the column and fire resistance. Kodur and Richard (2003) and Kodur *et al.* (2003)

presented the response of reinforced high strength concrete columns fabricated and tested under simulated fire conditions. Columns C1 and C2 were taken from Kodur *et al.* (2003) and Kodur and Richard (2003), respectively and used for the model validation. The columns were fixed (restrained against rotational and horizontal displacement) at both ends, with a height of 3760mm and a square section dimension of 305mm. They were fabricated with carbonate high strength concrete and reinforced bars.

Column C1 with a concrete strength of 72.7MPa was reinforced with 4 of 25mm diameter main bars and 10mm diameter bars as links. The yield strengths for the longitudinal and link bars were 420MPa and 280MPa, respectively. Column C2, having a compressive strength of 120MPa, was reinforced with 8 of 16mm diameter main bars and 6mm diameter bars as links. The yield strength for the reinforcement bars was 414MPa. The columns were subjected to axial concentric loading at the top of the columns and exposed to elevated temperatures with temperature controlled in accordance with a standard fire temperature curve. Further details of the columns are given in Figure 5.2 and Table 5.1.

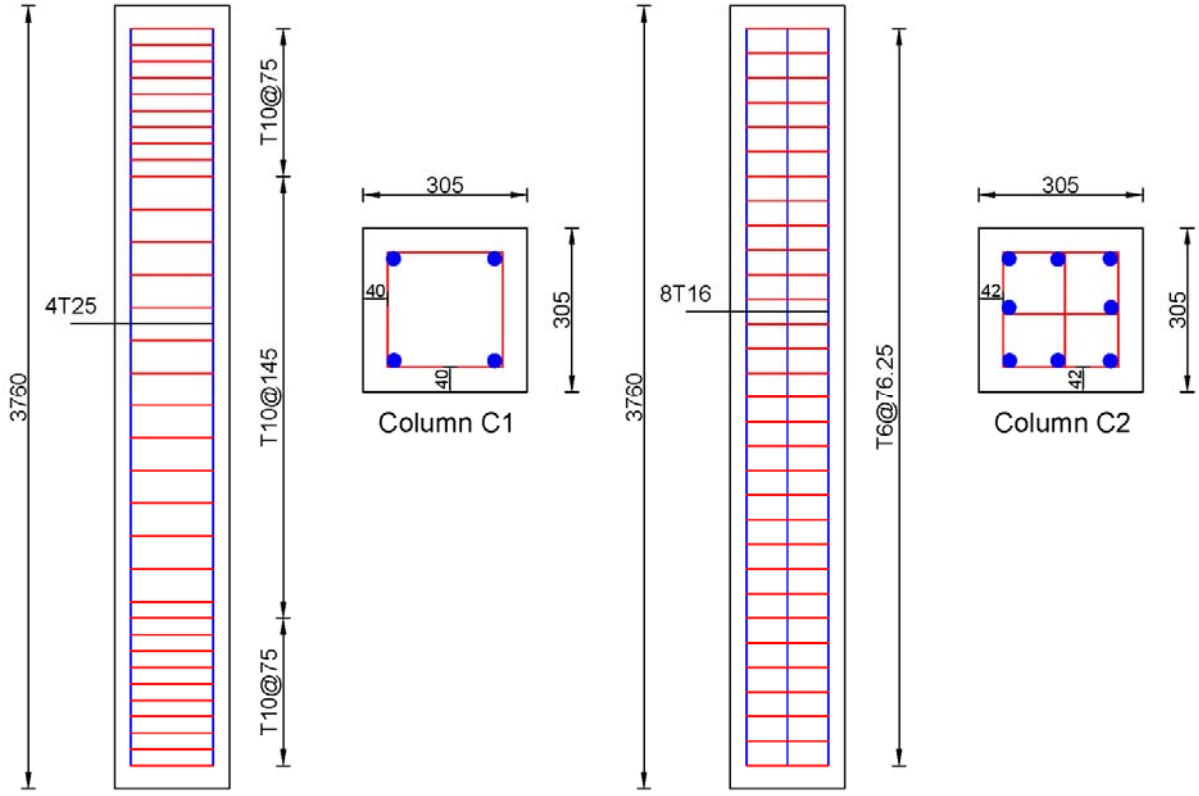

Figure 5:2: Details of RC column

Table 5:1: Column details

Column Parameters	C1	C2
Actual column size	305×305×3760mm	305×305×3760mm
Concrete strength	72.7MPa	120MPa
Reinforcement yield strength	420MPa for main bars	414MPa for main bars
	280MPa for link bars	414MPa for link bars
Number of reinforcement	4 ϕ 25mm main bars	8 ϕ 16mm main bars
	ϕ 10mm link bars @ 145c/c at the centre	ϕ 6mm link bars @ 76.25c/c at the centre
	ϕ 10mm link bars @ 75c/c at the support	ϕ 6mm link bars @ 76.25c/c at the support
Clear reinforcement cover	40mm	42mm
Total applied load (kN)	2000	2954
Aggregate type	Carbonate	Carbonate

5.3 Thermal Validation and Response of Column

The temperature − time response of the reinforced concrete column simulated under fire conditions was obtained from thermal analysis. This includes temperature distribution across the column at mid height and temperature evolution of concrete and steel reinforcement bars.

5.3.1 Temperature Distribution within Column

From the thermal analysis and as shown in Figure 5.3, the temperature distribution across the column section indicates that temperature decreases from the fire exposed surface to the centre of the column. This signifies that heat transfer occurs through conduction from a region with higher temperature to a region of lower temperature as the column is exposed to fire (Chapman, 1987). The temperature of the heated surface and through the column section also increases with a sustained and increase in fire exposure duration.

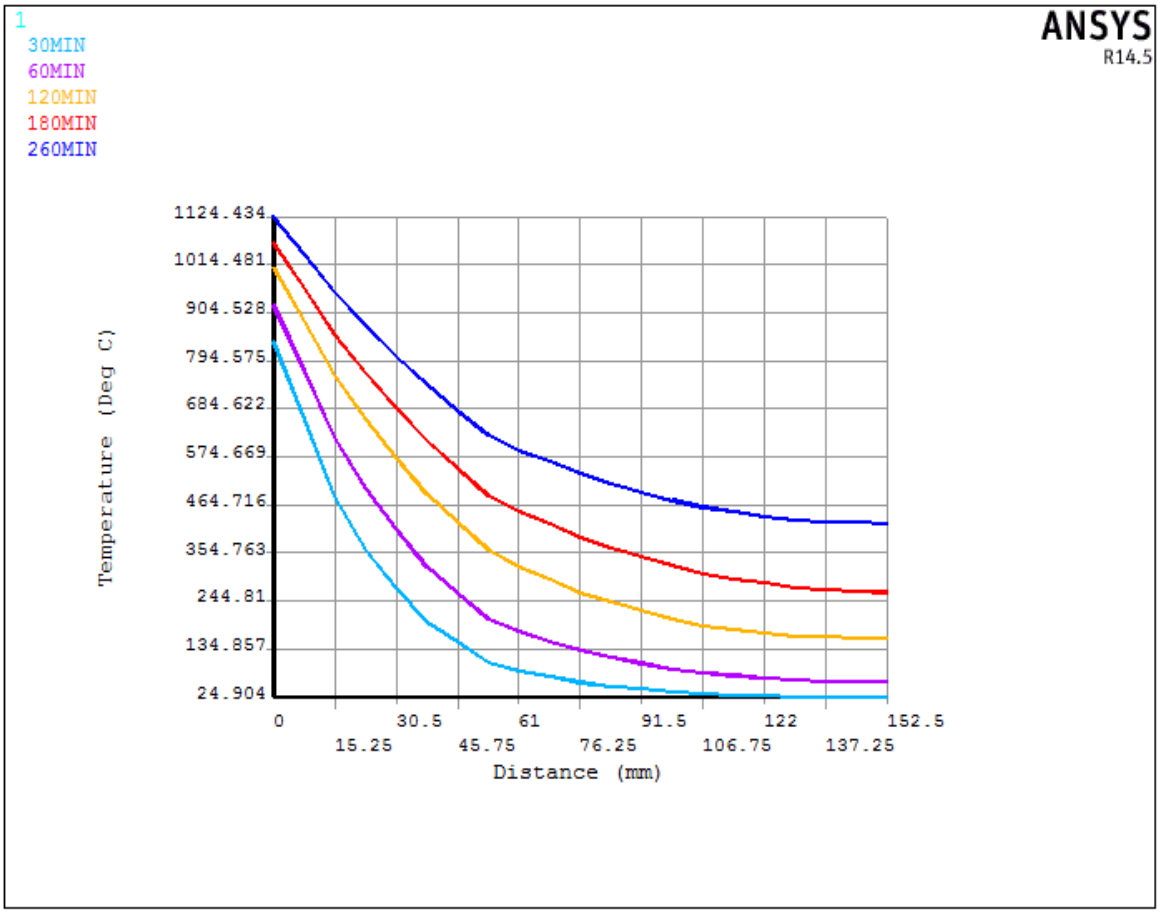

Figure 5:3: Temperature distribution across column

5.3.2 Temperature Variation of Column

Temperature evolution at the concrete surface, reinforcement and column centre are presented in Figure 5.4, which indicates that the surface temperature increases rapidly at the initial stages of fire exposure, attaining a temperature of about 800°C within 25minutes. Above this the surface temperature increases gradually with a less rapid rate. While throughout the heating duration, reinforcement and column centre temperatures increase gradually with an approximate linear relationship with time. This is attributed to the fact that heat conduction is the source of heat transfer across the column section and is dependent on the distance between the transfer medium and the point in question (Chapman, 1987).

In comparison with the exposed concrete surface, the reinforcement and concrete centre attain a temperature of about 125°C and 25°C respectively with 25 minutes of fire exposure, and after a

fire exposure time of 4 hours the concrete surface, reinforcement and concrete centre temperatures were about 1110°C, 700°C and 375°C, respectively.

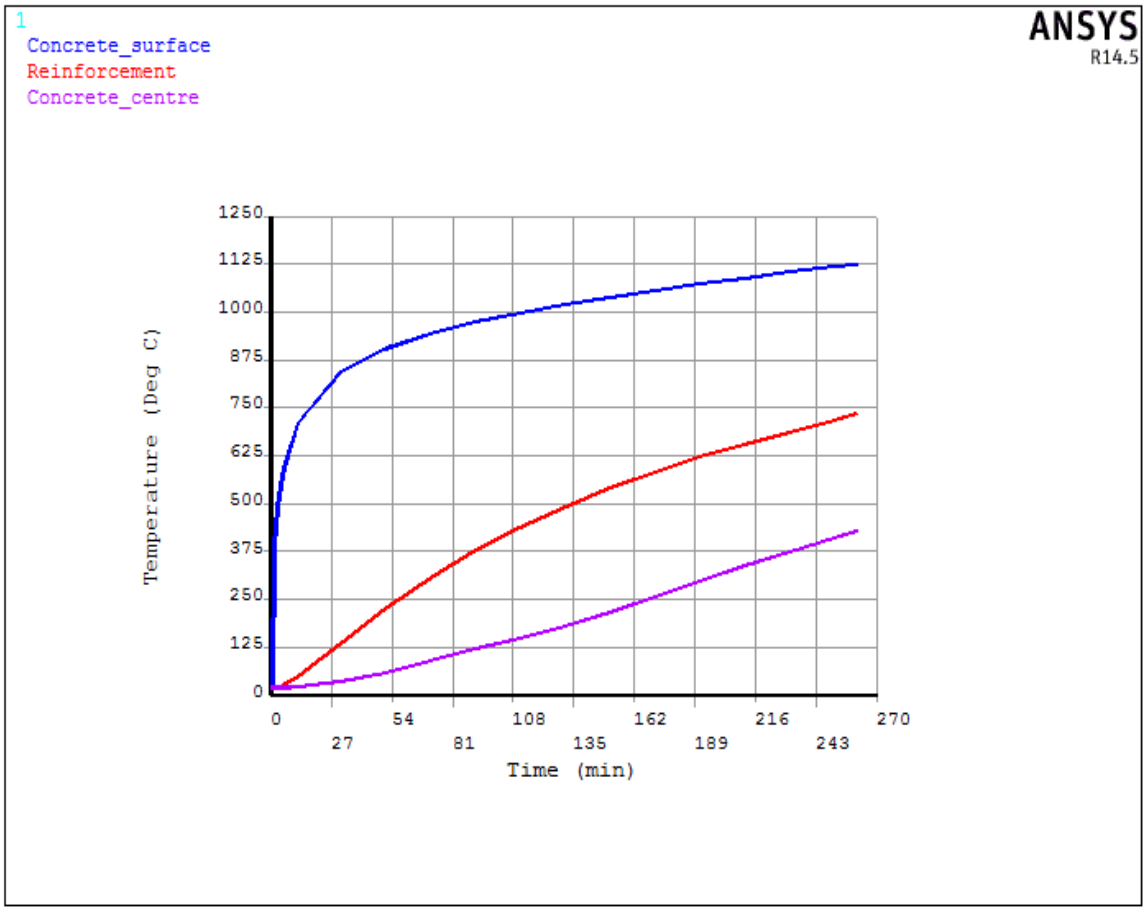

Figure 5:4: Temperature evolution within column C2

5.3.3 Thermal Validation of Column

The thermal validation of the FE model was established by comparing the predicted time dependent temperature at various points within the column with experiment results. The locations of these validated points are shown in Figure 5.5.

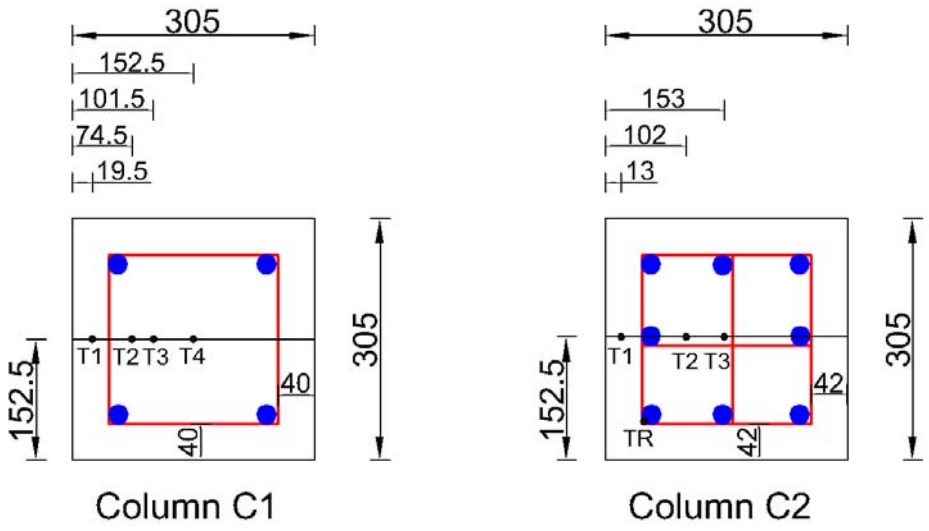

Figure 5:5: Validated temperature points within column

Figure 5.6 – 5.7 presents the comparisons of predicted column temperatures and experiment results. The comparison indicates that ANSYS predicted time dependent temperatures show a similar trend and are in close agreement with the measured experiment results. The predicted and measured temperatures both increase under fire exposure. Overall, the predicted result shows good agreement with fire test results and assuming the contact between the concrete and reinforcement to be perfectly bond proved to be adequate as predicted reinforcement temperature shows good agreement with experiment results.

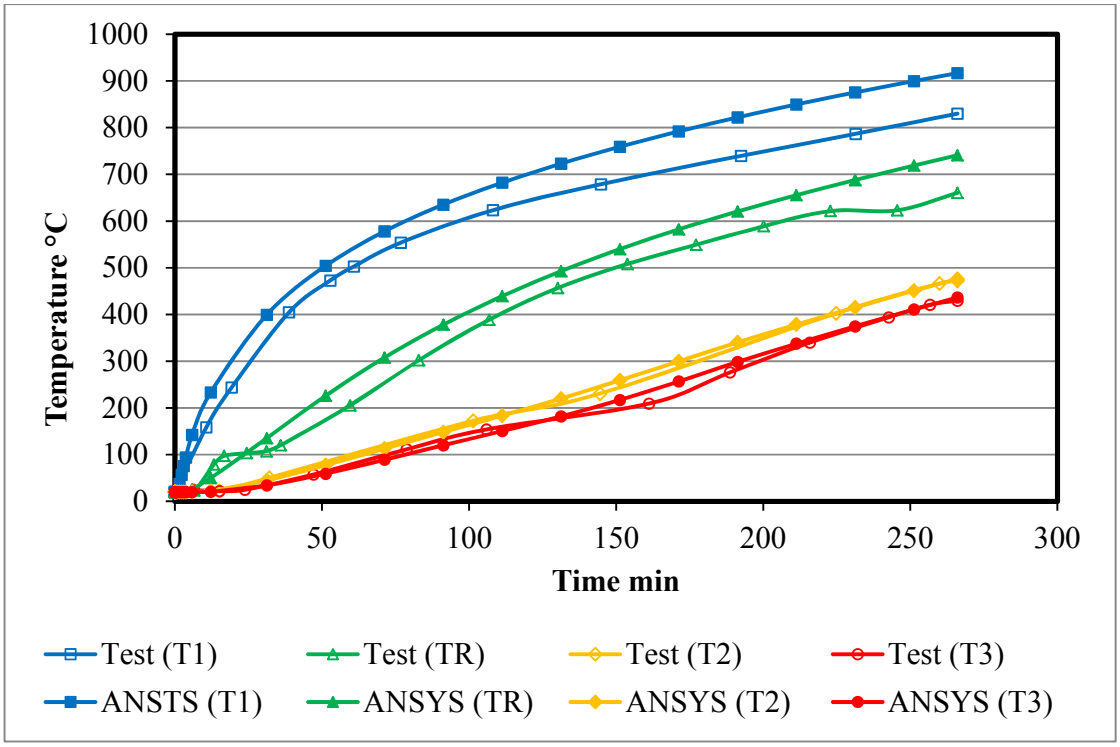

Figure 5:6: Predicted and experiment temperature evolution within column C2

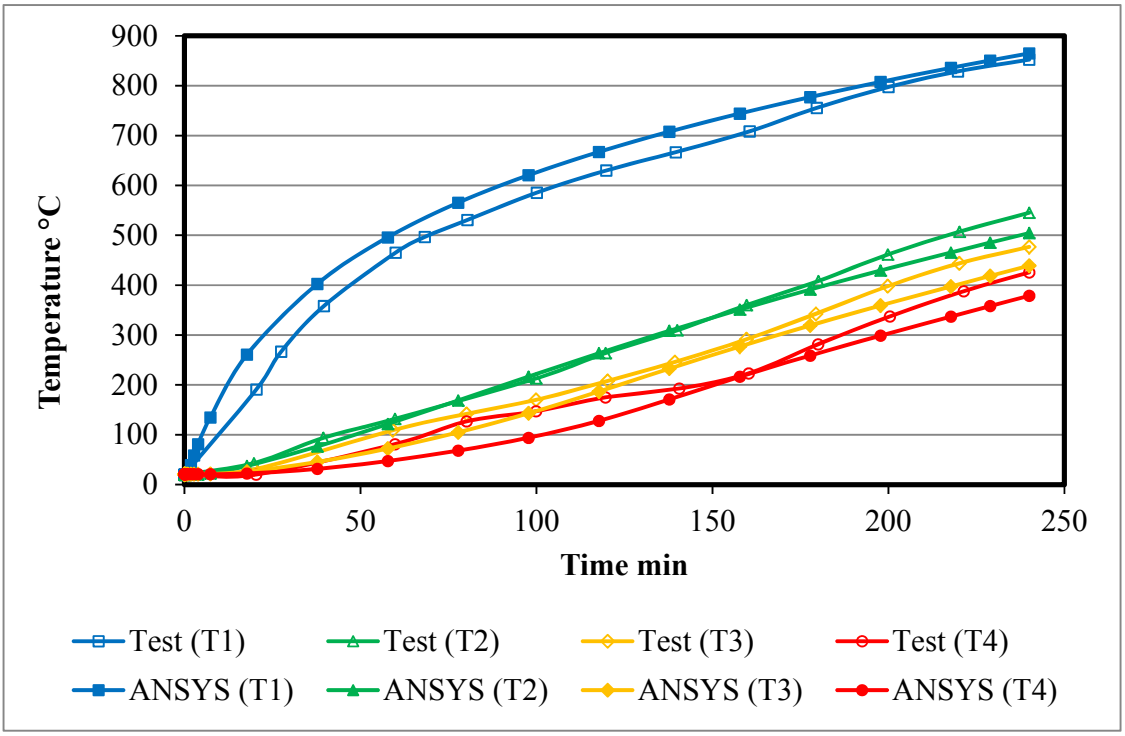

Figure 5:7: Predicted and experiment temperature evolution within column C1

5.4 Structural Validation and Response of Column

The structural time response of a reinforced concrete column was obtained by performing a coupled field analysis. This includes fire resistance, temperature − time dependent axial deformation and axial stress distribution across the column section.

5.4.1 Axial Deformation

Axial deformation of the reinforced concrete column simulated under structural load and fire, as illustrated in Figure 5.8, captures the full structural response of the column under fire and can be divided into three stages. In the first stage, only compressive load is applied to the column and therefore it undergoes compression and total compressive axial deformation. With temperature applied to the column in the second stage and with a sustained load, the column experiences expansion with the total deformation of the column still in compression. In the third stage, with heating and applied load sustained for longer periods, the column undergoes compression with a total compressive axial deformation. The compression of the column in the third stage is mainly attributed to loss of strength, stiffness and load bearing capacity of concrete and the steel material due to degradation of these materials under elevated temperatures (Ali *et al.*, 2010; Kodur *et al.*, 2003).

At heating range of about 1 – 60 minutes the column is under expansion deformation and with sustained heating and above 60minutes the column shows compressive deformation. Above 60 minutes to 120 minutes the compressive deformation in the column continually increases but at a slow rate. At 180 minutes and above the compressive deformation in column continue to increase with a higher rate of deformation until failure.

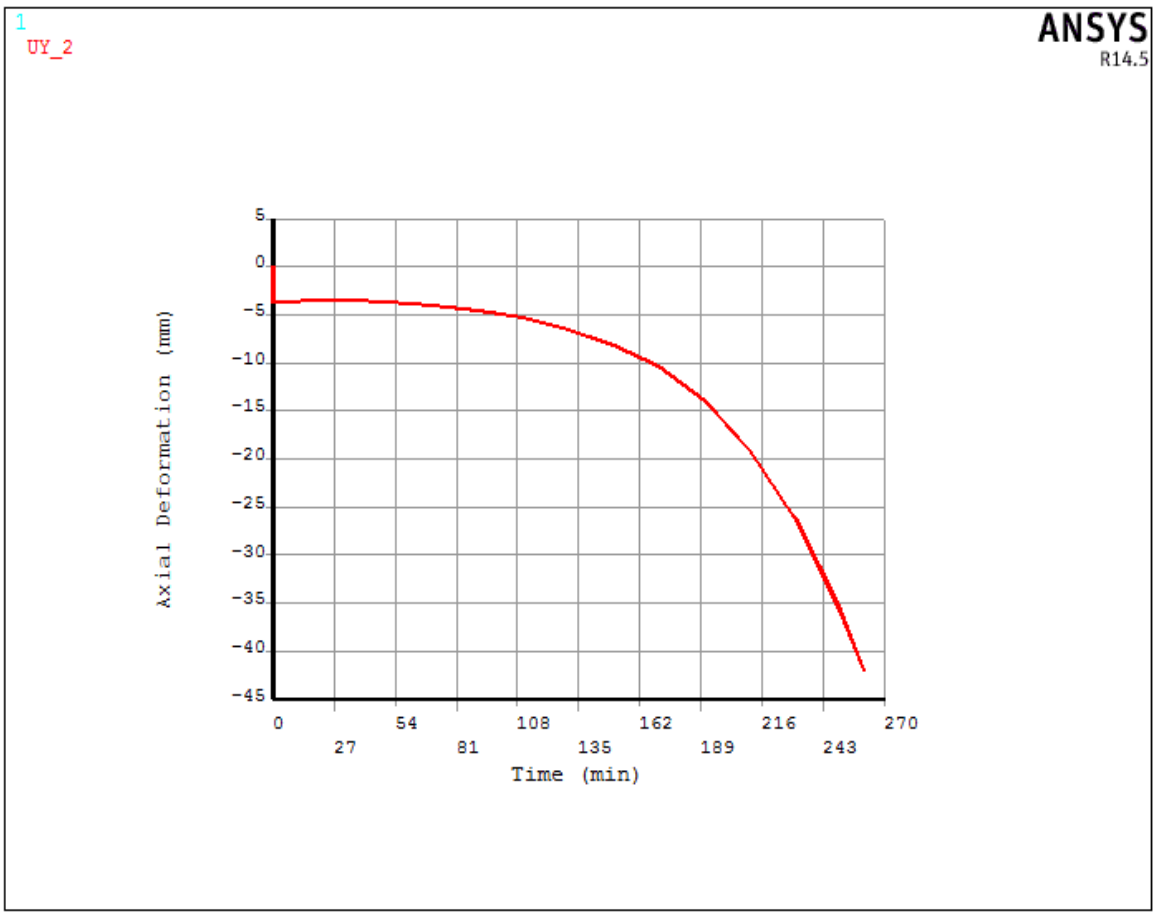

Figure 5:8: Predicted deformation of column C2

5.4.2 Axial Stress Distribution

Axial stress distributions and stress profile along the column section obtained from the FE model is presented in Figure 5.9 and Figure 5.10. From Figure 5.9, it can be seen that throughout the heating the column experiences mainly compressive axial stresses. This is because compressive load is applied to the column before subjecting it to elevated temperatures. With a high load level and degradation of materials, the load induced stresses are greater than thermal stresses and therefore, even when the column experiences expansion at some sections, the total axial stress is still compressive.

The stress distribution also indicates that, at initial heating duration of 60 minutes, the compressive stresses are lower when compared with results of column subjected to only structural load (at 0 minute). This is majorly attributed to thermal stresses caused by exposing the

column to elevated temperatures. While at 120 minutes and above, the column experiences maximum compressive stresses at column centre and minimum compressive stresses close to the heated surface, which is majorly attributed to loss of load bearing capacity accompanied with elevated temperatures.

This variation in stress distribution is mainly attributed to the fact that at early stages of heating the temperature at the concrete surface is much higher than at the inner section, which leads to loss of strength and stiffness at the surface with higher compressive stresses. With heating sustained, the column surface loses most of its load bearing capacity and the loads are gradually transferred to the inner sections, which leads to a higher compressive stress at the inner sections. Overall these large variations in stress during fire exposure will increase the loss of stiffness of the materials and cohesion within the concrete.

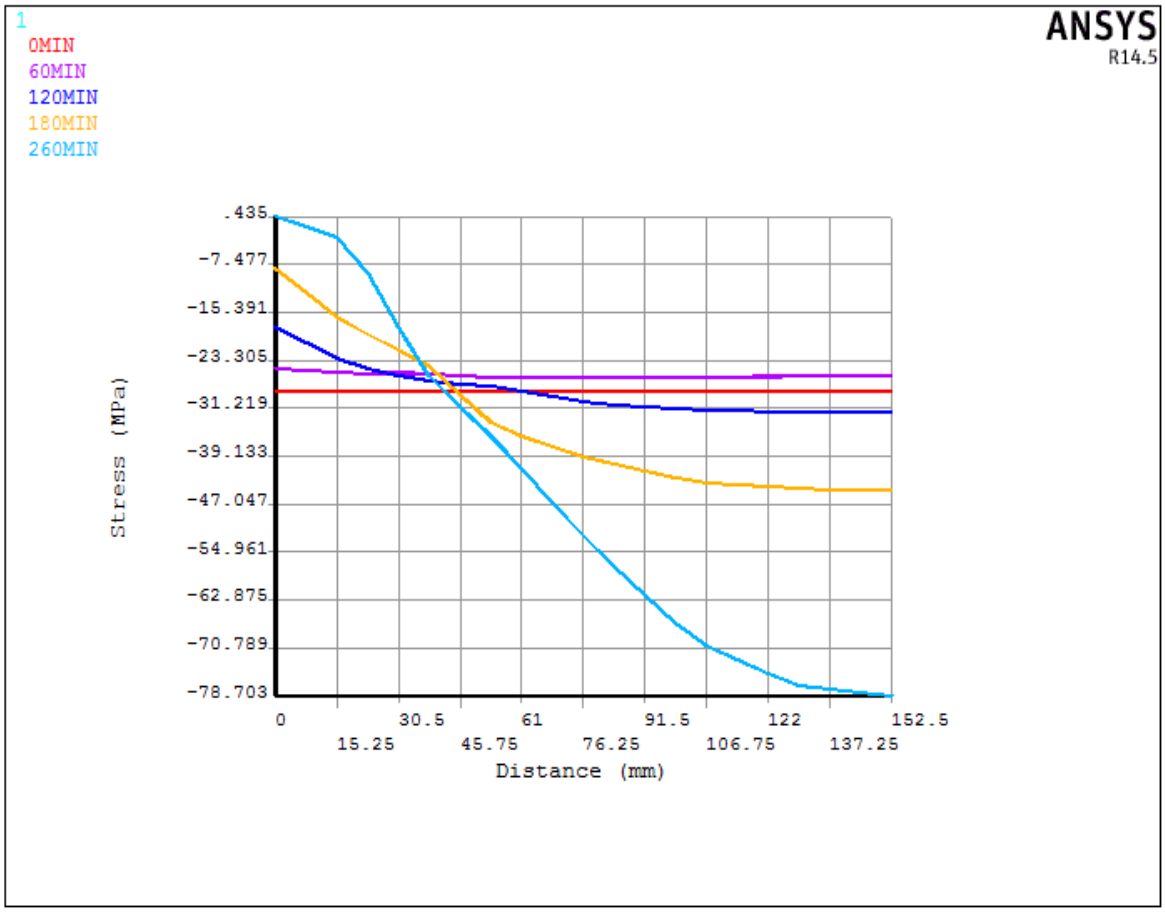

Figure 5:9: Axial stress distributions of column C2

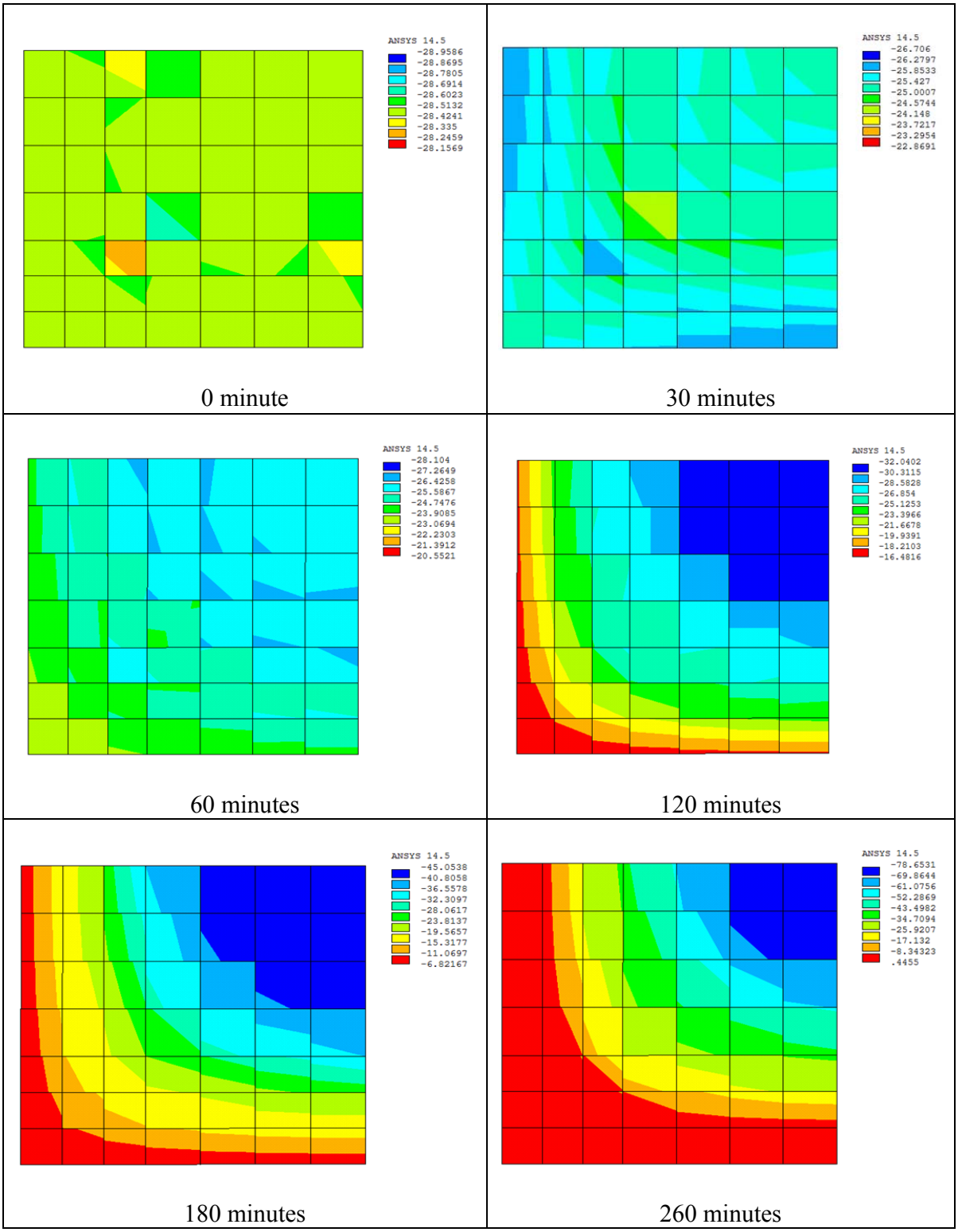

Figure 5:10: Axial stress profile of column C2

At failure the maximum compressive axial stress, which occurs at column centre is about 79MPa with a temperature of about 427°C. With the proposed stress – strain model at this temperature, the maximum compressive stress which concrete can retain is about 83MPa. Therefore this result indicates that the column fails before attaining its maximum compressive stress. Also using Drucker-Prager without a compressive cap proves to be satisfactory as compressive stresses in column section do not go beyond or reach its maximum stress before failure.

5.4.3 Structural Validation of Column

The numerical model for a high strength reinforced concrete column exposed to fire condition was validated by comparing the predicted ANSYS axial deformation and fire resistance with the measured experiment test results. These comparisons are presented in Figures 5.11 – 5.12 and Table 5.2.

From Figures 5.11 – 5.12 it can be seen that the ANSYS predicted axial deformation of the columns shows good agreement with the measured experiment result. The ANSYS model accurately captures the trend of the deformation of the column under fire, as under initial heating the column experiences expansion, and with sustained heating, temperature increase and decrease in material strength and stiffness, the column starts to be under compression until failure. Within the first 190 minutes of heating, the predicted axial deformation shows very close agreement with the experiment measured values. After 190 minutes the predicted axial deformation shows some discrepancies with the test result. These discrepancies can be attributed to having too much transient strain at later stages of fire and a high level of degradation of the steel and concrete material at higher temperatures, which makes it difficult to predict the exact behaviour and response as it approaches and reaches the failure stage. It can also be attributed to the heterogeneous nature of concrete, which makes it difficult to model the concrete behaviour accurately after the decomposition of its major binder component (portlandite) at 400 − 600°C (Naus, 2010), with the steel bars exceeding a critical temperature and the concrete and steel losing their load bearing capacity.

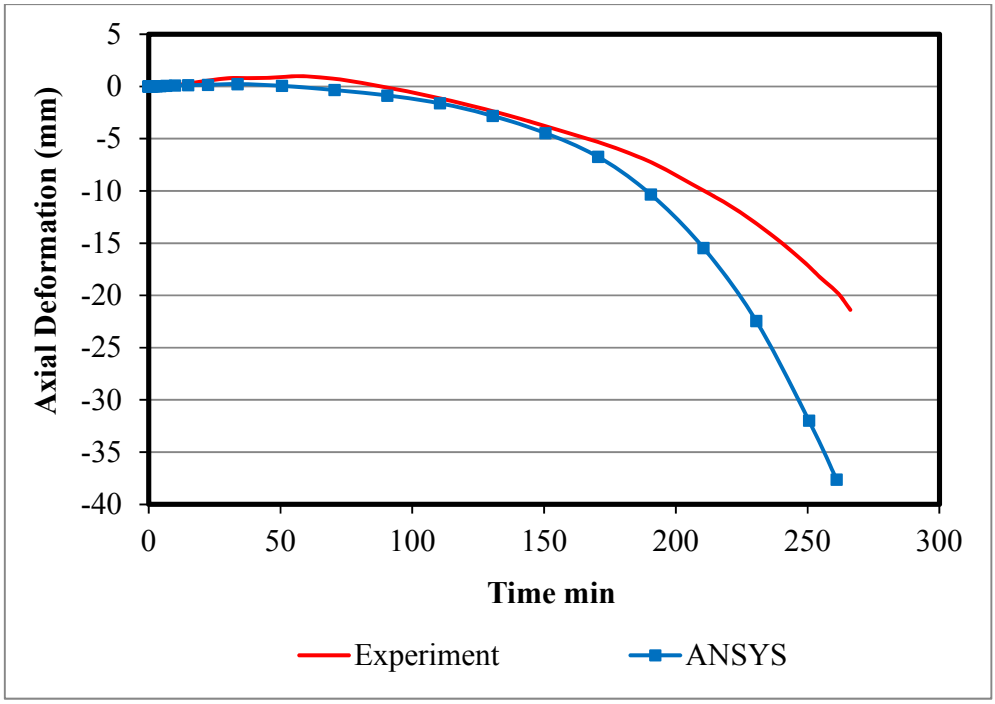

Figure 5:11: Experiment and predicted deformation of column C2

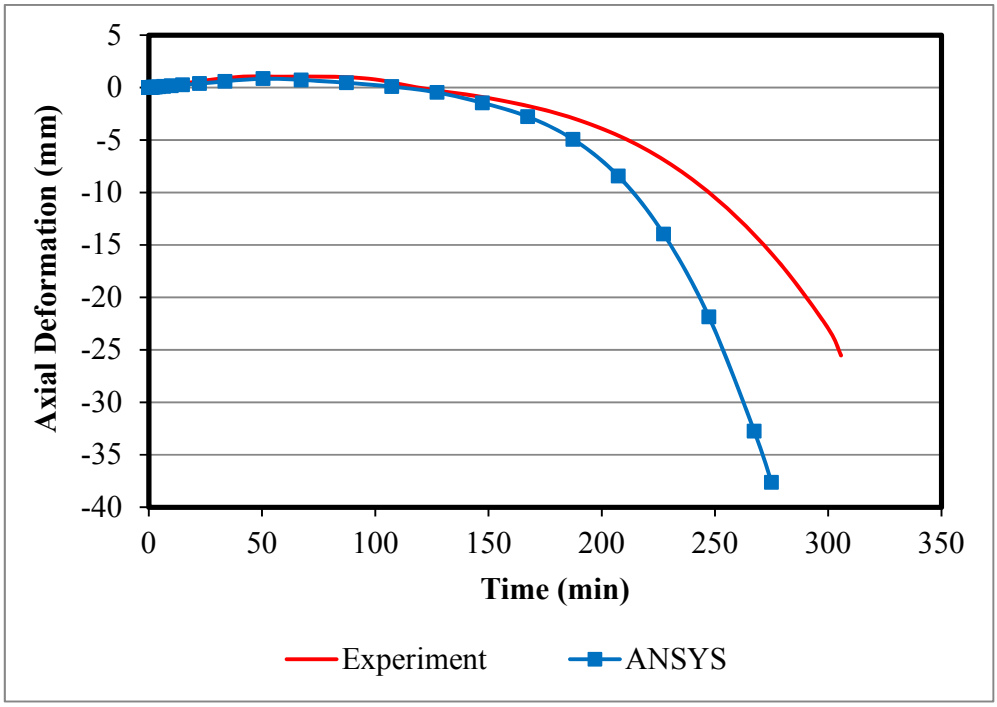

Figure 5:12: Experiment and predicted deformation of column C1

Overall the ANSYS model predicts an accurate fire resistance of the column, as this is the major target of the simulation. The fire resistance was predicted by using ISO 834 performance based failure criteria stated in Chapter 2. Table 5.2 presents a comparison of the experiment and predicted fire resistance of the column subjected to elevated temperatures.

The results presented in Table 5.2 indicate that the predicted fire resistances are very close to the measured experiment values. For column C2, the ANSYS predicted fire resistance was 261 minutes with a percentage difference of 1.88% when compared with the measured experiment results, while for Column C1, a fire resistance of 275 minutes was predicted, with a percentage difference of 9.84%. This has been a highly accurate numerical result compared with the testing data. The predicted axial deformation at failure, using ISO 834 failure criteria, showed discrepancies with the measured experiment results, but this was mainly introduced to assess the failure time rather than the maximum deformation in the column. As illustrated in Table 5.2, the predicted fire resistance with ANSYS shows a better agreement with the fire test result when compared with results obtained using the prescriptive design approach given in BS EN 1992-1-2:2004. Therefore, the FE model for simulating the fire resistance of the reinforced column is suitable and valid for this purpose.

Table 5:2: Experiment and predicted structural performance of column

Column	Column result	Test	ANSYS	EC2 prescriptive design	% Difference between test and ANSYS
C2	Fire resistance (mins)	266	261	116	1.88%
	Axial deformation (mm)	-22.0	-37.6	-	70.91%
C1	Fire resistance (mins)	305	275	134	9.84%
	Axial deformation (mm)	-25.0	-37.6	-	50.4%

5.5 Sensitivity Analysis for Column Model

A comprehensive sensitivity analysis was performed in order to determine the main influencing parameters of the FE model and their optimum values and also to determine the adequacy of the mesh size. These study parameters were thermal conductivity of concrete, moisture content and the concrete stress − strain model at elevated temperatures.

5.5.1 Concrete Thermal Conductivity Model for Column

As discussed in Chapter 4, the thermal conductivity model proposed in BS EN 1992-1-2:2004 was used for simulating heat conduction across the column in the FE model. Accordingly, BS EN 1992-1-2:2004 presents two models for predicting the thermal conduction of concrete under fire exposure. Sensitivity analysis was performed to evaluate the most efficient model and also to study the influence of thermal conductivity on the predicted response of the reinforced concrete column under fire. The upper and lower limits of thermal conductivity as presented in BS EN 1992-1-2:2004 were tested in simulating the reinforced concrete column at elevated temperatures. The predicted time dependent temperatures and axial deformations are compared and presented in Figures 5.13 and 5.14.

The predicted time dependent temperature at various points across the column as presented in Figure 5.13 shows the influence of thermal conductivity on the predicted response of the column exposed to fire conditions. The upper limit thermal conductivity values predict higher reinforcement and concrete temperatures when compared with the lower limit values, as conduction within the concrete is higher. Under sustained heating for 266 minutes, the predicted steel temperature (TR) was about 780°C and 740°C with upper limit and lower limit thermal conductivity models, respectively, while the predicted column centre temperature (T3) was around 500°C and 430°C with the upper limit and lower limit thermal conductivity values respectively. The lower limit thermal conductivity model predicted more accurate temperatures at various points across the column.

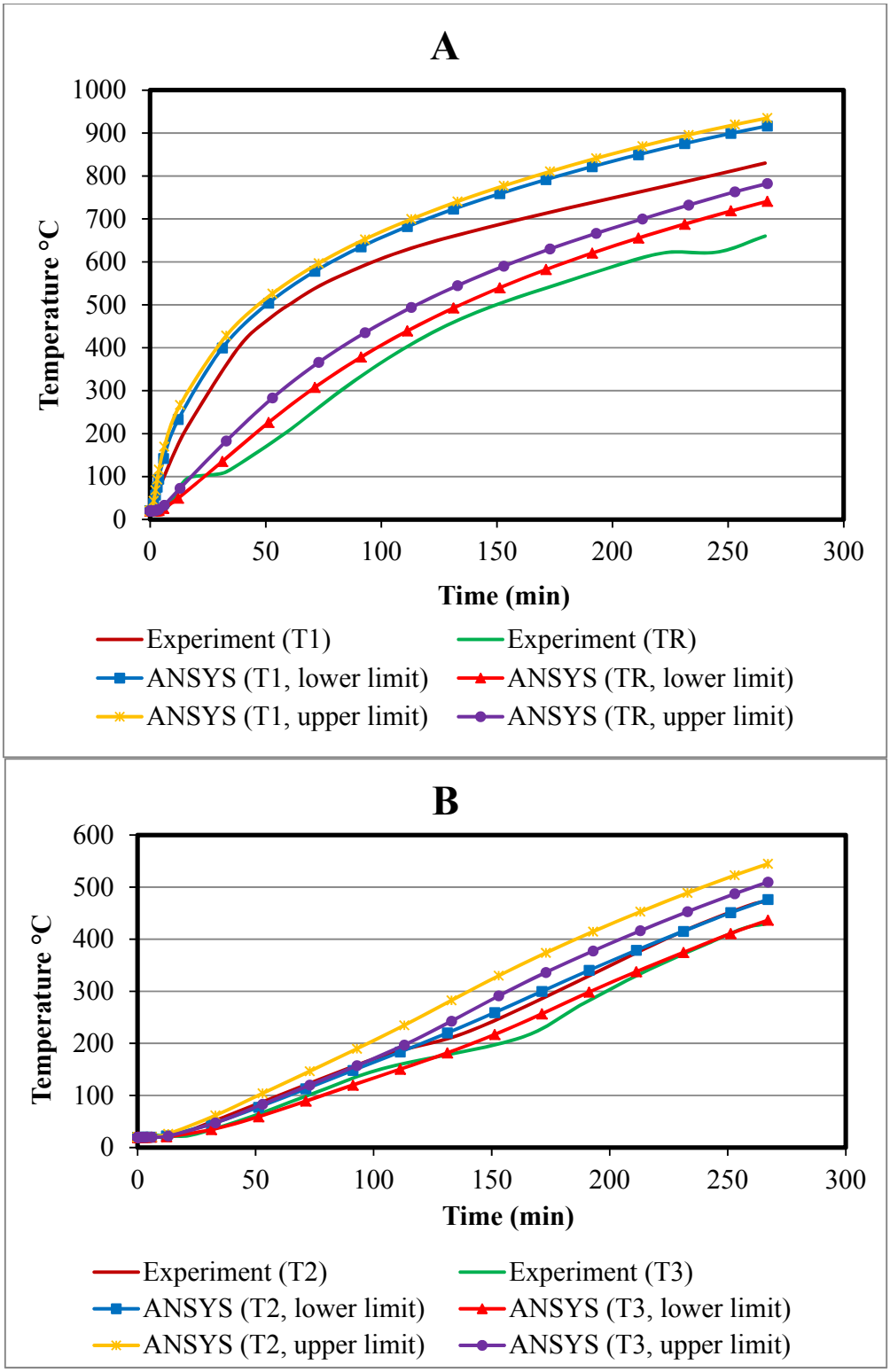

Figure 5:13: Comparison of experiment and predicted column temperature variation with different thermal conductivity models (a) at T1 and TR, (b) at T2 and T3

The ANSYS predicted axial deformation, presented in Figure 5.14, also indicates that lower limit thermal conductivity values predicted a more accurate response of the reinforced concrete column under fire exposure. Upper limit values of thermal conductivity predict a fire resistance of 226 minutes, while 261 minutes was predicted with the lower limit values. Overall, the lower limit values predicted a more accurate thermal and structural response of the concrete column under fire condition, Therefore, lower limits values were selected for FE modelling of the column. With the upper limit values predicting lower fire resistance, they are therefore recommended for worst case designs, while the lower limit values of thermal conductivity are recommended for best case designs of reinforced concrete columns under fire exposure.

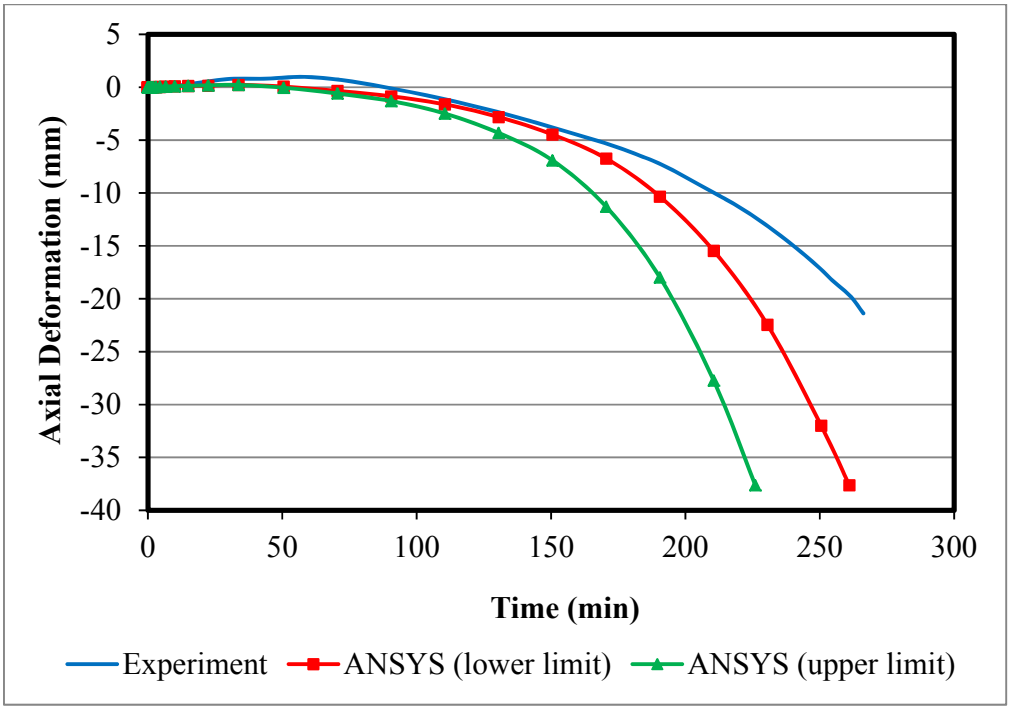

Figure 5:14: Comparison of experiment and predicted column deformation with different thermal conductivity models

5.5.2 Moisture Content Model for Column

As stated in Chapter 4, the moisture effect was indirectly accounted for in the FE model through the specific heat capacity model proposed in BS EN 1992-1-2:2004. BS EN 1992-1-2:2004 recommends specific heat peak values in the temperature range 100 − 115°C, as most of the heat energy in the column at these temperatures is used up in the evaporation process. The model considers two moisture content levels of 1.5% and 3.0% weight of concrete. A sensitivity study

was performed to determine the influence of these values on the predicted fire response of the reinforced concrete column. Values of specific heat capacity with 1.5% and 3.0% moisture content as presented in BS EN 1992-1-2:2004 were tested in simulating the reinforced concrete column at elevated temperatures. Predicted time dependent temperatures and axial deformations are compared and presented in Figures 5.15 and 5.16.

ANSYS predicted steel reinforcement (TR) and concrete centre (T3) time dependent temperatures with 1.5% moisture content are slightly higher than temperatures predicted with 3.0% moisture content. The predicted steel temperature with 1.5% moisture content and fire exposure time of 266 minutes was about 740°C, while the evaluated steel temperature was about 727°C using 3.0% moisture content. Predicted concrete centre temperatures were about 430°C and 406°C with 1.5% and 3.0% moisture content respectively. Using 3.0% moisture content, a slightly more accurate steel reinforcement temperature was predicted when compared with 1.5% moisture, while 1.5% moisture content predicted more accurate temperatures at the concrete centre than 3.0% moisture content. Overall, both moisture content levels predict very good temperature results in comparison with the test values.

The predicted axial deformations presented in Figure 5.16 indicate that with 3.0% moisture content a slightly more accurate response of the reinforced concrete column under elevated temperatures was predicted. This is in comparison with 1.5% moisture content where a less accurate axial deformation was predicted. Using 1.5% moisture content, a fire resistance time of 261 minutes was predicted, while 3.0% moisture content predicted a fire resistance time of about 274 minutes. Overall 1.5% moisture content was selected for FE modelling of the reinforced concrete column under fire exposure due to the fact that with 1.5% moisture a more accurate fire resistance was predicted.

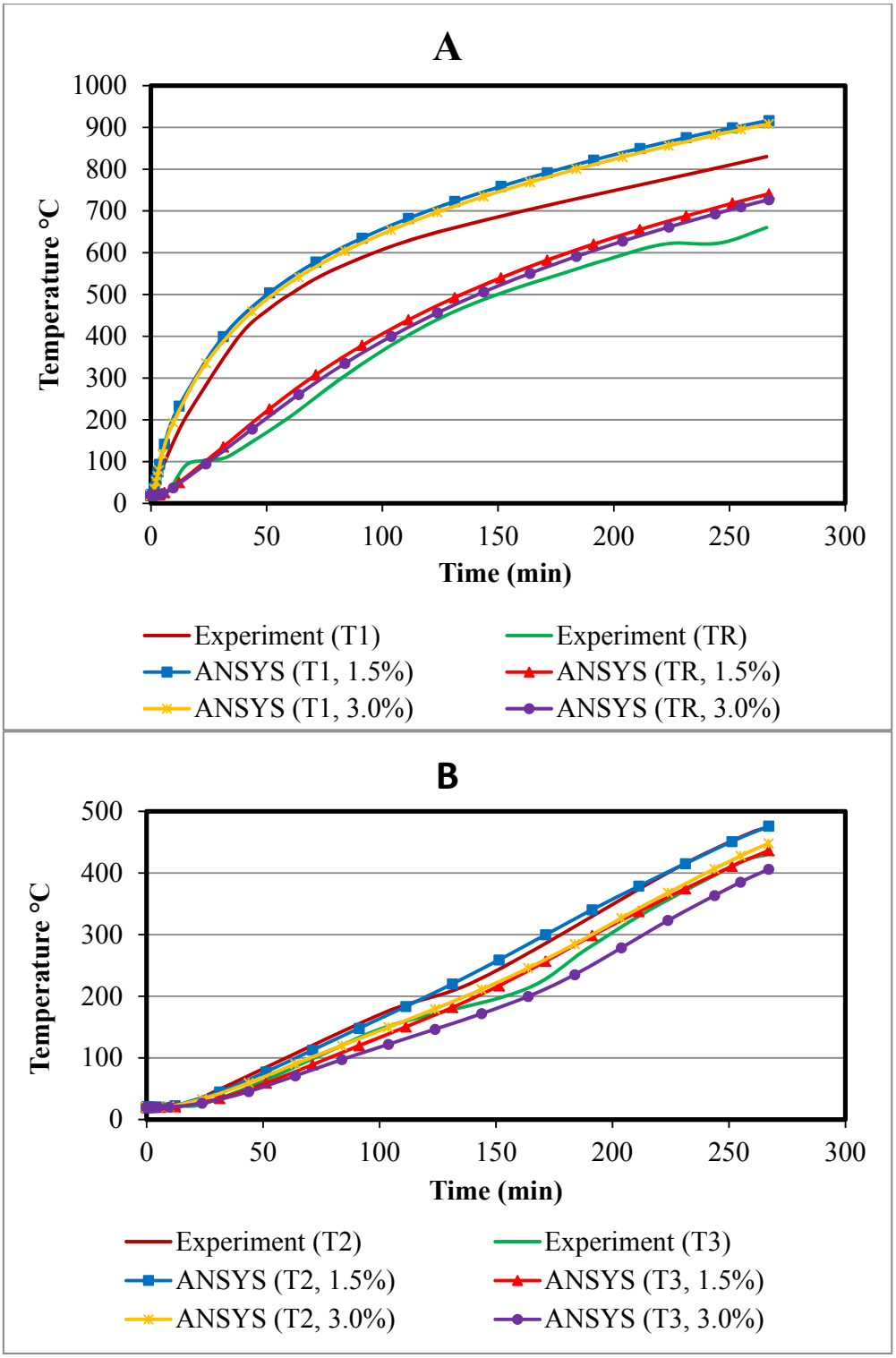

Figure 5:15: Comparison of experiment and predicted column temperature variation with different moisture levels (a) at T1 and TR, (b) at T2 and T3

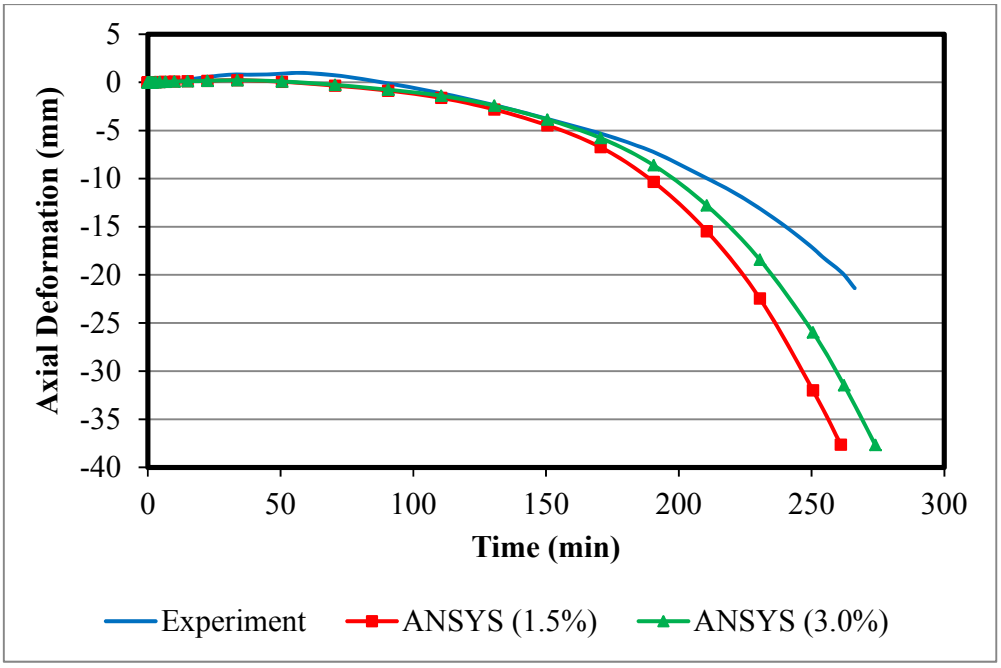

Figure 5:16: Comparison of experiment and predicted column deformation with different moisture levels

5.5.3 Concrete Stress – Strain Model for Column

Sensitivity analysis was performed in order to evaluate the influences of concrete's stress − strain model on ANSYS predicted column performance under fire conditions. The Kodur model, Knaack model, Eurocodes model and the proposed model in this study, as stated in Chapter 3, were selected for simulating the reinforced concrete column exposed to fire. The full stress – strain curve of the studied and proposed models were used. The axial deformations of the column using these models are compared and presented in Figure 5.17.

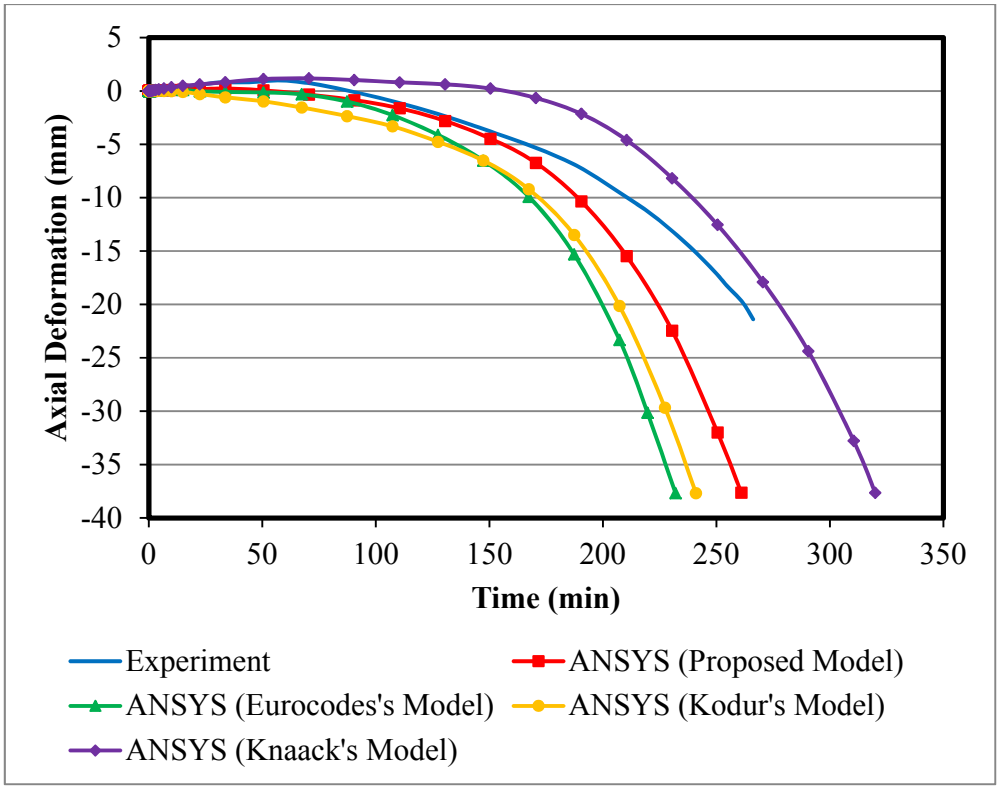

Figure 5:17: Comparison of experiment and predicted column deformation with different concrete mechanical models

As shown in Figure 5.17, the predicted axial deformation with the various concrete stress − strain models shows a similar trend to the measured experiment test result. The predicted result with these models captures the failure trend of reinforced column exposed to fire, with the column expanding at the initial stage and experiencing compression until failure at the later stages, due to sustained degradation of concrete and yielding of steel reinforced bars.

ANSYS predicted fire resistance times of the reinforced concrete column exposed to fire were 232, 241, 320 and 261 minutes with Eurocodes model, Kodur model, Knaack model and proposed model respectively. The Eurocodes model, Kodur model and the proposed model predicted a more accurate fire resistance time of the reinforced column, with the proposed model predicting a slightly more accurate fire resistance time than the Eurocodes and Kodur models. This also highlights the importance of the material model used, as different material models yield variations in the predicted fire resistance time of the column.

5.6 Parametric Studies for HSRC Column

The FE model was used to study various parameters affecting the performance of reinforced concrete column under fire. The parameters were fire type, structural load ratio, reinforcement ratio, column height, aggregate type and sectional dimension (concrete cover thickness, sectional shape and sizes).

5.6.1 Effect of Fire Type on HSRC Column

The influence of fire type was studied in order to evaluate its effect on temperature evolution and structural response of HSRC column subjected to fire conditions. The categories of fire used were standard and hydrocarbon fires. Temperature evolution and axial deformation obtained are presented and compared in Figures 5.18 − 5.19.

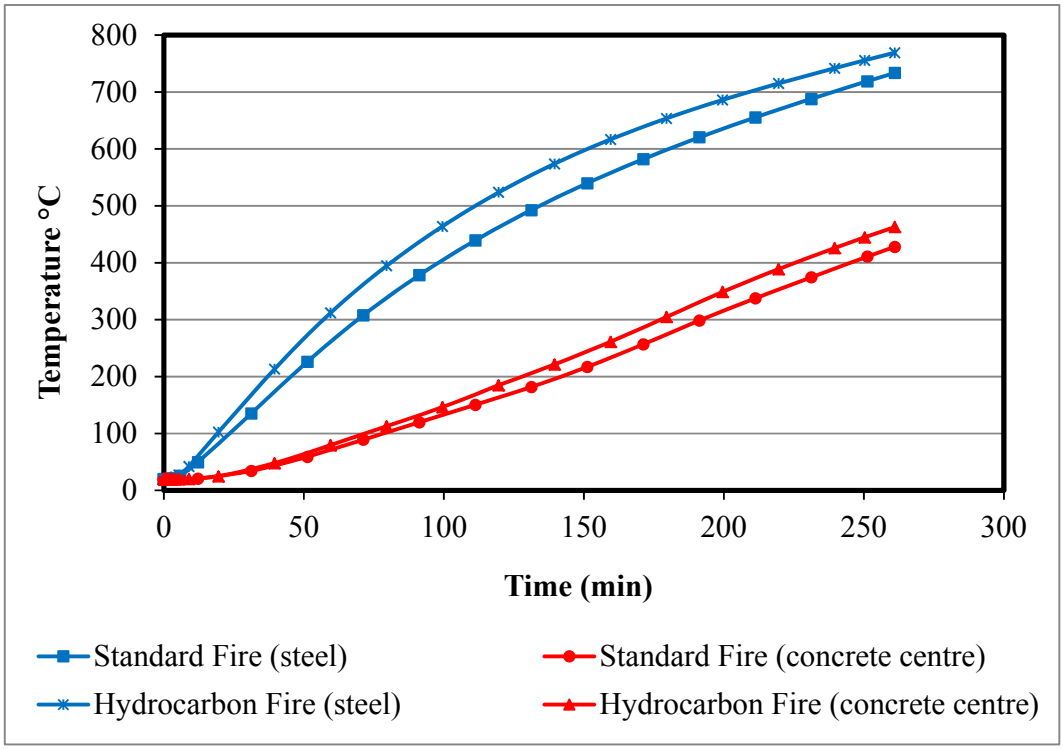

Figure 5:18: Effect of fire type on temperature evolution of column

Predicted time dependent temperatures of reinforcement bars as presented in Figure 5.18 are as expected, higher with hydrocarbon fires than with standard fires. The predicted steel temperatures of the column at a fire exposure of 261 minutes were about 770°C and 733°C with hydrocarbon and standard fires respectively. These higher temperatures are mainly attributed to the rapid rise of temperature within the first 10 minutes in hydrocarbon fires, while temperatures of standard fires increase at a less rapid rate. The predicted column centre temperatures with both fire types are very close at initial heating of about 140 minutes. Above this time range the concrete centre temperatures are higher with hydrocarbon fires, with a predicted temperature of about 465°C and 427°C using hydrocarbon and standard fires respectively. The similar concrete centre temperatures during the initial heating period can be attributed to less heat energy being transferred to the column centre at this stage, therefore exhibiting a low temperature difference, while with sustained fire exposure and increased heat energy transferred to the centre, the temperature difference becomes higher and therefore the effect of the fire type becomes more notable.

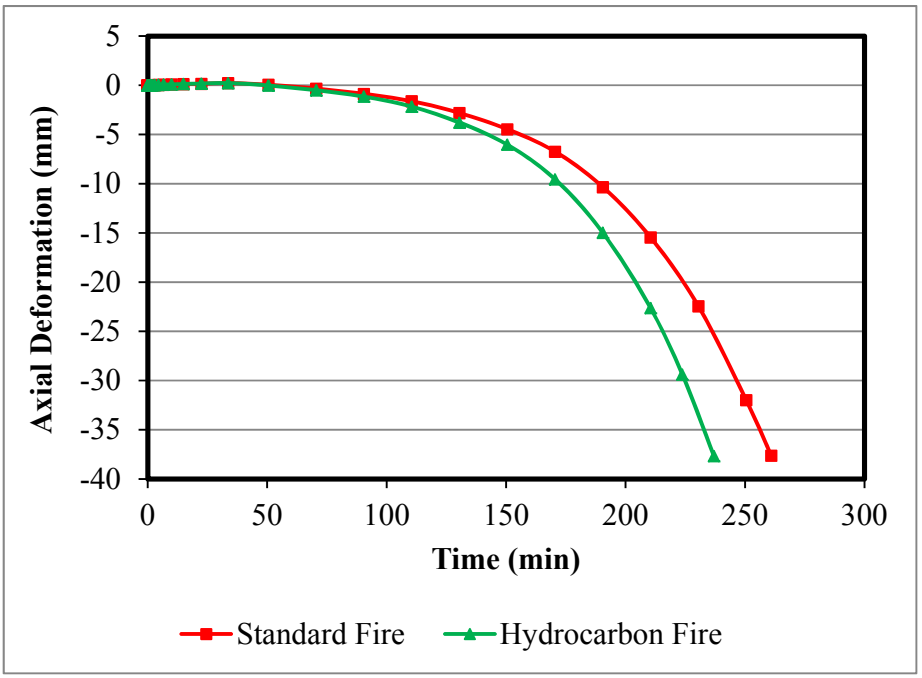

Figure 5:19: Effect of fire type on column deformation

The predicted axial deformation, as presented in Figure 5.19, indicated that with hydrocarbon fire the reinforced concrete column deforms at a faster rate than with standard fire, with an estimated fire resistance time of 237 and 261 minutes with hydrocarbon and standard fires respectively. This implies that fire type significantly affects the fire resistance of a reinforced concrete column, with a lower fire resistance for the column subjected to hydrocarbon fire and higher fire resistance under standard fire exposure.

5.6.2 Effect of Load Level on HSRC Column

The influence of load level was investigated in order to evaluate its effect on deformation and fire resistance of reinforced concrete column exposed to fire. Three load levels were considered for this study: 30%, 50% and 70%. The load level was evaluated as the ratio of applied load to column resistance at ambient temperature, as given in BS EN 1992-1-1:2004. The effects of load level on the performance of a reinforced concrete column subjected to elevated temperatures are illustrated in Figure 5.20.

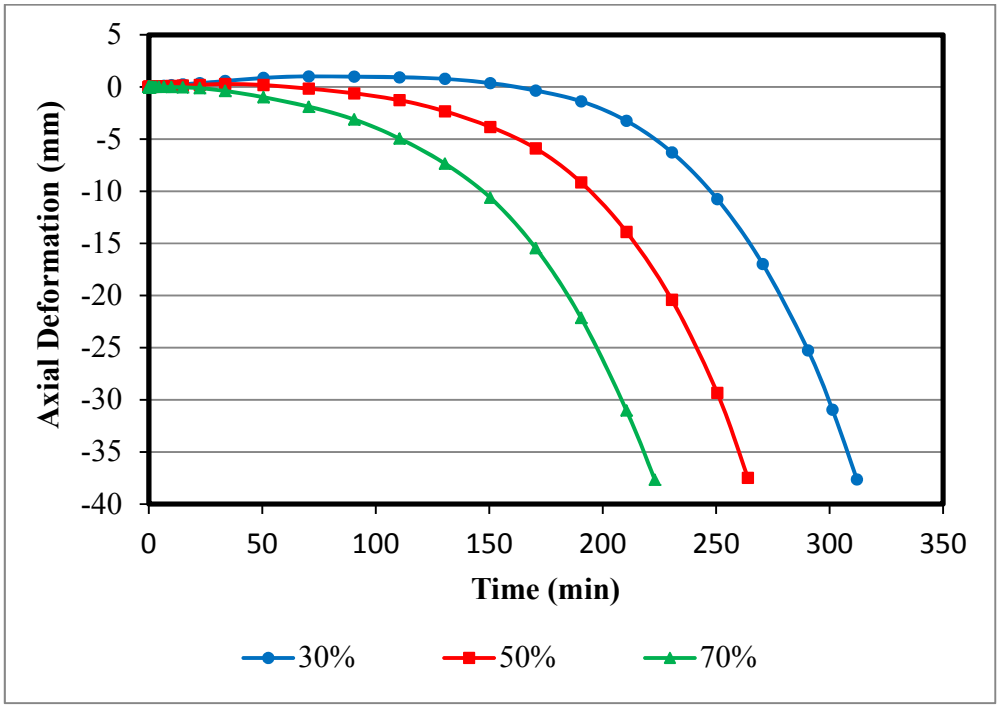

Figure 5:20: Effect of load level on column deformation

The predicted deformation of the column presented in Figure 5.20 implies that the performance of a reinforced concrete column is significantly influenced by the load level that the column supports. The column axial expansion is higher with a lower load level; this is because the total axial deformation of the column is a combination of thermal strain and load induced strains (elastic strain and transient stain). Therefore, with lower load levels the load induced strains are less, which leads to more expansion, and with higher load levels the load induced strains are more with less axial expansion and more axial compression of the column. The predicted fire resistances are 312, 264 and 223 minutes for 30%, 50% and 70% load ratios respectively. Overall the fire resistance of the column is lower with higher load ratios. This is attributed mainly to higher axial compressive deformation of the column under higher load ratios, with a reduction in the load bearing capacity of the reinforced concrete column due to continual degrading, loss of strength and stiffness of steel and concrete material under elevated temperatures in fire conditions.

5.6.3 Effect of Reinforcement Ratio on HSRC Column

The effect of the reinforcement ratio on the fire resistance of HSRC columns subjected to fire was investigated. Three reinforcement ratios, 1.0%, 2.5% and 4.0%, were selected for this study with a constant load ratio of 55%. The reinforcement ratio was calculated as the ratio of longitudinal steel cross section area to concrete sectional area as given in BS EN 1992-1-1:2004. The effect of reinforcement ratio on the performance of a reinforced concrete column exposed to fire is illustrated in Figure 5.21.

The column axial deformation and predicted fire resistance are similar for all three reinforcement ratios, when the column is loaded to a constant load ratio of 55%. This implies that reinforcement ratio has little or low influence on the fire performance of a reinforced concrete column with the column loaded with equal load ratios. The reinforcement ratio would have an influence on the fire performance of the column when the column is subjected to the same load values with different reinforcement ratios. Therefore, with higher reinforcement ratios, the column resistance increases and the load ratio decrease. As presented above, columns subjected to higher load levels have less fire resistance time in comparison to columns subjected to lower load levels.

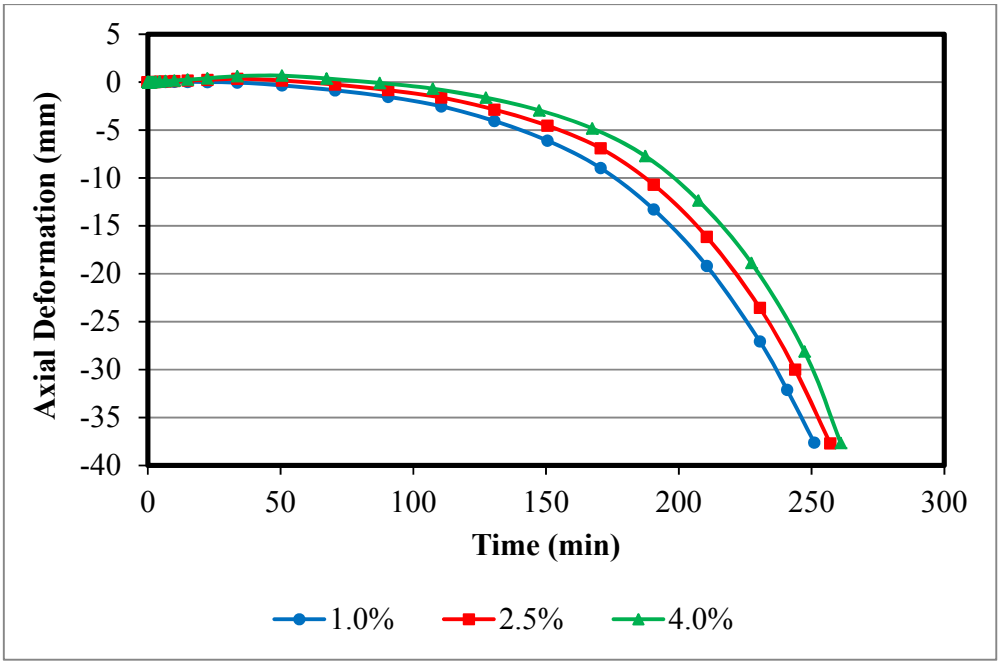

Figure 5:21: Effect of reinforcement ratio on column

5.6.4 Effect of Sectional Shape and Size on HSRC Column

The effect of sectional shape and size was investigated to evaluate its influence on the performance of reinforced concrete columns exposed to fire. To study the effect of sectional shape, square and rectangular shaped columns were selected with sectional dimensions of 305 x 305mm and 250 x 372mm. Both columns had approximately equivalent sectional areas and were subjected to equivalent load levels of 52%. The temperature distribution, axial deformation and fire resistance obtained are presented and compared in Figures 5.22 and 5.23.

From Figure 5.22, the temperature at the centre of the section is higher with 250mm width, with a value of around 467°C, while for 305mm width a temperature of about 427°C was obtained. This implies that with the column exposed to fire on all four sides, the heat transfer and concentration increases with smaller width.

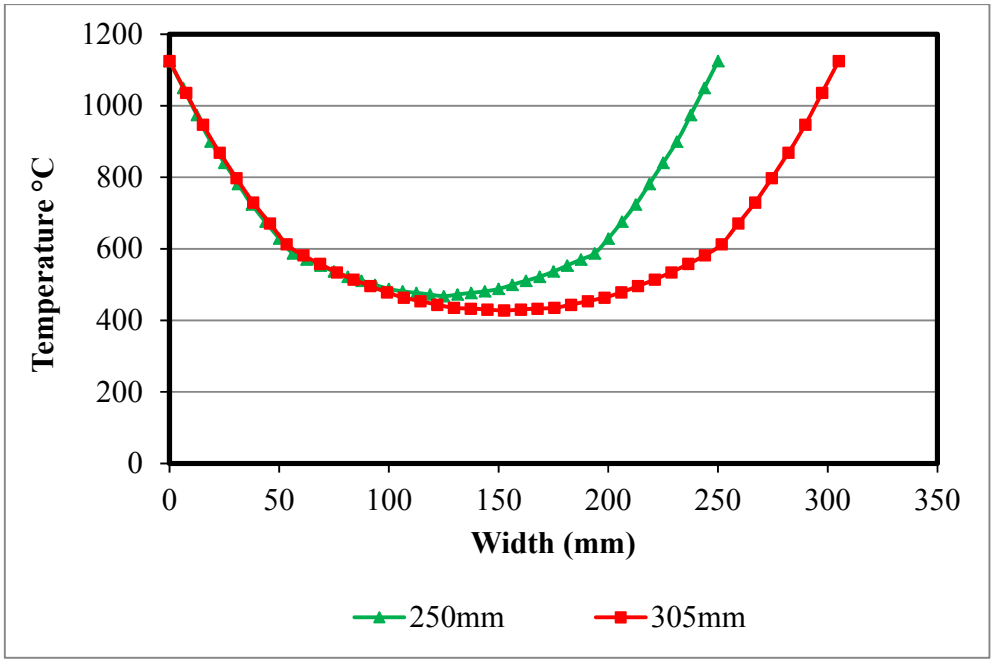

Figure 5:22: Effect of column width

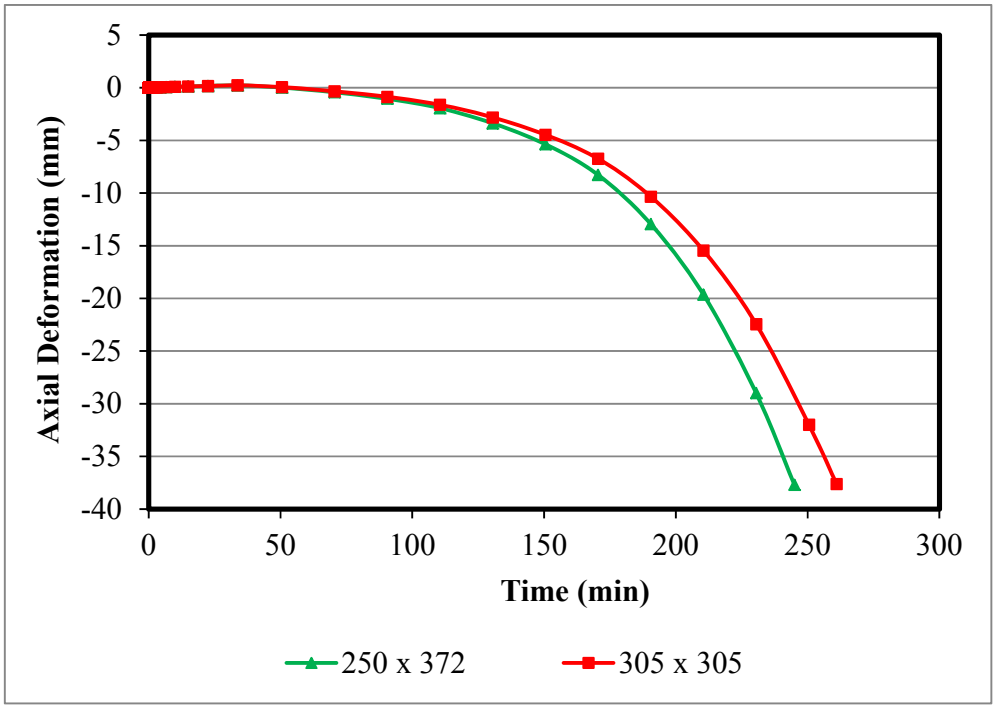

Figure 5:23: Effect of column shape

With a square sectional area, a fire resistance time of 261 minutes was predicted and 245 minutes with a rectangular section. The lower fire resistance with a rectangular section can be attributed to the smaller width, which significantly increases heat and temperature transmission across the section. Also, a rectangular section has a larger perimeter when compared with its equivalent square section and therefore has a larger surface area exposed to fire, which increases the heat energy distributed to the column.

The influence of column sectional size on the performance of reinforced concrete columns under fire conditions was investigated. Two square section sizes of 305 x 305mm and 250 x 250mm subjected to equivalent load level of 52% were selected. The effects of sectional size are illustrated in Figure 5.24.

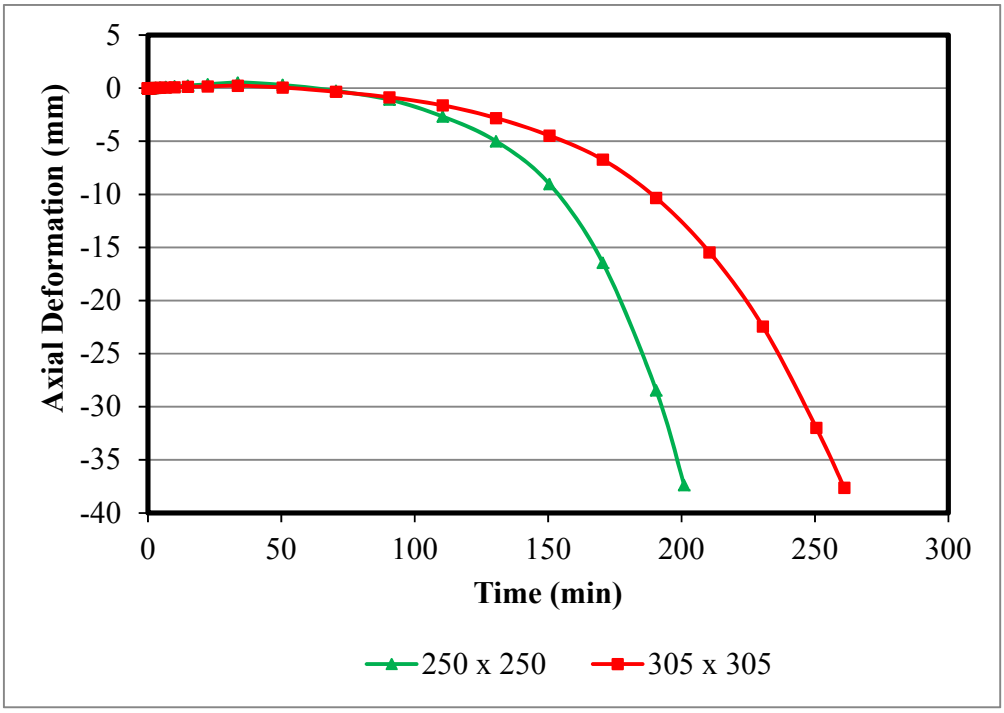

Figure 5:24: Effect of column sectional area

The results presented in Figure 5.24 indicate that sectional size has a significant influence on fire resistance of reinforced concrete columns. The column with 250mm square section has a lower fire resistance time of 201 minutes, while the column with 305mm square section has fire resistance time of 261 minutes. This can be attributed to the smaller sectional area, which increases heat concentration across the section as shown in Figure 5.22.

5.6.5 Effect of Concrete Cover Thickness on HSRC Column

The effect of concrete cover thickness was examined to determine its influence on the performance of reinforced concrete columns under fire conditions. Clear concrete cover thicknesses of 30mm and 50mm were used for this study, with the section size of 305 x 305mm maintained. The effects of the concrete cover are illustrated in Figures 5.25 – 5.26.

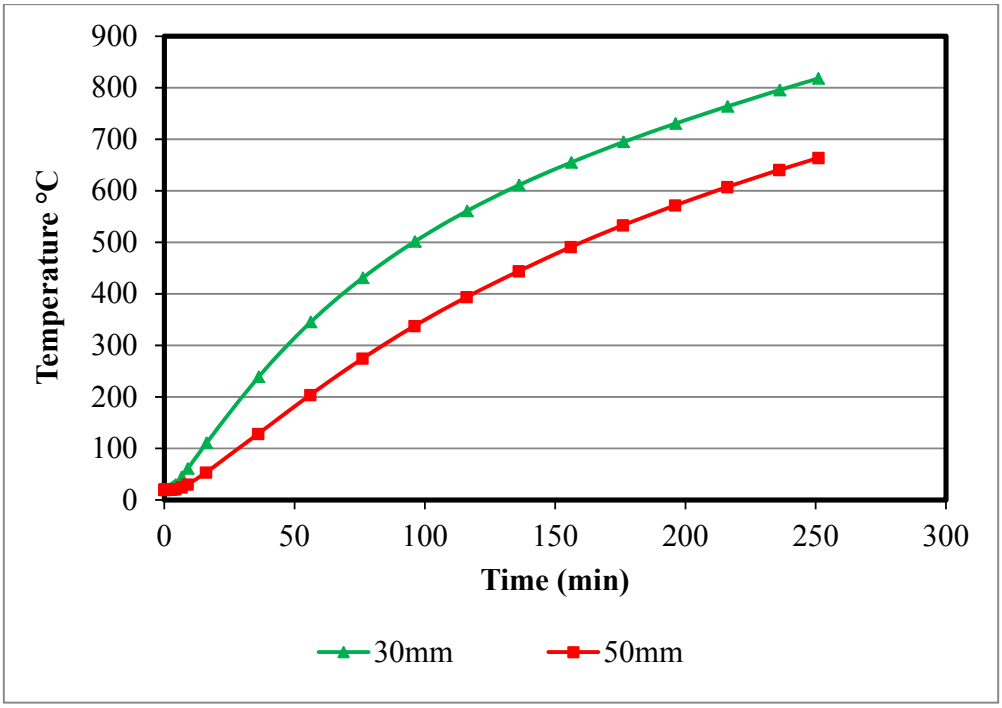

Figure 5:25: Effect of concrete cover on temperature evolution of reinforcement

It can also be seen from Figure 5.25 that the concrete cover significantly influences the steel temperature, with higher temperatures for a 30mm concrete cover. This is mainly attributed to the fact that heat transfers faster across a shorter distance and therefore with 30mm cover heat energy is transferred quicker to the steel in comparison with a 50mm concrete cover.

It can be seen from Figure 5.26 that the fire resistance of the column is slightly higher with 50mm concrete cover thickness, with a fire resistance time of 265 minutes, while a fire resistance time of 251 minutes was predicted using a 30mm concrete cover. Therefore, the concrete cover thickness has a moderate influences on fire resistance of the column.

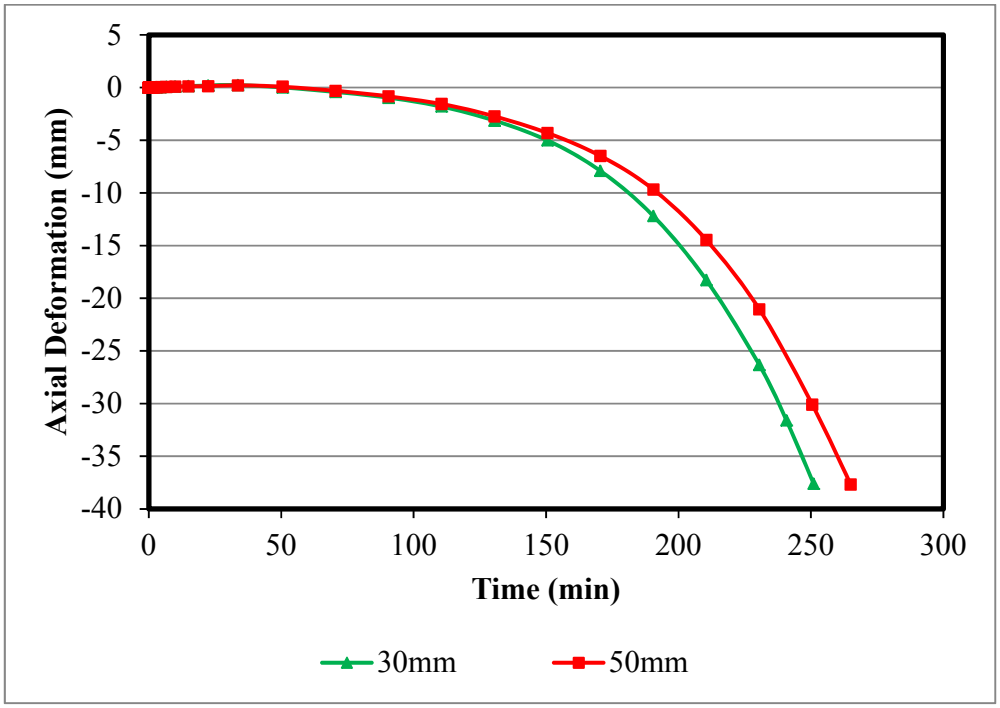

Figure 5:26: Effect of concrete cover on deformation of column

5.6.6 Effect of Column Height

The influence of column height was examined to determine its effect on fire performance of reinforced concrete columns under fire conditions. Column heights of 2520, 3150 and 3760mm were selected for this study with the section size of 305 x 305mm maintained and all other parameters kept constant. The effects of column height are presented in Figure 5.27.

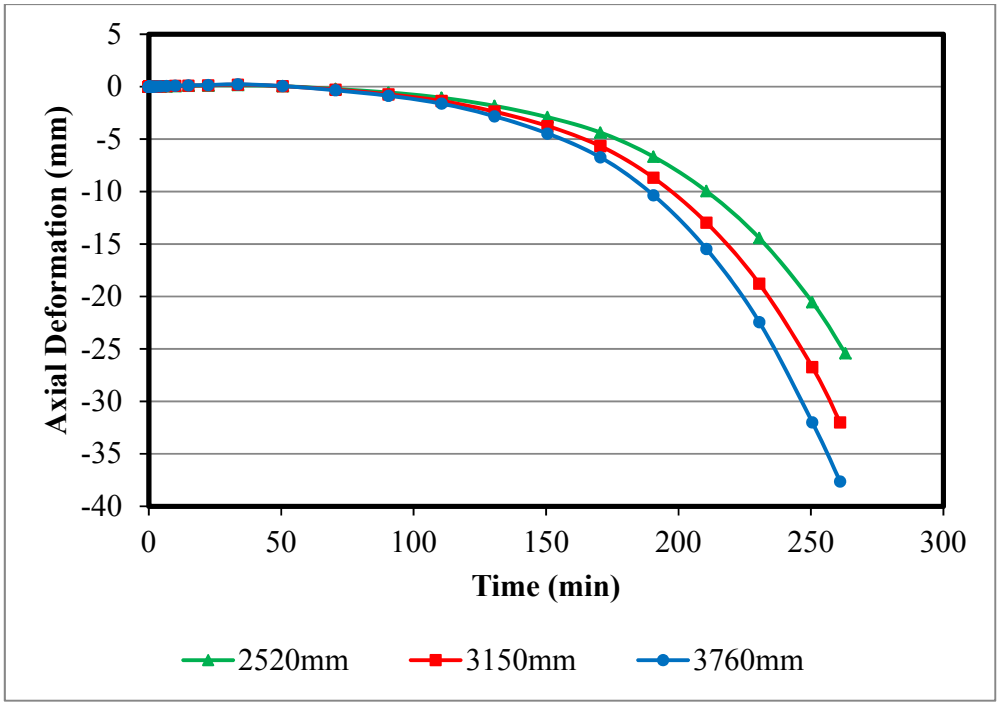

Figure 5:27: Effect of column height

As shown in Figure 5.27 and Table 5.3, the predicted fire resistance was 263, 261 and 261 minutes with column heights of 2520, 3150 and 3760mm respectively. This indicates that column height has little or low influences on fire performance of an axially loaded short reinforced concrete column.

5.6.7 Effect of Aggregate Type on HSRC Column

The effect of aggregate type on the fire resistance of reinforced concrete columns was examined. For this study, siliceous and carbonate aggregate concrete were tested and the predicted fire resistances and deformation of the columns are illustrated in Figure 5.28 and Table 5.3. The result indicates that the aggregate type has little or low effect on the fire resistance of an RC column, with a predicted fire resistance of 270 minutes and 261 minutes with siliceous and carbonate aggregate respectively.

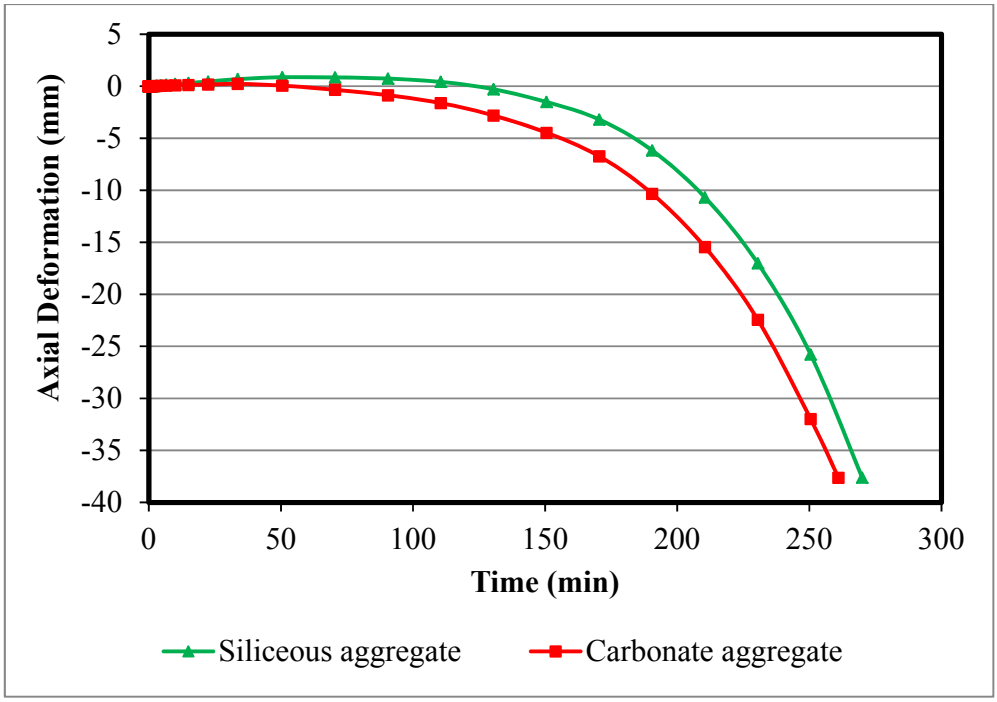

Figure 5:28: Effect of aggregate on HSRC column

5.6.8 Effect of Transient Strain HSRC Column

This study was conducted to determine the effect of including and excluding transient strain on the predicted column fire resistance. The effect of transient strain is presented in Figure 5.29. With inclusion of transient strain predicted column fire resistance was 261 minutes and was 305 minutes without transient. Therefore including transient strain predicts more accurate column fire resistance.

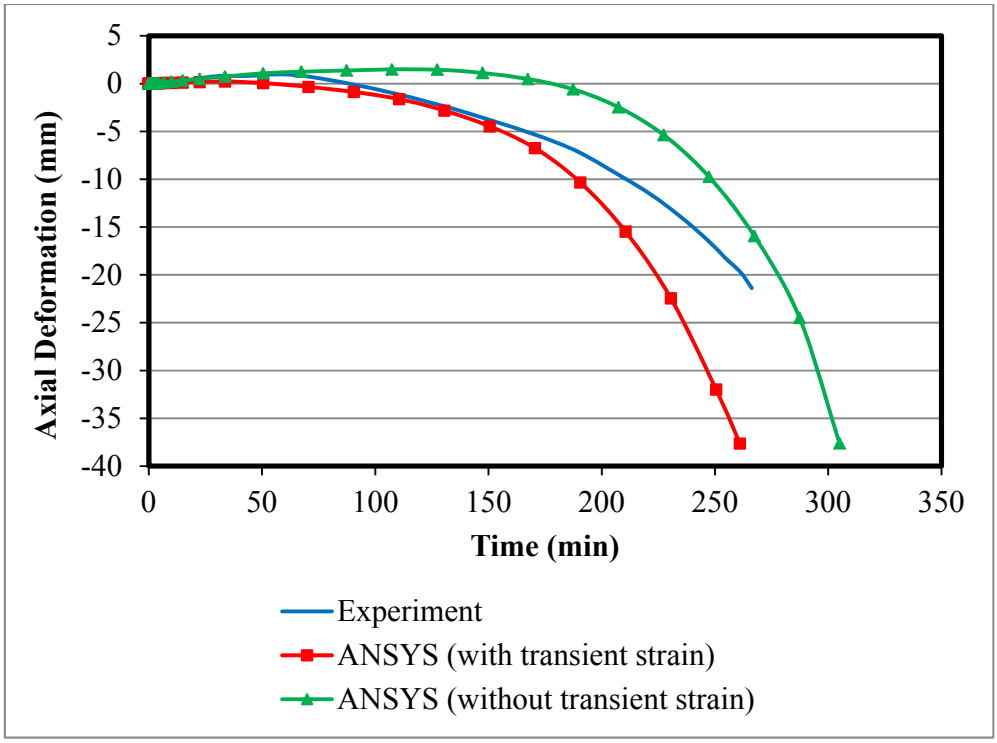

Figure 5:29: Effect of transient on HSRC column

A summary of the predicted HSRC column fire resistances from the conducted parametric studies is presented in Table 5.3.

5.7 Comparisons between Predicted Column Fire Resistance with ANSYS and EC2 Prescriptive Approach

Predicted column fire resistances presented in Tables 5.2 and 5.3 indicate that the prescriptive column design approach is conservative as it predicts a lower column fire resistance in comparison with ANSYS and the measured experiment column fire resistance. This result also indicates that the performance based approach using ANSYS predicts a more accurate column fire resistance than that of the EC2 prescriptive approach. Using the performance based approach, the fire performance of the column was evaluated under hydrocarbon fire curves as presented in Table 5.3, whereas the prescriptive design approach is only valid for standard fire.

Table 5:3: Predicted column fire resistance

Column size (mm)	Varying Parameter		Fire resistance (min)	
	Parameter	Value/type	Performance based (ANSYS)	Prescriptive (EC2)
305x305x3760	Fire type	Standard fire	261	116
305x305x3760		Hydrocarbon	226	-
305x305x3760	Load level (%)	30	312	186
305x305x3760		50	264	119
305x305x3760		70	223	103
305x305x3760	Reinforcement ratio (%)	1.0	251	114
305x305x3760		2.5	257	114
305x305x3760		4.0	261	114
250x250x3760	Sectional size (mm^2)	250	201	73
305x305x3760		305	261	116
305x305x3760	Concrete cover (mm)	30	251	90
305x305x3760		50	265	133
250x372x3760	Shape	Rectangular	245	73
305x305x3760		Square	261	116
305x305x2520	Column height (mm)	2520	263	116
305x305x3150		3150	261	116
305x305x3760		3760	261	116
305x305x3760	Aggregate type	Siliceous	270	116
305x305x3760		Carbonate	261	116

5.8 Summary

The FE model for predicting the fire resistance of an HSRC column was developed and verified by comparing the predicted temperature evolution, deformation and fire resistance with results from a fire resistance test. The predicted results show similar trends and good agreement with the fire test. Sensitivity analysis was conducted to ascertain the value of major aspects of the model that would yield optimum results and to verify the reliability of the proposed material model for

HSC. The result from the sensitivity analysis indicated that, using the lower limit thermal conductivity model given in BS EN 1992-1-1:2004, a moisture content of 1.5% and the proposed concrete stress − strain model predicted a more accurate fire resistance of HSRC columns.

By means of the verified FE model, parametric studies were performed to evaluate the influence of major factors affecting the fire performance of HSRC columns exposed to fire. The results indicated that fire scenarios, load level and sectional size significantly influence the fire resistance of HSRC columns. While concrete cover moderately influences fire performance of HSRC columns. Under constant load level, reinforcement ratio, aggregate type and column height has low influence on fire performance of HSRC columns exposed to fire.

Chapter 6 : Fire Resistance Simulation for HSRC Beam

This chapter presents the development, validation and FE analysis of an HSRC beams simulated under fire conditions. Based on a comprehensive sensitivity analysis, the optimum values of major parameters of the model are selected. Parametric studies on major factors influencing the fire performance of HSRC beams are evaluated. Fire resistances using a performance based approach with ANSYS are evaluated and compared with those obtained using the prescriptive design approach given in BS EN 1992-1-2:2004.

6.1 Development of Beam Finite Element Model

A high strength reinforced concrete beam under fire conditions was simulated by developing a three-dimensional (3D) Finite Element (FE) model using commercial Finite Element software ANSYS. The model includes the concrete thermal and mechanical properties, reinforced steel thermal and mechanical properties, restraint conditions, heat transfer, fire model and structural loads. The geometric parameters of the model include the beam length, breadth, depth, concrete cover and the size of the reinforcement bars. The model comprises concrete and steel reinforcement bars, owing to symmetry of the beam only half was modelled. Concrete was created as volume while the reinforcement bars were created as lines inside the concrete. This was achieved by creating the volume using the down-up modelling techniques and applying reinforcement bar sizes and steel properties for the required lines. The thermal and mechanical contacts between the reinforcement and concrete were assumed to be perfectly bond in order to simplify convergence of the solution and be less complicated. The concrete was meshed using SOLID70 hexagonal (8-node) thermal solid element with thermal capabilities, while the reinforcement bars were meshed with LINK33, which is a 2-node line element with thermal functions. In the structural phase of the analysis, these elements are substituted with their structural equivalent of SOLID185 and LINK180. The properties and attributes of these elements were given in Chapter 4. Element size was determined by using fracture energy method proposed by Carstensen *et al.*, (2013). From this method the suitable element sizes obtained was 18 – 192mm and therefore 20mm element size was adopted, which proved to be satisfactory for controlling the mesh density. The beam was simply supported at the bottom, the FE model is presented in Figure 6.1.

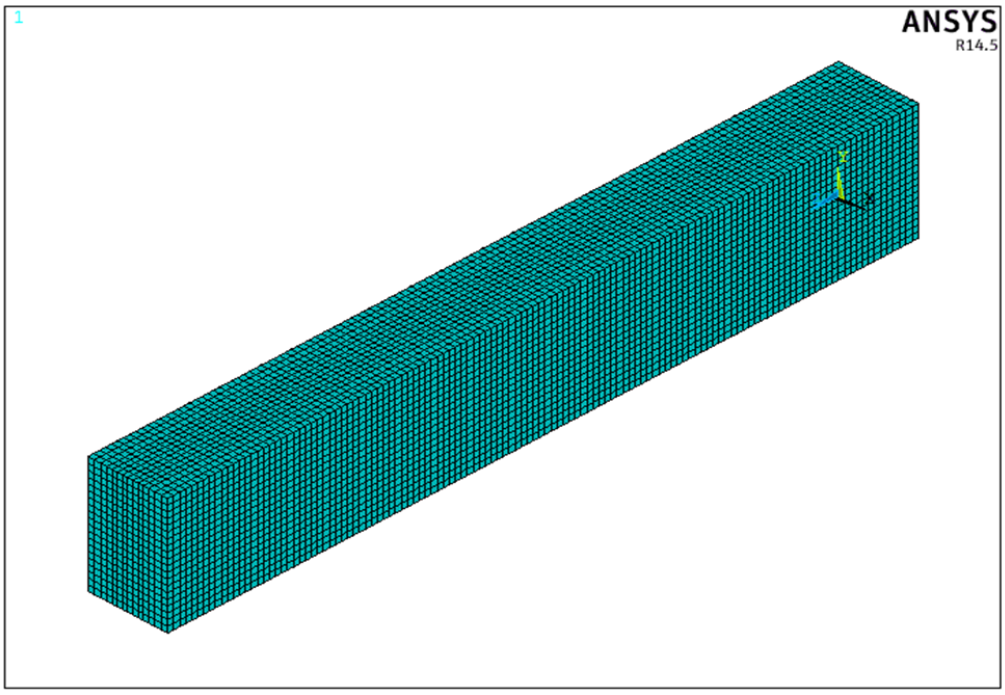

Figure 6:1: FE model of HSRC beam

6.2 Beam Model Validation

The FE model was validated in two stages. Firstly, the model was validated by comparing the thermal results with experiment test results, and in the next stage the structural response and fire resistance were validated with experiment results. The three-dimensional (3D) FE model was validated by comparing the results with Choi and Shin's (2011) experimental fire test on the structural behaviour of reinforced concrete simple supported beams under fire. The thermal response was validated with temperature variation at the concrete surface and reinforced steel, while the structural performance was validated with time dependent maximum deflection at the middle of the beam and fire resistance time.

Choi and Shin (2011) presented the response of four reinforced concrete beams fabricated and tested under elevated temperatures. Two beams were made of high strength reinforced concrete while the others were designed with normal strength reinforced concrete. For this study, only the high strength reinforced concrete beams were used. The beams were simply supported with a clear span of 4500mm between supports and a total length of 4700mm, with a section dimension of 250mm wide and 400mm deep. The compressive strength of the concrete was 55MPa and was

made with siliceous aggregate. It was reinforced with three high tensile 22mm bars at the tension zone and two high tensile 22mm bars at the compression zone, with 10mm bars provided as links at 150mm spacing. The strength and elastic modulus values for the longitudinal bars were 439MPa and 156GPa, and 390MPa and 172GPa for the link bars.

The beams were loaded under a four point loading system with a total load of 96.3kN and were subjected to elevated temperatures on 3 sides and approximately 4500mm length in a fire chamber, with temperatures controlled in accordance with the ISO 834 standard fire curve. Further details of the beams are given in Figure 6.2 and Table 6.1. Choi and Shin (2011) observed from their test, that significant spalling occurred at top half of the beam. This resulted in rapid rise of temperature at the top half of the beam. In order to account for this rapid raise in temperature, the top half of the beam was modelled with upper limit thermal conductivity, while the bottom half of the beam was modelled with lower limit thermal conductivity model proposed in BS EN 1992-1-2:2004. This helped in predicting more accurate temperatures at top section, when compared with lower limit thermal conductivity model as obtained in the sensitivity analysis in Section 6.5.

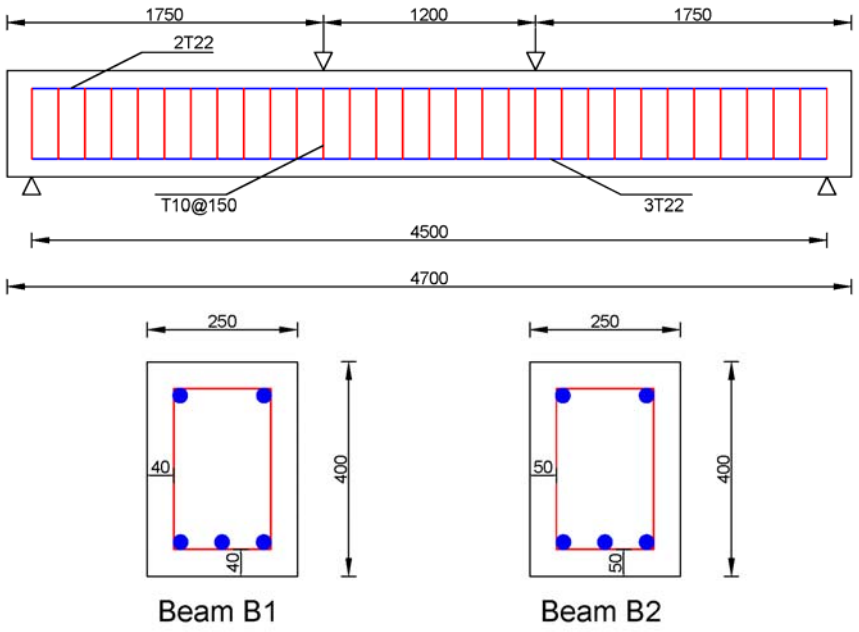

Figure 6:2: RC beam details

Table 6:1: Beam details

Beam Parameters	Beam B1	Beam B2
Beam size	250×400×4700mm	250×400×4700mm
Concrete strength	55MPa	55MPa
Reinforcement yield strength	439MPa for main bars	439MPa for main bars
	390MPa for link bars	390MPa for link bars
Number of reinforcements	3 ϕ 22mm bottom bars	3 ϕ 22mm bottom bars
	2 ϕ 22mm top bars	2 ϕ 22mm top bars
	ϕ 10mm link bars @ 150c/c	ϕ 10mm link bars @ 150c/c
Clear reinforcement cover	40mm	50mm
Total applied load (kN)	96.3	96.3
Aggregate type	Siliceous	Siliceous
Restraint	Simply supported	Simply supported

6.3 Thermal Validation and Response of Beam

The thermal response and heat transfer of a reinforced concrete beam simulated under fire conditions was obtained from thermal analysis. This includes temperature distribution across the beam at mid-span and temperature evolution of concrete and steel reinforcement bars.

6.3.1 Temperature Distribution within Beam

Temperature distributions across the beam width and along the geometric centroid of the beam, is presented in Figures 6.3. Across the beam width, the temperature decreases from the heated surface to the beam centre. This temperature distribution across the beam width indicates that heat transfer occurs through conduction from a region with high temperature to a region of lower temperature. The temperature of the heated surface and through the beam section also increases with a sustained and increase in fire exposure duration.

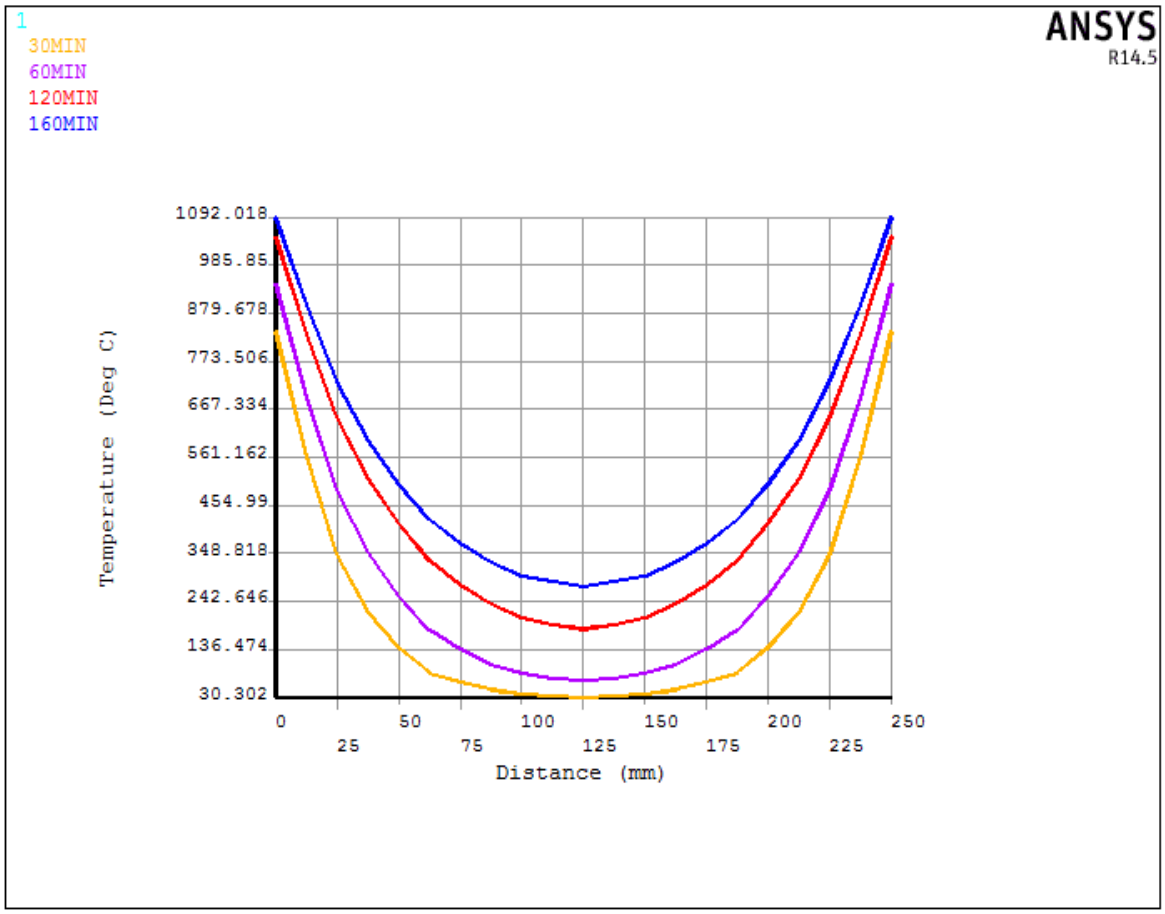

Figure 6:3: Temperature distribution across beam width

6.3.2 Temperature Variation of Beam

The temperature evolution at the concrete surface, concrete centre, corner and middle reinforcements are presented in Figure 6.4. These temperatures increase with sustained fire exposure due to heat transfer. At the early stages of heating, the temperature of the heated surface rises rapidly, reaching about 800°C within 25 minutes. Beyond this, the concrete's surface temperature increases gradually at a less rapid rate, as explained in Chapter 5, while throughout the heating duration, the reinforcement and beam centre temperatures increase gradually with an approximate linear relationship with time. This is attributed to the fact that heat conduction is the source of heat transfer across the beam section and is dependent on distance between the transfer medium and points. The temperature of the corner reinforcement is also higher than the temperature of the middle reinforcement. This is expected as heat energy and transfer is greater at the corner of the beam than at the middle due to two heated surfaces at the bottom corner of the beam.

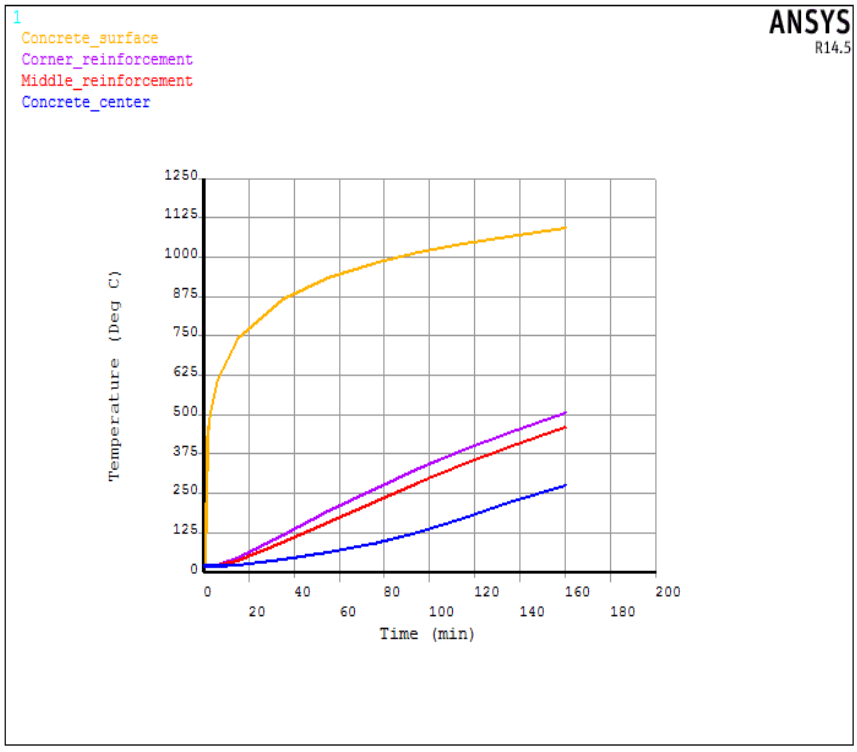

Figure 6:4: Temperature evolution within beam

6.3.3 Thermal Validation of Beam

Thermal validation was achieved by comparing the measured time dependent temperatures at various points within the beam with results from the FE analysis. The locations of these validated points are shown in Figure 6.5.

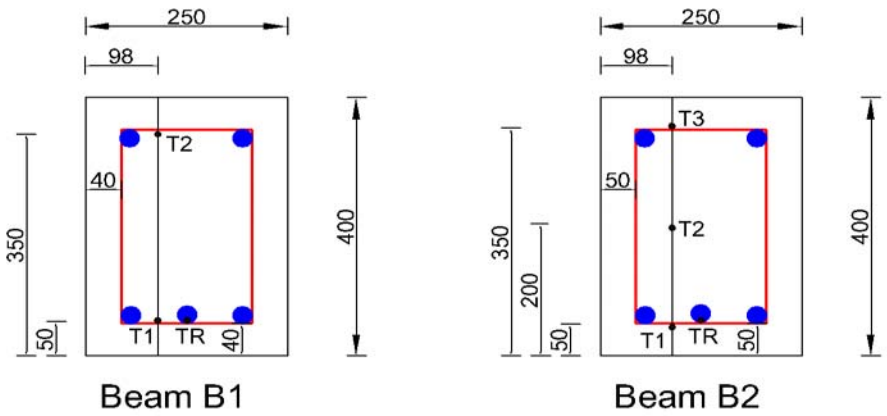

Figure 6:5: Validated temperature points within beam

Figure 6.6 – 6.7 presents the comparisons of predicted beam temperatures and experiment results.

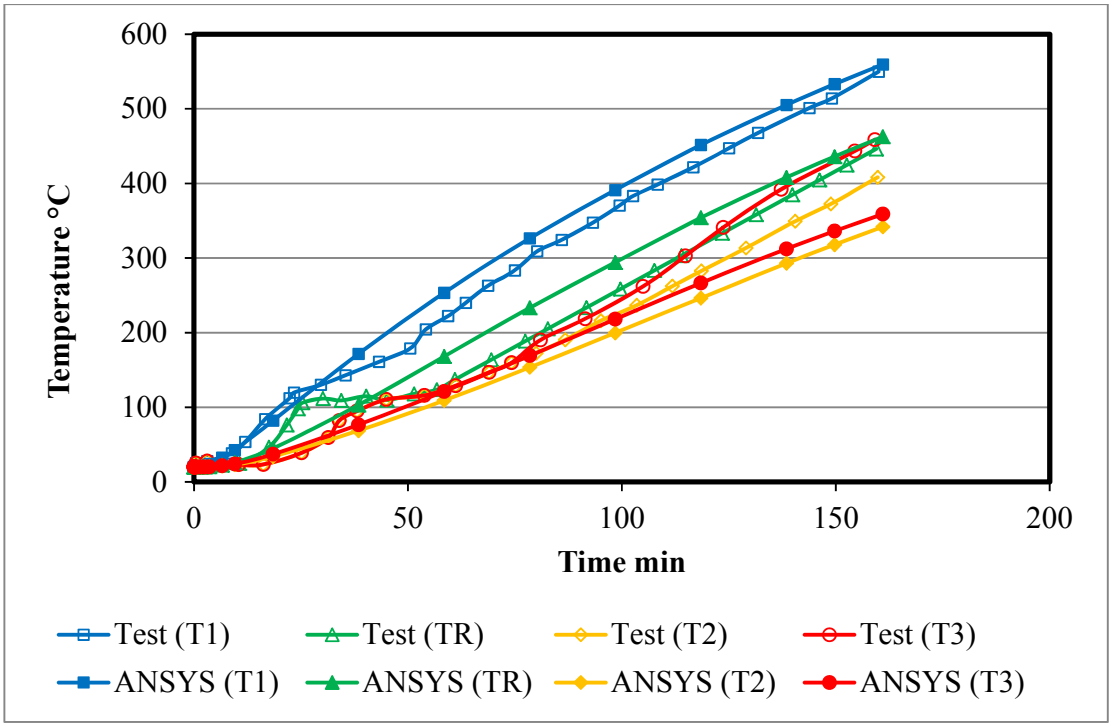

Figure 6:6: Predicted and experiment temperature evolution within beam B2

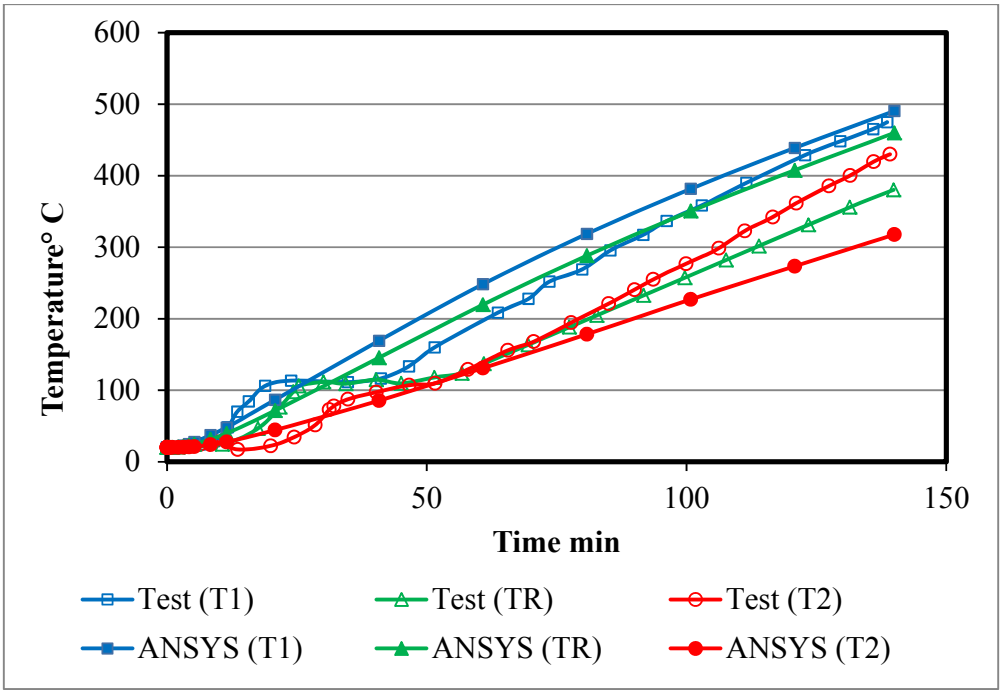

Figure 6:7: Predicted and experiment temperature evolution within beam B1

The predicted temperatures at point T1 and TR (steel) for beam B2 show good conformity when compared with fire test results, with slight differences. These variations can be attributed to a moisture evaporation effect; there is a significant delay in increase of test temperatures around 100 − 115°C within the beam, as most of the heat energy around this temperature range is used for evaporation and migration of moisture in the reinforced concrete. It should be noted that the moisture content was indirectly accounted for in the FE model through the specific heat capacity and in order to obtain more accurate temperature results a complete hydro-thermal simulation would be required, which would be very complex. These discrepancies can also be attributed to the fact that the contact between the concrete and reinforcement was assumed to be perfect rather than non-perfect bond, as a non-perfect bond would better represent the actual bond between the steel and concrete. As it is expected, the bond between the concrete and steel would lead to a delay in conduction from the concrete to the steel reinforcement bars. Again, due to complex nature of the problem in the modelling and solution convergences phase, it was modelled as a perfect contact. Predicted temperatures at point T1 for beam B1 shows good conformity when compared with fire test results while at point TR (steel) predicted temperatures show some variation with test result. As explained earlier this variations can be attributed to the moisture evaporation effect around 100 − 115°C and also the bond between the concrete and reinforcement, which was assumed to be perfect bond.

From Figure 6.6 – 6.7, it can be seen that FE simulation predicts accurate temperatures at point T2 and T3 at initial heating up to 100 minutes of fire. Above this heating range, predicted temperatures show discrepancies with measured temperatures. These discrepancies can be attributed to rapid rise in temperature due to spalling which occurred at the top section of the beams. It should be noted that the rapid rise in temperatures at top half of the beam was indirectly accounted for in the FE model by using upper limit thermal conductivity model as proposed in BS EN 1992-1-2:2004. This helped in predicting more accurate temperatures at top section, when compared with lower limit thermal conductivity model as obtained in the sensitivity analysis in Section 6.5. Overall, the predicted temperatures show some good agreement with fire test results.

6.4 Structural Validation and Response of Beam

The structural time response of a reinforced concrete beam was obtained from a coupled field analysis. This includes fire resistance and temperature − time dependent mid-span deflection.

6.4.1 Beam Deflection

The predicted mid-span deflection of the reinforced concrete beam simulated under fire is presented in Figure 6.8.

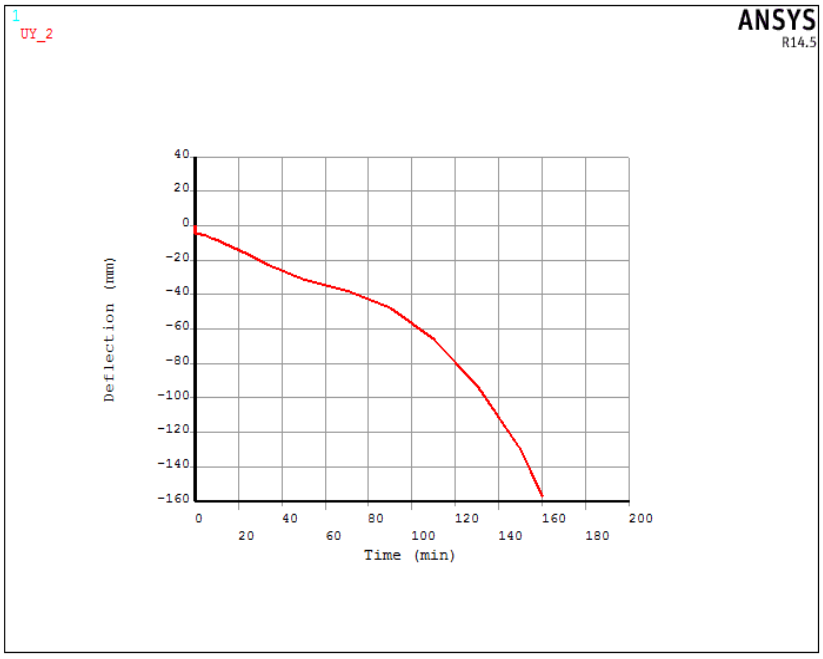

Figure 6:8: Predicted mid-span deflection of beam B2

The model captures the accurate response pattern of a reinforced concrete beam exposed to fire. This response can be categorised into two stages. In the first stage the beam deflects under structural load without the application of elevated temperature. In the second stage the deformation of the beam increases with elevated temperatures until failure. These continuous deflections of the beam under elevated temperatures are attributed to loss of strength and stiffness of the concrete and steel material.

Throughout the heating period the beam undergoes sagging deflections. At heating range of about 1 – 90 minutes the beam deflection continually increases but at a slow rate. At 120 minutes

and above the deflection in beam continue to increase with a higher rate of deflection until failure.

6.4.2 Beam Stress Distribution

Longitudinal stress distributions and stress profile along the beam centroid depth obtained from the FE model is presented in Figure 6.9 and Figure 6.10.

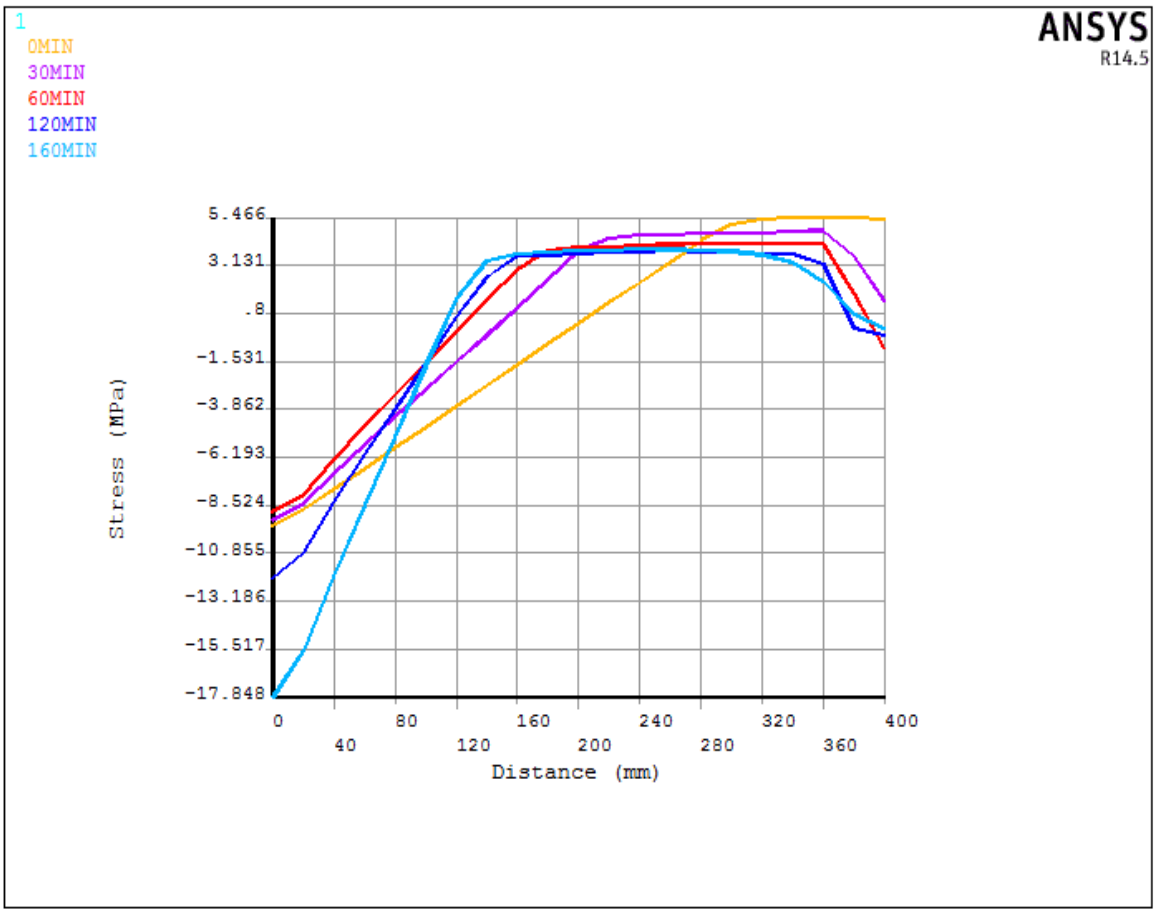

Figure 6:9: Stress distribution of beam B2 across beam depth at beam centre

From Figure 6.9, it can be seen that throughout the heating the beam experiences compressive stresses at the top and tensile stresses at bottom. The tensile stress continually decreases as the temperature increases which can be attributed to degradation of concrete material at elevated temperatures. The stress distribution also indicates that before subjecting the beam to elevated, the beam experiences maximum tensile stresses at the bottom surface.

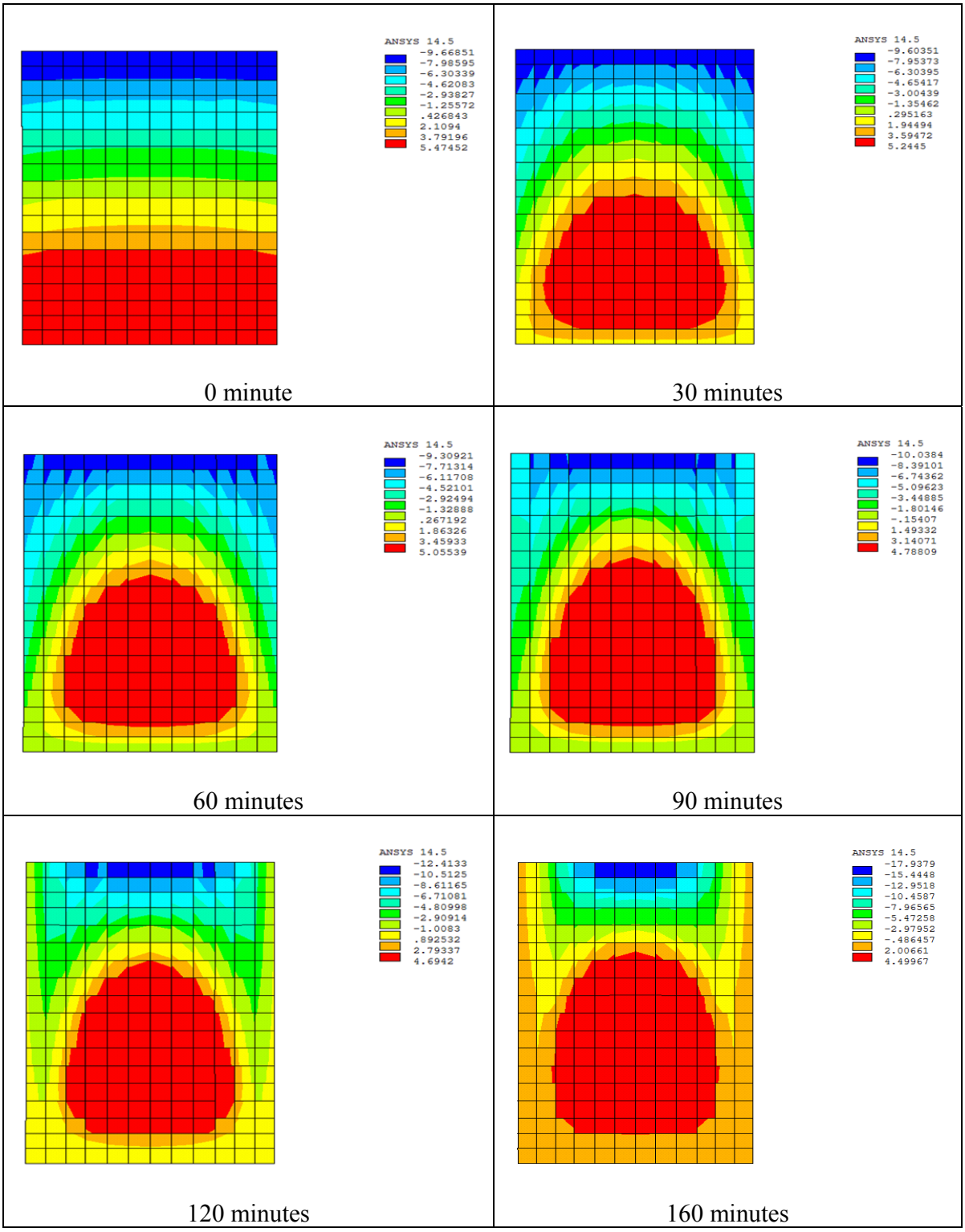

Figure 6:10: Stress profile of beam B2 at beam centre

As the beam is continually subject to elevated temperatures, the location where the maximum tensile stress occurs and neutral axis continues to move inward. This can be attributed to loss of load bearing capacity and material degradation at elevated temperatures.

6.4.3 Structural Validation of Beam

The structural validation of the FE model was achieved by comparing predicted temperature − time dependent mid-span deflections and fire resistance of the reinforced concrete beam with fire test results. These compared results for beams B1 and B2 are presented in Figures 6.11 and 6.12 and Table 6.2.

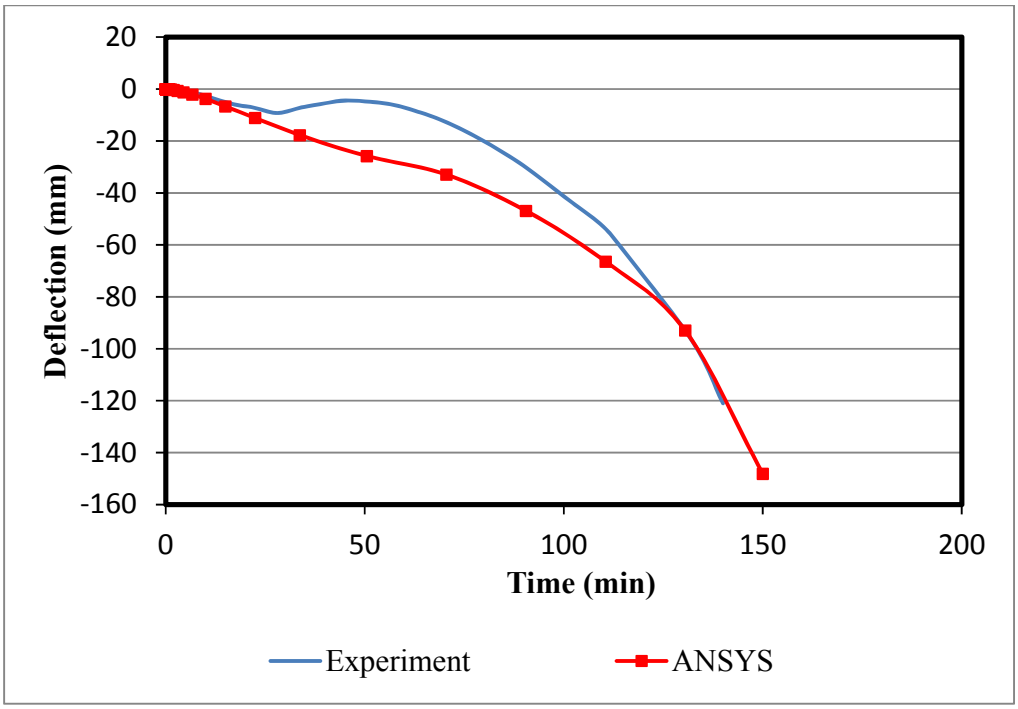

Figure 6:11: Experiment and predicted mid-span deflection for beam B1

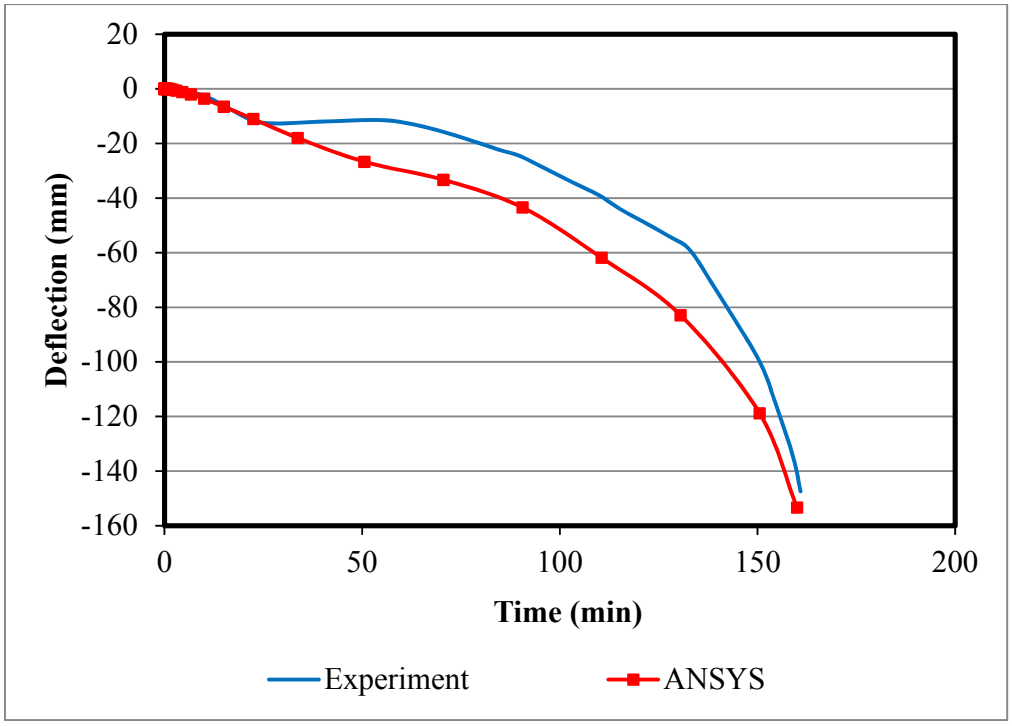

Figure 6:12: Experiment and predicted mid-span deflection for beam B2

From Figures 6.11 and 6.12 it can be seen that ANSYS predicted deflection of the beam shows fairly good agreement with the measured experiment result. The ANSYS model captures the trend of the deflection of the beam under fire accurately, as the deflection increases until failure. The discrepancies that exist between the predicted and measured deflections can be attributed to the fact that at heating durations of 20 to 50 minutes, there is a delay in increase in measured experiment beam deflection. Within this time range the beam deflection flattens and increases slightly in absolute value, and therefore there is a slight break in increase in beam deflection with increase in heating time. The effect can be attributed to the fact that at heating durations of 20 to 50 minutes, there is a delay in the increase of temperature inside the beam section. As shown in Figure 6.6 and 6.7, this is mainly due to heat energy being used up in the evaporation process of moisture present in the beam. The ANSYS model accounted for the moisture content but cannot predict the exact hydro-thermal response of the beam, as explained in chapter 5. Overall the ANSYS model predicts an accurate fire resistance of the beam, as this is the major target of the simulation. The fire resistance was predicted by using ISO 834 failure criteria. Table 6.2 presents the comparison of predicted fire resistance of the beam exposed to fire conditions with fire test results.

Table 6:2: Comparison of experiment and predicted beam response

Beam	Beam result	Test	ANSYS	EC2 prescriptive design	% Difference between test and ANSYS
B1	Fire resistance (mins)	140	150	129	10.00%
	Mid-span deflection (mm)	121.2	149.34	-	23.22%
B2	Fire resistance (mins)	161	160	158	0.63%
	Mid-span deflection (mm)	147.2	153.88	-	4.54%

From Table 6.2 it can be seen that the predicted fire resistances are very close to the fire test values. For beam B1, the predicted fire resistance was 150 minutes with a percentage difference of 10% when compared with the fire test results. For beam B2, the predicted fire resistance was closer to the fire result than for beam B1, with a percentage difference of 0.63%. The predicted maximum deflections using ISO 834 failure criteria are fairly close to the measured experiment results, with 149.34mm for beam B1 and 153.88mm for beam B2, with percentage differences of 23.22% and 4.54% respectively.

6.5 Sensitivity Analysis for Beam Model

Sensitivity analysis was performed to study the effect and determine the optimum values of the major model parameters that influence the predicted response of the reinforced concrete beam simulated under fire conditions. These parameters include moisture content, thermal conductivity and mechanical material model of concrete.

6.5.1 Concrete Thermal Conductivity Model for Beam

As discussed in chapter 4, the thermal conductivity model recommended in BS EN 1992-1-2:2004 was used for simulating heat conduction across the beam in the FE model. BS EN 1992-

1-2:2004 presents two models for predicting the thermal conduction of concrete under fire exposure. Sensitivity analysis was carried out to determine the optimal conductivity model and to also study the influence of thermal conductivity on the predicted performance of the reinforced concrete beam under fire. The upper limit and lower limit thermal conductivities as presented in BS EN 1992-1-2:2004 were tested in simulating the reinforced concrete beam at elevated temperatures. Predicted temperatures and deflections are compared and presented in Figures 6.13 − 6.14.

As illustrated in Figure 6.13, the predicted temperatures with lower and upper limit thermal conductivities show a similar trend with the experiment result. Lower limit thermal conductivity model predicts more accurate temperatures at point T1 and TR while the upper limit model predicts more accurate result at T2 and T3. As discussed earlier, Choi and Shin (2011) observed from their test, that significant spalling occurred at top half of the beam, which resulted in rapid rise of temperature at the top half of the beam. With the presented results and Choi and Shin (2011) observation, upper limit thermal conductivity model was selected for modelling the top half of the beam, while lower limit thermal conductivity was selected for the bottom half.

From the predicted mid-span deflections of the reinforced concrete beam illustrated in Figure 6.14, it can be seen that the deflection pattern of the beam is captured and is similar to the experiment results. With lower limit values, a fire resistance of 173 minutes was predicted, while upper limit values predicted a fire resistance time of 144 minutes. While using a combination model (upper limit at top half of beam and lower limit at bottom half of beam) produced more accurate fire resistance of 160 minutes. Overall using the combined model predicted more accurate temperatures and fire resistance. For these reasons, the combined model was selected for modelling of the reinforced concrete beam exposed to fire.

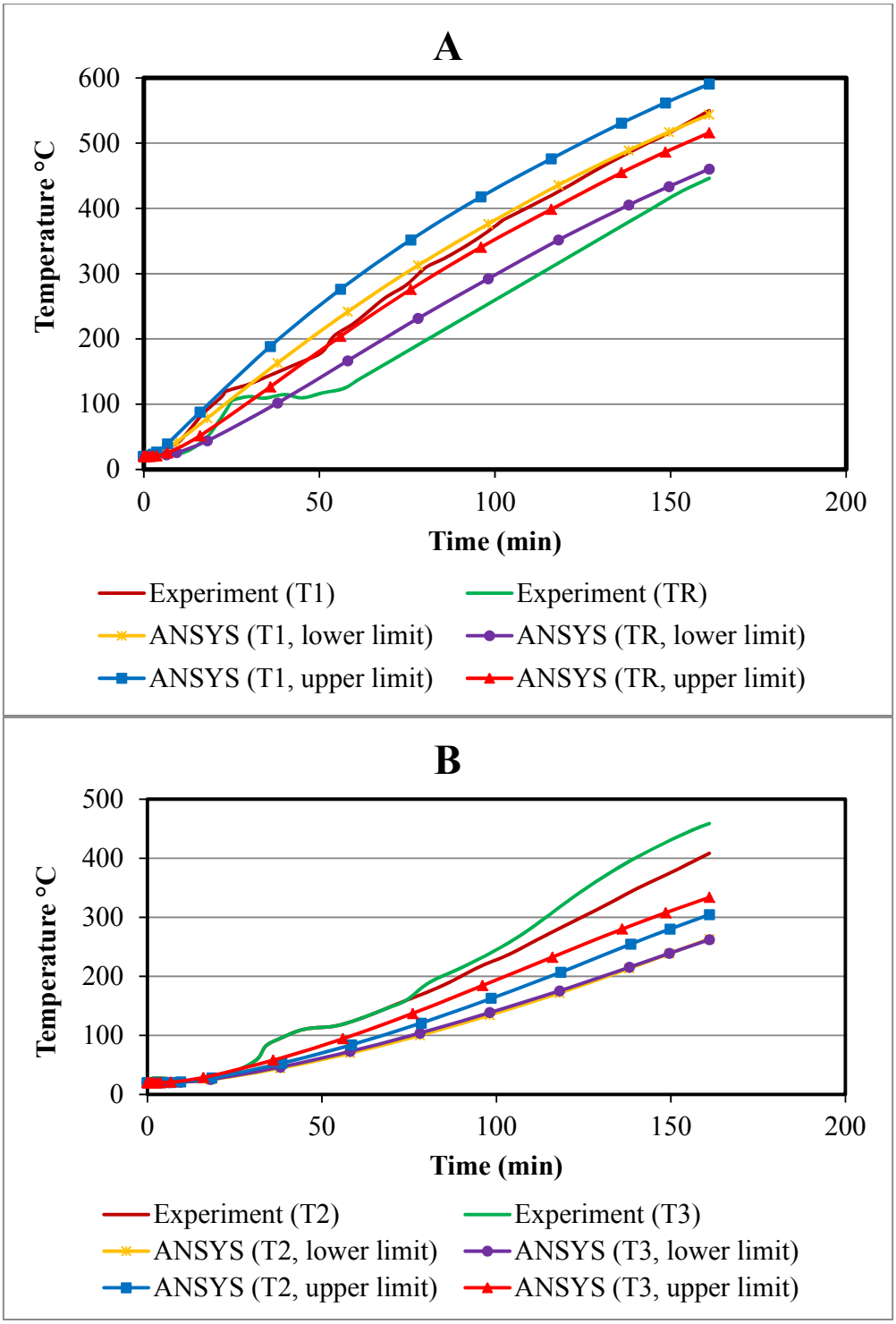

Figure 6:13: Comparison of experiment and predicted beam temperature variation with different thermal conductivity models

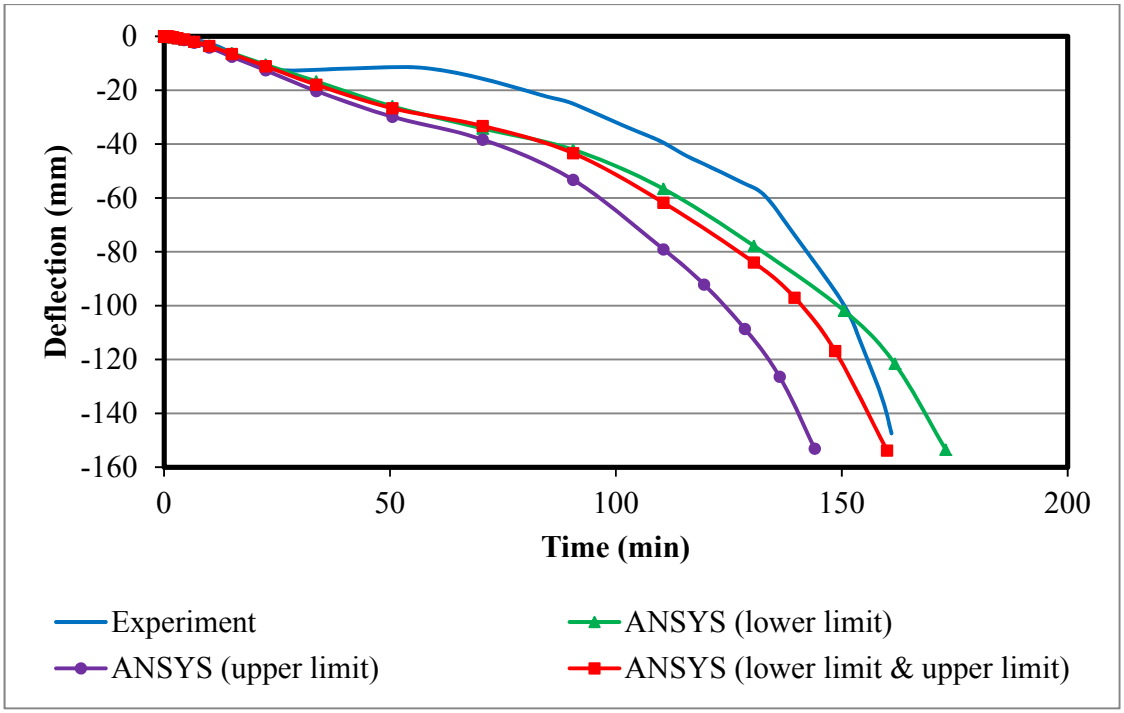

Figure 6:14: Comparison of experiment and predicted beam mid-span deflection with different thermal conductivity models

6.5.2 Moisture Content Model for Beam

In the FE model, the moisture content was indirectly accounted for through the specific heat capacity model proposed in BS EN 1992-1-2:2004. BS EN 1992-1-2:2004 recommends specific heat peak values at a temperature range of 100 − 115°C, as most of the heat energy in the beam at this temperature is used up in the moisture evaporation process. Sensitivity analysis was carried out to determine the optimum moisture content value and to analyse the influence of moisture content on the predicted response of the reinforced concrete beam under fire. Moisture content values of 1.5% and 3.0% were selected for this study. The predicted time dependent temperatures and mid-span deflections are compared and presented in Figures 6.15 – 6.16.

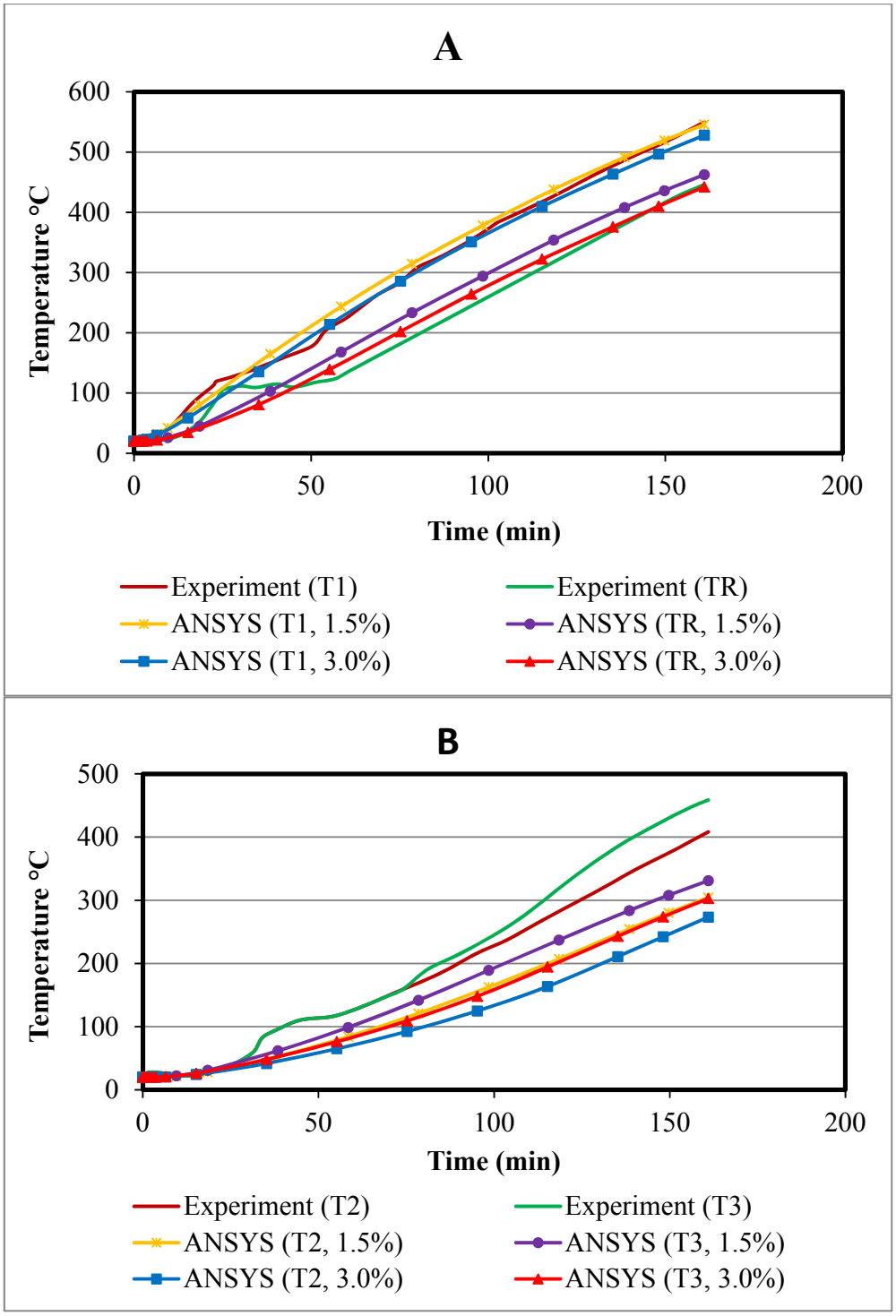

Figure 6:15: Comparison of experiment and predicted beam temperature variation with different moisture levels

As illustrated in Figure 6.15, the predicted temperature evolutions using 1.5% and 3.0% moisture content show good agreement with the experiment results. The predicted temperature at point T1 and TR are slightly more accurate with 3.0% moisture content in comparison with 1.5% moisture content. While at point T2 and T3 1.5% moisture content predicts slightly more accurate temperatures.

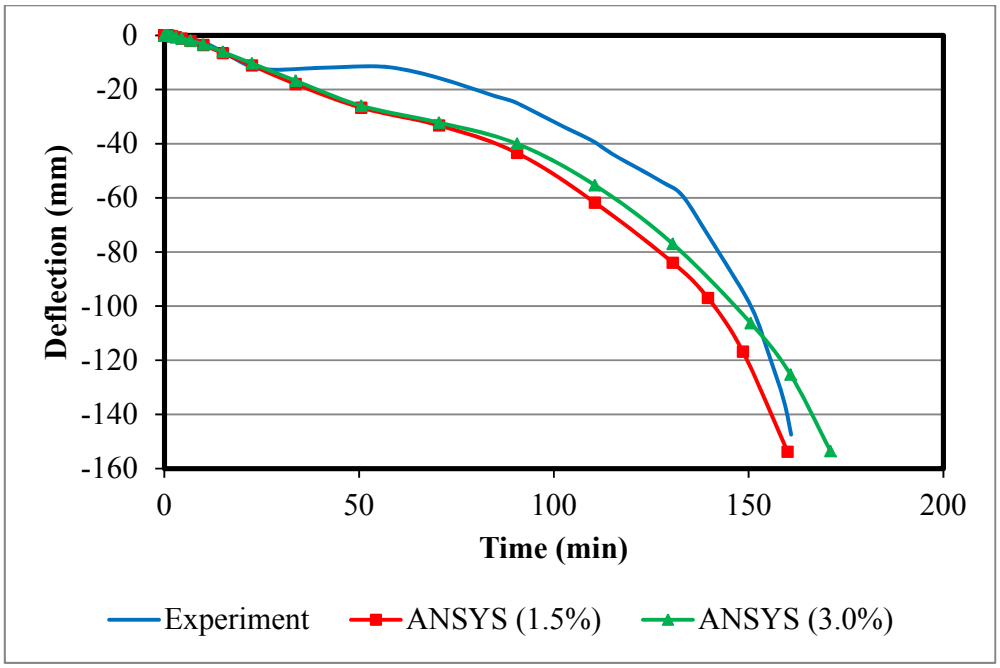

Figure 6:16: Comparison of experiment and predicted beam mid-span deflection with different moisture levels

The predicted mid-span deflection and fire resistance time of the reinforced concrete beam with 1.5% and 3.0% moisture contents are similar and show good agreement with the experiment. With 1.5% moisture content, a fire resistance time of 160 minutes was predicted, while 171 minutes was predicted using a 3.0% moisture content. Overall, 1.5% moisture content predicted a more accurate fire resistance time and was therefore selected for the modelling of the reinforced concrete beam exposed to fire.

6.5.3 Concrete Stress-Strain Model for Beam

This sensitivity analysis was performed to determine the effect of the concrete stress − strain model on the predicted structural performance of the reinforced concrete beam exposed to fire. The high strength concrete stress model proposed in this work, the Eurocodes model and the

Kodur model, as given in Chapter 3, were used in this sensitivity study. The deflections of the reinforced concrete beam obtained with these models are compared and presented in Figure 6.17.

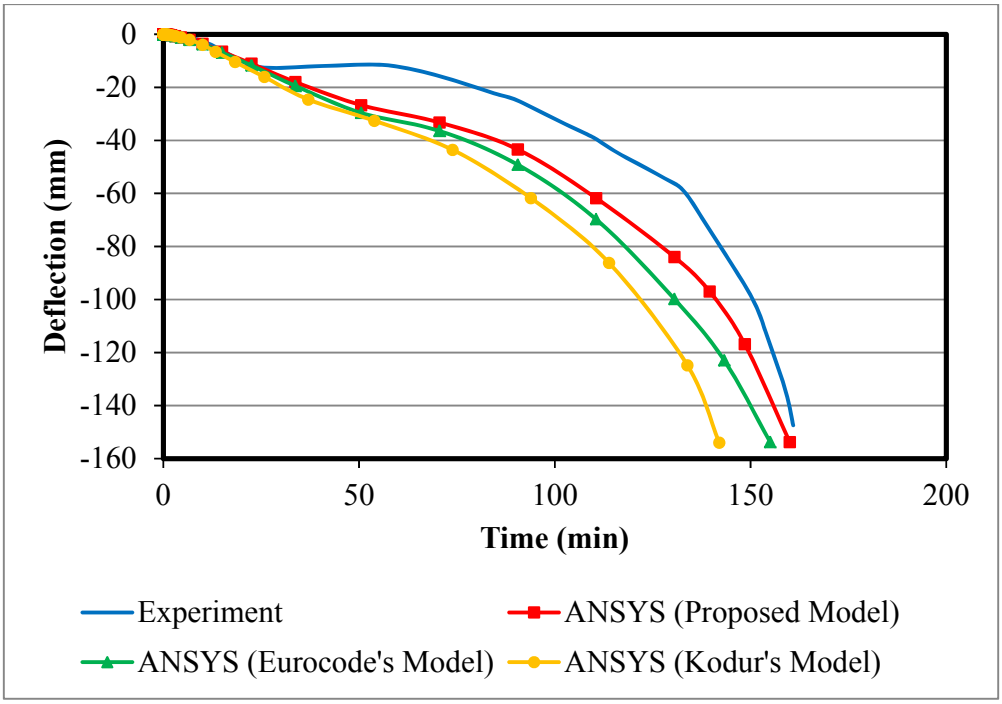

Figure 6:17: Comparison of experiment and predicted beam mid-span deflection with different concrete mechanical models

The predicted deflection shows that all three models capture the deflection pattern of a reinforced concrete beam subjected to fire conditions. With the proposed mechanical model in this study, a fire resistance time of 160 minutes was predicted, while with the Eurocodes and Kodur models fire resistance times of 155 minutes and 142 minutes were predicted, respectively. Overall, all three models predict a good and accurate deflection and fire resistance of the beam with the Eurocodes and proposed models predicting a slightly more accurate deflection and fire resistance time of the beam. The result also implies that the mechanical concrete model influences the predicted deflection and fire resistance of the simulated reinforced concrete beam under fire conditions.

6.6 Parametric Studies for HSRC Beam

The FE model was used to study various parameters affecting the performance of reinforced concrete beam under fire. The parameters were fire scenario, structural load ratio, sectional dimension (concrete cover thickness, beam width and span depth ratio) and effect of aggregate.

6.6.1 Effect of Fire Scenarios on HSRC Beam

This parametric study was performed in order to evaluate the effect of fire type on the performance of reinforced concrete beam exposed to fire. Hydrocarbon and standard fires (ISO 834) were selected for this study. The temperature evolution of the reinforcement, concrete centre and deflection of the beam are compared and illustrated in Figures 6.18 and 6.19.

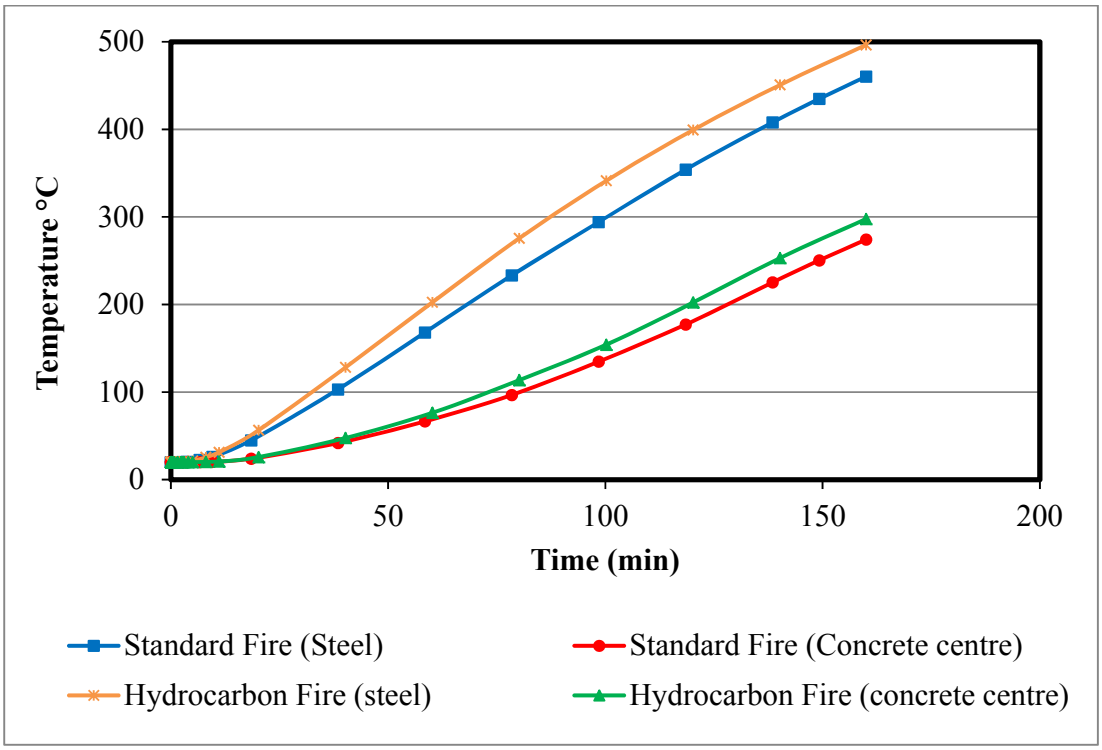

Figure 6:18: Effect of fire type on temperature evolution of beam

Steel and concrete temperatures are higher with hydrocarbon fires in comparison with standard fires, with predicted steel temperatures of about 460°C and 490°C using standard and hydrocarbon fire respectively. While predicted temperature at concrete centre was about 274°C and 297°C using standard and hydrocarbon fire respectively.

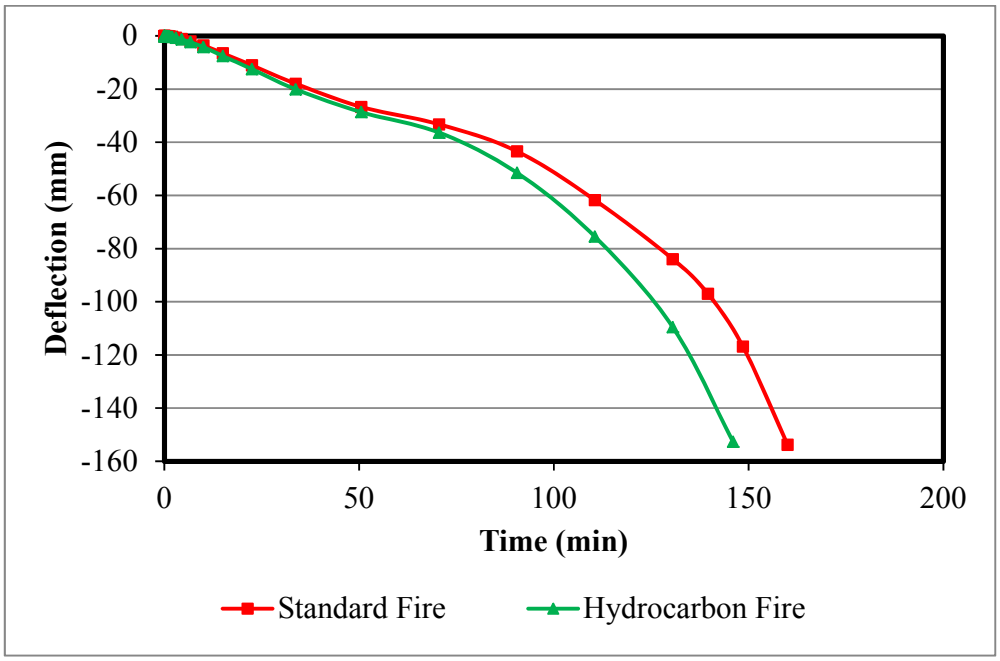

Figure 6:19: Effect of fire type on beam mid-span deflection

From Figure 6.19, the fire resistance of the reinforced concrete beam is much higher under standard fire, with a fire resistance time of 160 minutes. In comparison, under hydrocarbon fires a fire resistance time of 146 minutes was obtained. This reduced fire resistance time can be attributed to the rapid rise of temperature of the concrete and higher steel temperatures, which leads to rapid loss of strength, stiffness and load bearing capacity of the reinforced concrete beam. Overall, the result implies that the type of fire has a moderate level of influence on the performance of the reinforced concrete beam exposed to fire.

6.6.2 Effect of Load Level on HSRC Beam

The effect of load level on the performance of a reinforced concrete beam exposed to fire was investigated by varying the load level. For this study three load levels were considered: 40%, 55% and 70%. The load level was evaluated as the ratio of applied load under fire to the beam resistance at ambient temperature in accordance with BS EN 1992-1-1:2004. The effect of load ratio and deflection of the beam are compared and illustrated in Figure 6.20.

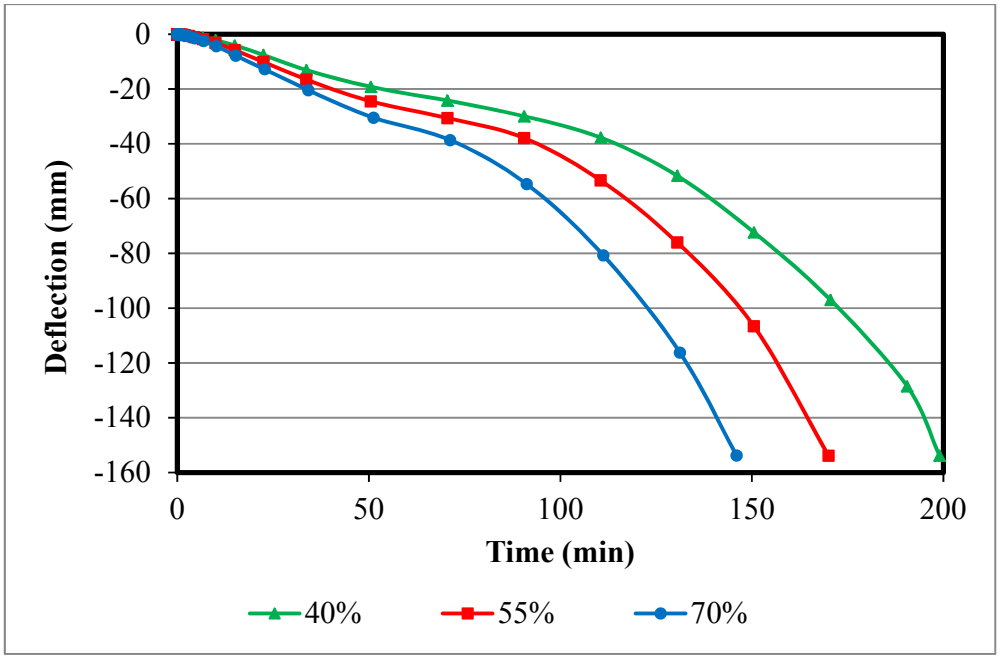

Figure 6:20: Effect of load level on fire performance of beam

It can be seen from Figure 6.20 that with the different load levels the deflection mode of the beam is similar. With increased load level the deflection of the beam increases; this is mainly attributed to the increase in mechanical strain (instantaneous strain and transient strain) due to the increase in load level. With increased load level the fire resistance of the beam decreases, which is mainly attributed to larger mid-span deflection of the beam. The fire resistances of the beam subjected to 40%, 55% and 70% load levels were 199 minutes, 170 minutes and 146 minutes respectively. Overall, the result implies that load level significantly influences the performance of reinforced concrete beam exposed to fire.

6.6.3 Effect of Beam Width and Concrete Cover on HSRC Beam

This parametric study was performed to evaluate the effect of beam width and concrete cover thickness on the performance of reinforced concrete beam exposed to fire conditions. To investigate the effect of beam width, three beam sizes of 250 x 400mm, 300 x 400mm and 350 x 400mm with a clear concrete cover of 50mm were selected. These beams were simulated under fire subjected to a structural load with a load level of 60%. The effects of beam width on the performance of reinforced concrete beam exposed to fire are illustrated in Figures 6.21 and 6.22.

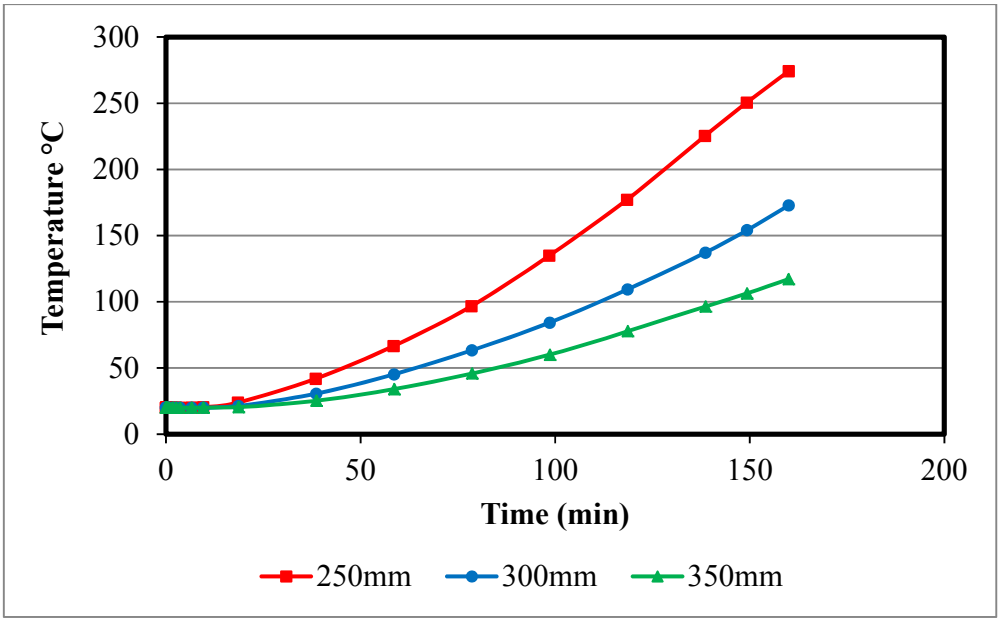

Figure 6:21: Effect of beam width on temperature evolution at beam centre

Temperatures at the centre of the beam presented in Figure 6.21 indicate that they are higher with smaller beam width. This is mainly attributed to heat transfer by conduction being a function of distance between the points of higher and lower temperature (Chapman, 1987). Therefore, across a smaller width, heat is transferred to the centre of the beam at a higher rate in comparison to a larger beam width. Temperatures at the centre of beams with widths of 250mm, 300mm and 350mm are 274°C, 172°C and 117°C, respectively.

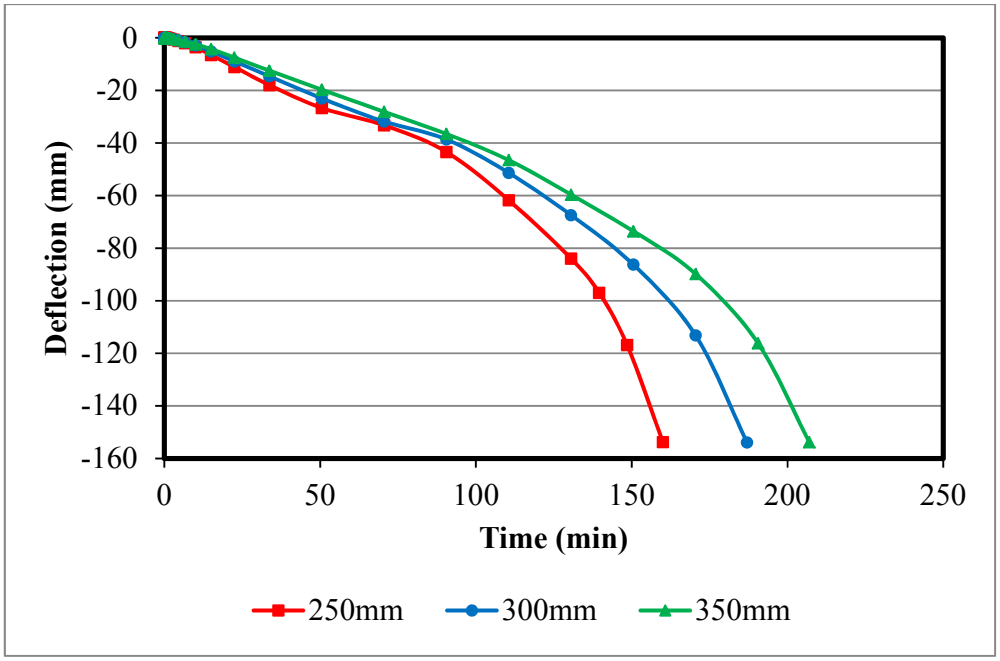

Figure 6:22: Effect of beam width on mid-span beam deflection

The mid-span deflection of the beam presented in Figure 6.22 indicates that at the early stages of exposure to elevated temperatures the deflections of the three beams are very close up to around 75 minutes. Beyond this time, the rate of beam deflection increases with decreased beam width. This is because temperatures at the inner section are higher within the beam of smaller width, which leads to an increase in the loss of strength and stiffness of the concrete. The fire resistance of the beam also increases with increased beam width, with a fire resistance time of 160 minutes, 187 minutes and 207 minutes for 250mm, 300mm and 350mm beam widths respectively. The result indicates that the beam width significantly affects the fire performance of reinforced concrete beams.

The effect of concrete cover thickness on the fire performance of reinforced concrete beam was investigated by varying the thickness. For this study, clear reinforcement covers of 30mm and 50mm were selected with a beam size of 250 x 400mm. The evaluated steel reinforcement temperature and deflection of beam obtained with these varied parameters are compared and presented in Figures 6.23 − 6.24.

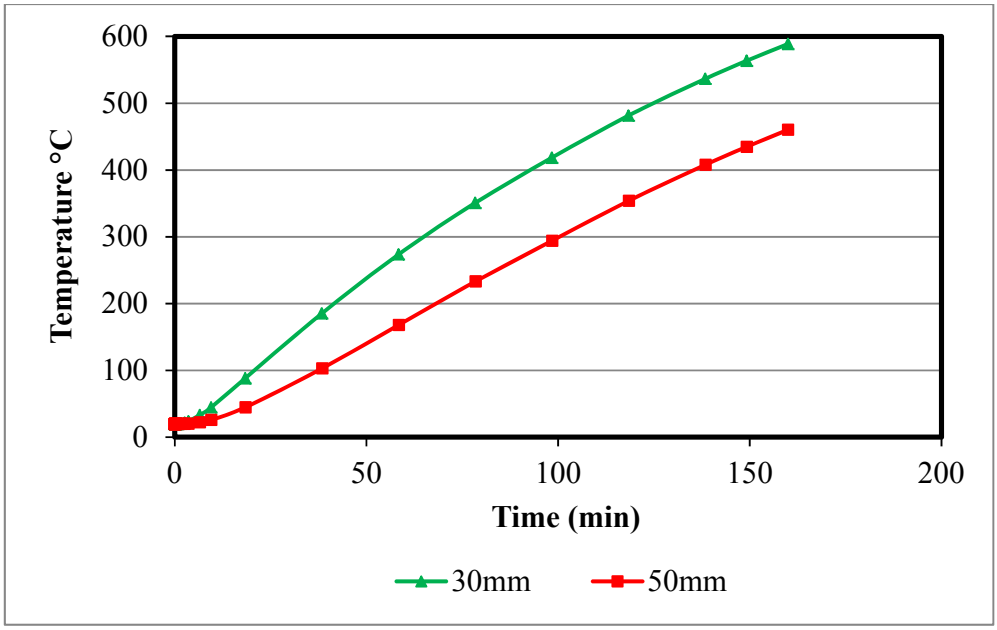

Figure 6:23: Effect of concrete cover on temperature evolution on beam reinforcement

From Figure 6.23 it can be seen that the steel reinforcement temperature increases with decreased concrete cover. This is because with smaller concrete cover, the distance between fire exposed concrete surface and reinforcement is shorter in comparison with larger concrete cover, which leads to more heat transfer to the reinforcement. The reinforcement temperatures with 30 mm and 50mm concrete covers are about 586°C and 460°C respectively.

Deflection of the beam illustrated in Figure 6.24 shows that the deflection results of the two beams are very similar at early stages, up to 50 minutes, of exposure to elevated temperatures. Beyond this time, the rate of deflection increases with decreased concrete cover thickness. This is mainly attributed to the higher temperatures of the steel reinforcement due to the smaller concrete cover, which leads to an increased rate of loss of strength and stiffness of the reinforcement. Fire resistance of the beam increases with increased concrete cover. Fire resistances of the beam with 30mm and 50mm clear covers are 133 minutes and 160 minutes respectively. The result implies that concrete cover thickness significantly affects the performance of reinforced concrete beam exposed to fire.

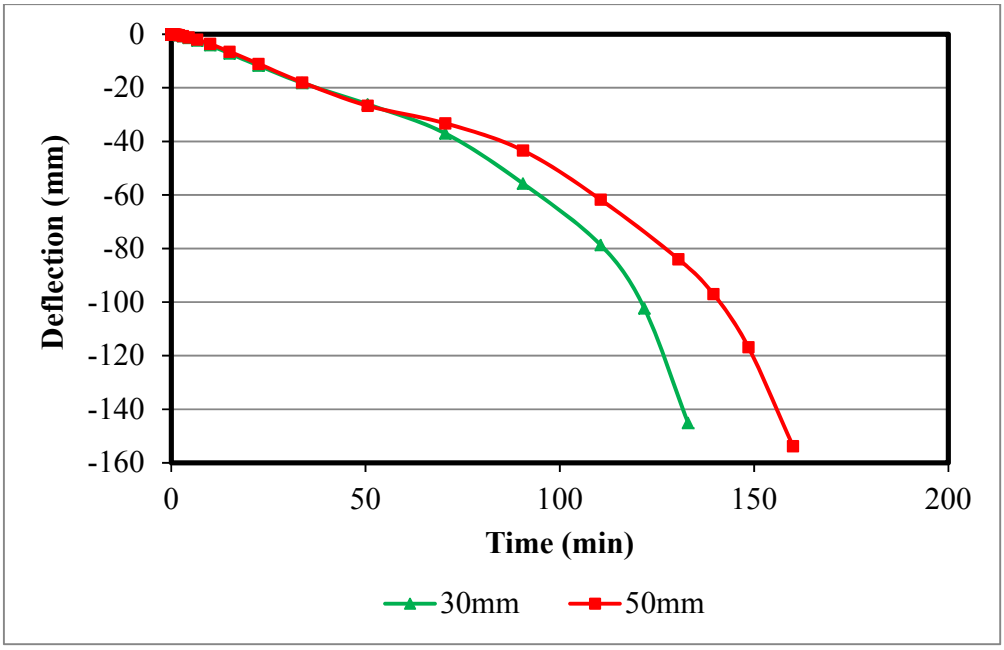

Figure 6:24: Effect of concrete cover on beam mid-span deflection

6.6.4 Effect of Span Depth/Ratio on HSRC Beam

The effect of span depth/ratio on the fire performance of reinforced concrete beams was investigated. This was achieved by varying the length and depth of the beam with a constant beam width and subjected to a structural load with a load ratio of 60%. Four beams were used for this study with beam details given in Table 6.3. The deflection and fire resistance of the beams are presented and compared in Figures 6.25 – 6.26.

Table 6:3: Span/depth ratio parametric studies

Beam size (mm)	Span/depth ratio	Maximum deflection (mm)	Fire resistance (min)
250 x 300 x 3200	10.0	-98.25	148
250 x 300 x 4700	15.0	-221.07	154
250 x 300 x 6200	20	-393.01	150
250 x 600 x 6200	10	-170.13	167

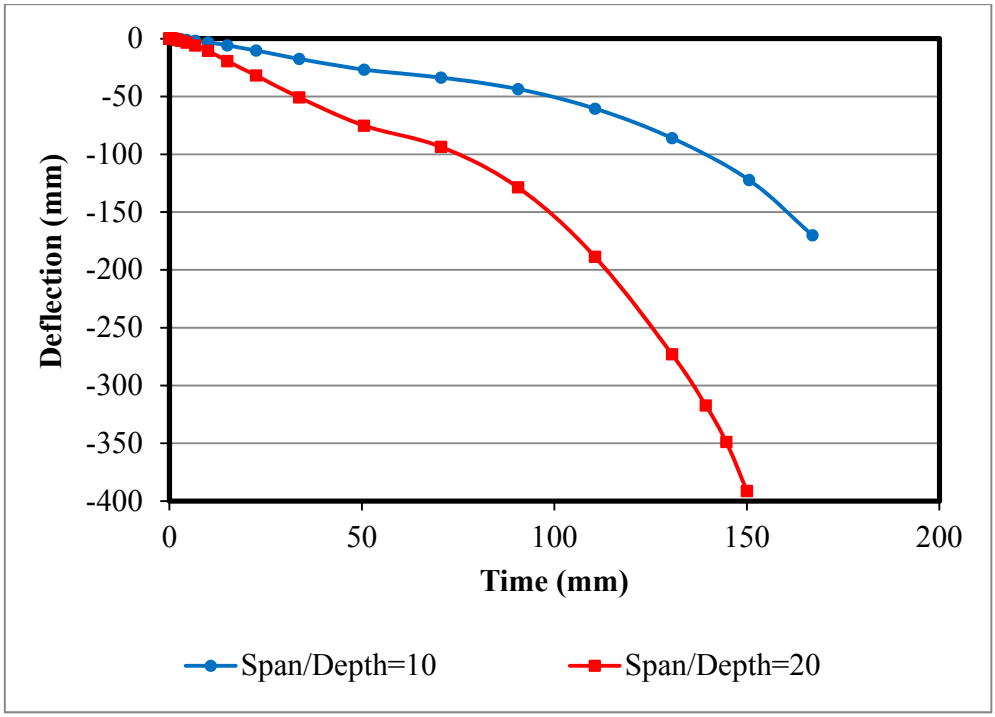

Figure 6:25: Effect of span/depth ratio on fire performance of beams with varying beam depth

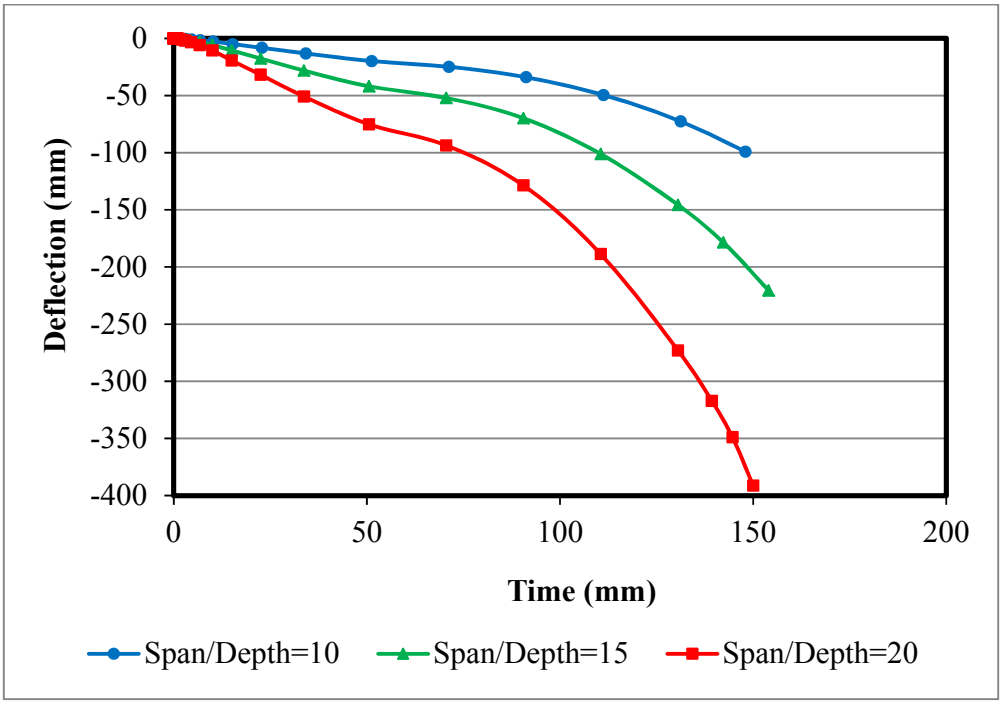

Figure 6:26: Effect of span/depth on fire performance of beams with varying beam span

From Figures 6.25 − 6.26 it can be seen that the deflection of the beams increases with fire exposure time. The rate of deflection of the beam and deflection increases with increased span/depth ratio. This is mainly attributed to reduced flexural beam stiffness due to larger span/depth ratios (Dwaikat, 2009). The predicted fire resistance of the beams indicates that varying beam depth has a moderate level of influence on fire performance of reinforced concrete beam. While beam length has little or low influence on the fire resistance of reinforced concrete beam.

6.6.5 Effect of Aggregate Type on HSRC Beam

The effect of aggregate type was examined to determine its influence on the performance of RC beams under fire conditions. Siliceous and carbonate aggregate RC beams were used for this study with a beam size of 250 x 400 x 4700mm and other parameters maintained. The effects of aggregate type are illustrated in Figure 6.27.

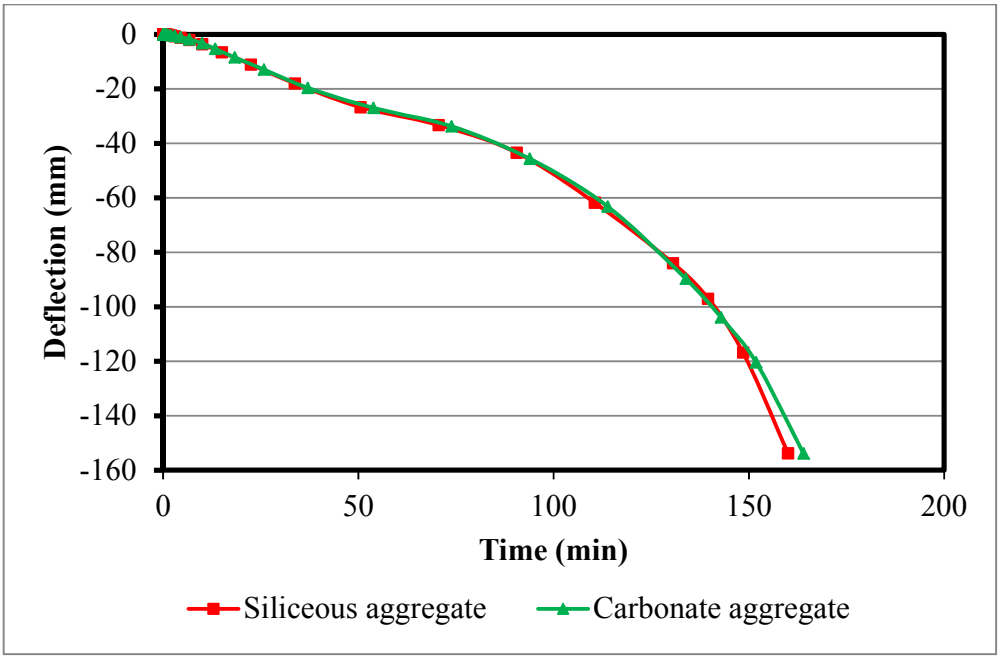

Figure 6:27: Effect of aggregate type on HSRC beam

The results presented in Figure 6.27 indicates that aggregate type has a little or low influence on the fire resistance of reinforced concrete beam, with a predicted fire resistance of 160 and 164 minutes for siliceous and carbonate aggregate, respectively.

6.6.6 Effect of Transient Strain HSRC Beam

This study was conducted to determine the effect of including and excluding transient strain on the predicted beam fire resistance. The effect of transient strain is illustrated in Figure 6.28.

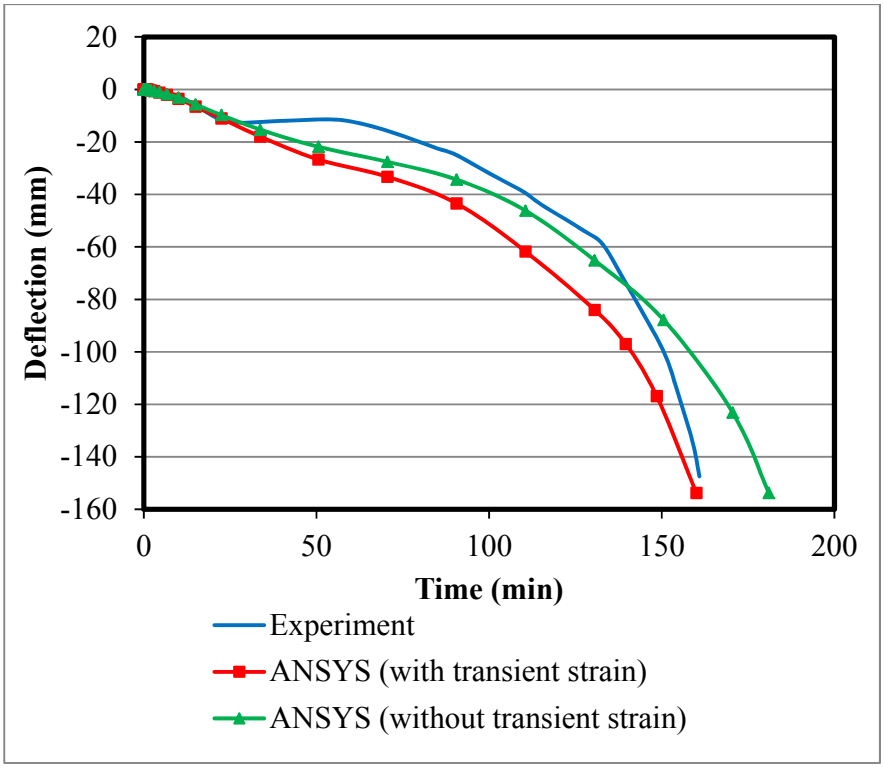

Figure 6:28: Effect of aggregate type on HSRC beam

With inclusion of transient strain predicted beam fire resistance was 160 minutes and was 181 minutes without transient. Therefore including transient strain predicts more accurate beam fire resistance.

A summary of the predicted fire resistance from the conducted parametric studies is presented in Table 6.4.

Table 6:4: Summary of parametric studies for HSRC beam

Beam size (mm)	Varying parameter		Fire resistance (min)	
	Parameter	Value/type	Performance based (ANSYS)	Prescriptive (EC2)
250x400x4700	Fire type	Standard	160	158
250x400x4700		Hydrocarbon	146	-
250x400x4700	Load level (%)	40	199	158
250x400x4700		55	170	158
250x400x4700		70	146	158
250x400x4700	Beam width (mm)	250	160	158
300x400x4700		300	187	180
350x400x4700		350	207	195
250x400x4700	Concrete cover (mm)	30	133	106
250x400x4700		50	160	158
250x300x3200	Span/depth ratio	10.0	148	158
250x300x4700		15.0	154	158
250x300x6200		20	150	158
250x600x6200		10	167	158
250x400x4700	Aggregate type	Siliceous	160	158
250x400x4700		Carbonate	164	158

6.7 Comparisons between Predicted RC Beam Fire Resistance with ANSYS and EC2 Prescriptive Approach

The predicted beam fire resistance presented in Table 6.2 indicated that the ANSYS model and EC2 prescriptive beam design approach predict accurately the fire resistance time of the tested RC beam. Parametric studies performed and presented in Table 6.4 imply that the type of fire, load ratio, beam sectional size and concrete cover influence the fire performance of RC beams. Using a performance based approach, the fire performance of the RC beam was evaluated under hydrocarbon fire curves as presented in Table 6.4, whereas the prescriptive design approach is only valid for standard fire. With the EC2 prescriptive design approach the fire resistance of RC

beams is unaffected by varying load level and fire scenario, while with a performance based approach using ANSYS the effect of these parameters is accounted for in the fire performance of the beams.

6.8 Summary

The FE model for predicting the fire resistance of HSRC beams was developed and verified by comparing the predicted temperature evolution, mid-span deflection and fire resistance with results from a fire resistance test. The predicted results show similar trends and close agreement with the fire test. Sensitivity analysis was conducted to ascertain the values of major aspects of the model which would yield an optimum results and to verify the reliability of the proposed material model for HSC stress – strain relationship. The result from sensitivity analysis indicated that using a combined thermal conductivity model (upper limit at top half of the beam and lower limit at bottom half of the beam) given in BS EN 1992-1-1:2004 and moisture content of 1.5% predicted a more accurate fire resistance of HSRC beams. With the proposed concrete stress − strain relationship an accurate fire resistance was predicted.

By means of the verified FE model, parametric studies were performed to evaluate the influence of major factors affecting the fire performance of HSRC beams exposed to fire. The results indicated that load level, beam width and concrete cover significantly influence the fire resistance of HSRC beams. While fire scenarios and beam depth indicates moderate influence on fire resistance of HSRC beams. Under constant load level, aggregate type and beam length indicates low influence on fire performance of HSRC beam exposed to fire.

Chapter 7 : Simple Model for Evaluating Fire Resistance

In this chapter a simple design method for evaluating the fire resistance of high strength reinforced concrete columns and beams is presented. The model accounts for major factors that govern the fire performance of high strength reinforced concrete columns and beams under standard fire and hydrocarbon fire exposure. These models are developed based on the predicted fire resistance using ANSYS and parametric studies presented in Chapter 5 and Chapter 6 with material models proposed in Chapter 3. The model is validated by comparing the obtained fire resistance with values from a fire resistance test and ANSYS. The model is simple to be applied and easy to be used.

7.1 Model for Calculating Fire Resistance of HSRC Column

The model developed for calculating the fire resistance of HSRC column accounts for the fire type, load ratio, column section size and concrete cover. As illustrated in Chapter 5, these factors significantly or moderately influence the fire performance of HSRC columns. The fire resistance increases with increase in section size, concrete cover and is higher under standard fire condition than hydrocarbon fires when loaded to a constant load level. The column fire resistance decreases with increase in load level. The model was proposed using Curve expert professional software. This was done by inputting predicted fire resistance from ANSYS and fire test with the considered parameters (section size, concrete cover and load ratio). The original model obtained using Curve expert professional is expressed as Equation 7.1.

$$F_{rc} = \left(\frac{4.593D_c + 3.394B_c}{11.212L_r + 0.096X} \right) \qquad 7.1$$

Where F_{rc} is the column fire resistance in minutes, B_c is the column sectional width in mm, D_c is the column sectional depth in mm, L_r is the load ratio and X is the clear concrete cover in mm.

The model presented in equation 7.1, does not effectively capture the variation of fire resistance with the concrete cover and load ratio. Therefore load ratio and concrete cover values which adequately capture the variation of fire resistance with these parameters was projected. A relationship was then obtained with this projected values (concrete cover factor and load ratio

factor) and actual values using Curve expert professional. The proposed and modified model for predicting the fire resistance is as expressed as Equation 7.2.

$$F_{rc} = f_f\left(\frac{4.593D_c + 3.394B_c}{1.121L_{rc} + 9.647X_c}\right) \quad 7.2$$

$$L_{rc} = 2.91\left(1 - \frac{1.13L_r}{1.244}\right)^{-0.885} \quad 7.3$$

$$X_c = 1.294\ \left(1 + \frac{1.474X}{9.927}\right)^{-0.678} \quad 7.4$$

f_f is the fire type factor and should be taken as 1 and 0.86 for standard and hydrocarbon fires respectively, L_{rc} is the column load ratio factor and X_c is the clear concrete cover factor for the column.

7.1.1 Validation of Proposed Simple Model for HSRC Column

The validation of the developed model for evaluating the fire resistance of a high strength reinforced concrete column was achieved by comparing the predicted fire resistance from the proposed approach with that obtain from numerical program (ANSYS) and a fire test. These comparisons are presented in Figure 7.1 and Table 7.1.

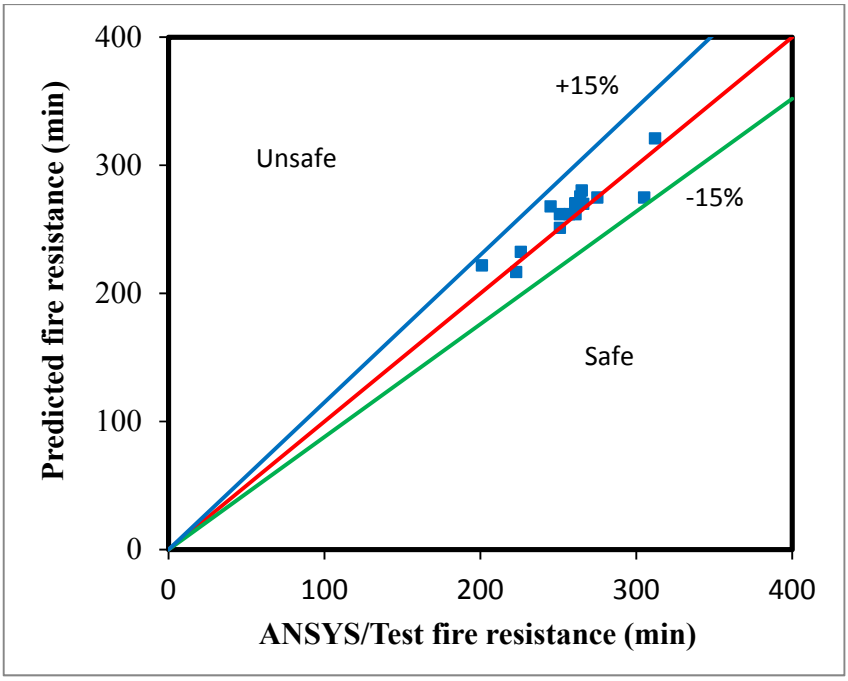

Figure 7:1: Predicted fire resistance of HSRC column using simple model

The predicted RC column fire resistance using the proposed simple model shows good agreement with the values from numerical studies using ANSYS and the fire resistance test. The predicted fire resistance falls within ±15% of the fire test and ANSYS values. The predicted values all fall within the safe limit and therefore the model is valid and safe for evaluating the fire resistance of HSRC columns under standard and hydrocarbon fire scenarios.

Table 7:1: Comparison of predicted HSRC column fire resistance with results from ANSYS and fire test

Width (mm)	Depth (mm)	Length (mm)	Concrete cover (mm)	Load ratio	Reinforcement ratio (%)	Aggregate type	Fire scenario	Fire resistance (min)		% difference
								Proposed model	ANSYS/Test	
305	305	3760	42	0.52	1.7	Carbonate	Standard	270	261	3.45
305	305	3760	42	0.52	1.7	Carbonate	Hydrocarbon	233	226	3.10
305	305	3760	42	0.30	1.7	Carbonate	Standard	321	312	2.88
305	305	3760	42	0.50	1.7	Carbonate	Standard	276	264	4.55
305	305	3760	42	0.70	1.7	Carbonate	Standard	217	223	2.69
305	305	3760	42	0.55	1.0	Carbonate	Standard	262	251	4.38
305	305	3760	42	0.55	2.5	Carbonate	Standard	262	257	1.95
305	305	3760	42	0.55	4.0	Carbonate	Standard	262	261	0.38
250	250	3760	42	0.52	1.7	Carbonate	Standard	222	201	10.45
250	372	3760	42	0.52	1.7	Carbonate	Standard	268	245	9.39
305	305	2520	42	0.52	1.7	Carbonate	Standard	270	263	2.66
305	305	3150	42	0.52	1.7	Carbonate	Standard	270	261	3.45
305	305	3760	42	0.52	1.7	Siliceous	Standard	270	261	3.45
305	305	3760	30	0.52	1.7	Carbonate	Standard	251	251	0.00
305	305	3760	50	0.52	1.7	Carbonate	Standard	280	265	5.66
305	305	3760	40	0.49	2.1	Carbonate	Standard	275	275	0.00
305	305	3760	40	0.49	2.1	Carbonate	Standard	275	305	9.84

305	305	3760	50	0.52	1.7	Carbonate	Standard	270	266	1.50

7.2 Model for Calculating Fire Resistance of HSRC Beam

The model proposed for calculating the fire resistance of HSRC beams accounts for the fire type, load ratio, beam section size and concrete cover. As illustrated in chapter 6, these factors significantly or moderately influence the fire response of HSRC beams. Under constant load ratio, RC beam fire resistance increases with increase in section size and concrete cover. The beam fire resistance is also higher under the standard fire condition than under hydrocarbon fires and decreases with increase in load level. The method used for proposing the column simple model was used to develop the model for the beam as well. The model was proposed using Curve expert professional software. This was done by inputting predicted fire resistance from ANSYS and fire test with the considered parameters (section size, concrete cover and load ratio). The original model obtained using Curve expert professional is expressed as Equation 7.5.

$$F_{rb} = f_f\left(\frac{0.289D_b + 3.196B_b}{3.345 + 8.818L_r - 0.059X}\right) \quad 7.5$$

Where F_{rb} is the beam fire resistance in minutes, B_b is the beam sectional width in mm, D_b is the beam sectional depth in mm, L_r is the load ratio and X is the clear concrete cover in mm.

The model presented in Equation 7.5, does not effectively capture the variation of fire resistance with the load ratio. Therefore load ratio values which adequately capture the variation of fire resistance was projected. A relationship was then obtained with this projected values (load ratio factor) and actual values using Curve expert professional. The proposed and modified model for predicting the fire resistance is expressed as Equation 7.6.

$$F_{rb} = f_f\left(\frac{0.289D_b + 3.196B_b}{3.345 + 8.818L_{rb} - 0.059X}\right) \quad 7.6$$

$$L_{rb} = 0.315\left(1 - \frac{0.916L_r}{1.216}\right)^{-1.092} \quad 7.7$$

f_f is the fire type factor and should be taken as 1 and 0.86 for standard and hydrocarbon fires respectively, L_{rb} is the beam load ratio factor

7.2.1 Validation of Proposed Simple Model for HSRC Beam

The validation of the proposed model for evaluating the fire resistance of high strength reinforced concrete beams was achieved by comparing the predicted fire resistance from the proposed model with that obtained from numerical program (ANSYS) and the fire resistance test. These comparisons are presented in Figure 7.2 and Table 7.2.

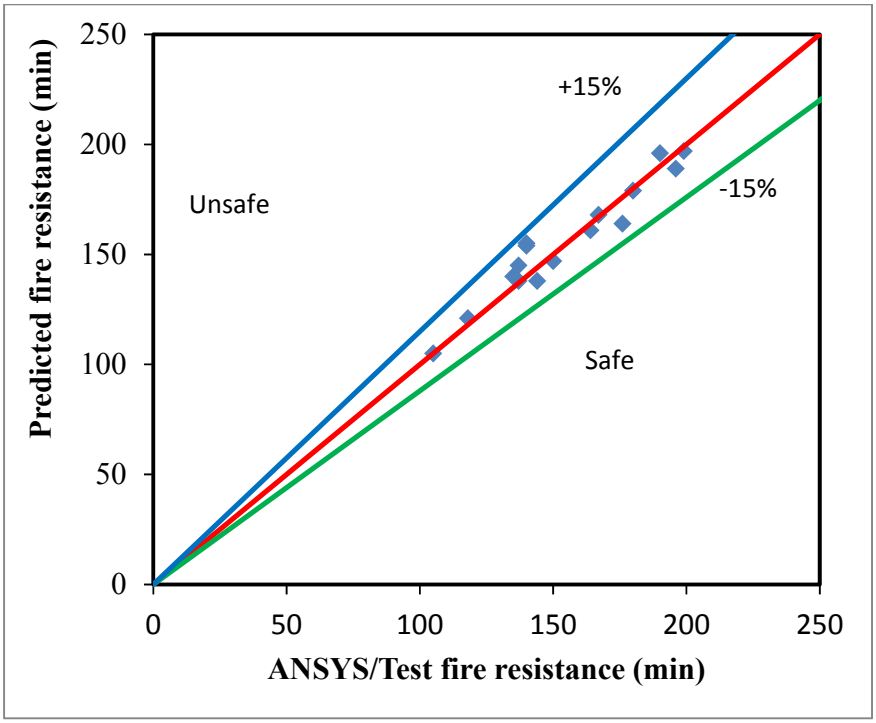

Figure 7:2: Predicted fire resistance of HSRC beam using simple model

The predicted fire resistance of HSRC beams using the proposed simple approach shows good agreement with the values from ANSYS and the fire resistance test. The predicted fire resistances with the simple equation are accurate with ±15% error and all fall within the safe limits. Therefore the model is valid and safe for evaluating the fire performance of HSRC beams under standard and hydrocarbon fire scenarios.

Table 7:2: Comparison of predicted HSRC beam fire resistance with result from ANSYS and fire test

Width (mm)	Depth (mm)	Length between support (mm)	Concrete cover (mm)	Load ratio	Aggregate type	Fire scenario	Fire resistance (min)		% Difference
							Proposed model	ANSYS/Test	
250	400	4500	50	0.6	Siliceous	Standard	159	160	0.63
250	400	4500	50	0.6	Siliceous	Hydrocarbon	137	146	6.16
250	400	4500	50	0.4	Siliceous	Standard	203	199	2.01
250	400	4500	50	0.55	Siliceous	Standard	170	170	0.00
250	400	4500	50	0.70	Siliceous	Standard	137	146	6.16
300	400	4500	50	0.6	Siliceous	Standard	187	187	0.00
350	400	4500	50	0.6	Siliceous	Standard	215	207	3.86
250	400	4500	30	0.6	Siliceous	Standard	132	133	0.75
250	300	3000	50	0.6	Siliceous	Standard	154	148	4.05
250	300	4500	50	0.6	Siliceous	Standard	154	154	0.00
250	300	6000	50	0.6	Siliceous	Standard	154	150	2.67
250	600	6000	50	0.6	Siliceous	Standard	169	167	1.20
250	400	4500	50	0.6	Carbonate	Standard	159	164	3.05
250	400	4500	50	0.6	Siliceous	Standard	159	161	1.24
250	400	4500	40	0.6	Siliceous	Standard	144	140	2.86
250	400	4500	40	0.6	Siliceous	Standard	144	150	4.00

7.3 Model Limitations

The developed model for HSRC column was only validated for square and rectangular shaped columns and it's not valid for circular and elliptical shaped RC columns .The developed model for HSRC column was only validated for short columns due to lack of availability of test data for slender columns and therefore the model is limited for predicted the fire resistance of short columns, up to 4000mm high. Column model captures the variation of the fire resistance with applied load ratio, the model was only validated for a loading ratio of 30 -70%. The model was validated for RC columns loaded axially in compression and does not consider biaxial loaded columns and columns under eccentric loading.

The developed model for HSRC beam was only validated for square and rectangular shaped beams and it's not valid for T and I section RC beams. The beam model was not tested and validated for tapered beams due to lack of availability of test data. Although the beam model captures the variation of fire resistance with beam depth and width, the model was only validated for a maximum beam width of 350mm and maximum beam depth of 600mm. The beam model is limited for HSRC beam with conventional reinforcing steel and does not cover prestressed beam. Beam model also capture the variation of the fire resistance with beam load ratio, the model was only validated for a loading ratio of 40 -70%.

7.4 Summary

In this chapter design models have been established for evaluating the fire resistance of HSRC columns and beams. The models were derived from the numerical and parametric studies on HSRC columns and beams exposed to fire. The approach accounts for several parameters that significantly influence the fire performance of HSRC columns and beams. These parameters include fire scenario, load ratio, concrete cover and size parameters. The proposed models were validated by comparing the predicted fire resistances with the values from ANSYS and a fire resistance test. The developed models present a rational and simple approach for evaluating the fire resistance of RC columns and beams exposed to standard or hydrocarbon fire scenarios. Using these models the fire resistances of HSRC columns and beams are obtained by inputting values of size parameters, load ratio and fire factor depending on the fire scenarios.

Chapter 8 : Conclusions

8.1 General Conclusions

This research was undertaken to present and develop rational approach for evaluating fire performance of HSRC members using performance based approach. The fire resistance of high strength reinforced concrete was investigated in this study through a numerical computational approach. A three-dimensional (3D) Finite Element (FE) model was developed for evaluating the fire resistance of high strength reinforced concrete columns and beams exposed to fire conditions using ANSYS numerical program via a robust material model for HSC proposed in this research. Elevated temperature material relationships for HSC were developed and were incorporated in the FE model, with other existing material models for HSC and reinforcement. Coupled field analysis was used to obtain the behaviour and fire performance of HSRC columns and beams exposed to fire. An extensive sensitivity analysis was performed on significant model parameters in order to ascertain their optimum values. The validity of the numerical model was established by comparing the predicted temperatures, time dependent deformation and fire resistance with values from fire test of high strength RC columns and beams. Parametric studies were conducted using the verified numerical model and the influences of various parameters on fire performance of HSRC columns and beams were quantified. Simple design models were developed from the parametric studies for evaluating fire resistance of RC columns and beams exposed to fire conditions. The proposed simple model accounts for fire scenarios, load ratio and size parameters of HSRC columns and beams exposed to fire. The numerical model and developed simple equations provide a rational approach for evaluating the fire resistance of HSRC columns and beams compared with the current prescriptive design approach.

8.2 Specific Conclusions

Based on the research work on fire resistance of high strength reinforced concrete columns and beams presented in this thesis, the following conclusions were drawn:

- The current approaches for evaluating the fire resistance of HSRC columns and beams are prescriptive and do not provide a rational method for evaluating the fire resistance.

- The proposed material model for HSC fits well with test data and is simple and convenient for both manual design calculations and computational analysis.
- The numerical model was validated with a fire resistance test of HSRC columns and beams. The model is capable of evaluating the fire performance and resistance of HSRC columns and beams exposed to fire. The model accounts for various factors which significantly influence the fire performance of RC columns and beams under fire, such as fire scenarios, load ratio, moisture content and size parameters.
- The predicted temperature, time − deformation pattern and fire resistance of HSRC columns and beams from the FE model with ANSYS software indicates that the numerical models are suitable for performing analysis of HSRC columns and beams under fire.
- The predicted temperature evolutions within the RC columns and beams show good agreement with test results.
- The predicted temperature − time deformation pattern shows good agreement with the fire test. The deformation of an HSRC column exposed to fire occurs in three stages. In the first stage the column undergoes compressive deformation under structural loading alone. In the second stage with elevated temperature being applied to the column, the column experiences expansion. In the third and final stage the column undergoes compressive deformation until failure, which is attributed to extensive degradation of the materials.
- The predicted temperature – time deflection of the HSRC beam shows a similar pattern with the fire resistance test of HSRC beams. The RC beam experiences sagging deflection at the mid-span under structural loading and continual sagging deflection with the application of elevated temperatures. This is mainly attributed to decomposition in the concrete and reinforcement materials.
- Using the numerical model the predicted fire resistances of HSRC columns and beams were validated with fire test results. The predicted results showed good agreement with the fire test and are within safe limits.

Some conclusions and recommendations on material modelling were made from the verified FE model and comprehensive sensitivity analysis:

- The material models proposed for the compressive strength, peak strain and elastic stress − strain curve of high strength concrete at elevated temperatures are in close agreement with the experimental data obtained.
- These proposed material models yield accurate results, when implemented into ANSYS with other existing models for transient strain and thermal properties for concrete, to perform FE analysis and evaluate fire resistance of high strength concrete reinforced columns and beams under fire.
- Through the proposed compressive strength model for HSC, the effect of sloughing off and aggregate type of spalling was partially accounted for implicitly. This was achieved by ensuring that regions within a temperature range of 800 − 1000°C had a retained strength between 1 – 16% of their unfired strength and therefore contributed little to the member exposed to fire.
- Using a constant density value of 2400kg/m^3 and 7850kg/m^3 for concrete and reinforcement respectively, without considering any variation with temperature, proved to be satisfactory for modelling concrete and steel material in RC columns and beams exposed to fire.
- Using a perfect bond between the concrete and reinforcement proved to be sufficient for evaluating the fire resistance of RC columns and beams exposed to fire.
- Modelling the reinforcements with line element proved to be adequate for evaluating the fire performance of RC columns and beams under fire.
- For modelling of RC columns the lower limit thermal conductivity model for concrete given in BS EN 1992-1-2:2004 gives a more accurate prediction of temperature evolution and fire resistance of RC columns. While for the beam using a combined thermal conductivity model (upper limit at top half of the beam and lower limit at bottom half of the beam) given in BS EN 1992-1-1:2004 predicts a more accurate temperature and fire resistance.
- Using proposed elastic stress − strain curve in this study predicts a more accurate column and beam resistance under fire.
- For RC columns and beams, optimum results were obtained with 1.5% moisture content.

Parametric studies were conducted with the verified FE model to evaluate the influence of major factors and parameters on fire resistance of RC columns and beams under fire. These factors are

fire scenarios, load ratio, reinforcement ratio, concrete cover, aggregate type and size parameters. From the parametric studies the following key findings were observed:

- The fire resistance of an HSRC column is significantly affected by column sectional size, load ratio and fire scenarios, while concrete cover moderately influence fire resistance of RC column. The fire resistance of the HSRC column decreases with increase in load ratio and under sustained load level it increases with increase in sectional size and concrete cover. A lower column fire resistance is also obtained in hydrocarbon fire type scenarios.
- Under constant load ratio, reinforcement ratio, aggregate type and column height has little or low influence on fire resistance of HSRC columns.
- The factors which have a significant influence on the fire resistance of high strength RC beams are load ratio, beam width and concrete cover, while beam depth and fire type moderately influence fire resistance of RC beam. The fire resistance of HSRC beams decreases with increase in load level. Under constant load ratio the fire resistance of HSRC beams increases with increase in sectional size, concrete cover and a lower beam fire resistance is obtained in hydrocarbon fire scenarios. Aggregate type and beam length has little or low influence on fire performance of HSRC beams exposed to fire.

From the verified FE model and parametric studies conducted, simple design equations were derived for evaluating the fire resistance of HSRC columns and beams exposed to fire. The simple model accounts for factors which significantly and moderately influence the fire resistance of HSRC columns and beams obtained from conducted parametric studies. These simple models were validated with the fire resistance obtained from the numerical model and fire test. The following conclusions are drawn from the developed simple models:

- The developed model for predicting the fire resistance of HSRC columns exposed to fire shows good agreement with results obtained from ANSYS and fire test. The model accounts for the effect of load ratio, concrete cover, sectional size and standard and hydrocarbon fire scenarios.
- The predicted fire resistances obtained with the developed simple model for evaluating the fire resistance of HSRC beams under fire show good agreement with results from the numerical model and fire test. Therefore it is adequate for evaluating the fire resistance of

high strength RC beams. The model accounts for the applied load level, sectional size and concrete cover, under standard and hydrocarbon fire scenarios.

- The model provides a simple, accurate and rational approach for evaluating the fire resistance of HSRC columns and beams subjected to fire. Therefore, it is recommended for this purpose.

8.3 Research Limitation and Future Work

The research work conducted in this study has provided an extensive contribution to knowledge in the research area of high strength reinforced concrete under fire. Given the extensive and complex scope of the problem and due to the limitation of the research studies, the following recommendations are made for future research works:

- This study is limited to HSRC columns and beams exposed to fire. The study should be expanded to cover high strength RC slabs and RC walls under fire. In this study only simply supported beams and stand-alone columns were considered. Therefore the study should be expanded to include continuous beams and columns in frames.
- In this study only square and rectangular shaped columns and beams were considered; for future works circular and elliptical shaped RC columns should be considered. For RC beams the research study should be extended to other shapes such as T and I sectional RC beams.
- The numerical model presented here for evaluating the fire performance of HSRC columns and beams should be extended to include fibre reinforced concrete columns and beams exposed to fire and high temperatures.
- The numerical model can only partially account for the effect of sloughing off and aggregate type of spalling. For future research the model should be extended to cover explosive spalling and fully account for sloughing off and aggregate type of spalling.
- In the model moisture content was considered by using specific heat capacity model given in BS EN 1992-1-1:2004. For future research and in order to predict more accurate temperatures and beam deflections, a hydro-thermal model should be used.
- In the FE model only standard and hydrocarbon fire models were considered; for future works the model should be expanded to consider the performance of high strength RC columns and beams under design parameter fires.

- This research only covers RC columns loaded axially in compression; therefore the study should be extended and validated for biaxial loaded columns and columns under eccentric loading.
- The load bearing performance failure criteria given by ISO 834-1:1999 and BS EN 1363-1:1999 for columns does not consider buckling failure criteria and therefore the numerical model and simple equation for evaluating fire resistance of high strength RC columns is limited to short and stocky columns. For future works a performance buckling failure criteria should be proposed and incorporated into various codes of practice.

8.4 Research Impact

The current method for evaluating the fire resistance of high strength reinforced concrete members is prescriptive and does not provide a realistic approach as it does not account for factors such as load ratio and hydrocarbon fires. The fire test approach is also expensive, time consuming and limited in space and size to a member which can be tested effectively and therefore it is not a rational approach for evaluating the fire resistance of full and complicated structures.

The numerical model and the developed simple design model provide a rational, accurate, safe and convenient method for evaluating the fire resistance of high strength RC columns and beams exposed to fire. The FE model and simple design equations can be used to evaluate the fire resistance of RC columns and beams with different section sizes, load level, concrete cover and beam length under standard and hydrocarbon fire scenarios. The developed design models are simple and straightforward to be used for evaluating fire resistance of high strength RC columns and beams and they can be incorporated into the various codes of practice. Overall the FE model and proposed design equation provide a rational approach which is suitable for a performance based design approach to high strength RC columns and beams exposed to fire.

References

Abrams, M. S. (1971) Compressive strength of concrete at temperatures of 1600F, *American Concrete Institute (ACI) SP 25, Temperature and Concrete,* .

Ali, F., Nadjai, A. and Choi, S. (2010) Numerical and experimental investigation of the behavior of high strength concrete columns in fire, *Engineering Structures,* 32 (5), pp. 1236-1243.

Anderberg, Y. and Thelandersson, S. (1976) Stress and deformation characteristics of concrete at high temperatures, 2-Experiment investigation and material behaviour model, *Bulletin 54, University of Lund, Sweden,* .

ANSYS (2010a) *ANSYS Mechanical APDL and mechanical applications theory reference.* Version 13.0. USA: ANSYS, Inc.

ANSYS (2010b) *ANSYS Mechanical APDL element reference.* Version 13.0. USA: ANSYS, Inc.

Arioz, O. (2007) Effects of elevated temperatures on properties of concrete, *Fire Safety Journal,* 42 (8), pp. 516-522.

Bailey, C. (2002) Holistic behaviour of concrete buildings in fire, in: *Proceedings of the Institution of Civil Engineers: Structures & Buildings,* 152 (3), pp. 199-212.

Bastami, M. and Aslani, F. (2010) Preloaded high temperature constitutive models and relationships for concrete, *Scientia Iranica,* 17 (1), pp. 11-25.

Behnood, A. and Ghandehari, M. (2009) Comparison of compressive and splitting tensile strength of high-strength concrete with and without polypropylene fibers heated to high temperatures, *Fire Safety Journal,* 44 (8), pp. 1015-1022.

Buchanan, A. H. (2001) *Structural design for fire safety.* Chichester: Wiley.

Carstensen, V.J., Jomaas, G. and Pankaj, P. (2013) Element Size and Other Restrictions in Finite-Element Modeling of Reinforced Concrete at Elevated Temperatures, *Journal of Engineering Mechanics,* 139 (10), pp. 1325-1333.

Chang, Y. F., Chen, Y. H., Sheu, M. S. and Yao, G. C. (2006) Residual stress–strain relationship for concrete after exposure to high temperatures, *Cement and Concrete Research,* 36 (10), pp. 1999-2005.

Chapman, A. J. (1987) *Fundamentals of heat transfer.* New York; London: Macmillan; Collier Macmillan.

Chen, W. (1988) *Plasticity for structural engineers.* New York: Springer-Verlag.

Chen, W. (1982) *Plasticity in reinforced concrete.* New York; London: McGraw-Hill.

Cheng, F., Kodur, V. K. R. and Wang, T. (2004) Stress-Strain Curves for High Strength Concrete at Elevated Temperatures, *Journal of Materials in Civil Engineering,* 16 (1), pp. 84-90.

Choi, E. G. and Shin, Y. S. (2011) The structural behavior and simplified thermal analysis of normal-strength and high-strength concrete beams under fire, *Engineering Structures,* 33 (4), pp. 1123-1132.

Comsa, T. (2013) *Spalling Mechanism in Concrete Exposed to Elevated Temperatures.* Aalborg University.

Connolly, Raymond J. (1995) *The spalling of concrete in fires.* University of Aston.

Cook, R. D., Malkus, D. S. and Plesha, M. E. (1989) *Concepts and applications of finite element analysis.* 3rd ed. New York: Wiley.

Cruz, C. R. and Gillen, M. (1980) Thermal expansion of Portland cement paste, mortar and concrete at high temperatures, *Fire and Materials,* 4 (2), pp. 66-70.

Dotreppe, J.-C. and Franssen, J.-M. (1985) The use of numerical models for the fire analysis of reinforced concrete and composite structures, *Engineering Analysis,* 2 (2), pp. 67-74.

Drucker, D.,C. and Prager, W. (1952) Soil Mechanics and Plastic Analysis or Limit Design, *Quarterly of Applied Mathematics,* 10 (2), pp. 157-165.

Drysdale, D. (2011) *An introduction to fire dynamics.* 3rd ed. Hoboken, N.J.: Wiley.

Dwaikat, M. B. M. (2009) *Flexural response of reinforced concrete beams exposed to fire.* Michigan State University.

Espinós Capilla, A., Hospitaler Pérez, A. and Romero García, M. (2012) *Numerical analysis of the fire resistance of circular and elliptical slender concrete filled tubular columns.* Valencia: Universidad Politécnica de Valencia.

European Committee for Standardization. (2002) *Eurocode 1: Actions on structures — Part 1-2: General actions — Actions on structures exposed to fire.* BS EN 1991-1-2:2002. BSI.

European Committee for Standardization. (2004a) *Eurocode 2: Design of concrete structures — Part 1-1: General rules and rules for buildings.* BS EN 1992-1-1:2004. BSI.

European Committee for Standardization. (2004b) *Eurocode 2: Design of Concrete Structures —Part 1-2: General Rules — Structural Fire.* BS EN 1992-1-2:2004. BSI.

European Committee for Standardization. (2005) *Eurocode 3: Design of steel structures — Part 1-2: General rules — Structural fire design* . BS EN 1993-1-2:2005. BSI.

European Committee for Standardization. (1999) *Fire resistance tests - Part 1: General requirements.* BS EN 1363-1:1999. BSI.

Ezekiel, S., Xiao, R. Y. and Chin, S. C. (2013) Constitutive model for compressive strength and elastic modulus for concrete under elevated temperature. *Structures Congress 2013,* Pittsburgh, USA. American Society of Civil Engineers (ASCE), pp. 2916-2925.

Ezekiel, S., Xiao, R. Y. and Kraincanic, I. (2013) Numerical modelling of reinforced concrete column under fire. *Fourteenth International Conference on Computational Structures Technology,* Cagliari, Sardinia, Italy, 2013. Kippen, Civil-Comp Press.

Felicetti, R. and Gambarova, P. G. (1998) Effects of high temperature on the residual compressive strength of high-strength siliceous concretes, *ACI Materials Journal*, 95 (4), pp. 395-405.

Fu, Y. F., Wong, Y. L., Poon, C. S. and Tang, C. A. (2005) Stress-strain behaviour of high-strength concrete at elevated temperatures, *Magazine of Concrete Research,* 57 (9), pp. 535-544.

Fu, Y. and Li, L. (2011) Study on mechanism of thermal spalling in concrete exposed to elevated temperatures, *Materials and Structures,* 44 (1), pp. 361-376.

Gao, W. Y., Dai, J., Teng, J. G. and Chen, G. M. (2013) Finite element modeling of reinforced concrete beams exposed to fire, *Engineering Structures,* 52 (0), pp. 488-501.

Gawin, D., Pesavento, F. and Schrefler, B. (2004) Modelling of deformations of high strength concrete at elevated temperatures, *Materials and Structures,* 37 (4), pp. 218-236.

Gibson, Henry R. (1994) *Elementary Statistics.* USA: Wm. C. Brown Publishers.

Han, C., Hwang, Y., Yang, S. and Gowripalan, N. (2005) Performance of spalling resistance of high performance concrete with polypropylene fiber contents and lateral confinement, *Cement and Concrete Research,* 35 (9), pp. 1747-1753.

Harmathy, T.,Z. (1970) Thermal properties of concrete at elevated temperatures, *ASTM Journal of Materials,* 5 (1), pp. 47-74.

Harmathy, T. Z. (1993) *Fire safety design and concrete.* Harlow: Longman.

Harmathy, T. Z. (1972a) A new look at compartment fires, part I, *Fire Technology,* 8 (3), pp. 196-217.

Harmathy, T. Z. (1972b) A new look at compartment fires, part II, *Fire Technology,* 8 (4), pp. 326-351.

Hassen, S. and Colina, H. (2006) Transient thermal creep of concrete in accidental conditions at temperatures up to 400C, *Magazine of Concrete Research,* 58 (4), pp. 201-208.

Hertz, K. D. (1981) *Sample Temperature Calculations of Fire Exposed Concrete Constructions.* Institute of Building Design, Technical University of Denmark.

Hertz, K. D. (2005) Concrete strength for fire safety design, *Magazine of Concrete Research,* 57 (8), pp. 445-453.

Hertz, K. (1984) Explosion of silica-fume concrete, *Fire Safety Journal,* 8 (1), p. 77.

Hou, X., Zheng, W., Kodur, V. and Sun, H. (2014) Effect of temperature on mechanical properties of prestressing bars, *Construction and Building Materials,* 61 , pp. 24-32.

Institution of Structural Engineers. (1975) *Fire resistance of concrete structures.* UK: Concrete Society.

International Standard Organisation. (1999) *Fire-resistance tests — Elements of building construction — Part 1: General requirements.* ISO 834-1:1999. Switzerland: ISO.

International Standard Organisation. (2000a) *Fire-resistance tests — Elements of building construction — Part 4: Specific requirements for loadbearing vertical separating elements.* ISO 834-4:2000. Switzerland: ISO.

International Standard Organisation. (2000b) *Fire-resistance tests — Elements of building construction — Part 5: Specific requirements for loadbearing horizontal separating elements.* ISO 834-5:2000. Switzerland: ISO.

International Standard Organisation. (2000c) *Fire-resistance tests — Elements of building construction — Part 6: Specific requirements for beams.* ISO 834-6:2000. Switzerland: ISO.

International Standard Organisation. (2000d) *Fire-resistance tests — Elements of building construction — Part 7: Specific requirements for columns.* ISO 834-7:2000. Switzerland: ISO.

Jensen, E., Horn, V. J. and Joshi, M. (2010) Deformation of Concrete Due to Mechanical and Fire Loads, in: *Structures in Fire: Proceedings of the Sixth International Conference,* DEStech, pp. 792-799.

Khoury, G. A., Dias, W. P. and Sullivan, P. J. (1986) Deformation of concrete and cement paste loaded at constant temperatures from 140 to 724°C, *Materials and Structures,* 19 (2), pp. 97-104.

Khoury, G. A., Grainger, B. N. and Sullivan, P. J. (1985) Transient thermal strain of concrete: literature review, conditions within specimen and behaviour of individual constituents, *Magazine of Concrete Research,* 37 (132), pp. 131-144.

Knaack, A. M., Kurama, Y. C. and Kirkner, D. J. (2010) Compressive Strength Relationships for Concrete under Elevated Temperatures, *ACI Material Journal,* 107 (2), pp. 164-175.

Knaack, A. M., Kurama, Y. C. and Kirkner, D. J. (2011) Compressive Stress-Strain Relationships for North American Concrete under Elevated Temperatures, *ACI Material Journal,* 108 (3), pp. 270-280.

Kodur, V., Cheng, F., Wang, T. and Sultan, M. (2003) Effect of Strength and Fiber Reinforcement on Fire Resistance of High-Strength Concrete Columns, *Journal of Structural Engineering,* 129 (2), pp. 253-259.

Kodur, V. K. R. *Integrating fire resistance into infrastructure projects.* Available from: http://www.nrc-cnrc.gc.ca/eng/ibp/irc/ctus/ctus-n31.html.

Kodur, V. K. R. (1999) Fire Performance of High-Strength Concrete Structural Members, *Construction Technology Update,* 31, pp. 1-4.

Kodur, V. K. R. and Dwaikat, M. (2008) A numerical model for predicting the fire resistance of reinforced concrete beams, *Cement and Concrete Composites,* 30 (5), pp. 431-443.

Kodur, V. K. R., Dwaikat, M. M. S. and Dwaikat, M. B. (2008) High-Temperature Properties of Concrete for Fire Resistance Modeling of Structures, *ACI Material Journal,* 105 (5), pp. 517-527.

Kodur, V. K. R. and Phan, L. (2007) Critical factors governing the fire performance of high strength concrete systems, *Fire Safety Journal,* 42 (6–7), pp. 482-488.

Kodur, V. K. R. and Sultan, M. A. (2003) Effect of Temperature on Thermal Properties of High-Strength Concrete, *Journal of Materials in Civil Engineering,* 15 (2), pp. 101-107.

Kodur, V. K. R., Wang, T. C. and Cheng, F. P. (2004) Predicting the fire resistance behaviour of high strength concrete columns, *Cement and Concrete Composites,* 26 (2), pp. 141-153.

Kodur, V. K. R. and Richard, M. (2003) Fire endurance of high strength concrete columns, *Fire Technology,* 39, pp. 73-87.

Kurowski, P. M. (2004) *Finite element analysis for design engineers.* USA: SAE International.

Lamont, S., Usmani, A. S. and Drysdale, D. D. (2001) Heat transfer analysis of the composite slab in the Cardington frame fire tests, *Fire Safety Journal,* 36 (8), pp. 815-839.

Larson, R. and Farber, B. (2012) *Elementary statistics: picturing the world.* 5th ed. Boston: Prentice Hall.

Li, L.,-J., Xie, W.,-F., Liu, F., Guo, Y.,-C. and Deng, J. (2011) Fire performance of high – strength concrete reinforced with recycled rubber particles, *Magazine of Concrete Research,* 63 (3), pp. 187-195.

Li, L. and Purkiss, J. (2005) Stress–strain constitutive equations of concrete material at elevated temperatures, *Fire Safety Journal,* 40 (7), pp. 669-686.

Li, M., Qian, C. and Sun, W. (2004) Mechanical properties of high-strength concrete after fire, *Cement and Concrete Research,* 34 (6), pp. 1001-1005.

Lie, T. T. and Irwin, R. J. (1993) Method to calculate the fire resistance of reinforced concrete columns with rectangular cross section, *ACI Structural Journal,* 90 (1), pp. 52-60.

Lie, T. T. (1992) *Structural fire protection.* New York: American Society of Civil Engineers.

Lie, T. T. (1974) Characteristic temperature curves for various fire severities, *Fire Technology,* 10 (4), pp. 315-326.

Mehta, P. K. and Monteiro, P. J. M. (1993) *Concrete: structure, properties, and materials.* 2nd ed. Prentice Hall.

Mugume, B.,Rodgers and Horiguchi, T. (2014) Prediction of spalling in fibre-reinforced high strength concrete at elevated temperatures, *Materials and Structures,* 47 (4), pp. 591-604.

Naus, D. J. (2010) *A Compilation of Elevated Temperature Concrete Material Property Data and Information for Use in Assessments of Nuclear Power Plant Reinforced Concrete Structures.* USA: .

Naus, D.,J. (2006) *The Effect of Elevated Temperature on Concrete Materials and Structures - A Literature Review.* USA: .

Nawy, E. G. (2001) *Fundamentals of high-performance concrete.* 2nd ed. New York; Chichester: Wiley.

Nawy, E. G. (2006) *Prestressed Concrete: A Fundamental Approach.* 5th ed. Upper Saddle River, NJ: Pearson Education.

Neville, A. M. (1995) *Properties of concrete.* 4th ed. Harlow: Longman Scientific & Technical.

Neville, A. M. and Brooks, J. J. (1987) *Concrete technology.* Harlow: Longman Scientific & Technical.

Noumowe, A. N., Siddique, R. and Debicki, G. (2009) Permeability of high-performance concrete subjected to elevated temperature (600 °C), *Construction and Building Materials,* 23 (5), pp. 1855-1861.

O'Brien, E. J., Dixon, A. S. and Sheils, E. (2012) *Reinforced and Prestressed Concrete Design to EC2 : The Complete Process.* 2nd ed. Abingdon, Oxon; New York: Spon Press.

Ollivier, J. P., Maso, J. C. and Bourdette, B. (1995) Interfacial transition zone in concrete, *Advanced Cement Based Materials,* 2 (1), pp. 30-38.

Park, J. E., Shin, Y. S. and Kim, H. S. (2011) Various Factors Influencing on Thermal Behaviors of High Strength Concrete (HSC) Columns under Fire, *Procedia Engineering,* 14 (0), pp. 427-433.

Phan, L. and Carino, N. (2003) Code provisions for high strength concrete strength-temperature relationship at elevated temperatures, *Materials and Structures,* 36 (2), pp. 91-98.

Phan, L. T. (2008) Pore pressure and explosive spalling in concrete, *Materials and Structures,* 41 (10), pp. 1623-1632.

Phan, L. T. and Carino, N. J. (1998) Review of Mechanical Properties of HSC at Elevated Temperature, *Journal of Materials in Civil Engineering,* 10 (1), pp. 58-65.

Poon, C. S., Shui, Z. H. and Lam, L. (2004) Compressive behavior of fiber reinforced high-performance concrete subjected to elevated temperatures, *Cement and Concrete Research,* 34 (12), pp. 2215-2222.

Purkiss, J. A. (1996) *Fire safety engineering design of structures.* Oxford: Butterworth-Heinemann.

Rao, S. Singiresu (1999) *The finite element method in engineering.* 3rd ed. USA: Butterworth-Heinemann.

Sabeur, H., Colina, H. and Bejjani, M. (2007) Elastic strain, Young's modulus variation during uniform heating of concrete, *Magazine of Concrete Research,* 59 (8), pp. 559-566.

Sadaoui, A. and Khennane, A. (2009) Effect of transient creep on the behaviour of reinforced concrete columns in fire, *Engineering Structures,* 31 (9), pp. 2203-2208.

Sancak, E., Dursun Sari, Y. and Simsek, O. (2008) Effects of elevated temperature on compressive strength and weight loss of the light-weight concrete with silica fume and superplasticizer, *Cement and Concrete Composites,* 30 (8), pp. 715-721.

Schneider, U. (1988) Concrete at high temperatures — A general review, *Fire Safety Journal,* 13 (1), pp. 55-68.

Shin, K., Kim, S., Kim, J., Chung, M. and Jung, P. (2002) Thermo-physical properties and transient heat transfer of concrete at elevated temperatures, *Nuclear Engineering and Design,* 212 (1–3), pp. 233-241.

Slate, F. O., Nilson, A. H. and Martinez, S. (1986) Mechanical properties of high-strength lightweight concrete, *ACI Journal Proceedings,* 83 (4), pp. 606-613.

Suhaendi, S. L. and Horiguchi, T. (2006) Effect of short fibers on residual permeability and mechanical properties of hybrid fibre reinforced high strength concrete after heat exposition, *Cement and Concrete Research,* 36 (9), pp. 1672-1678.

Terro, M. J. (1998) Numerical Modeling of the Behavior of Concrete Structures in Fire, *ACI Structural Journal,* 95 (2), pp. 183-193.

Tsuchiya, Y. and Sumi, K. (1971) Computation of the behavior of fire in an enclosure, *Combustion and Flame,* 16 (2), pp. 131-139.

Xiao, J. and König, G. (2004) Study on concrete at high temperature in China—an overview, *Fire Safety Journal,* 39 (1), pp. 89-103.

Xiao, R. Y. and Ezekiel, S. (2013). Constitutive model for high strength concrete (HSC) at elevated temperatures, *International Journal of Engineering and Technology*, 5(5), pp. 550-555.

Xu, Y., Wong, Y. L., Poon, C. S. and Anson, M. (2003) Influence of PFA on cracking of concrete and cement paste after exposure to high temperatures, *Cement and Concrete Research,* 33 (12), pp. 2009-2016.

Yang, S., Kim, J., Kim, N. and Park, J. (2003) Experimental Measurement of Concrete Thermal Expansion, *Journal of the Eastern Asia Society for Transportation Studies,* 5, pp. 1035-1048.

Yip, W. K. (1998) Generic Form of Stress-Strain Equations for Concrete, *Cement and Concrete Research,* 28 (4), pp. 499-508.

Youssef, M. A. and Moftah, M. (2007) General stress–strain relationship for concrete at elevated temperatures, *Engineering Structures,* 29 (10), pp. 2618-2634.

Zeiml, M., Leithner, D., Lackner, R. and Mang, H. A. (2006) How do polypropylene fibers improve the spalling behavior of in-situ concrete? *Cement and Concrete Research,* 36 (5), pp. 929-942.

Zha, X.,X. (2003) Three-dimensional non-linear analysis of reinforced concrete members in fire, *Building and Environment,* 38 (2), pp. 297-307.